frontiers | Research Topics

Advancing our understanding of the genetic and functional basis of skeletal dysplasia

Edited by
Long Guo, Rong Qiang, Pelin Ozlem Simsek-Kiper and Yi Zhang

Published in
Frontiers in Genetics
Frontiers in Pediatrics

ISSN 1664-8714
ISBN 978-2-8325-1646-1
DOI 10.3389/978-2-8325-1646-1

About Frontiers

Frontiers is more than just an open access publisher of scholarly articles: it is a pioneering approach to the world of academia, radically improving the way scholarly research is managed. The grand vision of Frontiers is a world where all people have an equal opportunity to seek, share and generate knowledge. Frontiers provides immediate and permanent online open access to all its publications, but this alone is not enough to realize our grand goals.

Frontiers journal series

The Frontiers journal series is a multi-tier and interdisciplinary set of open-access, online journals, promising a paradigm shift from the current review, selection and dissemination processes in academic publishing. All Frontiers journals are driven by researchers for researchers; therefore, they constitute a service to the scholarly community. At the same time, the *Frontiers journal series* operates on a revolutionary invention, the tiered publishing system, initially addressing specific communities of scholars, and gradually climbing up to broader public understanding, thus serving the interests of the lay society, too.

Dedication to quality

Each Frontiers article is a landmark of the highest quality, thanks to genuinely collaborative interactions between authors and review editors, who include some of the world's best academicians. Research must be certified by peers before entering a stream of knowledge that may eventually reach the public - and shape society; therefore, Frontiers only applies the most rigorous and unbiased reviews. Frontiers revolutionizes research publishing by freely delivering the most outstanding research, evaluated with no bias from both the academic and social point of view. By applying the most advanced information technologies, Frontiers is catapulting scholarly publishing into a new generation.

What are Frontiers Research Topics?

Frontiers Research Topics are very popular trademarks of the *Frontiers journals series*: they are collections of at least ten articles, all centered on a particular subject. With their unique mix of varied contributions from Original Research to Review Articles, Frontiers Research Topics unify the most influential researchers, the latest key findings and historical advances in a hot research area.

Find out more on how to host your own Frontiers Research Topic or contribute to one as an author by contacting the Frontiers editorial office: frontiersin.org/about/contact

Advancing our understanding of the genetic and functional basis of skeletal dysplasia

Topic editors

Long Guo — Laboratory for Bone and Joint Diseases, RIKEN Center for Integrative Medical Sciences, Japan

Rong Qiang — Medical Reproductive Center, Northwest Women's and Children's Hospital, China

Pelin Ozlem Simsek-Kiper — Hacettepe University, Türkiye

Yi Zhang — Central South University, China

Citation

Guo, L., Qiang, R., Simsek-Kiper, P. O., Zhang, Y., eds. (2023). *Advancing our understanding of the genetic and functional basis of skeletal dysplasia*. Lausanne: Frontiers Media SA. doi: 10.3389/978-2-8325-1646-1

The authors declare that the research was conducted in the absence of any commercial or financial relationships that could be construed as a potential conflict of interest

Table of contents

05 Editorial: Advancing our understanding of the genetic and functional basis of skeletal dysplasia
Long Guo, Rong Qiang, Yi Zhang and Pelin Ozlem Simsek-Kiper

08 Comprehensive Transcriptomic Profiling of Murine Osteoclast Differentiation Reveals Novel Differentially Expressed Genes and LncRNAs
Salman M. Toor, Sachin Wani and Omar M. E. Albagha

19 Genetic Variants and Protein Alterations of Selenium- and T-2 Toxin-Responsive Genes Are Associated With Chondrocytic Damage in Endemic Osteoarthropathy
Yujie Ning, Minhan Hu, Jiayu Diao, Yi Gong, Ruitian Huang, Sijie Chen, Feiyu Zhang, Yanli Liu, Feihong Chen, Pan Zhang, Guanghui Zhao, Yanhai Chang, Ke Xu, Rong Zhou, Cheng Li, Feng Zhang, Mikko Lammi, Xi Wang and Xiong Guo

30 Phenotypic Spectrum and Molecular Basis in a Chinese Cohort of Osteogenesis Imperfecta With Mutations in Type I Collagen
Peikai Chen, Zhijia Tan, Hiu Tung Shek, Jia-nan Zhang, Yapeng Zhou, Shijie Yin, Zhongxin Dong, Jichun Xu, Anmei Qiu, Lina Dong, Bo Gao and Michael Kai Tsun To

43 Identification of a Novel Missense Mutation of the *PHEX* Gene in a Large Chinese Family with X-Linked Hypophosphataemia
Yanting Yang, Yuanda Wang, Ying Shen, Mohan Liu, Siyu Dai, Xiaodong Wang and Hongqian Liu

53 Identification of Novel *FBN2* Variants in a Cohort of Congenital Contractural Arachnodactyly
Liying Sun, Yingzhao Huang, Sen Zhao, Wenyao Zhong, Jile Shi, Yang Guo, Junhui Zhao, Ge Xiong, Yuehan Yin, Zefu Chen, Nan Zhang, Zongxuan Zhao, Qingyang Li, Dan Chen,Yuchen Niu, Xiaoxin Li, Guixing Qiu, Zhihong Wu, Terry Jianguo Zhang, Wen Tian and Nan Wu

61 Novel Loss-of-Function Mutations in *NPR2* Cause Acromesomelic Dysplasia, Maroteaux Type
Jing Wu, Mengru Wang, Zhouyang Jiao, Binghua Dou, Bo Li, Jianjiang Zhang, Haohao Zhang, Yue Sun, Xin Tu, Xiangdong Kong and Ying Bai

72 A Novel Mutation c.3392G>T of *COL2A1* Causes Spondyloepiphyseal Dysplasia Congenital by Affecting Pre-mRNA Splicing
Lihong Fan, Longfei Ji, Yuqing Xu, Guosong Shen, Kefeng Tang, Zhi Li, Sisi Ye and Xueping Shen

80 ZPA Regulatory Sequence Variants in Chinese Patients With Preaxial Polydactyly: Genetic and Clinical Characteristics
Lei Zeng, Jie-Yuan Jin, Fang-Mei Luo, Yue Sheng, Pan-Feng Wu and Rong Xiang

88 Case Report: Prenatal Diagnosis of Postaxial Polydactyly With Bi-Allelic Variants in Smoothened (SMO)
Lihong Fan, Pengzhen Jin, Yeqing Qian, Guosong Shen, Xueping Shen and Minyue Dong

94 A Null Mutation of *TNFRSF11A* Causes Dysosteosclerosis, Not Osteopetrosis
Tarık Kırkgöz, Behzat Özkan, Filiz Hazan, Sezer Acar, Özlem Nalbantoğlu, Beyhan Özkaya, Melike Ataseven Kulalı, Semra Gürsoy, Shiro Ikegawa and Long Guo

101 *FGD1* Variant Associated With Aarskog–Scott Syndrome
Yilin Zhu, Qingqing Chen, Haiyan Lin, Huifei Lu, Yangbin Qu, Qingfeng Yan and Chunlin Wang

112 Exploring and expanding the phenotype and genotype diversity in seven Chinese families with spondylo-epi-metaphyseal dysplasia
Shanshan Lv, Jiao Zhao, Li Liu, Chun Wang, Hua Yue, Hao Zhang, Shanshan Li and Zhenlin Zhang

125 Novel SRY-box transcription factor 9 variant in campomelic dysplasia and the location of missense and nonsense variants along the protein domains: A case report
Carlos A. Calvache, Estefanía C. Vásquez, Vanessa I. Romero, Kazuyoshi Hosomichi and Juan C. Pozo

135 Clinical genetics of spondylocostal dysostosis: A mini review
Muhammad Umair, Muhammad Younus, Sarfraz Shafiq, Anam Nayab and Majid Alfadhel

frontiers | Frontiers in Genetics

TYPE Editorial
PUBLISHED 27 January 2023
DOI 10.3389/fgene.2023.1139228

OPEN ACCESS

EDITED AND REVIEWED BY
Jordi Pérez-Tur,
Institute of Biomedicine of Valencia,
Spanish National Research Council (CSIC),
Spain

*CORRESPONDENCE
Long Guo,
longguo601@gmail.com
Pelin Ozlem Simsek-Kiper,
poskiper@gmail.com

SPECIALTY SECTION
This article was submitted to Genetics of Common and Rare Diseases, a section of the journal Frontiers in Genetics

RECEIVED 06 January 2023
ACCEPTED 20 January 2023
PUBLISHED 27 January 2023

CITATION
Guo L, Qiang R, Zhang Y and Simsek-Kiper PO (2023), Editorial: Advancing our understanding of the genetic and functional basis of skeletal dysplasia.
Front. Genet. 14:1139228.
doi: 10.3389/fgene.2023.1139228

Editorial: Advancing our understanding of the genetic and functional basis of skeletal dysplasia

Long Guo[1,2]*, Rong Qiang[3], Yi Zhang[4] and Pelin Ozlem Simsek-Kiper[5]*

[1]Department of Laboratory Animal Science, School of Basic Medical Sciences, Xi'an Jiaotong University, Xi'an, China, [2]Shaanxi Institute for Pediatric Diseases, Xi'an Children's Hospital, Affiliated Children's Hospital of Xi'an Jiaotong University, Xi'an, China, [3]Center of Medical Genetics, Northwest Women's and Children's Hospital, Xi'an, China, [4]Department of Orthopaedics, Xiangya Hospital, Central South University, Changsha, China, [5]Hacettepe University Faculty of Medicine, Department of Pediatrics, Pediatric Genetics Unit, Ankara, Türkiye

KEYWORDS

skeletal dysplasia, genetics, development, WES, WGS

Editorial on the Research Topic
Advancing our understanding of the genetic and functional basis of skeletal dysplasia

Skeletal dysplasia is a group of disorders characterized by abnormal skeleton formation because of intrinsic derangement of growth, development, and/or differentiation. According to the latest International Classification of Skeletal Dysplasia, 42 subgroups with 461 disease entities have been established in this category. More than 90% of skeletal dysplasias are monogenic diseases. The incidence of each disease is low, but as a whole, skeletal dysplasias affect about one in 1,000 of the global population. Therefore, studies on skeletal dysplasia have essential clinical significance (*e.g.*, prenatal diagnosis, targeted therapy, prevention at the second pregnancy) and provide the highest evidence for the mechanism of development and maintenance of the human skeleton.

For this Research Topic, we collected high-quality research papers describing novel insights into genetic factors that decide heterogeneity, prognosis, and treatment of skeletal dysplasias. The final Research Topic has 14 published articles covering various types of skeletal dysplasias in different populations.

Osteogenesis imperfecta (OI) is a rare inherited connective tissue dysplasia characterized by skeletal fragility, recurrent fractures, and bone deformity, predominantly caused by mutations in *COL1A1* or *COL1A2* that encode the chains of type I collagen. Although mutation spectrums on autosomal dominant OI have been established in large cohorts of Chinese populations, the relationship between clinical manifestations and genetic mutations remains to be further explored due to the high genetic and clinical heterogeneity. Chen et al. performed a detailed analysis on 187 Chinese OI patients to further expand the mutational spectrum of type I collagen genes, and better establish the correlation between genotype and phenotype in OI patients. The findings coupled with the heterogeneity observed in the transcriptomic data derived from osteoblasts of six patients from the cohort. Notably, they highlighted that bisphosphonate treatment benefits bone density rather than height during the juvenile stage (10–15 years old). Observing effective bisphosphonate treatment in an age-specific manner would help improve OI patient management.

Dysosteosclerosis (DOS) is a rare sclerosing bone dysplasia characterized by unique osteosclerosis of the long tubular bones and platyspondyly. DOS is inherited in an autosomal recessive manner and is genetically and clinically heterogeneous. Pathogenic variants in *SLC29A3, TNFRSF11A, TCIRG1, LRRK1,* and *CSF1R* have been reported to be associated with DOS. Mutations in *TNFRSF11A* encoding RANK protein also cause osteopetrosis, autosomal recessive 7 (OPTB7). Based on the previous studies, it is hypothesized that mutations producing aberrant mutant RANK proteins (missense or truncated or elongated) cause DOS, while null mutations lead to OPTB7. Kırkgöz et al. presented the fifth case of TNFRSF11A-associated DOS with a novel homozygous frame-shift mutation. The mutation is predicted to cause non-sense mutation-mediated mRNA decay in all RANK isoform transcripts, resulting in a totally null allele. The finding opposes the previous hypothesis and suggests that the genotype-phenotype relationship in TNFRSF11A-associated OPTB7 and DOS remains unclear. Further studies are necessary to understand the phenotypic spectrum caused by *TNFRSF11A* mutations.

Congenital contractural arachnodactyly (CCA) is a rare autosomal dominant disorder of connective tissue characterized by crumpled ears, arachnodactyly, camptodactyly, large joint contracture, and kyphoscoliosis. CCA is caused by variants in *FBN2* encoding fibrillin-2, which is an integral component of elastin fibers in the extracellular matrix. The natural course of CCA has yet to be well-described. To decipher the genetic and phenotypic spectrum of CCA. Sun et al. enrolled a CCA cohort *via* the DISCO consortium (http://www.discostudy.org/) and identified ten pathogenic *FBN2* variants in 27 CCA patients from ten families. Among these ten variants, seven were novel. They also validated the clinical utility of a newly developed scoring system for CCA.

Polydactyly is a common congenital abnormality characterized by the presence of extra digit(s) on the preaxial or postaxial sides of the hand or foot. A complex network of intercellular communication and gene expression regulates limb growth in vertebrates. The sonic hedgehog protein (SHH), one of three mammalian hedgehog proteins, is expressed in the zone of polarizing activity (ZPA) of the limb bud and those of the notochord and floor plate in the neural tube, playing an essential role in regulating the patterning and growth of the developing limb. ZPA regulatory sequence (ZRS) is a limb-specific enhancer of *SHH*, located nearly 1 Mb from *SHH* and within intron 5 of *LMBR1*. Zeng et al. recruited 167 sporadic or familial cases (including 154 sporadic patients and 13 families) with preaxial polydactyly from Central-South China and identified four ZRS variants in four patients (2.40%, 4/167). This investigation preliminarily evaluated a ZRS variants rate in patients with preaxial polydactyly and described the general picture of preaxial polydactyly in Central-South China. Smoothened (SMO) is one of the significant components of the SHH pathway. Fan et al. identified bi-allelic novel variants of SMO in a patient with postaxial polydactyly and documented the detailed phenotype. These findings highlight the importance of the SHH pathway in human limb patterning by studying the etiology of polydactyly and contribute to a better understanding of the complex phenotypes and mechanisms associated with the defects of the SHH pathway.

Spondylo-epi-metaphyseal dysplasia (SEMD) is a heterogeneous group of disorders with different modes of inheritance and is characterized by disproportionate or proportionate short stature. More than 30 disease-causing genes have been identified to date, and different types of SEMD exhibit considerably overlapping clinical features, which usually complicate the diagnosis. Lv et al. enrolled seven families, including 11 patients with SEMD, and analyzed their clinical, radiographic, and genetic features. Seven variants were identified in *TRPV4, COL2A1, CCN6, SBDS*, and *ACAN*. In addition, Fan et al. reported a novel splicing variant of *COL2A1* in a Chinese family with SEMD and confirmed the pathogenicity of the variant by a minigene analysis. These studies expand the phenotypic and genetic spectrum of SEMD and provide evidence for the genotype-phenotype relations, contributing to molecular and clinical diagnosis of SEMD.

Kashin–Beck disease (KBD) is an endemic osteoarthropathy distributed throughout North Korea, Siberia, Japan, and China. Selenium deficiency and T-2 toxin have been considered the main environmental risk factors for KBD that induce cartilage damage, such as acceleration of chondrocyte apoptosis and an imbalance of the extracellular matrix. However, the role of selenium deficiency and T-2 toxin in KBD development remains unclear. Ning et al. took the cubital venous blood of 258 subjects including 129 sex-matched KBD patients and 129 healthy controls for single nucleotide polymorphisms (SNPs) detection and analysis. They selected these candidate SNP loci from selenium- and T-2 toxin–responsive genes in Comparative Toxicogenomics Database and verified the gene expression in knee cartilage of the patients and controls. These findings revealed the interaction between genetic and environmental factors and suggest that genomic variation in selenium deficiency- and T-2 toxin-responsive genes increase the risk of KBD by disturbing extracellular matrix homeostasis.

The Research Topic also included reports about acromesomelic dysplasia, Maroteaux type (Wu et al.), X-linked hypophosphataemia (Yang et al.), Aarskog–Scott syndrome (Zhu et al.), campomelic dysplasia (Calvache et al.), and spondylocostal dysostosis (Umair et al.) They either uncovered new genotype-phenotype associations by presenting exceptional cases or summarized the study progression of these skeletal dysplasias by designing a comprehensive review. Additionally, Toor et al. revealed novel differentially expressed coding genes and LncRNAs by profiling the transcriptome of murine osteoclast differentiation.

The above reports enrich our knowledge of skeletal dysplasia by reporting either large cohorts or atypical cases. These findings greatly expand the phenotypic and mutational spectrum, and contribute to the diagnosis, prevention and therapeutic innovation of skeletal dysplasia. These studies also provide insight into the underlying pathologic mechanisms, gene-environment interactions, and skeletal developmental biology. We sincerely appreciate the time and effort of all the authors, who contributed to the Research Topic, which significantly improves our understanding of the genetic and functional basis of the skeletal dysplasias.

Author contributions

LG and PS-K designed and initiated the paper collection. All authors are guest editors, who have made a substantial, direct and intellectual contribution to the work and approved it for publication.

Funding

LG was supported by Xi'an Jiaotong University (Young Talent Support Plan) and Japanese Society for Bone and Mineral Research (the JSBMR Rising Stars Grant); RQ was supported by Shaanxi Key R&D Program Project (2023-YBSF-518); YZ was supported by National Natural Science Foundation of China (No. 82102581).

Acknowledgments

The guest editors thank all the authors and reviewers for their valuable contributions to this Research Topic, and we hope this Research Topic of articles will interest the medical and genetics community.

Conflict of interest

The authors declare that the research was conducted in the absence of any commercial or financial relationships that could be construed as a potential conflict of interest.

Publisher's note

frontiers in Genetics

ORIGINAL RESEARCH
published: 15 November 2021
doi: 10.3389/fgene.2021.781272

Comprehensive Transcriptomic Profiling of Murine Osteoclast Differentiation Reveals Novel Differentially Expressed Genes and LncRNAs

Salman M. Toor[1†], *Sachin Wani*[2†] *and Omar M. E. Albagha*[1,2*]

[1]College of Health and Life Sciences, Hamad Bin Khalifa University, Doha, Qatar, [2]Rheumatology and Bone Disease Unit, Centre for Genomic and Experimental Medicine, Institute of Genetics and Cancer, University of Edinburgh, Edinburgh, United Kingdom

OPEN ACCESS

Edited by:
Long Guo,
RIKEN Center for Integrative Medical Sciences, Japan

Reviewed by:
Vincent Everts,
VU University Amsterdam, Netherlands
Helen Knowles,
University of Oxford, United Kingdom

***Correspondence:**
Omar M. E. Albagha
oalbagha@hbku.edu.qa

[†]These authors contributed equally to this study

Specialty section:
This article was submitted to Genetics of Common and Rare Diseases, a section of the journal Frontiers in Genetics

Received: 22 September 2021
Accepted: 22 October 2021
Published: 15 November 2021

Citation:
Toor SM, Wani S and Albagha OME (2021) Comprehensive Transcriptomic Profiling of Murine Osteoclast Differentiation Reveals Novel Differentially Expressed Genes and LncRNAs. Front. Genet. 12:781272. doi: 10.3389/fgene.2021.781272

Osteoclasts are the sole bone resorbing cells, which undertake opposing roles to osteoblasts to affect skeletal mass and structure. However, unraveling the comprehensive molecular mechanisms behind osteoclast differentiation is necessitated to overcome limitations and scarcity of available data, particularly in relation with the emerging roles of long non-coding RNAs (LncRNAs) in gene expression. In this study, we performed comprehensive and progressive analyses of the dynamic transcriptomes of murine osteoclasts, generated *in vitro*. We compared the total RNA-based transcriptomes of murine bone marrow derived cells with differentiated osteoclasts, while focusing on potentially novel genes and LncRNAs, to uncover critical genes and their associated pathways, which are differentially regulated during osteoclast differentiation. We found 4,214 differentially regulated genes during osteoclast differentiation, which included various types of LncRNAs. Among the upregulated protein coding genes not previously associated with osteoclast are *Pheta1*, *Hagh*, *Gfpt1* and *Nol4*, while downregulated genes included *Plau*, *Ltf*, *Sell* and *Zfp831*. Notably, we report *Nol4* as a novel gene related to osteoclast activity since *Nol4* knockout mice *Nol4*$^{em1(International\ Mouse\ Phenotyping\ Consortium)J}$ exhibit increased bone mineral density. Moreover, the differentially expressed LncRNAs included antisense and long intergenic non-coding RNAs, among others. Overall, immune-related and metabolism-related genes were downregulated, while anatomical morphogenesis and remodeling-related genes were upregulated in early-differentiated osteoclasts with sustained downregulation of immune-related genes in mature osteoclasts. The gene signatures and the comprehensive transcriptome of osteoclast differentiation provided herein can serve as an invaluable resource for deciphering gene dysregulation in osteoclast-related pathologic conditions.

Keywords: osteoclast, osteopororosis, bone resorption, RANK ligand (RANKL), differentiation

INTRODUCTION

The balance between osteoclast and osteoblast activity can dictate pathogenesis of bone diseases. Osteoclasts are the exclusive bone resorbing cells involved in bone remodeling and resorption, and perform opposing roles to osteoblasts to affect skeletal mass and structure (Teitelbaum and Ross, 2003). Augmented osteoclast activity can lead to bone loss in osteoporosis, inflammatory arthritis and tumor invasion in bone, while osteopetrosis is characterized by increased bone mass and results from attenuation in osteoclast function/recruitment or arrested osteoclastogenesis (Teitelbaum, 2007). Abnormalities in osteoclasts are considered the primary cause of many bone diseases including osteoporosis, the most common bone disorder, and Paget disease of the bone (PDB) in which accelerated osteoclastic bone resorption leads to osteolytic or osteosclerotic bone lesions (Shaker, 2009).

Osteoclasts are multi-nucleated cells belonging to myeloid lineage, and generated via the fusion of monocytes/macrophage precursor cells (Roodman, 1999). Importantly, signaling via tumor necrosis factor (TNF)-family cytokine, receptor activator of nuclear factor (NF)-kappaB ligand (RANKL) and macrophage colony-stimulating factor (M-CSF) are identified as the primary pathways associated with osteoclast differentiation (Asagiri and Takayanagi, 2007). Osteoclast precursors express receptor activator of nuclear factor kappa B (RANK), while its ligand (RANKL) is expressed on osteoblasts/stromal cell precursors, and inhibited by the decoy receptor osteoprotegerin (OPG) (Yasuda et al., 1998). Moreover, various genes including TNF receptor-associated factor (*TRAF*) 6, *NFKB1*, *FOS*, nuclear factor of activated T cells 1 (*NFATC1*), and dendritic cell-specific transmembrane protein (*DC-STAMP*) have been associated with osteoclastogenesis (Asagiri and Takayanagi, 2007), while the tartrate-resistant acid phosphatase (TRAcP) and cathepsin K (CTSK), released by osteoclasts during resorption are identified as specific osteoclast markers (Boyle et al., 2003; Kirstein et al., 2006). Osteoclast functionality in bone resorption is dependent on αvβ3 integrin-mediated induction, binding and polarization, while deficiencies in acidified bone resorptive components disrupt regulated bone remodeling, leading to osteopetrosis. Amplified stimulation of osteoclastogenesis primarily via NFKB signaling can lead to increased osteolysis in osteoporosis (Novack and Teitelbaum, 2008).

Genome-wide screening and the *in vitro* induction of osteoclastogenesis using osteoclast precursor cells and soluble mediators has enabled the identification of molecular mechanisms governing osteoclast differentiation (Asagiri and Takayanagi, 2007). Sequencing techniques and microarray analyses have also contributed to disclosing important genes related to osteoclast differentiation (Cappellen et al., 2002; Day et al., 2004; Nomiyama et al., 2005; Garlet et al., 2008; Coudert et al., 2014; Kim and Lee, 2014; Purdue et al., 2014; Madel et al., 2020). In addition, recent reports have highlighted the roles of long noncoding RNAs (LncRNAs), which have emerged as vital regulators of gene expression, epigenetics and protein translation (Fatica and Bozzoni, 2014), in osteoclast differentiation (Fei et al., 2020; Liu et al., 2020; Yang et al., 2021). However, available data have primarily focused on differences between fully differentiated/generated osteoclasts compared to precursors or focused predominantly on targeted sets of genes, previously linked with osteoclast differentiation/activity. Therefore, a comprehensive insight into the differentially regulated genes and their associated pathways during osteoclast differentiation is warranted.

In this study, we performed sequential and comprehensive transcriptomic profiling of murine osteoclasts generated *in vitro* by comparing the total RNA transcriptomes of bone marrow derived precursor cells with differentiated osteoclasts over different time points. Importantly, we focused on novel genes and LncRNAs, which have not been previously associated with osteoclast differentiation. These progressive analyses provide important insights into the differentially regulated genes and their associated pathways during osteoclast differentiation. Identification of novel gene signatures and LncRNAs associated with osteoclastogenesis can serve as molecular biomarkers for osteoclast differentiation or explored for therapeutic benefits, while the comprehensive transcriptome of osteoclast differentiation provided herein can serve as an invaluable resource for deciphering gene dysregulation in diseases related to osteoclast differentiation/activity.

MATERIALS AND METHODS

Samples

C57 black 6 (CBL/6) mice, with access to adequate nutrition (pelleted RM1; SDS diets, Essex, United Kingdom) and hydration, in a standard animal research facility were utilized in this study. All protocols were performed as per guidelines of the United Kingdom Animals Act of 1986 (Scientific Procedures). Bone marrow (BM) was flushed from long bones of 3-4-month-old CBL/6 mice and cultured in specialized media designed to induce osteoclast differentiation, as described below. All experiments were performed adhering to applicable guidelines and regulations.

Osteoclast Differentiation

Osteoclast cultures were maintained as described previously (Alonso et al., 2021). Briefly, BM cells from CBL/6 mice were cultured in complete growth media (α-MEM supplemented with 10% fetal calf serum, penicillin/streptomycin and glutamine) and in the presence of soluble M-CSF (Prospec Technology, United Kingdom) at 100 ng/ml to generate bone marrow derived macrophages (BMDM). Non-adherent cells were washed after 48 h, while adherent cells were removed using cell dissociation buffer (Gibco, United Kingdom) and re-cultured in parallel in 6-well plates at a density of 3×10^5 cells per well and in 96-well plates at 1×10^4 cells per well in the presence of M-CSF (25 ng/ml) and soluble RANKL (R&D Systems, United Kingdom) at 100 ng/ml. Cultures in 96-well plates were used to monitor osteoclast differentiation and mature osteoclasts were detected by staining for tartrate-resistant acid phosphatase (TRAcP). Cells with more than three nuclei and positive for TRAcP staining were considered osteoclasts. In addition, the resorptive activity of generated

osteoclasts was determined using Osteo Assay plates (Corning, New York, United States), as per manufacturer's guidelines. Quantification of resorption areas was carried out using ImageJ software (National Institutes of Health, Maryland, United States). Unpaired *t*-test was used to investigate statistical significance between two groups, while one-way Anova test was performed to determine statistical significance between more than two groups (GraphPad Prism, version 9.0; GraphPad Software, California, United States). A p value of <0.05 was considered statistically significant.

Cultures in 6-well plates were used to collect RNA for gene expression profiling. Cells were collected at the following time points for gene expression analysis: day 0 (BMDM), day 3 (osteoclast precursor) and day 4 (osteoclast) for subsequent investigations.

RNA Isolation

RNA was isolated from BMDM cells (Day 0) and differentiated osteoclasts from different time points (Day 3 and Day 4) using GenElute Mammalian Total RNA Kit (Sigma-Aldrich, Missouri, United States) by following manufacturer's protocol. Integrity and purity of RNA was assessed using Bioanalyzer 2100 (Agilent Technologies, California, United States). A total of nine RNA samples were obtained (representing three biological replicates at Day 0, Day 3 and Day 4).

Library Preparation and RNA-Sequencing

cDNA libraries were generated from isolated total RNA samples using TruSeq Stranded Total RNA kit with Ribo-Zero Globin (Illumina, California, United States) by following manufacturer's protocol. Quality-passed libraries were sequenced on NovaSeq6000 system (Illumina) using 100 bp paired-end protocol.

Data Processing and Differential Gene Expression Analyses

Data were analyzed and illustrated using multiple bioinformatics software under default settings unless otherwise stated. Reads were quality-trimmed using Cutadapt1 (version 1.9. dev2) and those with low quality and short reads (<35 bp) were trimmed along with Illumina TruSeq RNA kit adapters. Reads were aligned to the reference genome (*Mus* Musculus GRmc38) using STAR2 (version 2.5.2b) specifying paired-end reads. Reads were assigned to features of type 'exon' in the input annotation grouped by gene_id in the reference genome using featureCounts3 (version 1.5.1). The raw counts table was filtered to remove genes consisting predominantly of near-zero counts, filtering on counts per million (CPM) to avoid artefacts due to library depth. Overall, three biological replicate datasets were generated for each time point (Day 0, Day 3, and Day 4). Abundance data were successively subjected to differential gene expression analyses. Z-scores were calculated from CPM values as described previously (Malone et al., 2011) and heatmaps generated using GraphPad Prism software (GraphPad Software).

Differential gene expression analyses and gene ontology (GO) clustering analyses were performed using Integrated Differential Expression and Pathway (iDEP.92, South Dakota State University, United States) online tool. Raw CPM values were uploaded and computed (min. CPM = 1) to identify and generate various illustrations for gene clustering and differentially expressed genes. Differential expression analysis was performed using the DEseq2 method (Love et al., 2014). PCA and Volcano plots were generated with Log2-fold change (FC) > 2 and false discovery rate (FDR) cutoff <0.05. K-Means clustering were used for performing gene enrichment analyses using GO biological processes pathway database (Ashburner et al., 2000).

RESULTS

Transcriptomic Changes in Osteoclast Differentiation

An overview of the study design to decipher the transcriptomic changes during murine osteoclast differentiation *in vitro* is depicted in **Figure 1A**. The morphological changes in osteoclast differentiation showed the progressive and statistically significant differences in the number of TRAcP+ osteoclasts (≥3 nuclei) formed during differentiation of BMDM cells to osteoclast (**Figures 1B,C**). Osteoclast precursors exhibit a pre-fusion state whereby the cells cluster together to form multi-nucleated mature osteoclasts (Day 4). In addition, the functional activity of generated osteoclasts was assessed by Osteo Assay (resorptive activity assay), which showed statistically significant, distinct and large resorption areas with osteoclasts compared to osteoclast precursors and undifferentiated BMDM cells (**Figures 1D,E**). Comprehensive investigations were performed on the differentially regulated genes disclosed during osteoclast differentiation, using stringent criteria and cutoffs as described above.

We generated comprehensive datasets for the transcriptomes of undifferentiated BMDM cells (Day 0) and differentiated osteoclasts on Days 3 and 4 (**Supplementary Tables S1-3**). One replicate from day 3 failed the quality control measures and was removed from the analysis. PCA analyses showed close proximity of biological replicates for each time point: PC1 showed 87% variance and PC2 showed 7% variance (**Figure 2A**). Hierarchical gene clustering during osteoclast differentiation showed distinct gene clusters (**Figure 2B**). Overall, 4,214 differentially regulated genes (2,251 downregulated and 1,963 upregulated) were identified, which showed some overlap between the different timepoint comparisons, primarily between Day 3 versus Day 0 and Day 4 versus Day 0 comparisons (**Figure 2C**).

Importantly, K-Means clustering analyses revealed the corresponding pathways of gene enrichment observed during osteoclast differentiation (**Figure 2D**). Our data showed that genes related to immune and inflammatory response, and response to stimulus were downregulated during osteoclast differentiation. Concurrently, genes related to anatomical morphogenesis and developmental process were upregulated in differentiated osteoclasts. Moreover, upregulation of genes related to osteoclast differentiation, bone remodeling and resorption was observed during osteoclast differentiation. Further analyses revealed that the number of upregulated genes related to osteoclast differentiation (n = 12), tissue remodeling (n = 14), bone remodeling (n = 11) and bone resorption (n = 9) was lower compared to the number of

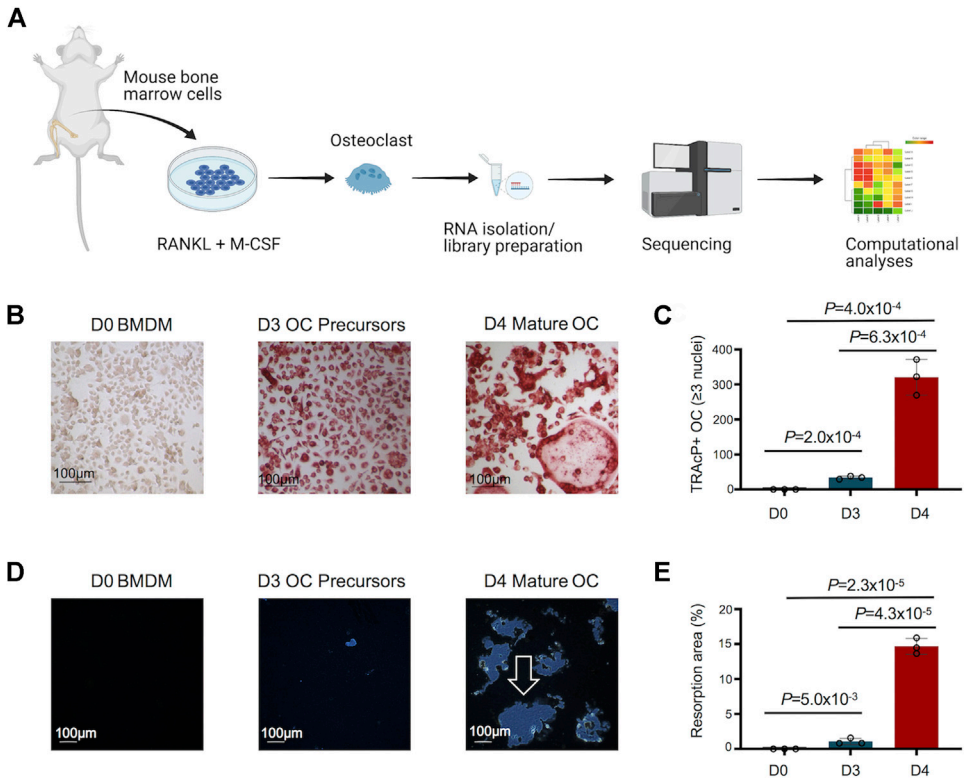

FIGURE 1 | Study design, and morphological and functional changes during osteoclast (OC) differentiation. **(A)** Bone marrow cells flushed from long bones of CBL/6 mice were cultured in the presence of soluble M-CSF and RANKL to induce OC differentiation. Libraries were generated from bone marrow derived macrophages (BMDM) (Day 0) and differentiated osteoclasts at different time points (Days 3 and 4) to perform comprehensive and progressive analyses of the dynamic transcriptomes of murine osteoclasts by RNA-Seq. Various bioinformatics tools were utilized for data analyses/visualization. Schematic representation of the study design is shown. **(B)** The generated OC were detected by staining for tartrate-resistant acid phosphatase (TRAcP). Cells positive for TRAcP staining and with more than three nuclei were identified as OC representative images of TRAcP stained cells show Bone marrow derived macrophages (BMDM) at day 0 (D0), OC precursors at D3 and mature OC at D4 of the culture. **(C)** Scatter/bar-hybrid plot shows the numbers with mean ± standard deviation (SD) of TRAcP+ OC in D0, D3 and D4 comparisons. **(D)** The bone resorption activity of OC was investigated using Osteo Assay. Representative images show cultures from BMDM cells at D0, OC precursors at D3 and mature OC at D4 of the culture. Resorption areas are indicated by white arrow. **(E)** Scatter/bar-hybrid plot shows the differences in percentage resorption area (mean ± SD) in D0, D3 and D4 cultures.

downregulated genes associated with immune response (n = 294), response to stress (n = 339), defense response (n = 198), inflammatory response (n = 131) and response to external stimulus (n = 260) (**Figure 2E**).

Of note, to confirm the *in vitro* generation of osteoclasts, we investigated the expression levels of critical genes known to be expressed in osteoclasts (Teitelbaum and Ross, 2003; Asagiri and Takayanagi, 2007). These selective genes included *Oscar*, *Ocstamp*, *Acp5* (TRAcP), *Ctsk*, *Dcstamp*, *Nfatc1*, *Traf6*, *Trap1* and *Nfkb1*, among others. We found that all genes in our selected panel of osteoclast-related genes were upregulated following induction of osteoclast differentiation (**Figure 2F**). These confirmatory data provided additional evidence for successful osteoclast generation.

Differentially Regulated Genes During Early Osteoclast Differentiation

An important aspect of this study was to uncover gene expression profiles during the course of osteoclast differentiation. In this pursuit, we first compared the transcriptomes of early-differentiated osteoclasts (Day 3) with BMDM cells (Day 0; **Figure 3**). Our data revealed 3,351 differentially regulated genes, of which 1,736 genes were upregulated while 1,615 genes were downregulated in early-differentiated osteoclasts (**Figure 3A**). Importantly, GO biological process enrichment analyses revealed distinct gene clusters between the transcriptomes of Day 3 versus Day 0 analyses (**Figure 3B**). Upregulated genes predominantly corresponded to metabolic processes, whereas downregulated genes primarily corresponded to immune and stimulus response. Generation of precursor metabolites and energy- (n = 102), small molecule metabolic process- (n = 256), phosphate containing compound metabolic process- (n = 365) and nucleotide metabolic process-related genes (n = 114) comprised upregulated genes. In contrast, response to stress- (n = 475), regulation of response to stimulus- (n = 467), immune system process- (n = 342) and inflammatory response-related genes (n = 139) comprised downregulated genes during early osteoclast differentiation (**Figure 3C**).

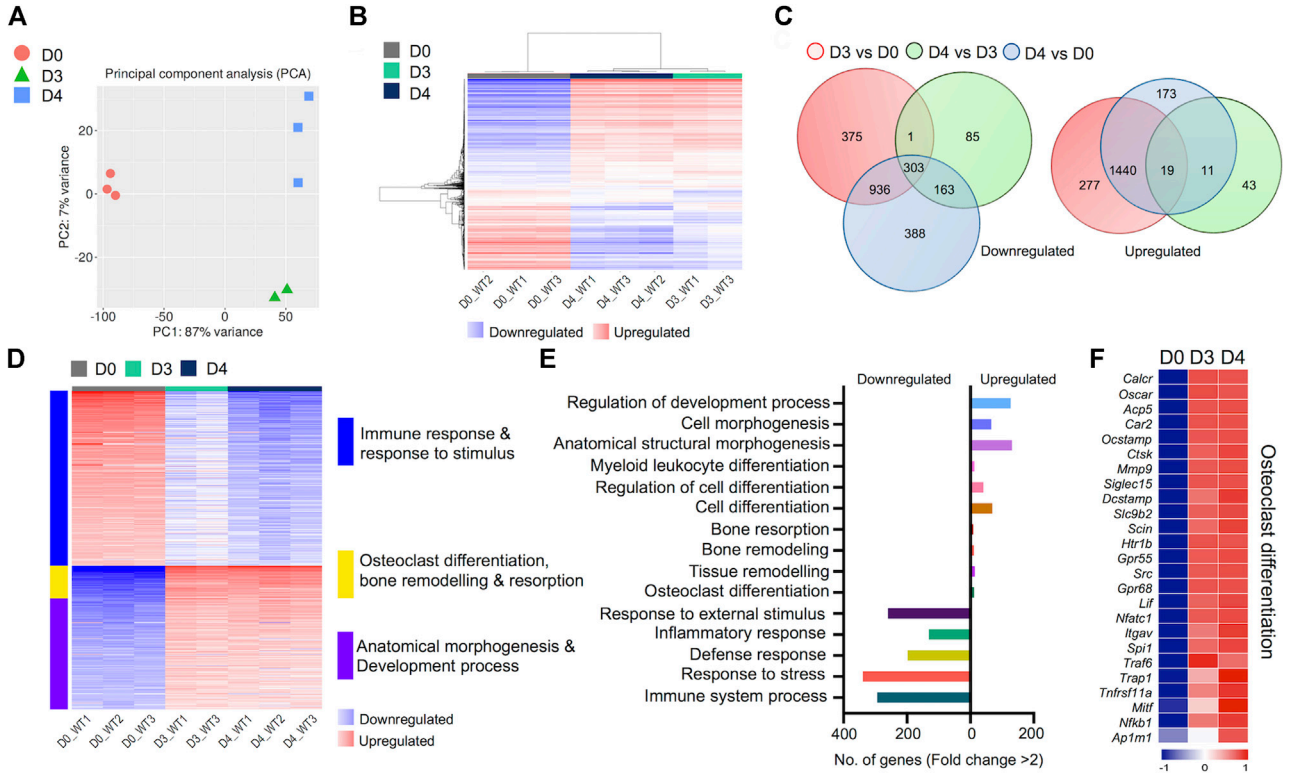

FIGURE 2 | Transcriptomic profiling of osteoclast differentiation. The transcriptomes of bone marrow derived macrophages (BMDM; D0) were compared with osteoclast precursors (D3) and fully differentiated osteoclasts (D4) by performing differential gene expression analyses. **(A)** PCA plot shows variability in gene expression among biological replicates between D0, D3 and D4. **(B)** Heatmap shows hierarchical clustering of gene expression in cells from D0, D3 and D4. **(C)** Venn diagram depicts the total numbers of overlapping differentially regulated (downregulated and upregulated) genes between D0, D3 and D4. **(D)** Heatmap shows gene enrichment and associated pathways in D0, D3 and D4. **(E)** Bar plot shows the numbers of genes corresponding to significantly up/downregulated functional pathways from gene ontology enrichment analyses. **(F)** Heat map shows the gene expression (Z-scores) of osteoclast-related gene panel for confirmation of osteoclast generation.

Distinct Long Non-coding RNA and Protein Coding Genes Upregulated During Early Osteoclast Differentiation

Apart from protein coding genes, the importance of LncRNAs in the regulation of osteoclast differentiation has been recently described (Fei et al., 2020; Liu et al., 2020; Yang et al., 2021). We compiled a list of differentially regulated LncRNAs during osteoclast differentiation (**Supplementary Figure S4**). These differentially regulated LncRNAs comprised of different subtypes as listed in **Table 1**. We found that 35 potentially novel LncRNAs were upregulated of which 20 LncRNAs showed Log2-FC ≥ 2, while 37 LncRNAs were downregulated with 15 LncRNAs showing Log2-FC ≥ 2 during early osteoclast differentiation. The top 20 differentially expressed LncRNAs during early osteoclast differentiation are presented in **Figure 3D**. These data reflect that these LncRNA genes may have significant roles in osteoclastogenesis and warrant further scrutiny.

In addition, we also identified the top upregulated protein coding genes, which have not been previously reported to be associated with osteoclast differentiation. The top 20 differentially expressed genes based on significance are presented in **Figure 3E** while, the complete list of potentially novel differentially expressed genes during osteoclast differentiation is provided in **Supplementary Table S5**. Additionally, the top 10 upregulated and 10 downregulated genes during osteoclast differentiation, based on FC and significance (p value), irrespective of novelty, are presented in **Supplementary Figure S1**.

Differentially Regulated Genes During Progressive Osteoclast Differentiation

Next, we compared the transcriptomes of early-differentiated osteoclasts (Day 3) with fully differentiated osteoclasts (Day 4). Interestingly, we found that the transcriptomes of committed osteoclasts did not show immense differences with fully differentiated osteoclasts. Overall, only 641 genes showed differential regulation between Day 4 and Day 3 comparison, of which 73 genes were upregulated while 552 genes were downregulated (**Figure 4A**). Importantly, these differentially regulated genes showed further enrichment in downregulation

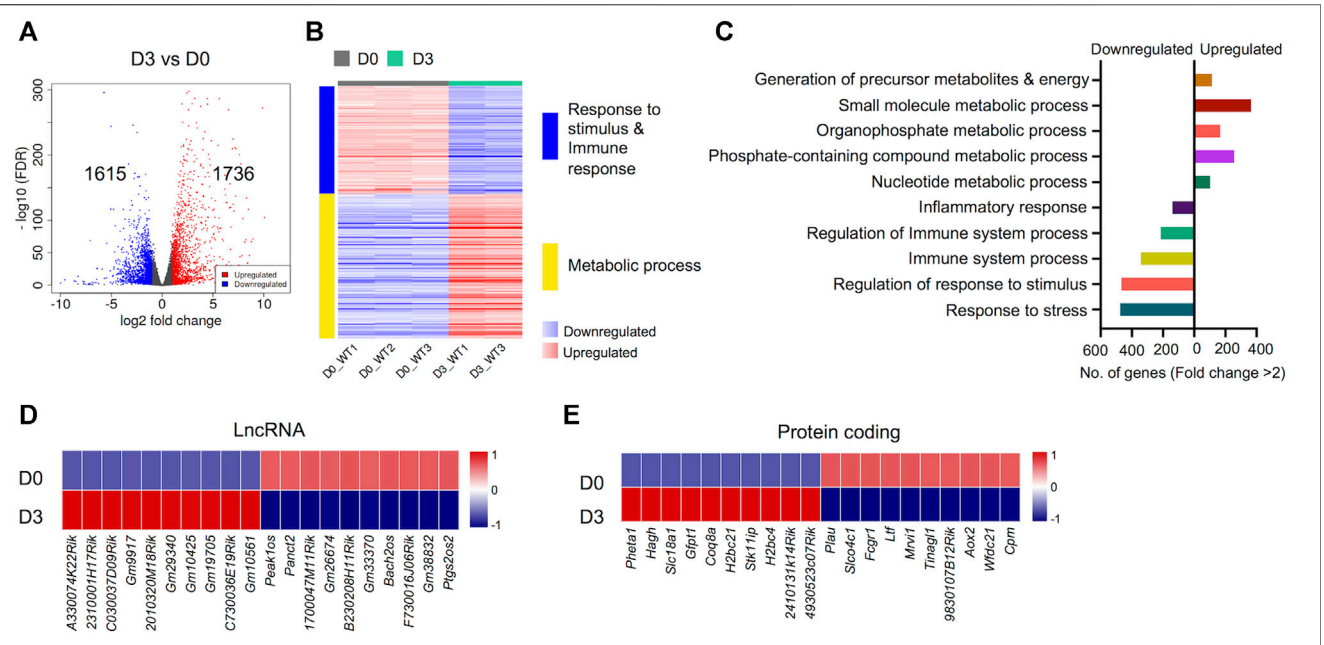

FIGURE 3 | Differentially regulated genes in early osteoclast differentiation. The transcriptomes of osteoclast precursors (D3) were compared with bone marrow derived macrophages (BMDM) (D0). **(A)** Volcano plot represents significantly upregulated (red), downregulated (blue) or genes with unchanged expression levels (gray) between D3 and D0 comparison. **(B)** Heatmap shows gene enrichment and associated pathways in D3 versus D0. **(C)** Bar plot shows the numbers of genes corresponding to significantly up/downregulated functional pathways from gene ontology enrichment analyses. Heat maps show the gene expression (Z-scores) of top differentially-regulated long non-coding RNAs (LncRNA) **(D)** and protein coding genes **(E)** in D3 versus D0 comparison (Log2-FC ≥ 2).

TABLE 1 | Differentially-regulated Long non-coding RNAs (LncRNAs) during osteoclast differentiation.

LncRNA type	Comparison	D3 vs D0		D4 vs D0		D4 vs D3	
	Regulation	↑	↓	↑	↓	↑	↓
Antisense		40	21	29	28	3	6
LincRNA (long intergenic ncRNA)		35	37	32	40	2	11
Bidirectional promoter LncRNA		12	—	4	—	—	—
Sense intronic		1	—	1	—	—	—
Sense overlapping		1	1	1	—	—	—
Total differentially-regulated LncRNAs		**89**	**59**	**67**	**68**	**5**	**17**

of immune response-related genes, whereas cell cycle and DNA replication-related processes were upregulated (**Figure 4B**). The downregulated genes corresponding to immune response-related processes were associated with process such as cytokine production (n = 68), leukocyte activation (n = 73), inflammatory (n = 68) and immune response (n = 112). The potentially novel genes not previously reported in association with osteoclast differentiation/activity are shown in **Figure 4D**, while the top differentially regulated genes based on FC and significance, irrespective of novelty are presented in **Supplementary Figure S1**.

Identifying *Nol4* as a Vital Gene in Mature Osteoclasts

The upregulation of selected potentially novel protein coding genes in mature osteoclasts prompted us to explore their prospective roles in osteoclast functionality. Since these genes have not been previously linked with osteoclast generation or activity, we investigated their associated phenotypes in the International Mouse Phenotyping Consortium (IMPC) database (Dickinson et al., 2016; International Mouse Phenotyping Consortium, 2021). Interestingly, we found that Selectin L (*Sell*), Myosin Light Chain 10 (*Myl10*), Resistin-like gamma (*Retnlg*) and Ceruloplasmin (*Cp*) *Signal Regulatory Protein Delta* (*Sirpd*/Gm9733), Zinc Finger Protein 831 (*Zfp831*) and Nuclear Protein 4 (*Nol4*) were previously investigated in relation with bone-related phenotypes. However, only *Nol4* showed statistically significant associations with bone mineral density (BMD) (**Figure 5A**), while *Zfp831* showed significant associations with tibia length (**Figure 5B**) in data from IMPC. Performing a body composition (DEXA lean/fat) phenotypic assay on 4,448 mice (male and female) showed that homozygous *Nol4* knockout mic ($Nol4^{em1(IMPC)J}$, n = 15) exhibited a significant increase in BMD compared to wild type mice (**Figure 5A**). While, performing phenotypic assays on *Zfp831* knockout mice ($Zfp831^{tm1b(KOMP)Wtsi}$) homozygote mutant mice (n = 10) compared to controls (n = 295) showed a significant reduction in bone (tibia) length (**Figure 5B**). The downregulation of *Zfp831* in mature osteoclasts in our dataset

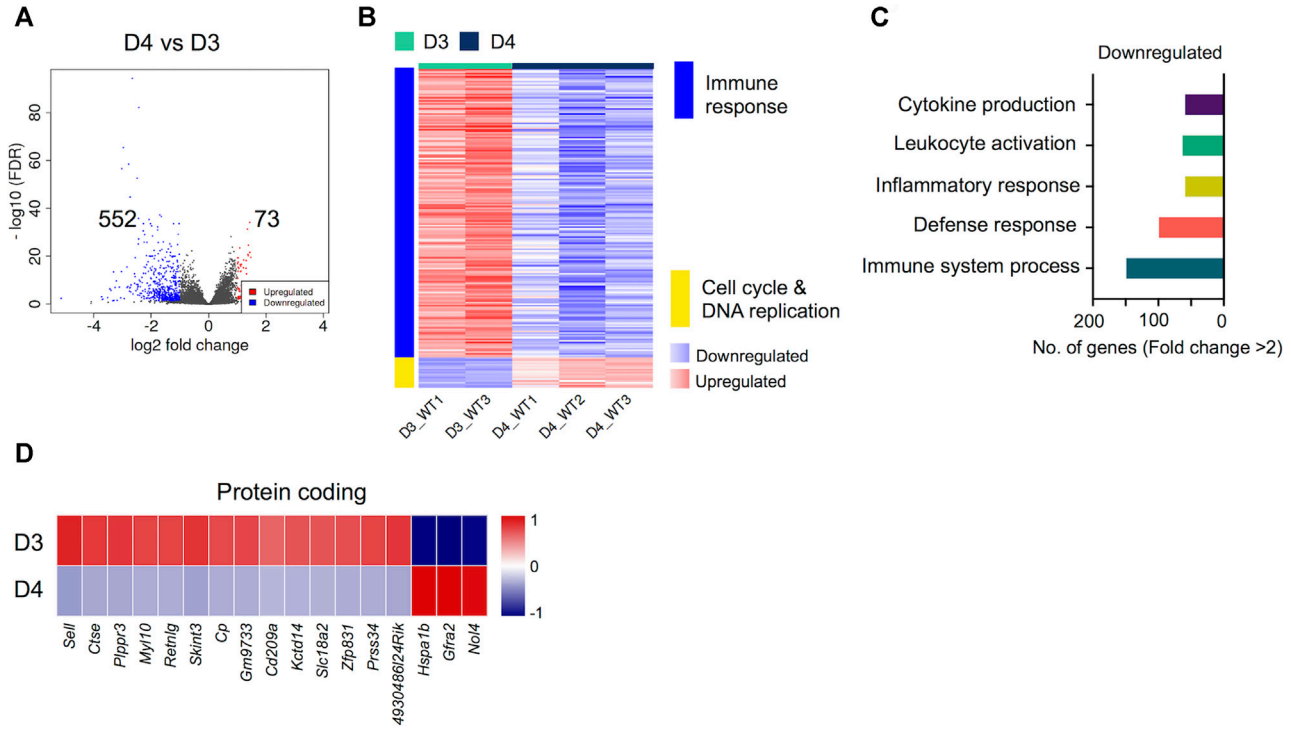

FIGURE 4 | Differentially regulated genes in late osteoclast differentiation. The transcriptomes of fully differentiated osteoclasts (D4) were compared with osteoclast precursors (D3). **(A)** Volcano plot represents significantly upregulated (red), downregulated (blue) or genes with unchanged expression levels (gray) between D4 and D3 comparison. **(B)** Heatmap shows gene enrichment and associated pathways in D4 versus D3. **(C)** Bar plot shows the numbers of genes corresponding to significantly up/downregulated functional pathways from gene ontology enrichment analyses. **(D)** Heat maps show the gene expression (Z-scores) of downregulated and upregulated protein coding genes in D4 versus D3 comparison.

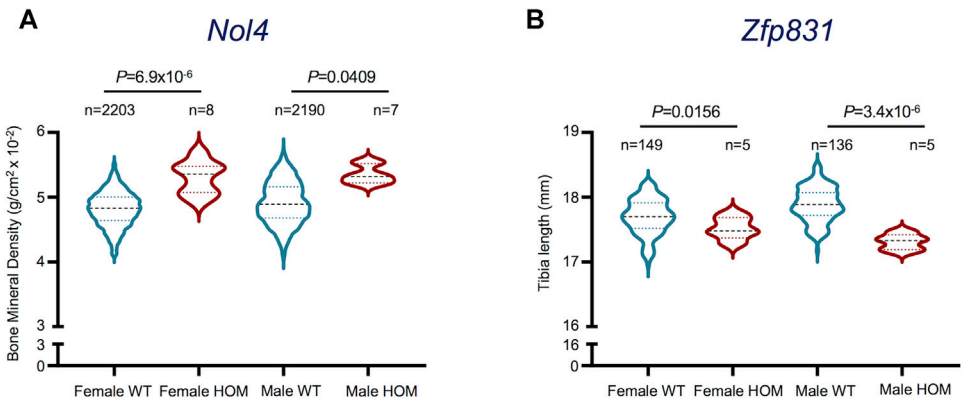

FIGURE 5 | Bone-related phenotypes of Nol4 and Zfp831 knockout mice in the International Mouse Phenotyping (IMPC) datasets. **(A)** Violin plot shows the differences in Bone Mineral Density (excluding skull) in female (n = 8), male (n = 7) homozygote (HOM) mutants for the *Nol4*$^{em1(IMPC)J}$ allele compared to female (n = 2,203), male (n = 2,190) wild type (WT) controls. **(B)** Violin plot shows the differences in Tibia length in female (n = 5), male (n = 5) HOM mutants for *Zfp831*$^{tm1b(KOMP)Wtsi}$ allele compared to female (n = 149) and male controls (n = 136). The interquartile range, minimum and maximum data points, and individual points representing outliers of each dataset are presented. *p* values represent the statistical significance between each comparison [Data taken from the International Mouse Phenotyping Consortium (IMPC) (Dickinson et al., 2016; International Mouse Phenotyping Consortium, 2021)].

therefore indicated its potential role in bone development/growth.

DISCUSSION

The molecular mechanisms behind osteoclast differentiation have been extensively explored. For instance, Capellen *et al.*, used microarray analyses to decipher changes in gene expression during osteoclast differentiation and showed synergy between MCSF and RANKL-induced gene expression (Cappellen et al., 2002). More recently, several potential genetic regulators of osteoclast differentiation have been identified. Nishikawa *et al.*, reported the epigenetic control of osteoclast differentiation via DNA (cytosine-5)-methyltransferase 3A (Dnmt3a) (Nishikawa et al., 2015) and Laha *et al.*, reported regulation of osteoclastogenesis by KLF2 (kruppel-like factor 2 [lung]) via reduction in autophagic cells (Laha et al., 2019). In addition, low-density lipoprotein receptor-related protein1 (LRP1), and COMMD1 were reported as critical regulators of osteoclastogenesis, osteoclast activity and bone mass (Murata et al., 2017; Bartelt et al., 2018), while leucine-rich repeat-containing G-protein-coupled receptor 4 (LGR4) has been identified as another putative receptor for RANKL (Luo et al., 2016).

While these studies revealed important osteoclast-related targets, a comprehensive list of genes provided in our study is of paramount significance in understanding the dynamic changes in gene expression during osteoclast differentiation. Irrefutably, the preexistent available literature related to osteoclast identification and functionality enabled us to confirm the generation of osteoclasts *in vitro*. However, our data revealed the dynamic changes in osteoclast transcriptome during osteoclastogenesis, showing diminishing of genes related to immune processes with concurrent upregulation of genes associated with anatomical morphogenesis and development. Moreover, these genes encoded for important mediators of cell differentiation, structural morphogenesis and bone and tissue remodeling.

The potentially novel genes related to osteoclast differentiation disclosed herein include PH Domain Containing Endocytic Trafficking Adaptor 1 (*Pheta1*), Hydroxyacylglutathione hydrolase (*Hagh*), Solute Carrier Family 18 Member A1 (*Slc18a1*), Glutamine-Fructose-6-Phosphate transaminase 1 (*Gfpt1*), Coenzyme Q8A (*Coq8a*), Solute Carrier Family 14 Member 2 (*Slc14a2*), Whirlin (*Whrn*) and C-Type Lectin Domain Family four Member A (*Clec4a4*), among others. The proteins encoded by these genes are primarily associated with biochemical or signaling pathways at the cellular level and defects in expression may lead to certain disorders. For instance, anomalies in PHETA1/2 have been associated with abnormal bone formation resulting in craniofacial defects (Ates et al., 2020), *HAGH* has been associated with skin, bone and joint infections in Yaws disease (Cheng et al., 2018) and mutations in *GFPT1* have been associated with muscle weakness in congenital myasthenic syndrome (Helman et al., 2019). In addition, histone-related genes H2B Clustered Histone 21 (*H2bc21*) and *H2bc4* were also significantly upregulated during osteoclast differentiation. Epigenetic regulation of bone development and remodeling has been extensively reported (Yi et al., 2019). The upregulation of histone-related genes in osteoclast differentiation indicates chromatin remodeling as a critical step in osteoclast generation.

One of the pivotal novel findings of this study is the upregulation and confirmatory evidence of the potential role of *Nol4* in mature osteoclasts, which has not been reported previously. Investigating bone-related phenotypes of some of the potentially novel genes we recorded showed that selective genes including *Pheta1*, *Hagh*, Plasminogen Activator urokinase (*Plau*), *Sell*, *Retnlg* and *Cp* are related to bone phenotypes in the IMPC database (Dickinson et al., 2016; International Mouse Phenotyping Consortium, 2021). However, only *Nol4* and *Zfp831* showed statistically significant associations with BMD or tibia length, respectively. Importantly, the knockout of *Nol4* led to increase in BMD compared to wild type mice, thereby providing evidence for its role in bone biology. Our differential gene analyses showed upregulation of *Nol4* expression in differentiated osteoclasts, which supports their contribution in affecting BMD in bone resorption and presents *Nol4* as a key gene related to osteoclast functionality. Of note, downregulation of *Zfp831* in mature osteoclasts in our data and association of *Zfp831* knockout with reduced bone (tibia) length in IMPC datasets suggest its potential roles in osteoclast-mediated effects on bone growth and remodeling. However, further investigations are necessitated to fully explore the effects of these genes on bone biology. The protein encoded by *Nol4* is associated with RNA binding and has been identified as a cancer/testis antigen in humans, recently presented as a candidate target in small cell lung cancer (Kim et al., 2021). However, the role of Nol4 in bone-related pathologies remains to be fully explored. Similarly, the protein encoded by *Zfb831* is associated with nucleic acid binding and was downregulated in tumor-infiltrating cytotoxic T lymphocytes (CTLs) compared to CTLs from spleen in a murine transplantable tumor model (Waugh et al., 2016), but its effects in bone-related diseases are not explored.

Accumulating evidences have highlighted the roles of LncRNAs in controlling gene expression to affect cell differentiation and development (Fatica and Bozzoni, 2014). Importantly, in relation with osteoclasts. Liu *et al.*, reported dysregulation in 1,117 LncRNAs in human osteoclasts differentiated from $CD14^{+}$ monocytes *in vitro* (Liu et al., 2020). Fei *et al.*, also reported 204 differentially expressed LncRNAs in male osteoporosis (Fei et al., 2020), while Yang *et al.*, identified 46 differentially expressed LncRNAs between osteoarthritis and osteolysis following total hip arthroplasty, and reported potential roles of specific LncRNA-mRNA pairs in regulating CD8A, CD8B and osteoclastogenesis in these patients (Yang et al., 2021). Moreover, Bu *et al.*, reported the role of LncRNA TSIX in promoting osteoblast apoptosis in particle induced osteolysis (PIO), evident from decreased BMD following implantation, via modulation of the microRNA miR-30a-5p (Bu et al., 2018). These reports rationalize the significance of LncRNAs in osteoclast generation and activity. We performed comprehensive total

RNA-based analyses to disclose the differentially regulated LncRNAs during osteoclast differentiation and exclusively reported LncRNA not previously reported or associated with osteoclasts. Importantly, we have highlighted the top 20 novel LncRNAs upregulated during murine osteoclast generation.

Osteoporosis is characterized by attenuated bone strength due to deterioration in bone microarchitecture and reduction in bone mass (Sozen et al., 2017). While various risk factors have been identified for predisposition to osteoporosis, endocrine diseases have also been liked with osteoporosis (Sozen et al., 2017). For instance, in diabetes-associated osteoporosis altered bone metabolism also leads to changes in BMD and has been linked with high osteoclast activity (Kemink et al., 2000; Reni et al., 2016). Importantly, insulin is identified as an essential mediator in osteoclast energy metabolism. Kim *et al.*, investigated the effects on gene expression in insulin-induced osteoclast differentiation and reported that insulin conducts similar roles as RANKL in osteoclast activity (Kim and Lee, 2014). These reports reflect the significance of energy and metabolism in osteoclast activity, which leads to osteoporosis. We found that numerous genes encoding important metabolism/energy-related mediators were significantly increased during early osteoclast generation.

Osteoclast progenitors are essentially immune cells, due to their origins from monocytes/macrophage precursors and may present as innate immune cells within the bone (Wu et al., 2008). Jacquin *et al.,* showed that osteoclast progenitor populations in murine BM comprise $CD45R^{-}$ $CD11b^{-/low}$ populations (Jacquin et al., 2006), while Jacome-Galarza *et al.*, reported that $B220^{-}CD3^{-}CD11b^{-/low}CD115^{+}CD117^{high}$ mouse BM cells possess high osteoclastic potential (Jacome-Galarza et al., 2013). Our data showed that osteoclast differentiation deviates their associations with other immunomodulatory cells, evident from downregulation of genes related to immune/inflammatory response and response to stress/stimulus in differentiated osteoclasts. Moreover, we found that the differences between the transcriptomes of fully-committed/differentiated and early-differentiated osteoclasts were predominantly limited to sustained downregulation of genes related to immune cell characteristics. These differentially expressed genes primarily encoded for cytokine production, leukocyte activation and immune response-related functions. Importantly, upregulation of genes related to cell cycle and DNA replication in fully differentiated osteoclasts exhibited the cellular expansion of committed osteoclasts. Of note, induction of bone resorption in inflammatory disorders and immune-related disorders results from the plethora of secreted cytokines, which induce osteoclastogenesis (Adamopoulos, 2018).

Overall, this study disclosed genes and their associated pathways during osteoclast differentiation which can be explored further in successive studies. Importantly, we highlighted the potentially novel genes and LncRNAs in relation to osteoclast differentiation and activity. However, functional studies are necessitated to disclose the roles of specific targets. The comprehensive list of differentially regulated genes provided herein can serve as an expedient tool in osteoclast-related research.

DATA AVAILABILITY STATEMENT

The datasets presented in this study can be found in online repositories. The names of the repository/repositories and accession number(s) can be found below: NCBI SRA, Accession no: PRJNA769960 (https://www.ncbi.nlm.nih.gov/bioproject/PRJNA769960/).

ETHICS STATEMENT

The animal study was reviewed and approved by Animal Welfare and the Ethical Review Body, University of Edinburgh.

AUTHOR CONTRIBUTIONS

ST: Data curation, Formal analysis, Visualization, Writing–original draft. SW: Data curation, Investigation, Methodology, Writing–review and editing. OA: Conceptualization, Funding acquisition, Project administration, Resources, Supervision, Writing–review and editing.

FUNDING

This work was supported by a grant from the Medical Research Council United Kingdom (Grant No. G0800933/87,390) and by the European Research Council (ERC) consolidator grant awarded to Prof. Omar ME Albagha (Grant No. 311723-GENEPAD).

SUPPLEMENTARY MATERIAL

The Supplementary Material for this article can be found online at: https://www.frontiersin.org/articles/10.3389/fgene.2021.781272/full#supplementary-material

REFERENCES

Adamopoulos, I. E. (2018). Inflammation in Bone Physiology and Pathology. *Curr. Opin. Rheumatol.* 30 (1), 59–64. doi:10.1097/bor.0000000000000449

Alonso, N., Wani, S., Rose, L., Van't Hof, R. J., Ralston, S. H., and Albagha, O. M. E. (2021). Insertion Mutation in Tnfrsf11a Causes a Paget's Disease-like Phenotype in Heterozygous Mice and Osteopetrosis in Homozygous Mice. *J. Bone Miner Res.* 36, 1376. doi:10.1002/jbmr.4288

Asagiri, M., and Takayanagi, H. (2007). The Molecular Understanding of Osteoclast Differentiation. *Bone* 40 (2), 251–264. doi:10.1016/j.bone.2006.09.023

Ashburner, M., Ball, C. A., Blake, J. A., Botstein, D., Butler, H., Cherry, J. M., et al. (2000). Gene Ontology: Tool for the Unification of Biology. *Nat. Genet.* 25 (1), 25–29. doi:10.1038/75556

Ates, K. M., Wang, T., Moreland, T., Veeranan-Karmegam, R., Ma, M., Jeter, C., et al. (2020). Deficiency in the Endocytic Adaptor Proteins PHETA1/2 Impairs Renal and Craniofacial Development. *Dis. Model. Mech.* 13 (5), dmm041913. doi:10.1242/dmm.041913

Bartelt, A., Behler-Janbeck, F., Beil, F. T., Koehne, T., Müller, B., Schmidt, T., et al. (2018). Lrp1 in Osteoblasts Controls Osteoclast Activity and Protects against Osteoporosis by Limiting PDGF-RANKL Signaling. *Bone Res.* 6, 4. doi:10.1038/s41413-017-0006-3

Boyle, W. J., Simonet, W. S., and Lacey, D. L. (2003). Osteoclast Differentiation and Activation. *Nature* 423 (6937), 337–342. doi:10.1038/nature01658

Bu, Y., Zheng, D., Wang, L., and Liu, J. (2018). LncRNA TSIX Promotes Osteoblast Apoptosis in Particle-Induced Osteolysis by Down-Regulating miR-30a-5p. *Connect. Tissue Res.* 59 (6), 534–541. doi:10.1080/03008207.2017.1413362

Cappellen, D., Luong-Nguyen, N.-H., Bongiovanni, S., Grenet, O., Wanke, C., and Šuša, M. (2002). Transcriptional Program of Mouse Osteoclast Differentiation Governed by the Macrophage Colony-stimulating Factor and the Ligand for the Receptor Activator of NFκB. *J. Biol. Chem.* 277 (24), 21971–21982. doi:10.1074/jbc.m200434200

Cheng, Z., VanPelt, J., Bergstrom, A., Bethel, C., Katko, A., Miller, C., et al. (2018). A Noncanonical Metal Center Drives the Activity of the Sediminispirochaeta Smaragdinae Metallo-β-Lactamase SPS-1. *Biochemistry* 57 (35), 5218–5229. doi:10.1021/acs.biochem.8b00728

Coudert, A. E., Del Fattore, A., Baulard, C., Olaso, R., Schiltz, C., Collet, C., et al. (2014). Differentially Expressed Genes in Autosomal Dominant Osteopetrosis Type II Osteoclasts Reveal Known and Novel Pathways for Osteoclast Biology. *Lab. Invest.* 94 (3), 275–285. doi:10.1038/labinvest.2013.140

Day, C. J., Kim, M. S., Stephens, S. b. R. J., Simcock, W. E., Aitken, C. J., Nicholson, G. C., et al. (2004). Gene Array Identification of Osteoclast Genes: Differential Inhibition of Osteoclastogenesis by Cyclosporin A and Granulocyte Macrophage colony Stimulating Factor. *J. Cel. Biochem.* 91 (2), 303–315. doi:10.1002/jcb.10780

Dickinson, M. E., Flenniken, A. M., Flenniken, A. M., Ji, X., Teboul, L., Wong, M. D., et al. (2016). High-throughput Discovery of Novel Developmental Phenotypes. *Nature* 537 (7621), 508–514. doi:10.1038/nature19356

Fatica, A., and Bozzoni, I. (2014). Long Non-coding RNAs: New Players in Cell Differentiation and Development. *Nat. Rev. Genet.* 15 (1), 7–21. doi:10.1038/nrg3606

Fei, Q., Li, X., Lin, J., Yu, L., and Yang, Y. (2020). Identification of Aberrantly Expressed Long Non-coding RNAs and Nearby Targeted Genes in Male Osteoporosis. *Cia* 15, 1779–1792. doi:10.2147/cia.s271689

Garlet, T. P., Coelho, U., Repeke, C. E., Silva, J. S., Cunha, F. d. Q., and Garlet, G. P. (2008). Differential Expression of Osteoblast and Osteoclast Chemmoatractants in Compression and Tension Sides during Orthodontic Movement. *Cytokine* 42 (3), 330–335. doi:10.1016/j.cyto.2008.03.003

Helman, G., Sharma, S., Crawford, J., Patra, B., Jain, P., Bent, S. J., et al. (2019). Leukoencephalopathy Due to Variants in GFPT1-Associated Congenital Myasthenic Syndrome. *Neurology* 92 (6), e587–e593. doi:10.1212/wnl.0000000000006886

International Mouse Phenotyping Consortium (2021). IMPC Data 2021. Available at: www.mousephenotype.org (Accessed August 18, 2021).

Jacome-Galarza, C. E., Lee, S.-K., Lorenzo, J. A., and Aguila, H. L. (2013). Identification, Characterization, and Isolation of a Common Progenitor for Osteoclasts, Macrophages, and Dendritic Cells from Murine Bone Marrow and Periphery. *J. Bone Miner Res.* 28 (5), 1203–1213. doi:10.1002/jbmr.1822

Jacquin, C., Gran, D. E., Lee, S. K., Lorenzo, J. A., and Aguila, H. L. (2006). Identification of Multiple Osteoclast Precursor Populations in Murine Bone Marrow. *J. Bone Miner Res.* 21 (1), 67–77. doi:10.1359/JBMR.051007

Kemink, S. A. G., Hermus, A. R. M. M., Swinkels, L. M. J. W., Lutterman, J. A., and Smals, A. G. H. (2000). Osteopenia in Insulin-dependent Diabetes Mellitus; Prevalence and Aspects of Pathophysiology. *J. Endocrinol. Invest.* 23 (5), 295–303. doi:10.1007/bf03343726

Kim, H. S., and Lee, N. K. (2014). Gene Expression Profiling in Osteoclast Precursors by Insulin Using Microarray Analysis. *Mol. Cell* 37 (11), 827–832. doi:10.14348/molcells.2014.0223

Kim, Y.-R., Kim, K.-U., Lee, J.-H., Kim, D.-W., Chung, J.-H., Kim, Y.-D., et al. (2021). Cancer Testis Antigen, NOL4, Is an Immunogenic Antigen Specifically Expressed in Small-Cell Lung Cancer. *Curr. Oncol.* 28 (3), 1927–1937. doi:10.3390/curroncol28030179

Kirstein, B., Chambers, T. J., and Fuller, K. (2006). Secretion of Tartrate-Resistant Acid Phosphatase by Osteoclasts Correlates with Resorptive Behavior. *J. Cel. Biochem.* 98 (5), 1085–1094. doi:10.1002/jcb.20835

Laha, D., Deb, M., and Das, H. (2019). KLF2 (Kruppel-like Factor 2 [lung]) Regulates Osteoclastogenesis by Modulating Autophagy. *Autophagy* 15 (12), 2063–2075. doi:10.1080/15548627.2019.1596491

Liu, W., Li, Z., Cai, Z., Xie, Z., Li, J., Li, M., et al. (2020). LncRNA-mRNA Expression Profiles and Functional Networks in Osteoclast Differentiation. *J. Cel Mol. Med.* 24 (17), 9786–9797. doi:10.1111/jcmm.15560

Love, M. I., Huber, W., and Anders, S. (2014). Moderated Estimation of Fold Change and Dispersion for RNA-Seq Data with DESeq2. *Genome Biol.* 15 (12), 550. doi:10.1186/s13059-014-0550-8

Luo, J., Yang, Z., Ma, Y., Yue, Z., Lin, H., Qu, G., et al. (2016). LGR4 Is a Receptor for RANKL and Negatively Regulates Osteoclast Differentiation and Bone Resorption. *Nat. Med.* 22 (5), 539–546. doi:10.1038/nm.4076

Madel, M. B., Ibáñez, L., Ciucci, T., Halper, J., Rouleau, M., Boutin, A., et al. (2020). Dissecting the Phenotypic and Functional Heterogeneity of Mouse Inflammatory Osteoclasts by the Expression of Cx3cr1. *Elife* 9, e54493. doi:10.7554/eLife.54493

Malone, B. M., Tan, F., Bridges, S. M., and Peng, Z. (2011). Comparison of Four ChIP-Seq Analytical Algorithms Using rice Endosperm H3K27 Trimethylation Profiling Data. *PLoS One* 6 (9), e25260. doi:10.1371/journal.pone.0025260

Murata, K., Fang, C., Terao, C., Giannopoulou, E. G., Lee, Y. J., Lee, M. J., et al. (2017). Hypoxia-Sensitive COMMD1 Integrates Signaling and Cellular Metabolism in Human Macrophages and Suppresses Osteoclastogenesis. *Immunity* 47 (1), 66–79. doi:10.1016/j.immuni.2017.06.018

Nishikawa, K., Iwamoto, Y., Kobayashi, Y., Katsuoka, F., Kawaguchi, S.-i., Tsujita, T., et al. (2015). DNA Methyltransferase 3a Regulates Osteoclast Differentiation by Coupling to an S-Adenosylmethionine-Producing Metabolic Pathway. *Nat. Med.* 21 (3), 281–287. doi:10.1038/nm.3774

Nomiyama, H., Egami, K., Wada, N., Tou, K., Horiuchi, M., Matsusaki, H., et al. (2005). Short Communication: Identification of Genes Differentially Expressed in Osteoclast-like Cells. *J. Interferon Cytokine Res.* 25 (4), 227–231. doi:10.1089/jir.2005.25.227

Novack, D. V., and Teitelbaum, S. L. (2008). The Osteoclast: Friend or Foe? *Annu. Rev. Pathol. Mech. Dis.* 3, 457–484. doi:10.1146/annurev.pathmechdis.3.121806.151431

Purdue, P. E., Crotti, T. N., Shen, Z., Swantek, J., Li, J., Hill, J., et al. (2014). Comprehensive Profiling Analysis of Actively Resorbing Osteoclasts Identifies Critical Signaling Pathways Regulated by Bone Substrate. *Sci. Rep.* 4, 7595. doi:10.1038/srep07595

Reni, C., Mangialardi, G., Meloni, M., and Madeddu, P. (2016). Diabetes Stimulates Osteoclastogenesis by Acidosis-Induced Activation of Transient Receptor Potential Cation Channels. *Sci. Rep.* 6, 30639. doi:10.1038/srep30639

Roodman, G. D. (1999). Cell Biology of the Osteoclast. *Exp. Hematol.* 27 (8), 1229–1241. doi:10.1016/s0301-472x(99)00061-2

Shaker, J. L. (2009). Paget's Disease of Bone: A Review of Epidemiology, Pathophysiology and Management. *Ther. Adv. Musculoskelet.* 1 (2), 107–125. doi:10.1177/1759720x09351779

Sozen, T., Ozisik, L., and Calik Basaran, N. (2017). An Overview and Management of Osteoporosis. *Eur. J. Rheumatol.* 4 (1), 46–56. doi:10.5152/eurjrheum.2016.048

Teitelbaum, S. L. (2007). Osteoclasts: what Do They Do and How Do They Do it? *Am. J. Pathol.* 170 (2), 427–435. doi:10.2353/ajpath.2007.060834

Teitelbaum, S. L., and Ross, F. P. (2003). Genetic Regulation of Osteoclast Development and Function. *Nat. Rev. Genet.* 4 (8), 638–649. doi:10.1038/nrg1122

Waugh, K. A., Leach, S. M., Moore, B. L., Bruno, T. C., Buhrman, J. D., and Slansky, J. E. (2016). Molecular Profile of Tumor-specific CD8+ T Cell Hypofunction in a Transplantable Murine Cancer Model. *J.I.* 197 (4), 1477–1488. doi:10.4049/jimmunol.1600589

Wu, Y., Humphrey, M. B., and Nakamura, M. C. (2008). Osteoclasts-the Innate Immune Cells of the Bone. *Autoimmunity* 41 (3), 183–194. doi:10.1080/08916930701693180

Yang, G., Tang, K., Qiao, L., Li, Y., and Sun, S. (2021). Identification of Critical Genes and lncRNAs in Osteolysis after Total Hip Arthroplasty and Osteoarthritis by RNA Sequencing. *Biomed. Res. Int.* 2021, 6681925. doi:10.1155/2021/6681925

Yasuda, H., Shima, N., Nakagawa, N., Yamaguchi, K., Kinosaki, M., Mochizuki, S.-i., et al. (1998). Osteoclast Differentiation Factor Is a Ligand for Osteoprotegerin/osteoclastogenesis-Inhibitory Factor and Is Identical to TRANCE/RANKL. *Proc. Natl. Acad. Sci.* 95 (7), 3597–3602. doi:10.1073/pnas.95.7.3597

Yi, S. J., Lee, H., Lee, J., Lee, K., Kim, J., Kim, Y., et al. (2019). Bone Remodeling: Histone Modifications as Fate Determinants of Bone Cell Differentiation. *Int. J. Mol. Sci.* 20 (13), 3147. doi:10.3390/ijms20133147

Conflict of Interest: The authors declare that the research was conducted in the absence of any commercial or financial relationships that could be construed as a potential conflict of interest.

Publisher's Note: All claims expressed in this article are solely those of the authors and do not necessarily represent those of their affiliated organizations, or those of the publisher, the editors and the reviewers. Any product that may be evaluated in this article, or claim that may be made by its manufacturer, is not guaranteed or endorsed by the publisher.

frontiers in Genetics

ORIGINAL RESEARCH
published: 11 January 2022
doi: 10.3389/fgene.2021.773534

Genetic Variants and Protein Alterations of Selenium- and T-2 Toxin-Responsive Genes Are Associated With Chondrocytic Damage in Endemic Osteoarthropathy

Yujie Ning[1], Minhan Hu[1], Jiayu Diao[2], Yi Gong[1], Ruitian Huang[1], Sijie Chen[1], Feiyu Zhang[1], Yanli Liu[1], Feihong Chen[1], Pan Zhang[1], Guanghui Zhao[3], Yanhai Chang[2], Ke Xu[3], Rong Zhou[1,4], Cheng Li[1,4], Feng Zhang[1], Mikko Lammi[1,5], Xi Wang[1] and Xiong Guo[1]**

[1]Key Laboratory of Trace Elements and Endemic Diseases, School of Public Health, Health Science Center, Xi'an Jiaotong University, National Health Commission of the People's Republic of China, Xi'an, China, [2]Shaanxi Provincial People's Hospital, Xi'an, China, [3]Xi'an Honghui Hospital, Xi'an, China, [4]Shaanxi Provincial Institute for Endemic Disease Control, Xi'an, China, [5]Department of Integrative Medical Biology, University of Umeå, Umeå, Sweden

OPEN ACCESS

Edited by:
Rong Qiang,
Northwest Women's and Children's Hospital, China

Reviewed by:
Yongjun He,
Xizang Minzu University, China
Yongmin Xiong,
Xian Jiaotong University, China
Wenyu Wang,
University of Helsinki, Finland

***Correspondence:**
Xi Wang
wn18andlife@xjtu.edu.cn
Xiong Guo
guox@xjtu.edu.cn

Specialty section:
This article was submitted to Genetics of Common and Rare Diseases, a section of the journal Frontiers in Genetics

Received: 10 September 2021
Accepted: 16 December 2021
Published: 11 January 2022

Citation:
Ning Y, Hu M, Diao J, Gong Y, Huang R, Chen S, Zhang F, Liu Y, Chen F, Zhang P, Zhao G, Chang Y, Xu K, Zhou R, Li C, Zhang F, Lammi M, Wang X and Guo X (2022) Genetic Variants and Protein Alterations of Selenium- and T-2 Toxin-Responsive Genes Are Associated With Chondrocytic Damage in Endemic Osteoarthropathy. Front. Genet. 12:773534. doi: 10.3389/fgene.2021.773534

The mechanism of environmental factors in Kashin–Beck disease (KBD) remains unknown. We aimed to identify single nucleotide polymorphisms (SNPs) and protein alterations of selenium- and T-2 toxin–responsive genes to provide new evidence of chondrocytic damage in KBD. This study sampled the cubital venous blood of 258 subjects including 129 sex-matched KBD patients and 129 healthy controls for SNP detection. We applied an additive model, a dominant model, and a recessive model to identify significant SNPs. We then used the Comparative Toxicogenomics Database (CTD) to select selenium- and T-2 toxin–responsive genes with the candidate SNP loci. Finally, immunohistochemistry was applied to verify the protein expression of candidate genes in knee cartilage obtained from 15 subjects including 5 KBD, 5 osteoarthritis (OA), and 5 healthy controls. Forty-nine SNPs were genotyped in the current study. The C allele of rs6494629 was less frequent in KBD than in the controls (OR = 0.63, p = 0.011). Based on the CTD database, PPARG, ADAM12, IL6, SMAD3, and TIMP2 were identified to interact with selenium, sodium selenite, and T-2 toxin. KBD was found to be significantly associated with rs12629751 of PPARG (additive model: OR = 0.46, p = 0.012; dominant model: OR = 0.45, p = 0.049; recessive model: OR = 0.18, p = 0.018), rs1871054 of ADAM12 (dominant model: OR = 2.19, p = 0.022), rs1800796 of IL6 (dominant model: OR = 0.30, p = 0.003), rs6494629 of SMAD3 (additive model: OR = 0.65, p = 0.019; dominant model: OR = 0.52, p = 0.012), and rs4789936 of TIMP2 (recessive model: OR = 5.90, p = 0.024). Immunohistochemistry verified significantly upregulated PPARG, ADAM12, SMAD3, and TIMP2 in KBD compared with OA and normal controls ($p < 0.05$). Genetic polymorphisms of PPARG, ADAM12, SMAD3, and TIMP2 may contribute to the risk of KBD. These genes could promote the pathogenesis of KBD by disturbing ECM homeostasis.

Keywords: single nucleotide polymorphism, Kashin–Beck disease, chondrocyte damage, selenium, T-2 toxin

INTRODUCTION

Kashin–Beck disease (KBD) is an endemic osteoarthropathy distributed throughout North Korea, Siberia, Japan, and China. In the 21st century, this condition has been most prevalent in China. Endemic areas encompass 13 provinces (or city/autonomous regions) and 379 counties from the northeast to the southwest. Monitoring data reported in the 2018 China Health Statistical Yearbook documents 535,878 patients, including 8,540 juvenile cases and more than 104 million residents at risk (http://www.nhfpc.gov.cn). Moreover, new cases have been diagnosed in Tibet recently (Ya-qun et al., 2014). The main pathogenic sites of KBD were irreversible coagulation necrosis and apoptosis in chondrocytes from articular cartilage, epiphyseal cartilage, and epiphyseal plate cartilage. Selenium deficiency and T-2 toxin (Guo et al., 2014; Sun et al., 2019; Wang et al., 2020) have been established and widely accepted as the main environmental risk factors for KBD that induce cartilage damage such as acceleration of chondrocyte apoptosis and an imbalance of the extracellular matrix (Wang et al., 2006; Li et al., 2012). However, the role of selenium deficiency and T-2 toxin in KBD development remains unclear, which limits the effective treatment options. Osteoarthritis (OA) is another cartilage-damaging osteoarthropathy that affects people worldwide (Ji et al., 2019). The aetiology and pathogenesis of OA are also poorly understood, but OA mainly occurs in elderly individuals, with chondrocyte apoptosis starting from the superficial zone of cartilage, whereas KBD mainly occurs in childhood, with chondrocyte apoptosis starting from the deep zone of cartilage (Guo et al., 2014; He et al., 2018; Wang et al., 2021).

Single nucleotide polymorphisms (SNPs) typically indicate disease susceptibility. Recently, a number of studies have suggested that SNPs play a crucial role in revealing the pathogenesis of osteochondral diseases such as OA (den Hollander et al., 2018) and KBD (Zhang et al., 2016). For example, ITPR2 has been identified as a susceptibility gene for KBD in both Han and Tibetan Chinese individuals (Ehret, 2010; Zhang et al., 2015). Shi et al. (2011) found that genetic variants in the HLA-DRB1 gene significantly increased susceptibility to KBD. Recently, TP63 was also identified as a novel susceptibility gene for KBD (Cheng et al., 2021). Advanced KBD is similar to osteoarthritis in clinical manifestations, such as arthritic pain, morning stiffness, and the deformity of limb joints. However, few studies have compared the differences in SNPs between OA and KBD, which could be helpful in genetically distinguishing the two diseases. In addition, accumulating evidence suggests that cartilage damage in patients with KBD is driven by the interaction between genetic and environmental factors (Guo et al., 2014). However, no previous study has provided any insight into SNPs in environmentally responsive genes before.

In this study, we selected 49 SNPs of 41 genes to perform SNP genotyping in 129 KBD and 129 normal controls. A Sequenom MassARRAY®SNP analysis was used to detect the associations between KBD and the 49 candidate SNPs. Immunohistochemistry was used to verify the distribution and protein expression of five candidate genes that interacted with selenium, sodium selenite, and T-2 toxin. Our results identify potential SNP biomarkers of selenium deficiency– and T-2 toxin–responsive genes to help reveal the pathogenesis of KBD.

METHODS AND MATERIALS

Ethics

All subjects provided informed consent (orally, if the subject was illiterate) for sample collection. The study protocol was approved by the ethics committee of Xi'an Jiaotong University (Approval No. 2018-206).

Subjects and Sample Collection

Diagnosis and degree classification of juvenile and adult KBD patients were strictly applied according to the national criteria of KBD in China [WS/T 207-2010]. Patients with OA were strictly diagnosed according to the Modified Outerbridge Classification. All subjects were diagnosed with KBD if they manifested X-ray alterations such as defects and sclerosis on the bone end of phalanges combined with compression changes of the calcaneus and talus and enlarged/deformed limb joints (hand, elbow, knee, ankle, etc.). KBD subjects were excluded if they were suffering or had previously suffered from any other osteoarticular diseases such as osteoarthritis, rheumatoid arthritis, gout, or skeletal fluorosis. Patients with any type of macrosomia, disorder of osteochondrodysplasia, chronic disease (such as hypertension, diabetes, or a coronary heart disease), or autoimmune disease were excluded if they had accepted any treatments that could affect the skeletal system within the last 6 months. All healthy controls lacked musculoskeletal pathologies or recent injuries and were selected from the same endemic areas as the KBD cases. All subjects were of Chinese Han lineage from Tongde and Guide Counties in Qinghai Province. The subjects were summoned to the local CDC and township health center for sample collection. Using the inclusion and exclusion criteria described above, we selected 129 patients with KBD and 129 healthy controls for this study. The articular cartilage samples from KBD and OA patients were collected from individuals who underwent arthroplasty of the knee. Healthy controls were obtained from patients who had suffered trauma or amputation due to an accident.

For SNP detection, approximately 5–7 ml of venous blood was collected from 258 subjects (129 KBD and 129 normal). The samples were rested for 5–10 min. First, the samples were centrifuged at 1,500×g for 5 min, and the supernatant was collected. The samples were then centrifuged at 12,000×g for 10 min, and the supernatant was collected. The resulting serum was then frozen in liquid nitrogen overnight and preserved at −80°C until testing. None of the samples was thawed more than twice before being analyzed.

Because the incidence of KBD has decreased dramatically and there are almost no new juvenile cases, it is extremely difficult to collect juvenile samples for verification. Moreover, the adult samples used here were typical KBD cases that were strictly screened. In addition, the OA patients were all adults. For

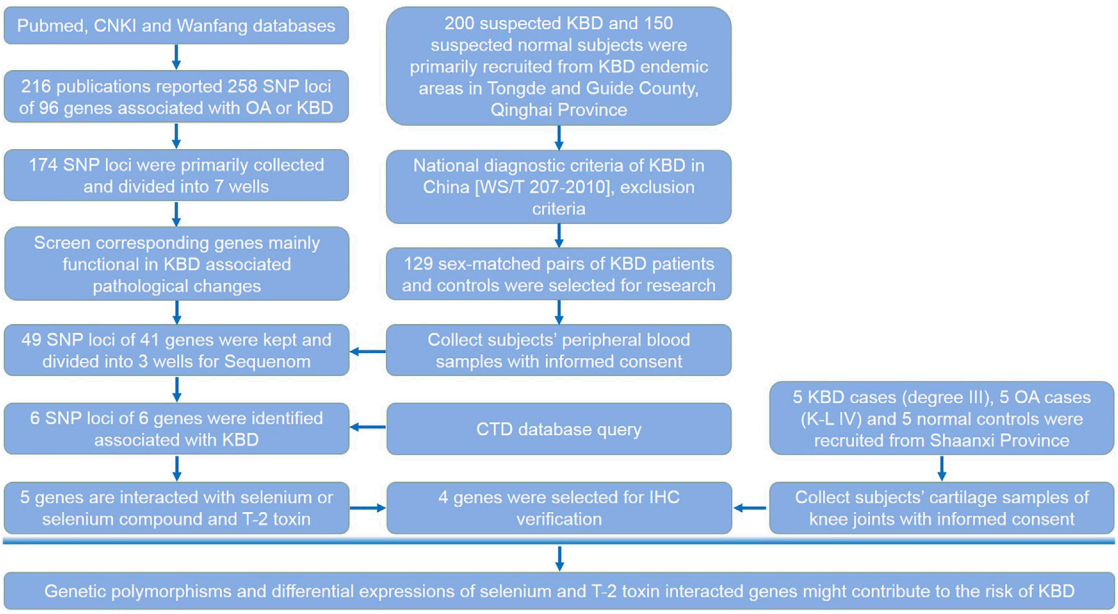

FIGURE 1 | Research design. This flow chart shows the selection process of candidate SNP loci and corresponding genes, subjects recruited and sample collection procedures, and the main methods and technologies used in this study.

these reasons, we chose only adult KBD patients for immunohistochemistry (IHC) verification. We included 15 adult subjects (5 KBD patients, 5 OA patients, and 5 normal controls) who had undergone arthroplasty of the knee or had died due to accidents or other diseases (not related to osteochondrosis) in Shaanxi Province to verify the protein expression of candidate genes in articular cartilage using immunohistochemistry. The knee joint samples were collected with the informed consent of patients and their families.

Selection of Candidate SNP Loci

We determined the SNP loci reported in the literatures (**Supplementary Table S1**). For unpublished results, we determined the fold change value of the corresponding genes tested in KBD chondrocytes or monocytes by microarray analysis. Up to the date of the experiment, 216 publications have reported SNP loci associated with OA or KBD; these were searched from the Pubmed, CNKI, and Wanfang databases. Candidate loci also met the following criteria: the Hardy–Weinberg law (PHWE >0.05), a minimal allele frequency (MAF) > 0.05, and an $R^2 > 0.8$ (default value). First, 258 SNP loci of 96 corresponding genes were collected from previous publications. Of these, 49 SNP loci of 41 corresponding genes that were differentially expressed in KBD or OA articular cartilage and/or peripheral blood mononuclear cells were selected for verification. These genes were mainly functional in KBD-associated pathological changes such as apoptosis, extracellular matrix metabolism, aggrecan, collagen, selenoprotein synthesis, and signal transduction. The selection process of candidate SNP loci and their corresponding genes is shown in detail in the research design (**Figure 1**).

Primer Design

PCR amplification primers and single-base extension primers for the tested SNP loci were designed using Sequenom's (United States) Genotyping Tools and MassARRAY Assay Design software and submitted to Biotech for synthesis.

DNA Extraction

DNA was extracted from blood samples using a Wizard Genomic DNA Purification Kit (Promega, United States). DNA quantification and quality testing were determined by spectrophotometry and agarose gel electrophoresis, respectively. Qualified DNA was adjusted to 50 ng/μl, transferred to a 384-well plate, and stored at −20°C.

SNP Detection

Sequenom MassARRAY SNP detection was applied to reflect the base difference caused by SNP polymorphisms using the difference in molecular weight. Using matrix-assisted laser desorption ionization time-of-flight mass spectrometry (MALDI-TOF-MS), the molecular weight of the elongated product was determined and processed using MassArray TYPER 4.0 software. The analysis was conducted in cooperation with CapitalBio Corporation (Beijing, China).

Interactions Between Selenium, T-2 Toxin, and Genes Corresponding to SNP Loci

The Comparative Toxicogenomics Database (CTD, http://ctdbase.org/) provides manually curated information about chemical–gene/protein interactions and chemical–disease and gene–disease relationships mainly based on publications. These data are integrated with functional and pathway data to assist in

developing hypotheses regarding the mechanisms of environmentally influenced diseases. This database was used to explore whether selenium, sodium selenite, and/or T-2 toxin interact with a corresponding gene to a candidate SNP locus.

Cartilage Tissue Collection and Immunohistochemistry Verification

We identified six genes with differential SNPs: TLR3, IL6, PPARG, ADAM12, SMAD3, and TIMP2. Of these, IL6 had already been verified in the cartilage tissue or cells of KBD (Zhou et al., 2014) and OA patients (Ansari et al., 2019). However, the PPARG, ADAM12, SMAD3, and TIMP2 genes have either not been compared/verified with respect to KBD/OA, and the research conclusions are inconsistent. In addition, compared with the CTD database, no interaction was found between the TLR3 gene and T-2 toxin/low selenium, whereas PPARG, ADAM12, SMAD3, and TIMP2 interacted with both selenium and T-2 toxin. Therefore, we chose to verify the protein levels of these four genes: PPARG, ADAM12, SMAD3, and TIMP2.

All articular cartilage samples, including all of the cartilage zones (including the calcified zone) and the subchondral bone, were harvested from the lateral tibial plateau 1 h after operation. Cartilage tissues were fixed with 4% (w/v) paraformaldehyde for 24 h immediately after acquisition and decalcified in 10% (w/v) ethylenediaminetetraacetic acid disodium salt (·EDTA-2Na) for 2–3 weeks. The samples were dehydrated in an alcohol series, cleared in xylene, and embedded in paraffin wax. Paraffin sections were cut into 5-μm sections, mounted on slides, and stored at room temperature until use for staining. The paraffin-embedded sections were baked at 65°C for 1 h, deparaffinized with xylene, and then rehydrated in decreasing concentrations of ethanol. Endogenous peroxidase activity was blocked with 0.3% (w/v) hydrogen peroxide for 10 min at room temperature, and then the sections were washed with 1×PBS. The sections were then incubated in a 10 mol/L urea solution diluted with water at 37°C for 20 min and washed with 1×PBS. The sections were then treated with 2 mg/ml hyaluronidase at pH 5.0 and 37°C for 30 min. Blocking with 5% (w/v) goat serum for 20 min at room temperature was followed by the addition of anti-PPARG (1: 100; Abcam, United Kingdom), anti-ADAM12 (1:100; Abcam, United Kingdom), anti-SMAD3 (1:100; Abcam, United Kingdom), and anti-TIMP2 (1:100; Abcam, United Kingdom) primary antibodies overnight at 4°C with IgG as a negative control. The slides were removed and held at room temperature for 30 min and then washed three times with PBS. Next, secondary antibodies were added at 37°C for 20 min. After washing, SABC reagent (Zhongshan Jinqiao, China) was added, and the slides were incubated at 37°C for 20 min. Finally, DAB (Abcam) staining, haematoxylin slight counterstaining, and neutral balsam fixation were performed. Instead of the primary antibody, PBS was used in each experiment as a negative control. Chondrocytes with brown granules in the nucleus and the cytoplasm were considered to be positive for the target protein.

Statistical Analysis

For the SNP polymorphisms of candidate genes in KBD, PLINK 1.90 was used to perform an association analysis based on an additive model, a dominant model, and a recessive model to identify significant SNPs associated with the disease. Specifically, for an SNP at a certain locus, whether a genotype increased the risk of disease was considered. For example, in the GT mutation, G is less prevalent and T is prevalent. When GG, GT, and TT differ in diseases, we designated this as an additive model (i.e., if there is a G or T, it will increase the possibility of onset). The analysis of (GG + GT) vs. TT represents the dominant model of G. The analysis of GG vs. (TT + GT) represents the recessive model of G. In most cases, the less prevalent nucleotide is the disease onset SNP, which invokes the referred dominant model or recessive model. The results of each model can be divided into two parts, adjusted covariates and unadjusted covariates, depending on the presence of uncorrected confounding factors, such as age and sex.

For immunohistochemistry, a German semiquantitative scoring system was used to evaluate the staining. The staining intensity and area extent were evaluated separately with a 0 for no staining, one for weak staining, two for moderate staining, and three for strong staining. In addition, the percentage of staining was given a score of 0 (<5%), 1 (5–25%), 2 (25–50%), 3 (51–75%), or 4 (>75%). These two scores were multiplied to obtain the final score for comparison.

SPSS18.0 was used for the comparative analyses. A Student's *t*-test was applied to determine the difference in continuous variables between two groups. A chi-square test was applied to determine the difference in categorical variables between two groups. A p value <0.05 indicates a statistically significant difference.

RESULTS

Characteristics of the Population

The population included for SNP analysis was sex-matched. The composition of males and females between the KBD and control groups was not significantly different ($p = 0.081$). There were more juveniles ($n = 90$) than adults ($n = 39$) in the KBD group, whereas the opposite situation existed in the control group (juveniles = 3 and adults = 126; $p < 0.001$, **Table 1**). **Table 2** shows the general information of the 15 subjects for the immunohistochemistry analysis. Five subjects were separately included in the KBD, OA, and normal control groups.

Association Analyses of Candidate SNP Loci

Forty-nine SNPs with qualifing Hardy–Weinberg test results (**Supplementary Table S2**) were genotyped in the current study. In our sample, allele C of rs6494629 was less frequent in cases than in controls (OR = 0.63, $p = 0.011$, **Table 3**). SNP rs12629751 of PPARG was significantly associated with KBD under the additive (OR = 0.46, $p = 0.012$), dominant (OR = 0.45, $p = 0.049$), and recessive (OR = 0.18, $p = 0.018$) models after

TABLE 1 | General information of subjects for SNP detection.

		KBD (*n* = 129)	Normal (*n* = 129)	χ^2	*p*
Sex	Male	71	57	3.039	0.081
	Female	58	72		
Age groups	Juvenile (≤18 years)	90	3	127.260	1.63E-29
	Adult (>18 years)	39	126		

Notes: p < *0.05 denotes significant difference. KBD, is short for Kashin-Beck disease.*

TABLE 2 | General information of subjects for IHC verification.

Number	KBD			OA			NC	
	Sex	Age	Degree	Sex	Age	K-L score	Sex	Age
1	Female	63	III	Female	69	IV	Male	37
2	Male	56	III	Male	76	IV	Male	70
3	Male	50	III	Female	81	IV	Female	62
4	Female	58	III	Male	55	IV	Male	40
5	Male	57	III	Male	63	IV	Male	56

Notes: All cartilage samples were harvested from the lateral tibial plateau of knee joints of subjects. KBD, is short for Kashin-Beck disease; OA, is short for osteoarthritis; NC, is short for normal control. Such abbreviations mean the same in the following tables and figures.

TABLE 3 | Comparison of genotypes and alleles between the KBD and control groups.

Chromosome/SNP	Genotype/allele	KBD (*n*, %)	Control (*n*, %)	χ^2	*p* value
3/rs12629751 T/C	TT	5 (3.91)	12 (9.52)	3.336	0.189
	TC	47 (36.72)	41 (32.54)		
	CC	76 (59.37)	73 (57.94)		
	T	57 (22.27)	65 (25.79)	0.866	0.352
	C	199 (77.73)	187 (74.21)		
4/rs3775296 A/C	AA	9 (6.98)	6 (4.76)	6.191	0.045
	AC	39 (30.23)	57 (45.24)		
	CC	81 (62.79)	63 (0.50)		
	A	57 (22.09)	69 (27.38)	1.916	0.166
	C	201 (77.91)	183 (72.62)		
7/rs1800796 G/C	GG	8 (6.20)	23 (18.11)	8.958	0.011
	GC	60 (46.51)	47 (37.01)		
	CC	61 (47.29)	57 (44.88)		
	G	76 (29.46)	93 (36.61)	2.965	0.085
	C	182 (70.54)	161 (63.39)		
10/rs1871054 T/C	TT	29 (22.48)	15 (11.81)	5.223	0.073
	TC	62 (48.06)	67 (52.76)		
	CC	38 (29.46)	45 (35.43)		
	T	120 (46.51)	97 (38.19)	3.63	0.057
	C	138 (53.49)	157 (61.81)		
15/rs6494629 C/T	CC	15 (11.72)	23 (17.97)	6.847	0.033
	CT	52 (40.63)	64 (0.50)		
	TT	61 (47.65)	41 (32.03)		
	C	82 (32.03)	110 (42.97)	6.533	0.011
	T	174 (67.97)	146 (57.03)		
17/rs4789936 T/C	TT	11 (8.59)	9 (7.03)	0.398	0.819
	TC	45 (35.16)	49 (38.28)		
	CC	72 (56.25)	70 (54.69)		
	T	67 (26.17)	67 (26.17)	0	1
	C	189 (73.83)	189 (73.83)		

Notes: p < *0.05 denotes significant difference. SNP, is short for single nucleotide polymorphism, and such abbreviation means the same in the following tables and figures.*

TABLE 4 | Candidate SNP loci with KBD identified by association analysis.

Chromosome/SNP	Model	OR (95%CI)	*p* value	Adjusted OR (95% CI)	Adjusted *p* value
3/rs12629751 T/C	Additive	0.78 (0.52, 1.17)	0.226	0.46 (0.25, 0.85)	0.012
	Dominant	0.93 (0.56, 1.53)	0.775	0.45 (0.20, 0.99)	0.049
	Recessive	0.38 (0.13, 1.12)	0.071	0.18 (0.05, 0.75)	0.018
4/rs3775296 A/C	Additive	0.77 (0.51, 1.17)	0.226	0.76 (0.42, 1.40)	0.382
	Dominant	0.60 (0.36, 0.99)	0.045	0.67 (0.32, 1.38)	0.272
	Recessive	1.51 (0.52, 4.38)	0.443	1.16 (0.20, 6.63)	0.870
7/rs1800796 G/C	Additive	0.75 (0.52, 1.08)	0.120	0.78 (0.46, 1.33)	0.359
	Dominant	0.92 (0.56, 1.51)	0.750	1.04 (0.50, 2.16)	0.909
	Recessive	0.30 (0.13, 0.70)	0.003	0.31 (0.10, 0.97)	0.043
10/rs1871054 T/C	Additive	1.38 (0.96, 1.99)	0.085	1.54 (0.92, 2.59)	0.102
	Dominant	1.30 (0.77, 2.20)	0.328	1.32 (0.62, 2.81)	0.475
	Recessive	2.19 (1.11, 4.31)	0.022	2.89 (1.08, 7.75)	0.035
15/rs6494629 C/T	Additive	0.65 (0.45, 0.93)	0.019	0.84 (0.48, 1.46)	0.541
	Dominant	0.52 (0.31, 0.87)	0.012	0.71 (0.34, 1.50)	0.371
	Recessive	0.60 (0.30, 1.21)	0.152	1.05 (0.35, 3.15)	0.934
17/rs4789936 T/C	Additive	1.03 (0.70, 1.52)	0.879	1.31 (0.73, 2.36)	0.368
	Dominant	0.96 (0.58, 1.57)	0.856	1.00 (0.48, 2.06)	0.998
	Recessive	1.40 (0.54, 3.60)	0.485	5.90 (1.26, 27.59)	0.024

Notes: Data have been adjusted by age and sex; p < *0.05 denotes significant difference.*

adjustment for age and sex. SNP rs6494629 of SMAD3 was significantly associated with KBD under the additive (OR = 0.65, $p = 0.019$) and dominant (OR = 0.52, $p = 0.012$) models. SNP rs3775296 of TLR-3 (OR = 0.60, $p = 0.045$) was significantly associated with KBD under the dominant model. SNP rs1800796 of IL6 (OR = 0.30, $p = 0.003$) and SNP rs1871054 of ADAM12 (OR = 2.19, $p = 0.022$) were significantly associated with KBD under the dominant model before and after adjustment for age and sex. SNP rs4789936 of TIMP2 (OR = 5.90, $p = 0.024$) was significantly associated with KBD under the recessive model after adjustment for age and sex (**Table 4**).

Interactions Between Environmental Risk Factors and Responsive Genes With Candidate SNPs

Based on the CTD, five candidate genes (PPARG, ADAM12, IL6, SMAD3, and TIMP2) were found to interact with selenium, sodium selenite, and T-2 toxin. These chemicals could affect the expression of the above genes at both the gene and protein levels to participate in KBD-associated pathogenic processes such as apoptosis, changes to the extracellular matrix, and ROS reactions. Details of the interactions are summarized in **Table 5**.

Immunohistochemistry Verification of Candidate Genes

Immunohistochemistry was used to verify the distribution and protein expression of PPARG, ADAM12, SMAD3, and TIMP2 in adult articular cartilage obtained from KBD and OA patients and normal controls. The gene PPARG was barely expressed in normal controls but significantly upregulated in KBD, particularly in the superficial zone and the deep zone (**Figure 2A**, $p = 0.016$, $p = 0.034$). This protein was also significantly upregulated in OA compared with the controls ($p = 0.041$) and showed slight but insignificant upregulation in the middle and deep zones compared with KBD. TIMP2 was significantly upregulated in all zones of KBD compared with OA and the normal control and upregulated in the middle zone of OA compared with the normal control (**Figure 2B**, $p = 0.026$). The genes ADAM12 (**Figure 3A**, $p = 0.002$) and SMAD3 (**Figure 3B**, $p = 0.036$) were significantly upregulated in all zones of KBD compared with OA and the normal control.

DISCUSSION

Gene–environment interactions have been widely used in studying the aetiology and pathogenesis of complex diseases (Li et al., 2019) and have been demonstrated to be associated with KBD and OA (He et al., 2021). Gene polymorphisms may participate in the development of KBD (Wu et al., 2019) and OA (Styrkarsdottir et al., 2018). Our study recruited 49 candidate SNPs from publications on osteochondropathy. KBD was found to be significantly associated with SNPs rs12629751 T/C of PPARG on chromosome 3, rs3775296 A/C of TLR-3 on chromosome 4, rs1800796 G/C of IL6 on chromosome 7, rs1871054 T/C of ADAM12 on chromosome 10, rs6494629 C/T of SMAD3 on chromosome 15, and rs4789936 T/C of TIMP2 on chromosome 17. These responsive genes (PPARG, ADAM12, SMAD3, and TIMP2) were selected for verification based on the interactions with environmental risk factors for KBD such as low selenium and T-2 toxin. The candidate genes were verified mainly upregulated in articular cartilage in KBD compared with those in OA patients and controls. Therefore, SNP and protein alterations of these genes could participate in the pathogenic process of KBD.

The gene PPARG (peroxisome proliferator activated receptor gamma), also known as PPARγ, is involved in cell apoptosis and necessary in cartilage differentiation (Monemdjou et al., 2012). However, PPARG plays a double-edged role in cartilage. The

TABLE 5 | Candidate SNP loci corresponding genes and associated interactions with selenium and T-2 toxin.

SNP loci	Gene name	Associated chemicals	Interactions from the CTD database	References: Pubmed ID
rs12629751	PPARG	Selenium	PPARG protein promotes the reaction [Selenium inhibits the reaction [lipopolysaccharide, *Escherichia coli* O111 B4 results in increased expression of PTGS2 protein]]	17439952
			Selenium promotes the reaction [lipopolysaccharide, *Escherichia coli* O111 B4 results in increased activity of PPARG protein]	17439952
		Sodium selenite	Sodium selenite inhibits the reaction [2-cresol results in increased expression of PPARG mRNA]	21705299
			Sodium selenite results in increased expression of PPARG protein	24140496
		T-2 toxin	T-2 toxin results in increased expression of PPARG mRNA	26141394
rs1800796	IL6	Selenium	[Cadmium analog co-treated with selenium analog co-treated with zinc sulfide analog] results in increased expression of IL6 mRNA	21481475
			Selenium affects the reaction [mercuric chloride results in decreased expression of IL6 protein]	26089086
		Sodium selenite	[Sodium selenite co-treated with plant extracts] inhibits the reaction [sodium arsenite results in increased expression of IL6 protein]	26085057
			Sodium selenite inhibits the reaction [cadmium chloride results in increased expression of IL6 protein]	24954678
			Sodium selenite inhibits the reaction [IL6 protein results in increased activity of AR protein]	17346688
			Sodium selenite inhibits the reaction [IL6 protein results in increased expression of KLK3 protein]	17346688
			Sodium selenite inhibits the reaction [sodium arsenite results in increased expression of IL6 protein]	26085057
			Sodium selenite inhibits the reaction [TGFB1 protein results in increased expression of IL6 protein]	16757516
			Sodium selenite results in increased expression of IL6 mRNA	18175754
		T-2 toxin	AKNA protein affects the reaction [T-2 toxin results in increased expression of IL6 mRNA]	29079362
			Alpha-cyano-(3,4-dihydroxy)-N-benzylcinnamide inhibits the reaction [T-2 toxin results in increased expression of IL6 mRNA]	22454431
			Stattic inhibits the reaction [T-2 toxin results in increased expression of IL6 mRNA]	22454431
			T-2 toxin results in increased expression of IL6 mRNA	29079362
rs1871054	ADAM12	Sodium selenite	Sodium selenite results in decreased expression of ADAM12 mRNA	18175754
rs6494629	SMAD3	Sodium selenite	Sodium selenite results in increased expression of SMAD3 mRNA	18175754
rs4789936	TIMP2	Selenium	Selenium inhibits the reaction [T-2 toxin results in decreased expression of TIMP2 protein]	21144892
			Selenium results in decreased expression of TIMP2 mRNA	17390030
		T-2 toxin	Selenium inhibits the reaction [T-2 toxin results in decreased expression of TIMP2 protein]	21144892
			T-2 toxin affects the expression of TIMP2 mRNA	21112371
			T-2 toxin results in decreased expression of TIMP2 protein	21144892

Note: CTD, is short for Comparative Toxicogenomics Database.

PPARG polymorphism rs12629751 was identified to be significantly associated with susceptibility to knee OA in a southeast Chinese population (Ding et al., 2014). Overexpression of miR-27b inhibited the expression of PPARG, matrix metalloproteinase 13 (Mmp13), and type X collagen (Col10a1), while significantly promoting the expression of type II collagen (Col2a1) and sex-determining region-box 9 (Sox9) at both the mRNA and protein levels. However, agonist- and siRNA-mediated knockdown of PPARG suppressed Col2a1 expression while promoting the expression of Col10a1 and runt-related transcription factor 2 (Runx2) in a concentration-dependent manner (Xu et al., 2018). Aberrant alterations in these genes and proteins are the main molecular characteristics of KBD cartilage injury (Wang et al., 2008; Wang et al., 2017). One of our unpublished results demonstrated that exosomal hsa-miR-27b-3p was significantly downregulated in KBD chondrocytes (FC = 0.53, p = 0.0176). Therefore, the upregulation of PPARG might contribute to KBD cartilage damage. Moreover, the treatment of KBD by injecting hyaluronic acid into the knee joint is effective in alleviating arthritic pain and morning stiffness, hence promoting patient quality of life (Yu et al., 2014; Xia et al., 2016; Tang et al., 2019). Sodium hyaluronate could protect articular cartilage against degeneration by inhibiting PPARG mRNA expression (Zhou et al., 2009). This could represent a partial therapeutic mechanism of hyaluronic acid injection for KBD therapy.

The gene ADAM12 (ADAM metallopeptidase domain 12) encodes a member of the matrix metalloproteinases and is involved in skeletal growth and development (Kveiborg et al., 2008). It is capable of stimulating longitudinal bone growth by modulating chondrocyte proliferation and maturation (Kveiborg et al., 2006). However, a meta-analysis including 5,048 cases and 6,848 controls suggested that rs1871054 was significantly associated with the risk of knee OA (Hu et al., 2017). In addition, upregulation of ADAM12 may participate in abnormal chondrocyte differentiation and accelerate OA development (Yang et al., 2017). The gene ADAM12 was expressed in 87% of OA cartilages at both the mRNA and protein levels compared with normal controls (Okada et al., 2008). ADAM12 was upregulated prior to Col10a1 during

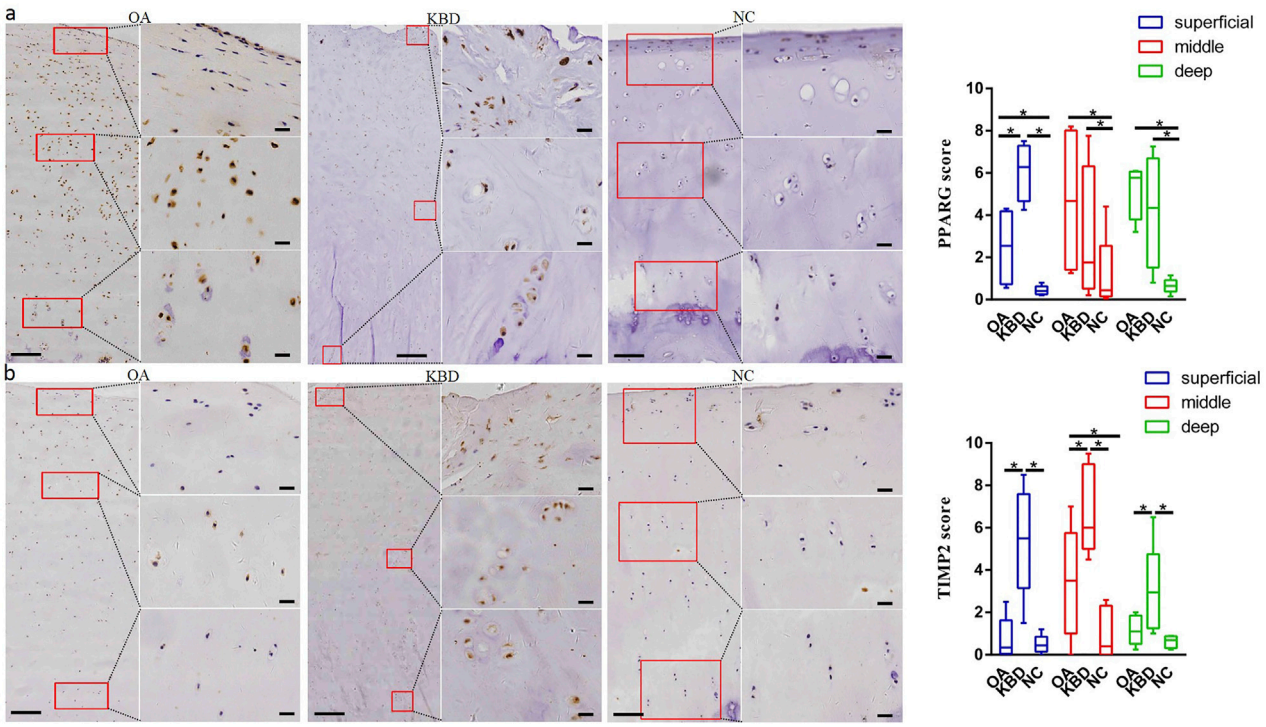

FIGURE 2 | Representative immunohistochemistry staining of PPARG **(A)** and TIMP2 **(B)** in OA, KBD, and normal control cartilage tissues. The scores of different areas (superficial, middle, and deep) in cartilage tissues displayed by box plot (n = 5). *p < 0.05.

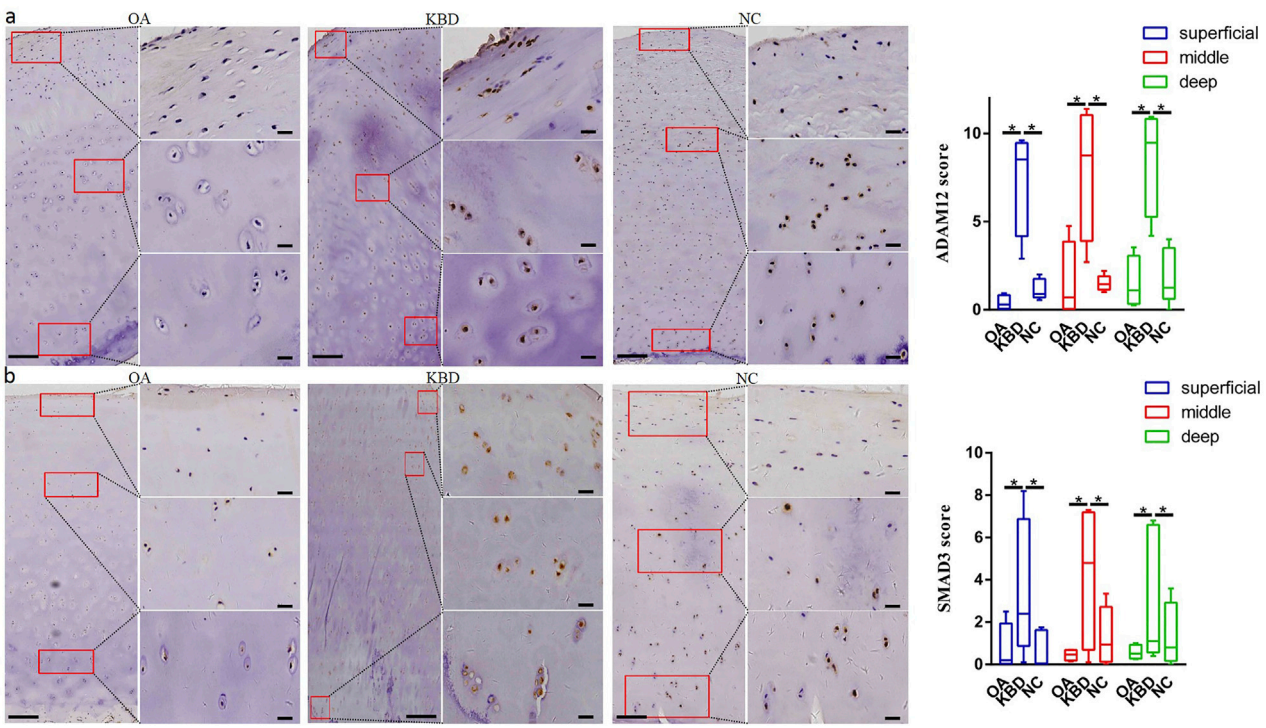

FIGURE 3 | Representative immunohistochemistry staining of ADAM12 **(A)** and SMAD3 **(B)** in OA, KBD, and normal control cartilage tissues. The scores of different areas (superficial, middle, and deep) in cartilage tissues displayed by box plot (n = 5). *p < 0.05.

chondrogenic differentiation in ATDC5 cells. In addition, TGF-β1–induced ADAM12 overexpression resulted in upregulation of Igf-1 and downregulation of Runx2 expression (Horita et al., 2019). The protein RUNX2 is a crucial transcription factor for type X collagen expression and chondrocyte hypertrophy and is known to regulate endochondral ossification through the control of chondrocyte proliferation and differentiation (Chen et al., 2014). Abnormal endochondral ossification during childhood is the main pathogenesis of KBD. Downregulation of COL2A1 and RUNX2 and upregulation of COL10A1 are consistently observed in KBD chondrocytes (Guo et al., 2006; Wang et al., 2008). Therefore, upregulated ADAM12 could be an accelerating factor for KBD development.

SMAD3 (SMAD Family Member 3) is a protein-encoding gene. The SMAD3 protein transmits signals from the cell surface to the nucleus and functions in the TGF-β signaling pathway, which is critical in the proliferation, differentiation, migration, and apoptosis as well as extracellular matrix (ECM) synthesis and degradation (Heldin et al., 1997; Wharton and Derynck, 2009). SMAD3 polymorphisms are associated with the risk of both hip and knee arthritis. Specifically, the SNP locus rs6494629 mapping to intron one of SMAD3 was associated with knee OA (Sharma et al., 2018). Thus, abnormal SMAD3 expression was expected in damaged cartilage. Previously, SMAD3 expression was reported to be, on average, 83% higher in OA cartilage than that in controls (Aref-Eshghi et al., 2016). Indeed, the SMAD3 protein was significantly overexpressed in KBD and OA cartilages in our study. The TGF-β1/SMAD3 signaling pathway has been reported to be essential for the inhibition of chondrocyte differentiation. Interestingly, T-2 toxin reduced the expression of type II collagen while promoting the expression of MMP13 through the activation of SMAD3 and the stimulation of TGF-β1 signaling, which ultimately led to chondrocyte damage. Chondrocytes undergo abnormal terminal differentiation, which is another pathogenic characteristic of KBD (Li et al., 2017).

The gene TIMP2 (tissue inhibitor of matrix metalloproteinase 2) maintains extracellular balance. The SNP rs4789936 on TIMP-2 was observed to decrease the risk of alcohol-induced osteonecrosis of the femoral head (ONFH) in the Chinese Han population under allele, dominant, overdominant, and log-additive models after adjusting for age and sex (Chen et al., 2016). Choi et al. found that hyperactivation of SMAD3 signaling during the osteogenic differentiation of Costello syndrome (CS) MSCs leads to aberrant expression of ECM remodeling proteins such as MMP13, TIMP1, and TIMP2. Specifically, enhanced TIMP1/2 expression induced by hyperactivated SMAD3 signaling impairs the osteogenic development of CS MSCs *via* inactivation of wnt/β-catenin signaling (Choi et al., 2021). Compared with normal nucleus pulposus (NP) tissues, intervertebral disc degeneration (IDD) samples exhibited higher levels of circular RNA derived from TIMP2 (circ-TIMP2) expression levels. In addition, overexpression of circ-TIMP2 promoted ECM catabolism and suppressed ECM anabolism. Furthermore, circ-TIMP2 sequesters miR-185-5p, which potentially upregulates the target genes associated with ECM degradation (Guo et al., 2020). Therefore, TIMP2 imbalance could disturb ECM homeostasis in KBD cartilage.

The results were obtained based on a literature review, Sequenom MassARRAY SNP detection, CTD database query, and IHC verification. However, due to the dramatically decreased incidence of KBD in recent years, the sample size for SNP analysis is relatively small, which indicates that we may have missed other SNP loci indicative of susceptibility to KBD as affected by low selenium and T-2 toxin.

CONCLUSION

The evidence suggests that SNPs and upregulated expression of low selenium– and T-2 toxin–responsive genes, including PPARG, ADAM12, SMAD3, and TIMP2, could participate in the pathogenesis of KBD by disturbing ECM homeostasis. The functions of these genes appear to be linked through the TGF-β and wnt/β-catenin pathways, which needs further investigation.

DATA AVAILABILITY STATEMENT

The datasets presented in this study can be found in online repositories. The names of the repository/repositories and accession number(s) can be found in the article/https://www.frontiersin.org/articles/10.3389/fgene.2021.773534/full#**Supplementary Material**.

ETHICS STATEMENT

The studies involving human participants were reviewed and approved by the ethics committee of Xi'an Jiaotong University (Approval No. 2018-206). The patients/participants provided their written informed consent to participate in this study.

AUTHOR CONTRIBUTIONS

Conception and design: YN, XW, and XG. Sample collection: JD, GZ, YC, and KX. Study conduct and data collection: YN, MH, JD, YG, RH, GZ, PZ, SJC, FYZ, FHC, YLL, CL, and RZ. Data interpretation and drafting manuscript: YN, MH, and XW. Revising manuscript content: XW, XG, FZ, and ML. Approving final version of manuscript: all authors. YN and XW take responsibility for the integrity of the data analysis.

FUNDING

This study was financially supported by the National Natural Science Foundation of China (81803178, 81803179, and 81620108026), the China Postdoctoral Foundation (2021M692543), the National Key

R&D Program of China (China-Korea, 2016YFE0119100), the Shaanxi Postdoctoral Foundation (2018BSHYDZZ47 and 2018BSHEDZZ96), and the Fundamental Research Funds for the Central Universities (xjj2018147 and xjj2018149).

ACKNOWLEDGMENTS

We appreciate the support and cooperation provided by the Center for Disease Control of Tongde and Guide Counties in Qinghai Province. We are grateful to Xi'an Honghui Hospital and Shaanxi Provincial People's Hospital for blood and articular cartilage sample collection.

SUPPLEMENTARY MATERIAL

The Supplementary Material for this article can be found online at: https://www.frontiersin.org/articles/10.3389/fgene.2021.773534/full#supplementary-material

REFERENCES

Ansari, M. Y., Khan, N. M., Ahmad, N., Green, J., Novak, K., and Haqqi, T. M. (2019). Genetic Inactivation of ZCCHC 6 Suppresses Interleukin-6 Expression and Reduces the Severity of Experimental Osteoarthritis in Mice. *Arthritis Rheumatol.* 71 (4), 583–593. doi:10.1002/art.40751

Aref-Eshghi, E., Liu, M., Razavi-Lopez, S. B., Hirasawa, K., Harper, P. E., Martin, G., et al. (2016). SMAD3 Is Upregulated in Human Osteoarthritic Cartilage Independent of the Promoter DNA Methylation. *J. Rheumatol.* 43 (2), 388–394. doi:10.3899/jrheum.150609

Chen, H., Ghori-Javed, F. Y., Rashid, H., Adhami, M. D., Serra, R., Gutierrez, S. E., et al. (2014). Runx2 Regulates Endochondral Ossification through Control of Chondrocyte Proliferation and Differentiation. *J. Bone Miner Res.* 29 (12), 2653–2665. doi:10.1002/jbmr.2287

Chen, J. Y., Guo, Y. C., Jin, T. B., Li, J., Du, J. L., Cao, Y. J., et al. (2016). Association of MMPs/TIMPs Polymorphism with Alcohol-Induced Osteonecrosis of Femoral Head in the Chinese Han Population. *Int. J. Clin. Exp. Pathol.* 9 (8), 8231–8238.

Cheng, B. L., Liang, C. J., Yang, X. N., Li, P., Liu, L., Cheng, S. Q., et al. (2021). Genetic Association Scan of 32 Osteoarthritis Susceptibility Genes Identified TP63 Associated with an Endemic Osteoarthritis, Kashin-Beck Disease. *Bone* 150, ARTN 115997. doi:10.1016/j.bone.2021.115997

Choi, J. B., Lee, J., Kang, M., Kim, B., Ju, Y., Do, H.-S., et al. (2021). Dysregulated ECM Remodeling Proteins lead to Aberrant Osteogenesis of Costello Syndrome iPSCs. *Stem Cel Rep.* 16, 1–14. doi:10.1016/j.stemcr.2021.06.007

Ehret, G. B. (2010). Genome-Wide Association Studies: Contribution of Genomics to Understanding Blood Pressure and Essential Hypertension. *Curr. Sci. Inc* 12 (1), 17–25. doi:10.1007/s11906-009-0086-6

Guo, W., Zhang, B., Sun, C., Duan, H. Q., Liu, W. X., Mu, K., et al. (2020). Circular RNA Derived from TIMP2 Functions as a Competitive Endogenous RNA and Regulates Intervertebral Disc Degeneration by Targeting miR-185-5p and M-atrix M-etalloproteinase 2. *Int. J. Mol. Med.* 46, 621–632. doi:10.3892/ijmm.2020.4621

Guo, X., Ma, W.-J., Zhang, F., Ren, F.-L., Qu, C.-J., and Lammi, M. J. (2014). Recent Advances in the Research of an Endemic Osteochondropathy in China: Kashin-Beck Disease. *Osteoarthritis and Cartilage* 22 (11), 1774–1783. doi:10.1016/j.joca.2014.07.023

Guo, X., Zuo, H., Cao, C.-X., Zhang, Y., Geng, D., Zhang, Z.-T., et al. (2006). Abnormal Expression of Col X, PTHrP, TGF-β, bFGF, and VEGF in Cartilage with Kashin-Beck Disease. *J. Bone Miner Metab.* 24 (4), 319–328. doi:10.1007/s00774-006-0690-3

He, Y., Zhang, Y., Zhang, D., Zhang, M., Wang, M., Jiang, Z., et al. (2018). 3-morpholinosydnonimine (SIN-1)-Induced Oxidative Stress Leads to Necrosis in Hypertrophic Chondrocytes *In Vitro*. *Biomed. Pharmacother.* 106, 1696–1704. doi:10.1016/j.biopha.2018.07.128

He1, Y., Fan, L., Aaron, N., Feng, Y., Fang, Q., Zhang, Y., et al. (2021). Reduction of Smad2 Caused by Oxidative Stress Leads to Necrotic Death of Hypertrophic Chondrocytes Associated with an Endemic Osteoarthritis. *Rheumatology (Oxford).* doi:10.1093/rheumatology/keab286

Heldin, C.-H., Miyazono, K., and ten Dijke, P. (1997). TGF-β Signalling from Cell Membrane to Nucleus through SMAD Proteins. *Nature* 390(6659), 465–471. doi:10.1038/37284

Hollander, W., Pulyakhina, I., Boer, C., Bomer, N., Breggen, R., Arindrarto, W., et al. (2019). Annotating Transcriptional Effects of Genetic Variants in Disease-Relevant Tissue: Transcriptome-Wide Allelic Imbalance in Osteoarthritic Cartilage. *Arthritis Rheumatol.* 71, 561–570. doi:10.1002/art.40748

Horita, M., Nishida, K., Hasei, J., Furumatsu, T., Sakurai, M., Onodera, Y., et al. (2019). Involvement of ADAM12 in Chondrocyte Differentiation by Regulation of TGF-B1-Induced IGF-1 and RUNX-2 Expressions. *Calcif Tissue Int.* 105 (1), 97–106. doi:10.1007/s00223-019-00549-6

Hu, X., Sun, G., and Wang, W. (2017). Association of ADAM 12 Polymorphisms with the Risk of Knee Osteoarthritis: Meta-Analysis of 5048 Cases and 6848 Controls. *Rheumatol. Int.* 37 (10), 1659–1666. doi:10.1007/s00296-017-3778-2

Ji, Q., Zheng, Y., Zhang, G., Hu, Y., Fan, X., Hou, Y., et al. (2019). Single-cell RNA-Seq Analysis Reveals the Progression of Human Osteoarthritis. *Ann. Rheum. Dis.* 78 (1), 100–110. doi:10.1136/annrheumdis-2017-212863

Jian-lin, Z., Shi-qing, L., Bo, Q., Qiong-jie, H., Jiang-hua, M., and Hao, P. (2009). The Protective Effect of Sodium Hyaluronate on the Cartilage of Rabbit Osteoarthritis by Inhibiting Peroxisome Proliferator-Activated Receptor-Gamma Messenger RNA Expression. *Yonsei Med. J.* 50 (6), 832–837. doi:10.3349/ymj.2009.50.6.832

Kveiborg, M., Albrechtsen, R., Couchman, J. R., and Wewer, U. M. (2008). Cellular Roles of ADAM12 in Health and Disease. *Int. J. Biochem. Cel Biol.* 40 (9), 1685–1702. doi:10.1016/j.biocel.2008.01.025

Kveiborg, M., Albrechtsen, R., Rudkjaer, L., Wen, G., Damgaard-Pedersen, K., and Wewer, U. M. (2006). ADAM12-S Stimulates Bone Growth in Transgenic Mice by Modulating Chondrocyte Proliferation and Maturation. *J. Bone Miner Res.* 21 (8), 1288–1296. doi:10.1359/Jbmr.060502

Li, J., Li, X., Zhang, S., and Snyder, M. (2019). Gene-Environment Interaction in the Era of Precision Medicine. *Cell* 177 (1), 38–44. doi:10.1016/j.cell.2019.03.004

Li, S., Cao, J., Caterson, B., and Hughes, C. E. (2012). Proteoglycan Metabolism, Cell Death and Kashin-Beck Disease. *Glycoconj J.* 29 (5-6), 241–248. doi:10.1007/s10719-012-9421-2

Li, Y., Zou, N., Wang, J., Wang, K. W., Li, F. Y., Chen, F. X., et al. (2017). TGF-β1/Smad3 Signaling Pathway Mediates T-2 Toxin-Induced Decrease of Type II Collagen in Cultured Rat Chondrocytes. *Toxins (Basel)* 9 (11), Artn 359. doi:10.3390/toxins9110359

Monemdjou, R., Vasheghani, F., Fahmi, H., Perez, G., Blati, M., Taniguchi, N., et al. (2012). Association of Cartilage-specific Deletion of Peroxisome Proliferator-Activated Receptor γ with Abnormal Endochondral Ossification and Impaired Cartilage Growth and Development in a Murine Model. *Arthritis Rheum.* 64 (5), 1551–1561. doi:10.1002/art.33490

Okada, A., Mochizuki, S., Yatabe, T., Kimura, T., Shiomi, T., Fujita, Y., et al. (2008). ADAM-12 (Meltrin α) Is Involved in Chondrocyte Proliferation via Cleavage of Insulin-like Growth Factor Binding Protein 5 in Osteoarthritic Cartilage. *Arthritis Rheum.* 58 (3), 778–789. doi:10.1002/art.23262

Sharma, A. C., Srivastava, R. N., Srivastava, S. R., and Raj, S. (2018). Smad3 Genepolymorphisms and Expression in Serum and Cartilage Influence the Risk of Knee Osteoarthritis. *Osteoarthritis and Cartilage* 26, S186. doi:10.1016/j.joca.2018.02.400

Shi, Y., Lu, F., Liu, X., Wang, Y., Huang, L., Liu, X., et al. (2011). Genetic Variants in the HLA-DRB1 Gene Are Associated with Kashin-Beck Disease in the Tibetan Population. *Arthritis Rheum.* 63 (11), 3408–3416. doi:10.1002/art.30526

Styrkarsdottir, U., Lund, S. H., Thorleifsson, G., Zink, F., Stefansson, O. A., Sigurdsson, J. K., et al. (2018). Meta-analysis of Icelandic and UK Data Sets Identifies Missense Variants in SMO, IL11, COL11A1 and 13 More New Loci

Associated with Osteoarthritis. *Nat. Genet.* 50(12), 1681, 1687. doi:10.1038/s41588-018-0247-0

Sun, L., Cui, S., Deng, Q., Liu, H., Cao, Y., Wang, S., et al. (2019). Selenium Content And/or T-2 Toxin Contamination of Cereals, Soil, and Children's Hair in Some Areas of Heilongjiang and Gansu Provinces, China. *Biol. Trace Elem. Res.* 191 (2), 294–299. doi:10.1007/s12011-018-1620-7

Tang, X., Zhou, Z. k., Shen, B., Kang, P. d., Pei, F. x., and Li, J. (2019). Long-term Efficacy of Repeated Sodium Hyaluronate Injections in Adult Patients with Kashin-Beck Disease of the Knee. *Int. J. Rheum. Dis.* 22 (3), 392–398. doi:10.1111/1756-185X.13435

Wang, L., Yin, J., Yang, B., Qu, C., Lei, J., Han, J., et al. (2020). Serious Selenium Deficiency in the Serum of Patients with Kashin-Beck Disease and the Effect of Nano-Selenium on Their Chondrocytes. *Biol. Trace Elem. Res.* 194 (1), 96–104. doi:10.1007/s12011-019-01759-7

Wang, S. J., Guo, X., Zuo, H., Zhang, Y. G., Xu, P., Ping, Z. G., et al. (2006). Chondrocyte Apoptosis and Expression of Bcl-2, Bax, Fas, and iNOS in Articular Cartilage in Patients with Kashin-Beck Disease. *J. Rheumatol.* 33 (3), 615–619.

Wang, W., Guo, X., Chen, J., Xu, P., and Lammi, M. J. (2008). Morphology and Phenotype Expression of Types I, II, III, and X Collagen and MMP-13 of Chondrocytes Cultured from Articular Cartilage of Kashin-Beck Disease. *J. Rheumatol.* 35 (4), 696–702.

Wang, X., Ning, Y. J., Zhang, P., Poulet, B., Huang, R. T., Gong, Y., et al. (2021). Comparison of the Major Cell Populations Among Osteoarthritis, Kashin-Beck Disease and Healthy Chondrocytes by Single-Cell RNA-Seq Analysis. *Cel Death Dis.* 12 (6), ARTN 551. doi:10.1038/s41419-021-03832-3

Wang, X., Ning, Y., Zhang, P., Yang, L., Wang, Y., and Guo, X. (2017). Chondrocytes Damage Induced by T-2 Toxin via Wnt/β-Catenin Signaling Pathway Is Involved in the Pathogenesis of an Endemic Osteochondropathy, Kashin-Beck Disease. *Exp. Cel Res.* 361 (1), 141–148. doi:10.1016/j.yexcr.2017.10.012

Wharton, K., and Derynck, R. (2009). TGFβ Family Signaling: Novel Insights in Development and Disease. *Development* 136 (22), 3691–3697. doi:10.1242/dev.040584

Wu, R., Zhang, R., Xiong, Y., Sun, W., Li, Y., Yang, X., et al. (2019). The Study on Polymorphisms of Sep15 and TrxR2 and the Expression of AP-1 Signaling Pathway in Kashin-Beck Disease. *Bone* 120, 239–245. doi:10.1016/j.bone.2018.03.026

Xia, C.-t., Yu, F.-f., Ren, F.-l., Fang, H., and Guo, X. (2016). Hyaluronic Acid and Glucosamine Sulfate for Adult Kashin-Beck Disease: a Cluster-Randomized, Placebo-Controlled Study. *Clin. Rheumatol.* 35 (5), 1263–1270. doi:10.1007/s10067-014-2809-6

Xu, J., Lv, S., Hou, Y., Xu, K., Sun, D., Zheng, Y., et al. (2018). miR-27b Promotes Type II Collagen Expression by Targetting Peroxisome Proliferator-Activated Receptor-Γ2 during Rat Articular Chondrocyte Differentiation. *Biosci. Rep.* 38, Artn Bsr20171109. doi:10.1042/BSR20171109

Ya-qun, K., Bu-Ci-ren, P., Jun, W., Cun-qun-pei, J., Ze-Wang-gong, J., and Dun-Zhu-Si, T. (2014). To Investigate and Analyze the Condition of Kaschin-Beck Disease Around 7-12 Years Old Children in Bianba County of Tibet in 2013. *Chin. J. Control. Endemic Dis.* 29, 350–351.

Yang, C.-Y., Chanalaris, A., and Troeberg, L. (2017). ADAMTS and ADAM Metalloproteinases in Osteoarthritis - Looking beyond the 'usual Suspects'. *Osteoarthritis and Cartilage* 25 (7), 1000–1009. doi:10.1016/j.joca.2017.02.791

Yu, F. F., Xia, C. T., Fang, H., Han, J., Younus, M. I., and Guo, X. (2014). Evaluation of the Therapeutic Effect of Treatment with Intra-articular Hyaluronic Acid in Knees for Kashin-Beck Disease: A Meta-Analysis. *Osteoarthritis and Cartilage* 22 (6), 718–725. doi:10.1016/j.joca.2014.04.012

Zhang, F., Dai, L., Lin, W., Wang, W., Liu, X., Zhang, J., et al. (2016). Exome Sequencing Identified FGF12 as a Novel Candidate Gene for Kashin-Beck Disease. *Funct. Integr. Genomics* 16 (1), 13–17. doi:10.1007/s10142-015-0462-z

Zhang, F., Wen, Y., Guo, X., Zhang, Y., Wang, X., Yang, T., et al. (2015). Brief Report: Genome-wide Association Study IdentifiesITPR2as a Susceptibility Gene for Kashin-Beck Disease in Han Chinese. *Arthritis Rheumatol.* 67 (1), 176–181. doi:10.1002/art.38898

Zheru, D., Peiliang, F., Yuli, W., Haishan, W., Qirong, Q., Xiaohua, L., et al. (2014). Association of PPARγ Gene Polymorphisms with Osteoarthritis in a Southeast Chinese Population. *J. Genet.* 93 (3), 719–723. doi:10.1007/s12041-014-0444-2

Zhou, X., Wang, Z., Chen, J., Wang, W., Song, D., Li, S., et al. (2014). Increased Levels of IL-6, IL-1β, and TNF-α in Kashin-Beck Disease and Rats Induced by T-2 Toxin and Selenium Deficiency. *Rheumatol. Int.* 34 (7), 995–1004. doi:10.1007/s00296-013-2862-5

Conflict of Interest: The authors declare that the research was conducted in the absence of any commercial or financial relationships that could be construed as a potential conflict of interest.

The reviewer YMX declared a shared affiliation with the authors YJN, MHH, YG, RH, SJC, FYZ, YLL, FHC, RZ, CL, FZ, XW, and XG to the handling editor at the time of review.

Publisher's Note: All claims expressed in this article are solely those of the authors and do not necessarily represent those of their affiliated organizations, or those of the publisher, the editors, and the reviewers. Any product that may be evaluated in this article, or claim that may be made by its manufacturer, is not guaranteed or endorsed by the publisher.

frontiers in Genetics

ORIGINAL RESEARCH
published: 28 January 2022
doi: 10.3389/fgene.2022.816078

Phenotypic Spectrum and Molecular Basis in a Chinese Cohort of Osteogenesis Imperfecta With Mutations in Type I Collagen

Peikai Chen[1,2†], Zhijia Tan[1,3†], Hiu Tung Shek[1], Jia-nan Zhang[2], Yapeng Zhou[1], Shijie Yin[1], Zhongxin Dong[1], Jichun Xu[1], Anmei Qiu[1], Lina Dong[1], Bo Gao[1,2*] and Michael Kai Tsun To[1,3*]*

[1]Department of Orthopaedics and Traumatology, The University of Hong Kong-Shenzhen Hospital (HKU-SZH), Shenzhen, China, [2]School of Biomedical Sciences, Li Ka Shing Faculty of Medicine, The University of Hong Kong, Hong Kong, China, [3]Department of Orthopaedics and Traumatology, Li Ka Shing Faculty of Medicine, The University of Hong Kong, Hong Kong, China

OPEN ACCESS

Edited by:
Long Guo,
RIKEN Center for Integrative Medical Sciences, Japan

Reviewed by:
Andre Travessa,
Centro Hospitalar Lisboa Norte (CHLN), Portugal
Karen E. Heath,
University Hospital La Paz, Spain

***Correspondence:**
Zhijia Tan
tanzj@hku-szh.org
Bo Gao
gaobo@hku.hk
Michael Kai Tsun To
duqj@hku-szh.org

[†]These authors have contributed equally to this work

Specialty section:
This article was submitted to Genetics of Common and Rare Diseases, a section of the journal Frontiers in Genetics

Received: 16 November 2021
Accepted: 04 January 2022
Published: 28 January 2022

Citation:
Chen P, Tan Z, Shek HT, Zhang J-n, Zhou Y, Yin S, Dong Z, Xu J, Qiu A, Dong L, Gao B and To MKT (2022) Phenotypic Spectrum and Molecular Basis in a Chinese Cohort of Osteogenesis Imperfecta With Mutations in Type I Collagen. Front. Genet. 13:816078. doi: 10.3389/fgene.2022.816078

Osteogenesis imperfecta (OI) is a rare inherited connective tissue dysplasia characterized with skeletal fragility, recurrent fractures and bone deformity, predominantly caused by mutations in the genes *COL1A1* or *COL1A2* that encode the chains of type I collagen. In the present study, clinical manifestations and genetic variants were analysed from 187 Chinese OI patients, majority of whom are of southern Chinese origin. By targeted sequencing, 63 and 58 OI patients were found carrying mutations in *COL1A1* and *COL1A2* respectively, including 8 novel *COL1A1* and 7 novel *COL1A2* variants. We validated a novel splicing mutation in *COL1A1*. A diverse mutational and phenotypic spectrum was observed, coupling with the heterogeneity observed in the transcriptomic data derived from osteoblasts of six patients from our cohort. Missense mutations were significantly associated (χ^2 p = 0.0096) with a cluster of patients with more severe clinical phenotypes. Additionally, the severity of OI was more correlated with the quality of bones, rather than the bone mineral density. Bone density is most responsive to bisphosphonate treatment during the juvenile stage (10–15 years old). In contrast, height is not responsive to bisphosphonate treatment. Our findings expand the mutational spectrum of type I collagen genes and the genotype-phenotype correlation in Chinese OI patients. The observation of effective bisphosphonate treatment in an age-specific manner may help to improve OI patient management.

Keywords: osteogenesis imperfecta, targeted amplicon sequencing, COL1A1, COL1A2, bisphosphonate, bone mineral density

INTRODUCTION

Osteogenesis imperfecta (OI), also known as "brittle bone disease", is a group of hereditary connective-tissue disorders with an incidence of ~1:15,000 births (Lindahl et al., 2015). Patients with OI are more susceptible to long bone fractures and generally characterized by various degrees of bone deformity, blue sclerae, dentinogenesis imperfecta, scoliosis, hearing loss in young adulthood and decreased pulmonary function (Forlino et al., 2011; Marini et al., 2017). The spectrum of clinical manifestation ranges from mild to severe. The original grading system proposed by Sillence *et al.* classifies OI patients into four categories (Sillence et al., 1979), based on clinical and radiographic

characteristics. Type I OI is the mildest form characterized by increased bone fragility and blue sclerae without obvious deformity. Type II OI causes perinatal lethality with intrauterine fracture. Patients with type III OI present multiple fractures and progressive skeletal deformities during the neonatal period. Type IV OI shows variable degrees of bone deformity with a severity intermediate between type I and III. This classical grading system has been re-defined, adding type V OI characterized by unique interosseous ossification, radial head dislocation and hyperplastic callus formation (Van Dijk and Sillence, 2014).

Since early 1980s, OI has been known as an autosomal dominant disease caused by mutations in *COL1A1* and *COL1A2*, which encodes the α1 and α2 chains of type I collagen, the most abundant extracellular matrix in bone, tendon and skin (Forlino et al., 2011). With the development of next-generation sequencing (NGS), new genes have been identified with different inheritance patterns. To date, over 19 OI causative genes have been identified, with functions covering bone mineralization, collagen modification, crosslinking and osteoblast differentiation (Forlino and Marini, 2016; Marini et al., 2017; Moosa et al., 2019; van Dijk et al., 2020).

Autosomal dominant variants in *COL1A1* and *COL1A2* are the most prevalent mutations causing OI (Zhytnik et al., 2019). Type I collagen consists of two α1 and one α2 chains, each of which contains a triple-helical domain composed of Gly-X-Y repeats flanked by N and C terminal pro-peptides. The heterotrimer is assembled from C-terminal toward N-terminal, secreted from the endoplasmic reticulum, and finally cleaved by proteinases (Marini et al., 2017). Mutations resulting in quantitative change of type I collagen cause a mild OI phenotype. Such haploinsufficiency is usually caused by nonsense, frameshift or splicing mutations. In contrast, qualitative mutations alter the structure of type I collagen and weaken the connective tissues, leading to more severe forms of OI. Substitution of glycine with a bulkier or charged residue within the Gly-X-Y tripeptide repeat is the most common mutation disrupting the triple-helical assembly (Van Dijk and Sillence, 2014; Forlino and Marini, 2016; Marini et al., 2017; Tournis and Dede, 2018).

Mutation spectrums on autosomal dominant OI have been established in large cohorts of Swedish (Lindahl et al., 2015), Canadian (Bardai et al., 2016), Indian (Mrosk et al., 2018), Italian (Maioli et al., 2019), Japanese (Higuchi et al., 2021) and Chinese populations (Li L. et al., 2019; Xi et al., 2021), highlighting the genetic heterogeneity of OI. However, the relationship between clinical manifestations and genetic mutations, and the mutational spectrum of type I collagen remain to be further explored. *COL1A1* and *COL1A2* contain 51 and 52 exons spanning genomic regions of 18 and 38 kb respectively. More than 1,065 (Last update: Nov 18, 2020) and 612 unique (Last update: Nov 19, 2020) mutations have been respectively identified in *COL1A1* and *COL1A2* loci (http://www.le.ac.uk/ge/collagen/). In the present study, clinical manifestations and genetic variants were analysed from 187 Chinese OI patients, with the intention to further expand the mutational spectrum of type I collagen, and better establish the correlation between genotype and phenotype in OI patients. Analyses of transcriptomic data from osteoblasts with different dominant mutations further reflected the heterogeneity of OI patients.

MATERIALS AND METHODS

Subjects

This study was approved by the Institutional Review Board of the University of Hong Kong–Shenzhen Hospital. In all, 187 patients diagnosed as OI in Department of Orthopaedics and Traumatology, the University of Hong Kong-Shenzhen Hospital (HKU-SZH, a tertiary general hospital in China) were included in this study. Informed consent was obtained for all patients or legal guardians of children under 18. Detailed medical history and physical examination were assessed and collected by clinicians. Peripheral blood was obtained for genetic test. Skeletal samples were collected for analyses after osteotomy operation based on availability.

BMD and Selection of Control Groups

To assess the growth curve of OI patients under the influence of bisphosphonate treatment, in terms of height, weight and bone mineral density (BMD), we retrieved a set of age and gender-matched controls for such information from the hospital information system. The BMD were measured by the Discovery DXA system (Hologic Inc., Massachusetts) at HKU-SZH. The total hip and total spine (the lumbar regions combined) BMDs were used. Weight and height of each BMD measurements were also collected. If multiple scans of the same measurements were available, the maximum shall be taken.

To begin with, the 187 OI patients were divided into 5-year age groups and further separated according to gender, starting from 0–5 years as the first group. We randomly selected BMD data from non-OI records as controls. However, there is a strong age disparity between the OI and non-OI BMD records, with OI records being much younger than non-OI ones. For example, 664 and 92 records of measurements were retrieved from individuals below 20 y/o for OI and non-OI, respectively. On the other hand, 67 and over 20,000 measurements were obtained for those aged above 20, in the two same groups, respectively. To cope with this, we developed an age- and gender-stratified selection procedure. First, the ratio of non-OI to OI records in the 15–20 age-group was about 1:4 for both genders and dropped significantly afterwards. Next, we used this ratio to determine the optimal number of non-OI control to be 12 for the hip and 26 for the spine in each group. As such, we used all the non-OI data below 20 as controls, and randomly select another 12 and 26 records per each 5-year age-group from the non-OI hip and spine respectively, for those aged above 20.

The non-OI data were fitted with LOESS (Local Polynomial Regression Fitting) regression with default parameters using R function loess (), to produce a normal growth curve, denoted as $f()$. For any successive two readings of the same individual, a normal growth slope was calculated: $k = [f(t_2) - f(t_1)]/(t_2 - t_1)$. The actual growth slope was calculated $k' = (b_2 - b_1)/(t_2 - t_1)$, where b_2 and b_1 are either

BMD or height readings at t_2 and t_1, respectively, with $t_2 > t_1$. The angle α was calculated as $\alpha = \tan^{-1}(k^{'}/C^{'}) - \tan^{-1}(k/C)$, where $C^{'}$ and C are normalising scaling factors to ensure that angles for BMD and height are comparable.

Targeted Amplicon Sequencing

DNA samples isolated from peripheral blood were subjected to targeted amplicon sequencing of *COL1A1* and *COL1A2* (Bybee et al., 2011). Libraries were prepared by a two-stage PCR process and incorporated with a unique 8-bp index for sample-specific barcoding, allowing all samples to be mixed for library purification and sequencing in a single run. Sequencing was performed on the NovaSeq 6000 system (Illumina) with a 150bp paired-end protocol in DynastyGene Co. (Shanghai) and aligned to GRCh37/hg19 genome reference. The GATK toolkit (version 4.0.4.0) (McKenna et al., 2010) was then used to call the variants from the aligned BAM files. The results were annotated by SNPeff (Cingolani et al., 2012) and ANNOVAR (Wang et al., 2010), and deposited in VCF (variant calling format) files to be reviewed by our team of clinicians and geneticists. Qualitative mutations were defined as missense variants, and quantitative as non-missense ones. The variants were visualized (**Figures 1C,D**) using custom scripts, with exon coordinates for *COL1A1* (NM_000088.4) and *COL1A2* (NM_000089.4) obtained from NCBI.

Minigene Splicing Assay

The minigene splicing assay was performed to assess the effects of two intronic mutations in *COL1A1* (c.805–2A > G) and *COL1A2* (c.792+2T > G) on mRNA splicing. Target genome DNA fragments containing the mutated intron and the flanking upstream and downstream genome regions (exon10 to exon15 in *COL1A1* and exon14 to exon18 in *COL1A2*) were cloned into pcDNA3.1 (+) vector at *EcoRI* and *NotI* sites. Point mutations were generated by site-directed mutagenesis and validated by Sanger sequencing. Purified *COL1A1* and *COL1A2* minigene constructs were transfected into HEK293T cells using polyethylenimine. RNA was extracted from transfected cells by TRIzol reagent (Invitrogen) after 24-h, and reversely transcribed into cDNA using PrimeScript RT reagent kit with gDNA Eraser (TakaRa). Spliced mature mRNA fragments can be amplified from the cDNA with specific *COL1A1* (forward: 5′-TGGA AAACCTGGTCGTCCTGGTGA-3′, reverse:5′-CCAGTAGCACCATCATTTCCACGA-3′) and *COL1A2* (forward: 5′-TTCCTGGTGAGAGAGGACGTGTTG-3′, reverse:5′-CACCAGT AAGGCCGTTTGCTCCA-3′) primers. Amplified PCR products were separated on 2% agarose gel and purified by MiniBEST Agarose Gel DNA Extraction Kit V4.0 (TaKaRa). The specific splicing pattern was determined by subsequent Sanger sequencing.

Bone Histology

The skeletal samples collected after necessary operations were fixed in 4% paraformaldehyde and decalcified with 0.5M EDTA before embedding in paraffin. 6 μm sections were cut and mounted on glass slides. The rehydrated sections were stained with Goldner's trichrome and visualised with Leica DM3000 microscope.

Bulk RNA Sequencing

Skeletal specimens from 1) six patients with type I collagen mutations after operations (e.g. osteotomy), 2) a normal boy with humerus fracture and 3) a patient with leg length discrepancy were collected for osteoblast isolation. Soft tissues were removed completely and blood cells were washed away with PBS. Bone samples were then minced into small pieces and immersed in osteoblast culture medium (aMEM with 10% fetal bovine serum, penicillin [100 U/ml] and streptomycin [100 μg/ml]) for 1–2 weeks for osteoblast migration and proliferation.

Confluent cells were lysed with Trizol (Invitrogen) and total RNA were extracted according to manufacturer's instruction. RNA concentration was measured by Qubit and RNA integrity was assessed using the Agilent 2100. A total amount of 2 μg RNA per sample was used as input material. Sequencing libraries were generated using VAHTS mRNA-seq v2 Library Prep Kit from Illumina following manufacturer's recommendations and sequenced on an Illumina NovaSeq platform to generate 150 bp paired-end reads by a commercial company (Berry Genomics, Beijing).

Bioinformatic Analyses of RNA Sequencing Data

Raw data (raw reads) of fastq format were firstly processed through primary quality control. Clean data were aligned to the reference human genome (GRCh38/hg38) and gene expression (FPKM values) was calculated for each transcript using the HISAT2 (Kim et al., 2015) and Cufflinks package (Trapnell et al., 2012). HTSeq package sequencing read count was calculated as described (Anders et al., 2015). Differential expression analysis between two conditions was performed using the cuffdiff tool in the Cufflink package. Differentially expressed genes were defined with adjusted p-value < 0.01 and the log2(Fold change) > 2. Genes with average values < 1 in both groups under comparisons were excluded.

Statistics

Data presented are the averages with standard deviation. Statistical significance level was evaluated by student's t-test (two-tailed, unpaired) between two groups. The difference with $p < 0.05$ was considered significant. Wilcoxon signed rank tests were used for testing if the normalised angles are positive (>0) in the BMD and height tracking data.

RESULTS

Clinical Characteristics of Our OI Cohort

In all, 187 patients diagnosed with OI in the past 5 years were included. Familial information was collected and the patients were found to group into 175 unrelated families, where 167 families have one patient only and 8 (20 patients) have

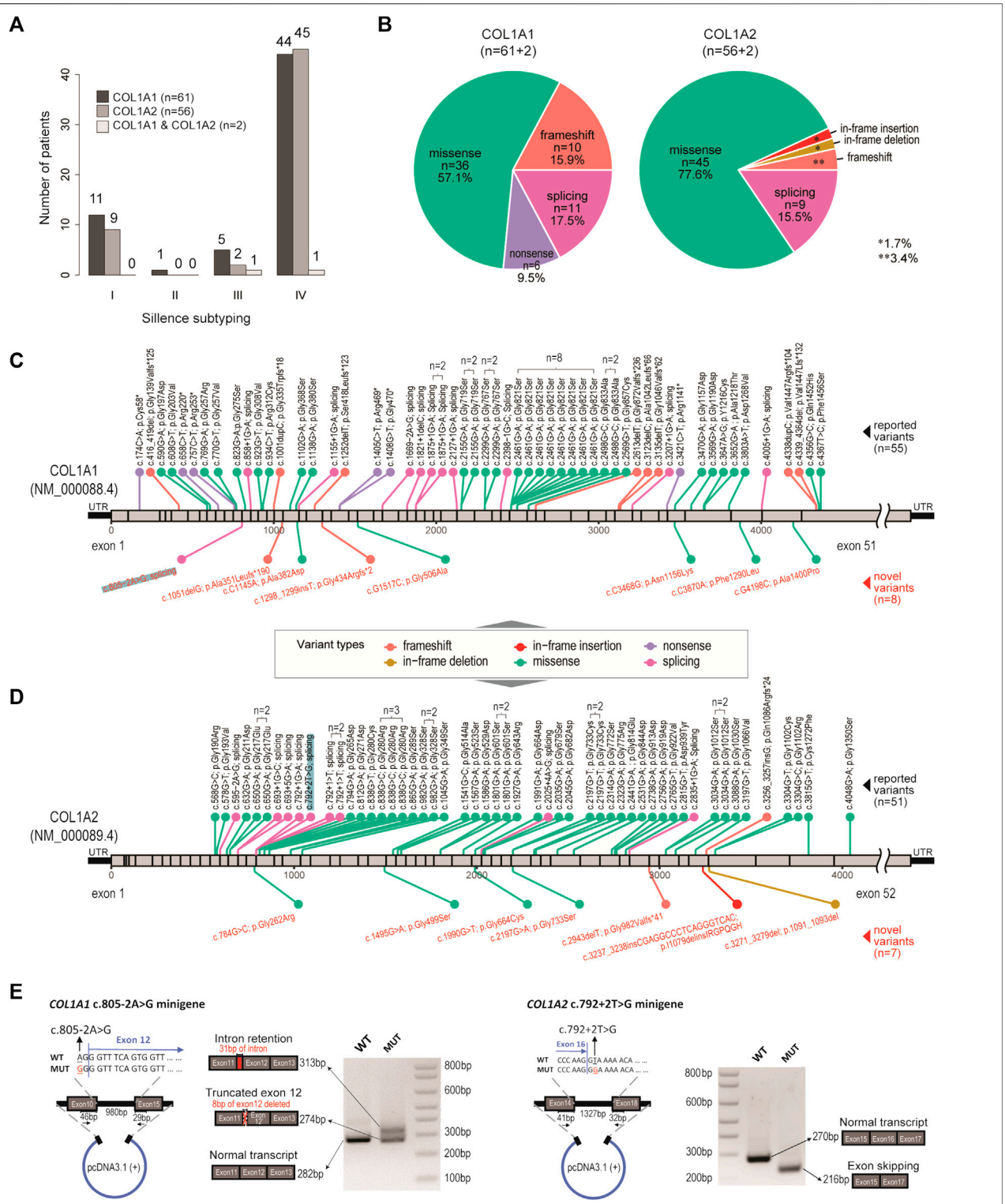

FIGURE 1 | Genetic spectrum in our OI cohort. **(A)** Bar charts showing the distribution of OI cases, with respect to genotypes and clinical subtyping (Sillence scales). **(B)** Pie charts showing the distribution of variant types, with respect to genotypes. **(C)** Diagram showing location and mutation information of the pathogenic variants identified in COL1A1. n number indicates number of recurrences in the cohort. Black texts indicate reported variants. Red texts indicate novel variants. **(D)** Diagram showing location and mutation information of the pathogenic variants identified in COL1A2. n number indicates number of recurrences in the cohort. Black texts indicate reported variants. Red texts indicate novel variants. **(E)** Validation of a novel splicing variant (COL1A1, c.805–2A > G) and a positive control (COL1A2, c.792+2T > G), which were also highlighted in **(C)** and **(D)**.

multiple (**Supplementary Table S1**). The patients were admitted to the Hospital for orthopaedic surgeries, drug treatment or physiotherapy, which include 113 males and 74 females with hospital admission ages ranging from 1 to 38 (median 11, IQR 7–17). Geographically, 88.5% of the cohort came from southern China (south of Yangtze River). According to Sillence classification, the cohort displayed predominantly moderate to severe features, with 24 (14.6%), 1 (0.6%), 20 (11.7%) and 125 (73.1%) patients classified as subtypes I, II, III and IV, respectively. Another 17 patients showed typical type V OI features, including radial head dislocation, interosseous ossification and hyperplastic callus (Hanagata, 2016). Fractures were frequently reported, with 140 (74.5%) patients reporting at least one prior fracture event on their admission/visit to the Hospital, with an average of 13.5 previous fractures per patient. About two thirds (122 out of 187) reported previous surgical treatments and 117 (62.5%) patients reported previous drug treatments, with pamidronate and zoledronate accounting for 26.5 and 73.5%, respectively. Only one patient was treated with denosumab. Physical inspections for typical OI traits, including blue sclerae, limb deformity, dentinogenesis imperfecta, scoliosis, joint laxity, flat feet, basilar invagination, etc. were also recorded, which shall be discussed in later sections.

Targeted Sequencing Revealed Pathogenic Variants in *COL1A1* and *COL1A2*

By targeted amplicon sequencing covering the coding regions and exon-intron boundaries of *COL1A1* and *COL1A2* loci, 119 patients (63.6%) were found to be carrying pathogenic mutations on *COL1A1* (n = 61), *COL1A2* (n = 56) or both (n = 2) (**Figure 1A**; **Supplementary Table S1**). The other 68 patients (referred to as the OI-nonCOL1 group) shall be investigated in future, by an expanded gene-panel, copy number variation (CNV) analysis by MLPA or by whole-genome sequencing. Clinical subtypes of these 119 OI-COL1 patients were predominantly Types I and IV, with no detectable difference between the two affected genes (χ^2 p = 0.84) (**Figure 1A**). Interestingly, the compositions of variant types are significantly different (χ^2 p = 0.013) between individuals carrying *COL1A1* and *COL1A2*, with missense mutations representing 57.1 and 77.6% of all events in the two genes, respectively (**Figure 1B**). Frameshift and nonsense mutations were much more frequent in *COL1A1* (15.9 and 9.5%, respectively) than in *COL1A2* (3.4 and 0%, respectively); whereas variants affecting splicing were comparable (17.5% in *COL1A1* and 15.5% in *COL1A2*). For the two patients carrying mutations on both *COL1A1* and *COL1A2*, one (glycine substitution mutations in both genes) displayed type III features, and the other (alanine substitution on *COL1A1* and frameshift on *COL1A2*) was classified as type IV (**Supplementary Table S2**).

The positions and nature of these variants were displayed in the *COL1A1* and *COL1A2* locus chart, with 8 and 7 novel pathogenic mutations detected, respectively (**Figures 1C,D**). We noted that a "hotspot" missense mutation was present in 8 patients (*COL1A1*, c. 2461G > A), though four of them came from a consanguineous family (**Supplementary Table S1**). A number of other recurrent variants can be found in both genes (**Figures 1C,D**). A novel splicing mutation (*COL1A1*, c.805–2A > G) was selected to validate its deleterious effect on mRNA splicing.

The *COL1A2* (c.792+2T > G) splicing mutation was selected as a positive control (Zolezzi et al., 1995). Splicing mutations causing premature termination may produce mild phenotypes, while variants resulting in reading frame shift and impaired triple helix structures may be associated with more severe phenotypes (Marini et al., 2007). The patient with c.805-2A > G (*COL1A1*) variant displayed severe skeletal deformity (type IV) including scoliosis and low bone density in the spine (Z score: −4.8). The patient with c.792+2T > G (*COL1A2*) variant showed mild type I features (**Supplementary Table S2**). The minigene assay showed that the mutation (*COL1A1*, c.805-2A > G) resulted in mRNA splicing abnormalities, including intron retention and exon truncation (**Figure 1E**). Consistently, exon 16 skipping was observed in the *COL1A2* (c.792+2T > G) variant (Zolezzi et al., 1995). These data expanded the genetic spectrum for OI patients affected by *COL1A1/2* mutations.

Clinical, Histological and Molecular Diversification Coupled With Genetic Spectrum

Twenty critical clinical traits for OI patients, including blue sclera, dentinogenesis imperfecta, hearing loss, joint and skeletal issues, etc. were collected from 90 of the 119 patients. Based on the hierarchical clustering of these data, two clusters of patients can be identified, one with 39 patients (Cluster 1) and the other with 51 (Cluster 2) (**Figure 2A**). Visually, more negative entries (in blue) were observed in Cluster 2. Interestingly, although no association was found between the genotypes and the two clusters (χ^2 p = 0.11); there is a strong tendency (χ^2 p = 0.0096) of higher missense mutations in Cluster 1 (33/39, 84.6%) than in Cluster 2 (29/51, 56.8%) (**Figure 2B**).

The 20 traits contributed differently to the two-cluster patterns, with 8 of them being significantly correlated with the two-cluster classification (χ^2 $p < 0.05$) (**Figure 2C**, top chart). Of note, ratios of flat-fleet, dentinogenesis imperfecta, pectus carinatum, over sweating, scoliosis and pregnancy screening abnormality were higher in Cluster 1 than in Cluster 2, indicating overall more severe clinical phenotypes in the Cluster 1 (**Figure 2C**, bottom chart). Limb deformity was found to be lower in Cluster 1. Limb deformity was not based on pre-orthopaedic correction conditions, but on physical inspection upon the patients' presentation to the physicians. Lower limb deformity rate in Cluster 1 may in fact suggest a higher chance of prior orthopaedic corrections and thus a more severe prior deformity condition in this cluster. The lower rate of blue sclerae in cluster 1 was also found, consistent with the fact that blue sclera was typically more prevalent in less severe OI (Marini et al., 2017).

The mechanical strength of bone is determined not only by the degree of mineralization but also the alignment of collagen fibres. To understand the molecular basis correlated with the severity of OI patients, we further characterized the bone geometrical property in the control and affected individuals. Transaxial

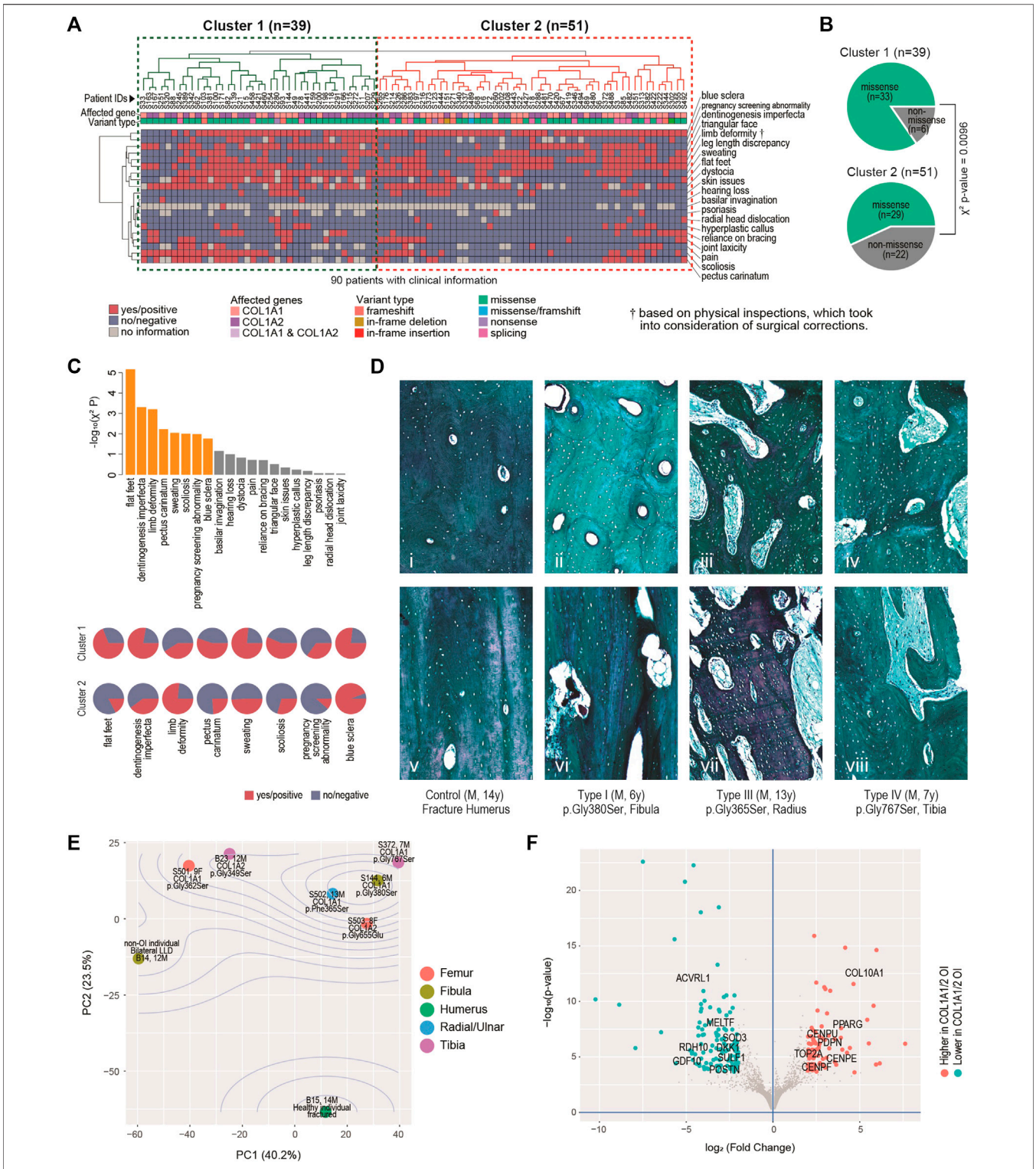

FIGURE 2 | Clinical, histological and molecular phenotypes. **(A)** Heatmap showing clinical characteristics for 90 patients affected by COL1A1 or COL1A2, and with available information. Euclidean distance and complete linkage were used in constructing the dendrograms. **(B)** Enriched types of variants in the identified clusters. **(C)** Top: bar charts showing the clinical traits most correlated with the two clusters. Bars in orange have $p < 0.05$. Bottom: arrays of pie charts showing the percentages of positive traits in each of the two clusters, for the 8 clinical traits that have $p < 0.05$. **(D)** Analyses of bone histology. Goldner trichrome staining of skeletal samples from control individual (n = 1) (i, v), proband with type I OI (n = 2) (ii, vi), proband with type III OI (n = 2) (iii, vii) and proband with type IV OI (n = 3) (iv, viii) harbouring different mutations in COL1A1. Haversian structure was shown by transaxial sections (i-iv). Collagen matrix alignment was shown by sagittal sections (v-viii). **(E)** Diagram of Principal component (PC) analyses showing the sample-sample relationships in a set of eight bulk transcriptome data derived from osteoblasts of six OI and two non-OI patients. Percentages on axes indicate fraction of variance explained. **(F)** Volcano plot showing the differentially expressed genes between the six OI samples with mutations on COL1A1/2 and the two controls.

sections indicated that the size and number of haversian canals and resorption cavities were significantly increased in the cortical bones from type I OI patients (**Figure 2Dii**), when compared to control samples (fracture humerus, 13 years/o, male) with compact haversian structure (**Figure 2Di**). The structure became even worse in type III and type IV patients, showing more severe clinical features (**Figures 2Diii,iv**). Bone histology from sagittal sections also indicated similar trends. The control sample showed condensed and organized lamellar pattern (**Figure 2Dv**), whereas the bones from affected individuals displayed increasing porosity with disorganized collagen alignment from type I to type III and IV (**Figures 2Dvi–viii**), suggesting that the severity of clinical manifestations was positively correlated with the degree of abnormal bone geometry.

To build up more connections between genetics and clinical/histological changes, we conducted bulk transcriptomic profiling on osteoblasts derived from six OI individuals and two non-OI samples. Principal component analyses (PCA) showed that the first two PCs captured 63.7% of the data variance in combination (**Figure 2E**). The two non-OI samples lie on one side (lower left) of the PCA chart, while all the six OI samples lie on the other side, with the fractured sample from normal individual lying furthest from the OIs. The OI group also showed some degree of variation, although the majority of osteoblasts were isolated from patients with glycine substitution mutation (**Figure 2E**). The transcriptomic variation may partially explain the diversity of clinical features among OI patients. To identify the gene expression changes commonly affected by type I collagen mutations, we went on to detect the differentially expressed genes (DEGs) between the two groups. At FDR<0.01 (false discovery rate) and $\log_2$ (fold change) > 2, we detected 85 DEGs higher and 121 DEGs lower in the OI-COL1 group, as compared with the two non-OIs (**Figure 2F**; **Supplementary Table S3**; **Supplementary Figure S1**). It was noteworthy that *COL10A1* and *PPARG* were listed among the genes higher in the OI-COL1 group. COL10A1 is a marker for hypertrophic chondrocytes, which can become osteoblasts (Yang et al., 2014; Tsang et al., 2015). *PPARG* encodes a transcription factor PPARγ critical for adipogenesis (Rosen, 2005). It was reported that osteogenesis and adipogenesis were counteracting forces in normal bone formation, and compromised osteogenesis may lead to more active adipogenesis (Akune et al., 2004; Zhang et al., 2006). The increased expression of *COL10A1* and *PPARG* observed in OI samples may suggest the change of cell fate in the mutant osteoblasts. The genes lower in OI-COL1 group included osteochondrogenic marker *GDF10* (Kratochvilova et al., 2021), indicating reduced bone formation activities in the OI group.

Compromised Weight, Height and BMD in OI Patients

It is of interest to track several key growth indicators, including weight, height and BMD in OI-COL1 patients with consideration of age and gender, in comparison with non-OI individuals. Since many OI patients have metal rodding inside their limbs, BMD readings in these sites may not be suitable for analyses. Instead, the spine BMD was often used, although readings on the hip may also be valuable. We first carefully selected a set of patients without OI features as controls (referred to as the non-OIs) (Methods). Majority of the OI patients had BMD measurements (181 out of 187), with matching height and weight measurements. **Figures 3A,B** showed the weight and height readings for the four groups of individuals. Statistically, the readings of weight and height from OI patients were significantly lower than the non-OI for the age-groups 15–20, 20–25 and 25–30 years of the females; and for age-groups 10–15, 15–20 and 25–30 years of the males (**Supplementary Figure S2A,B**). Not much difference was found among the three OI groups in both genders. For height, although in both genders, the divergence starts as early as the 5–10 years group, the biggest gap occurs from the 15–20 group, which was maintained into the 25–30 years group (**Figure 3B**; **Supplementary Figure S2C,D**). The total BMD in the spine and in the hip showed a similar trend, where the gap between non-OI and OI widens from the 10–15 age-group and onwards (**Figures 3C,D**; **Supplementary Figure S2E,F**). Indeed, the spine and hip BMD showed a strong correlation (Pearson correlation $r = 0.898$) (**Figure 3E**), although this correlation dropped slightly (Pearson correlation $r = 0.766$) in the OIs (**Figure 3F**). Interestingly, the growth behaviours between *COL1A1* and *COL1A2* patients showed much less divergence, in weight, height and BMD.

We also asked if mutation types (qualitative or quantitative, defined in Methods) may impact the growth curves of height. We fitted the data with a non-linear mixed-effect model using SITAR (Cole et al., 2010), using height data from individuals with more than 4 separate measurements and spline degree of freedom of 3, just to avoid model unidentifiability. We found that the patient-specific random effects for qualitative and quantitative mutations were on average 4.1 cm below and 3.1 cm above population average, respectively. This is consistent with our earlier findings that missense mutations have more negative phenotypes (**Figures 2A–C**).

Tracking the Impact of Bisphosphonates on BMD Revealed Age-specific Improvement

Among the 108 (out of 119) OI-COL1 and 60 (out of 68) OI-nonCOL1 patients with BMD data, 281 and 178 records were retrieved, amounting to an average of 2.6 and 3.0 records per individual, respectively. About 3/4 of these patients reported being treated by bisphosphonates (BP), with 72.1, 75.6 and 78.6% for the COL1A1, COL1A2, and OI-nonCOL1 groups, respectively (**Supplementary Figure S3A**). On average, an OI patient reported receiving 4.6 prior BP treatments (IQR 2.0–6.0) (**Supplementary Figure S3B**). Based on current records, 64 patients had two or more BMD records for the spine, 54 of which treated with BP. Given the linear relation between spine and hip (**Figures 3E,F**) and the quadratic relation between height and weight (**Supplementary Figure S3C**), we focused on the spine BMD and height for treatment response analyses. Line segments linking successive spine BMD (**Figure 4A**) and height

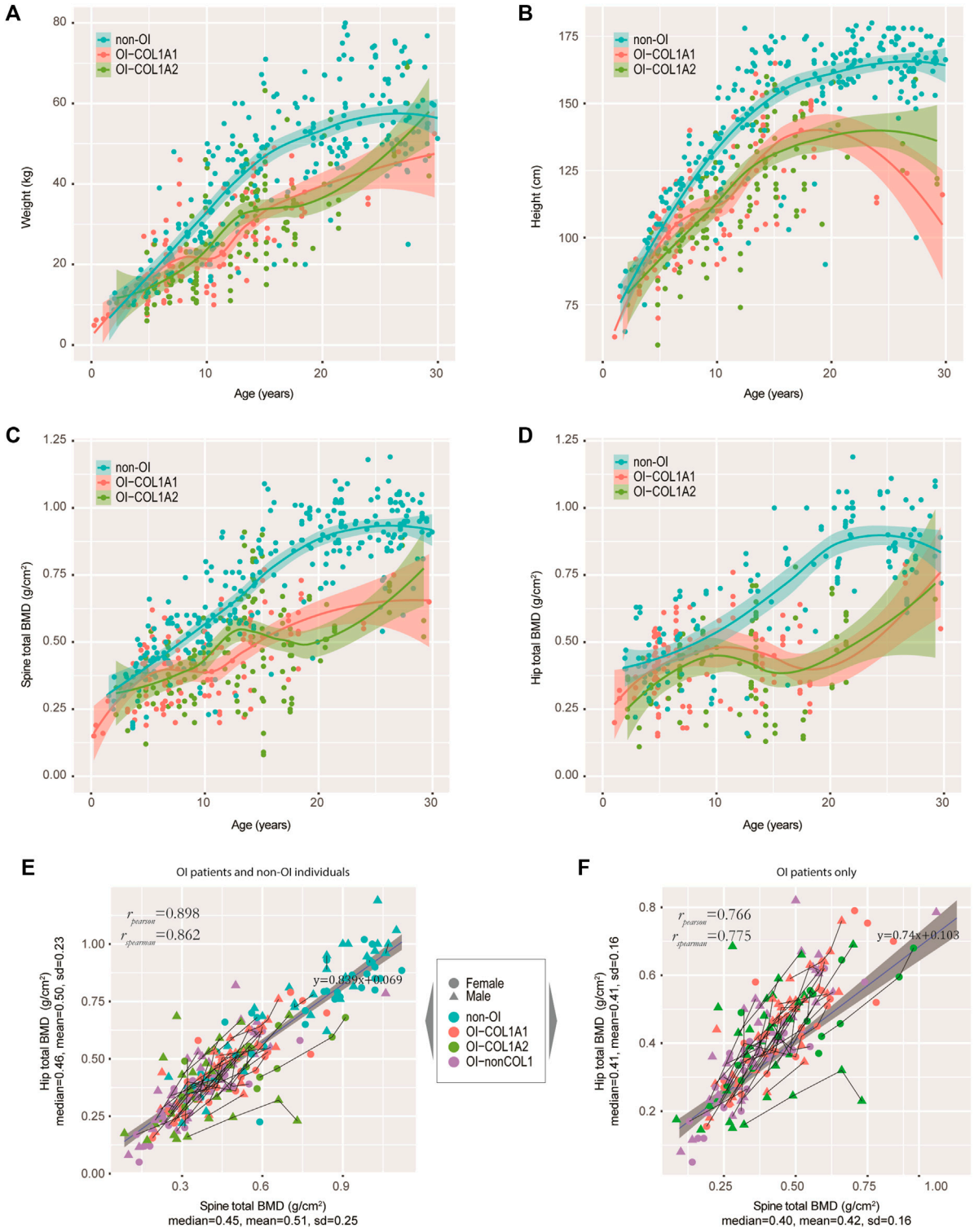

FIGURE 3 | Tracking the weight, height and BMD in our OI cohort. **(A–D)** Growth curves of weight **(A)**, height **(B)**, spine BMD **(C)**, and hip BMD **(D)** were tracked. Non-OIs were randomly retrieved from our hospital information system with gender and aged matched (per age group), and served as controls for comparison. Each dot represents one measurement for one individual. **(E)** Scatter plot showing the correlation between spine and hip BMDs in our OI and non-OI cohorts combined. **(F)** Scatter plot showing the correlation between spine and hip BMDs in our OI cohort only. Line segments indicated measurements of the same individuals.

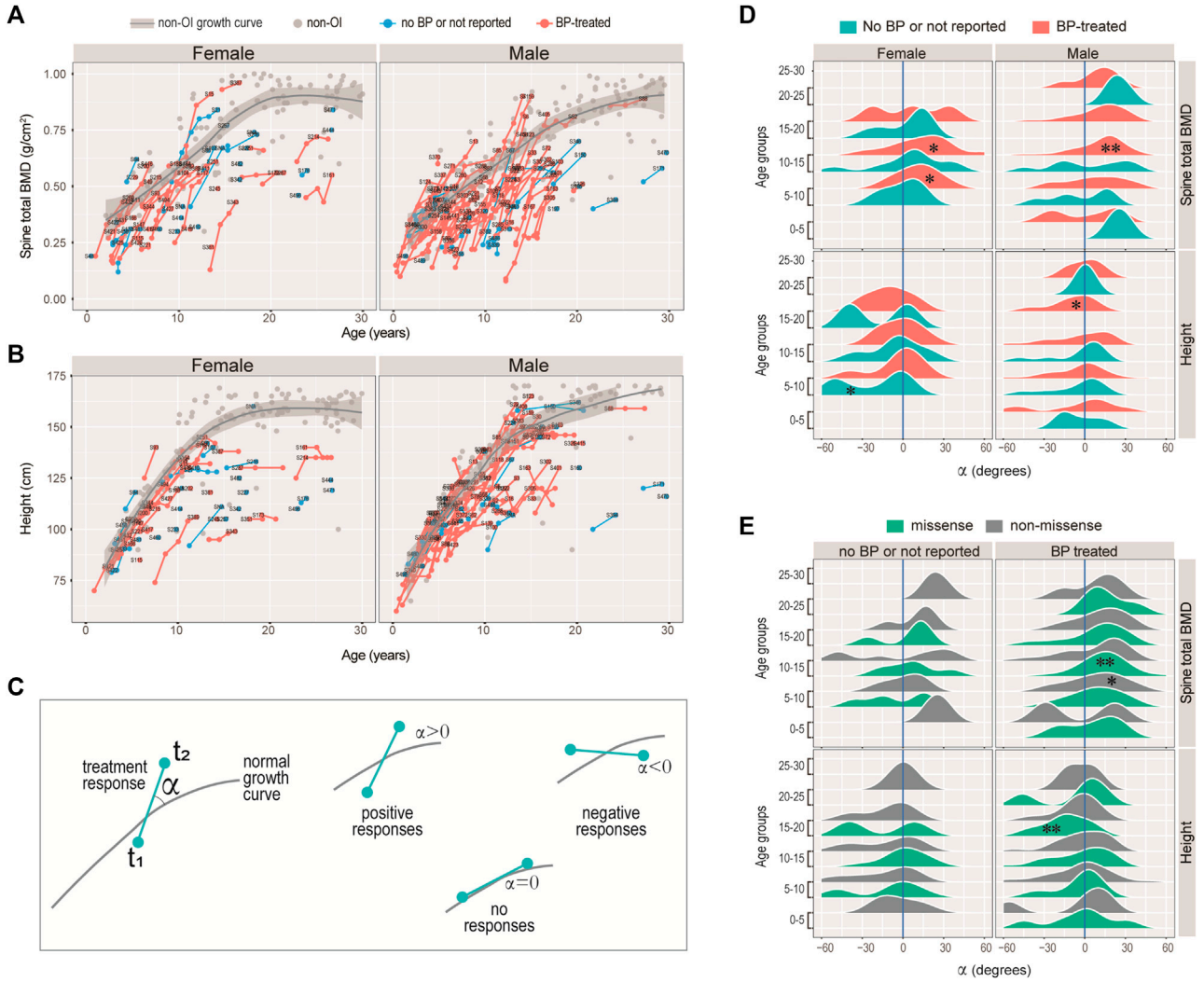

FIGURE 4 | Responses of bisphosphonate (BP) treatment. **(A–B)** Growth curves for spinal BMD **(A)**, and height **(B)** for the female and male patients with *COL1A1/2* variants in our cohort. Line segments indicated measurements of the same individuals. Text labels were anonymized patient IDs. **(C)** Diagram illustrating the strategy measuring BP responses. The angle α was measured between the slope of the consecutive measurements and the tangential slope in the controls. A positive angle indicates stronger growth rate as compared with the controls, and a negative one indicates otherwise. **(D–E)** Ridge plots showing the BP responses of spinal BMD and height with respect to sex, BP-history and age-groups **(D)**, or to variant type, BP-history and age-groups **(E)**. *: Wilcoxon test $p < 0.05$; **: $p < 0.01$; unmarked box: no significant difference.

(**Figure 4B**) readings of the same individuals were shown, with grey dots indicating the non-OI readings of BMD and height, and their fitted curves (Methods) with standard error band.

Intuitively, we noticed that although the BMD and height readings tend to fall below the non-OI fitted growth curves, the BMDs' slopes appeared to be steeper than the non-OI fitted curve, whereas the heights' slopes were more or less tangent to the curve. We asked if BMD was more responsive to BP than height, and if the response was age-dependent. Nonlinear mixed effect models were frequently used to fit the growth curves (Cole et al., 2010; Susman et al., 1998), where both the deviation from normal and transient velocity (growth rate) can be estimated. Unfortunately, extensive data points per individual are needed to avoid model unidentifiability. Alternatively, we used an *ad hoc* approach to measure the normalised angle (Methods) between the slope of the successive readings and that on the fitted curve (**Figure 4C**). A positive angle would indicate a growth rate faster than normal (i.e. non-OI), a negative angle would mean a slower response and a zero angle for no response (**Figure 4C**). **Figures 4D,E** showed the angle, with respect to data type (BMD or height), gender, and treatment history. It appeared that the angles for height were either not different from zero, or significantly lower (lower panels of **Figures 4D,E**). In particular, height growth appeared to be significantly lower in the BP-treated OI in the 15–20 age-group, which was consistent with a mouse study showing BP-treatment inhibits long bone growth (Evans et al., 2003). In comparison, the angles for spine BMD showed a strong tendency to deviate to the right of the zero axis (upper panels of **Figures 4D,E**). In addition, the significantly positive angles tended to occur in the 5–15 age-groups. These results suggest that BP treatment may not be

helpful to improving height, but it does improve bone density, particularly when administered in the juvenile age-groups (5–15 years).

DISCUSSION

Considering the clinical complexity and genetic heterogeneity of OI, NGS-based genotyping enables precise diagnosis and genetic counselling for OI cases. In the current study, we analyzed the pathogenic variants in the type I collagen of 187 patients diagnosed with OI, and revealed the correlation between genotype and phenotype. Our results expand the clinical features, genetic spectrum and molecular basis to the Chinese cohorts of OI (Zhang et al., 2016; Liu et al., 2017; Li L. et al., 2019; Li L.-J. et al., 2019; Xi et al., 2021), with a particular focus on the OI population from southern China. OI is generally considered a monogenic skeletal disorder. At current stage, we identified a total of 102 unique mutations in *COL1A1* and *COL1A2*, including 15 novel mutations. Variants in type I collagen accounted for the majority of all patients (63.6%, 119 out of 187). With regard to the proportion of collagen-related OI in different cohorts, the detection rates were high up to 85–90% in Italian (Maioli et al., 2019), Canadian (Bardai et al., 2016) and Japanese (Higuchi et al., 2021) populations. It is noteworthy that type I mild OI predominates in these cohorts. While in the cohort from Indian with majority of moderate to severe OI, only 46% of OI cases were caused by mutations in *COL1A1* and *COL1A2*, and the moderate to severe form of OI accounts for a higher proportion (Mrosk et al., 2018). The deviation may lie in the bias of individuals with severe phenotypes to seek orthopaedic treatment, geographical isolation with higher risk of consanguineous history, genetic heterogeneity vulnerable to autosomal recessive defects, epigenetic, environmental, and other unidentified factors associated with the corresponding variability. Our cohort only consists of 16.8% type I mild OI (20/119), while moderate to severe OI types dominate the cohort. Compared with patients with autosomal dominant OI, those with recessive inheritance tend to show more severe skeletal deformities (Marini et al., 2017; Li et al., 2020). Population-based studies would be more representative to determine the OI mutations spectrum by removing the inheriting biases and hospital-based referral trends.

In accordance with the literature, mild OI cases in our cohort were caused both by quantitative and qualitative defects in type I collagen defects (Forlino and Marini, 2016). Although mild form of OI was generally caused by mutations in *COL1A1* and *COL1A2* (Bardai et al., 2016), we observed four patients without suspicious variants detected in type I collagen, where no record of extraskeletal features was known to us. No correlation was observed between the variant position and clinical manifestations, since mutations associated with mild to severe OI types were dispersed throughout the genomic loci of *COL1A1* and *COL1A2*. Interestingly, a frequent variant detected in Chinese patients (c. 2299G > A; p.Gly767Ser in *COL1A1*) (Xi et al., 2021) was also identified in our cohort. Another hotspot (c. 2461G > A; p.Gly821Ser in *COL1A1*) was present in 8 patients (belonging to five unrelated families). Interestingly, remarkable phenotypic variability ranging from moderate to severe was observed among individuals bearing this variant (**Supplementary Figure S4**). It was recently suggested that haploinsufficiency in familial cases may cause similar features, whereas structural abnormality results in higher phenotypic variability (Zhytnik et al., 2020).

Obtaining a precise diagnosis of OI in different populations expands the understanding of molecular basis in OI and improves the personalized care. Notably, no nonsense variants were identified in *COL1A2* loci, consistent with a previous study in Chinese OI cohort (Li L. et al., 2019). This bias may originate from the composition proportion of the heterotrimer (two α1 and one α2 chains), suggesting a significant difference between *COL1A1* and *COL1A2* where a decreased amount of the α2 chain causes minor interruption of type I collagen (Rauch et al., 2010). The proportion of missense mutations in *COL1A1* in our study was lower than reports in India (85.7%), Vietnam (67.6%), and Sweden (60.9%) (Stephen et al., 2014; Lindahl et al., 2015; Ho Duy et al., 2016), but was still the dominant variant in the spectrum. Two patients were found harboring compound mutations of *COL1A1* and *COL1A2*. One of them with two known pathogenic variants (c.590G > A in *COL1A1* and c. 650G > A in *COL1A2*) displayed severe phenotypes (type III), while the other patient with two novel variants (c.4918G > C in *COL1A1* and c.2943delT in *COL1A2*) showed moderate features (type IV). The variant c.2943delT in *COL1A2* was considered as the likely pathogenic factor because it was inherited from his father with OI, while the mutation c. 4918 G > C in *COL1A1* was considered as variant of uncertain significance (VUS) that requires further validation. In our study, we only identified a homozygous mutation in *COL1A1* (c. 3803A > T; p. Asp1268Val) leading to embryonic lethality, which was not found in the variants involved in the lethal outcome (Maioli et al., 2019). On the other hand, a lethal mutation in the same Italian cohort was found recurrent in our spectrum, which may further reveal the genetic heterogeneity among different ethnic populations.

The relationship between the genetic mutations and clinical severity is complex in OI patients. Glycine substitutions and splicing mutations are the dominant variants, leading to structural defects (qualitative) or quantitative change in type I collagen (Forlino and Marini, 2016). Glycine is the only amino acid small enough to fit into the restricted space of the helical centre. Glycine substitutions usually disrupt the helix stability and produce moderate-to-severe phenotypes (Marini et al., 2017), which was corroborated by the unbiased clustering analyses in our study. Splicing variants that cause reading frame shifted and impaired triple helix structures may result in severe phenotypes. Conversely, mutations resulting in premature termination may produce mild phenotypes (Marini et al., 2007), which may explain the different severities in the patients carrying novel splicing variants in our study. The patient with c.805–2A > G in *COL1A1* was classified in type III OI, while the patient with c.792+2T > G in *COL1A2* displayed type IV features.

Consistent with previous studies, blue sclera was associated with the mild form of OI, while dentinogenesis imperfecta was

detected more in patients with moderate-to-severe features, suggesting the similarity of dentin and bone with regard to the composition in the extracellular matrix (**Figure 2C**) (Bardai et al., 2016; Li L. et al., 2019; Higuchi et al., 2021). Hearing loss, a common secondary feature of OI with mixed conductive and sensorineural deficiency, often develops between the second and fourth decades of adult patients (Hald et al., 2018). In the current study, only two probands encountered hearing loss, with much lower proportion than those reported in Chinese (7.5%) and European (24%) populations (Hald et al., 2018; Xi et al., 2021), which may be explained by the majority of paediatric patients in our cohort. Furthermore, four individuals presented with hearing impairment in adolescence and young adulthood, but the number of cases was insufficient for the assessment of genotypic associations (Higuchi et al., 2021). Consistently, the height of OI patients, particularly in the severe forms, was significantly lower than that of the normal population (Bardai et al., 2016; Li L.-J. et al., 2019), while there was no difference between patients with mutations in *COL1A1* and *COL1A2*.

Bisphosphonates, as the mainstay of pharmacological intervention for osteoporosis, are widely used to improve the BMD for OI patients, aiming to increase their bone mass and reduce the limb deformity (Sato et al., 2016; Kashii et al., 2019). Bisphosphonate treatment in our cohort improved the BMD of the OI patients, in particular in the 10–15 age-range. We noticed that although it was not specifically assessed in their work, the treatment responses (their **Figure 1**) in (Astrom and Soderhall, 2002) demonstrated highly similar patterns as ours, with sharpest responses in the 10–15 age-range. The effects of BP treatment on the height, however, was trivial. In fact, height growth rate at 15–20 appears to be lower than expected in the BP treated patients (**Figure 4E**). A study showed that children with OI receiving BP treatment have their height Z-scores decrease from -4.8 to -5.1, (Palomo et al., 2015). Another previous study reported that pamidronate therapy increased the Z-scores of heights in type III OI patients after 1 year treatment, but not in type I and type IV groups. After 4 years of treatment, only the Z-scores from type IV patients was improved (Zeitlin et al., 2003). In this regard, the application of bisphosphonate therapy in paediatric patients with low bone mass remains controversial (Bachrach and Ward, 2009).

In summary, our study detected known and novel mutations in *COL1A1* and *COL1A2* in OI patients of southern Chinese origin, revealed genotype-phenotype correlation and diversification, and assessed age-specific treatment response of bisphosphonate therapy. A novel splicing event was validated by functional assays. Histological and transcriptomic analyses offered some insights on bone microstructure and osteoblast differentiation. Further studies are needed to characterize the actual prevalence of OI in more representative cohorts, consummate the mutational spectrum both in dominant and recessive forms of OI, decipher the complicated connection between genotypes and phenotypes, and develop more effective therapeutic pharmacies and interventions.

DATA AVAILABILITY STATEMENT

The Sillence subtyping, genotypes, variant types and anonymized patient IDs were attached in **Supplementary Table S1**. The transcriptome data was deposited on NCBI GEO (accession: GSE186141). Scripts for processing the data and producing the figures are deposited on: https://github.com/HKUSZH/COL1.

ETHICS STATEMENT

The studies involving human participants were reviewed and approved by The university of Hong Kong—Shenzhen Hospital Institutional Review Board. Written informed consent to participate in this study was provided by the participants (aged 18 or above) or their legal guardians/next-of-kin (aged below 18).

AUTHOR CONTRIBUTIONS

PC, ZT, BG, and MT conceived and designed the research studies. MT, ZD, YZ, SY and JX provided diagnoses and performed surgeries on the patients. AQ and LD provided nursing care and documented the clinical data. ZT, HS and J-nZ conducted the experiments and acquired the data. PC designed the analytical framework, and conducted biostatistical and bioinformatics analyses. PC, ZT and MT analysed the data and wrote the original manuscript. BG helped with data interpretation and manuscript editing. MT and BG acquired research funding and supervised the study. All authors revised and approved the manuscript.

FUNDING

This work was supported by "Shenzhen Key Medical Discipline Construction Fund" (No. SZXK077) and Hong Kong Health and Medical Research Fund (No.07181676).

ACKNOWLEDGMENTS

We thank the Fu Tak Iam foundation (Hong Kong) (www.ftifoundation.org) and Chow Tai Fook charity foundation (Hong Kong) (www.ctfcf.org) for covering part of the medical costs. PC and ZT thank the Shenzhen Peacock Plan for the awards and support. We thank all our patients and their families for their participation in this study.

SUPPLEMENTARY MATERIAL

The Supplementary Material for this article can be found online at: https://www.frontiersin.org/articles/10.3389/fgene.2022.816078/full#supplementary-material

Supplementary Figure S1 | DEGs between control and OI-COL1.

Supplementary Figure S2 | Growth curves and inter-group comparisons.

Supplementary Figure S3 | Growth curves and treatment responses.

Supplementary Figure S4 | Radiographic images of eight patients carrying COL1A1 c.2461G>A, p.Gly821Ser mutation.

Supplementary Table S1 | A full list of the 187 patients and their genetic information.

Supplementary Table S2 | Clinical features of patients with splicing mutations selected for validation.

Supplementary Table S3 | A full list of the 206 differentially expressed genes between the two non-OI samples and the six COL1 OI samples.

REFERENCES

Akune, T., Ohba, S., Kamekura, S., Yamaguchi, M., Chung, U.-i., Kubota, N., et al. (2004). PPAR γ Insufficiency Enhances Osteogenesis through Osteoblast Formation from Bone Marrow Progenitors. *J. Clin. Invest.* 113, 846–855. doi:10.1172/jci200419900

Anders, S., Pyl, P. T., and Huber, W. (2015). HTSeq--a Python Framework to Work with High-Throughput Sequencing Data. *Bioinformatics* 31, 166–169. doi:10.1093/bioinformatics/btu638

Astrom, E., and Soderhall, S. (2002). Beneficial Effect of Long Term Intravenous Bisphosphonate Treatment of Osteogenesis Imperfecta. *Arch. Dis. Child.* 86, 356–364. doi:10.1136/adc.86.5.356

Bachrach, L. K., and Ward, L. M. (2009). Clinical Review: Bisphosphonate Use in Childhood Osteoporosis. *J. Clin. Endocrinol. Metab.* 94, 400–409. doi:10.1210/jc.2008-1531

Bardai, G., Moffatt, P., Glorieux, F. H., and Rauch, F. (2016). DNA Sequence Analysis in 598 Individuals with a Clinical Diagnosis of Osteogenesis Imperfecta: Diagnostic Yield and Mutation Spectrum. *Osteoporos. Int.* 27, 3607–3613. doi:10.1007/s00198-016-3709-1

Bybee, S. M., Bracken-Grissom, H., Haynes, B. D., Hermansen, R. A., Byers, R. L., Clement, M. J., et al. (2011). Targeted Amplicon Sequencing (TAS): A Scalable Next-Gen Approach to Multilocus, Multitaxa Phylogenetics. *Genome Biol. E* 3, 1312–1323. doi:10.1093/gbe/evr106

Cingolani, P., Platts, A., Wang, L. L., Coon, M., Nguyen, T., Wang, L., et al. (2012). A Program for Annotating and Predicting the Effects of Single Nucleotide Polymorphisms, SnpEff. *Fly* 6, 80–92. doi:10.4161/fly.19695

Cole, T. J., Donaldson, M. D. C., and Ben-Shlomo, Y. (2010). SITAR-a Useful Instrument for Growth Curve Analysis. *Int. J. Epidemiol.* 39, 1558–1566. doi:10.1093/ije/dyq115

Evans, K. D., Lau, S. T., Oberbauer, A. M., and Martin, R. B. (2003). Alendronate Affects Long Bone Length and Growth Plate Morphology in the Oim Mouse Model for Osteogenesis Imperfecta. *Bone* 32, 268–274. doi:10.1016/s8756-3282(02)00974-2

Forlino, A., and Marini, J. C. (2016). Osteogenesis Imperfecta. *Lancet* 387, 1657–1671. doi:10.1016/s0140-6736(15)00728-x

Forlino, A., Cabral, W. A., Barnes, A. M., and Marini, J. C. (2011). New Perspectives on Osteogenesis Imperfecta. *Nat. Rev. Endocrinol.* 7, 540–557. doi:10.1038/nrendo.2011.81

Hald, J. D., Folkestad, L., Swan, C. Z., Wanscher, J., Schmidt, M., Gjørup, H., et al. (2018). Osteogenesis Imperfecta and the Teeth, Eyes, and Ears-A Study of Non-skeletal Phenotypes in Adults. *Osteoporos. Int.* 29, 2781–2789. doi:10.1007/s00198-018-4663-x

Hanagata, N. (2016). IFITM5 Mutations and Osteogenesis Imperfecta. *J. Bone Miner Metab.* 34, 123–131. doi:10.1007/s00774-015-0667-1

Higuchi, Y., Hasegawa, K., Futagawa, N., Yamashita, M., Tanaka, H., and Tsukahara, H. (2021). Genetic Analysis in Japanese Patients with Osteogenesis Imperfecta: Genotype and Phenotype Spectra in 96 Probands. *Mol. Genet. Genomic Med.* 9, e1675. doi:10.1002/mgg3.1675

Ho Duy, B., Zhytnik, L., Maasalu, K., Kändla, I., Prans, E., Reimann, E., et al. (2016). Mutation Analysis of the COL1A1 and COL1A2 Genes in Vietnamese Patients with Osteogenesis Imperfecta. *Hum. Genomics* 10, 27. doi:10.1186/s40246-016-0083-1

Kashii, M., Kanayama, S., Kitaoka, T., Makino, T., Kaito, T., Iwasaki, M., et al. (2019). Development of Scoliosis in Young Children with Osteogenesis Imperfecta Undergoing Intravenous Bisphosphonate Therapy. *J. Bone Miner Metab.* 37, 545–553. doi:10.1007/s00774-018-0952-x

Kim, D., Langmead, B., and Salzberg, S. L. (2015). HISAT: A Fast Spliced Aligner with Low Memory Requirements. *Nat. Methods* 12, 357–360. doi:10.1038/nmeth.3317

Kratochvilova, A., Ramesova, A., Vesela, B., Svandova, E., Lesot, H., Gruber, R., et al. (2021). Impact of FasL Stimulation on Sclerostin Expression and Osteogenic Profile in IDG-SW3 Osteocytes. *Biology* 10 (8), 757. doi:10.3390/biology10080757

Li, S., Cao, Y., Wang, H., Li, L., Ren, X., Mi, H., et al. (2020). Genotypic and Phenotypic Analysis in Chinese Cohort With Autosomal Recessive Osteogenesis Imperfecta. *Front. Genet.* 11, 984. doi:10.3389/fgene.2020.00984

Li, L., Mao, B., Li, S., Xiao, J., Wang, H., Zhang, J., et al. (2019). Genotypic and Phenotypic Characterization of Chinese Patients with Osteogenesis Imperfecta. *Hum. Mutat.* 40, 588–600. doi:10.1002/humu.23718

Li, L.-J., Lyu, F., Song, Y.-W., Wang, O., Jiang, Y., Xia, W.-B., et al. (2019). Genotype-phenotype Relationship in a Large Cohort of Osteogenesis Imperfecta Patients with COL1A1 Mutations Revealed by a New Scoring System. *Chin. Med. J. (Engl)* 132, 145–153. doi:10.1097/cm9.0000000000000013

Lindahl, K., Åström, E., Rubin, C.-J., Grigelioniene, G., Malmgren, B., Ljunggren, Ö., et al. (2015). Erratum: Genetic Epidemiology, Prevalence, and Genotype-Phenotype Correlations in the Swedish Population with Osteogenesis Imperfecta. *Eur. J. Hum. Genet.* 23, 1112. doi:10.1038/ejhg.2015.129

Liu, Y., Asan, Ma, D., Lv, F., Xu, X., Wang, J., et al. (2017). Gene Mutation Spectrum and Genotype-Phenotype Correlation in a Cohort of Chinese Osteogenesis Imperfecta Patients Revealed by Targeted Next Generation Sequencing. *Osteoporos. Int.* 28, 2985–2995. doi:10.1007/s00198-017-4143-8

Maioli, M., Gnoli, M., Boarini, M., Tremosini, M., Zambrano, A., Pedrini, E., et al. (2019). Genotype-phenotype Correlation Study in 364 Osteogenesis Imperfecta Italian Patients. *Eur. J. Hum. Genet.* 27, 1090–1100. doi:10.1038/s41431-019-0373-x

Marini, J. C., Forlino, A., Cabral, W. A., Barnes, A. M., San Antonio, J. D., Milgrom, S., et al. (2007). Consortium for Osteogenesis Imperfecta Mutations in the Helical Domain of Type I Collagen: Regions Rich in Lethal Mutations Align with Collagen Binding Sites for Integrins and Proteoglycans. *Hum. Mutat.* 28, 209–221. doi:10.1002/humu.20429

Marini, J. C., Forlino, A., Bächinger, H. P., Bishop, N. J., Byers, P. H., Paepe, A. D., et al. (2017). Osteogenesis Imperfecta. *Nat. Rev. Dis. Primers* 3, 17052. doi:10.1038/nrdp.2017.52

McKenna, A., Hanna, M., Banks, E., Sivachenko, A., Cibulskis, K., Kernytsky, A., et al. (2010). The Genome Analysis Toolkit: a MapReduce Framework for Analyzing Next-Generation DNA Sequencing Data. *Genome Res.* 20, 1297–1303. doi:10.1101/gr.107524.110

Moosa, S., Yamamoto, G. L., Garbes, L., Keupp, K., Beleza-Meireles, A., Moreno, C. A., et al. (2019). Autosomal-Recessive Mutations in MESD Cause Osteogenesis Imperfecta. *Am. J. Hum. Genet.* 105, 836–843. doi:10.1016/j.ajhg.2019.08.008

Mrosk, J., Bhavani, G. S., Shah, H., Hecht, J., Krüger, U., Shukla, A., et al. (2018). Diagnostic Strategies and Genotype-Phenotype Correlation in a Large Indian Cohort of Osteogenesis Imperfecta. *Bone* 110, 368–377. doi:10.1016/j.bone.2018.02.029

Palomo, T., Fassier, F., Ouellet, J., Sato, A., Montpetit, K., Glorieux, F. H., et al. (2015). Intravenous Bisphosphonate Therapy of Young Children With Osteogenesis Imperfecta: Skeletal Findings During Follow Up Throughout the Growing Years. *J. Bone Miner Res.* 30, 2150–2157. doi:10.1002/jbmr.2567

Rauch, F., Lalic, L., Roughley, P., and Glorieux, F. H. (2010). Genotype-phenotype Correlations in Nonlethal Osteogenesis Imperfecta Caused by Mutations in the Helical Domain of Collagen Type I. *Eur. J. Hum. Genet.* 18, 642–647. doi:10.1038/ejhg.2009.242

Rosen, E. D. (2005). The Transcriptional Basis of Adipocyte Development. *Prostaglandins, Leukot. Essent. Fatty Acids* 73, 31–34. doi:10.1016/j.plefa.2005.04.004

Sato, A., Ouellet, J., Muneta, T., Glorieux, F. H., and Rauch, F. (2016). Scoliosis in Osteogenesis Imperfecta Caused by COL1A1/COL1A2 Mutations - Genotype-

Phenotype Correlations and Effect of Bisphosphonate Treatment. *Bone* 86, 53–57. doi:10.1016/j.bone.2016.02.018

Sillence, D. O., Senn, A., and Danks, D. M. (1979). Genetic Heterogeneity in Osteogenesis Imperfecta. *J. Med. Genet.* 16, 101–116. doi:10.1136/jmg.16.2.101

Stephen, J., Shukla, A., Dalal, A., Girisha, K. M., Shah, H., Gupta, N., et al. (2014). Mutation Spectrum ofCOL1A1andCOL1A2genes in Indian Patients with Osteogenesis Imperfecta. *Am. J. Med. Genet.* 164, 1482–1489. doi:10.1002/ajmg.a.36481

Susman, E. P., Murphy, J. R., Zerbe, G. O., and Jones, R. H. (1998). Using a Nonlinear Mixed Model to Evaluate Three Models of Human Stature. *Growth Dev. Aging* 62, 161–171.

Tournis, S., and Dede, A. D. (2018). Osteogenesis Imperfecta - A Clinical Update. *Metabolism* 80, 27–37. doi:10.1016/j.metabol.2017.06.001

Trapnell, C., Roberts, A., Goff, L., Pertea, G., Kim, D., Kelley, D. R., et al. (2012). Differential Gene and Transcript Expression Analysis of RNA-Seq Experiments with TopHat and Cufflinks. *Nat. Protoc.* 7, 562–578. doi:10.1038/nprot.2012.016

Tsang, K. Y., Chan, D., and Cheah, K. S. E. (2015). Fate of Growth Plate Hypertrophic Chondrocytes: Death or Lineage Extension? *Develop. Growth Differ.* 57, 179–192. doi:10.1111/dgd.12203

Van Dijk, F. S., and Sillence, D. O. (2014). Osteogenesis Imperfecta: Clinical Diagnosis, Nomenclature and Severity Assessment. *Am. J. Med. Genet.* 164, 1470–1481. doi:10.1002/ajmg.a.36545

van Dijk, F. S., Semler, O., Etich, J., Köhler, A., Jimenez-Estrada, J. A., Bravenboer, N., et al. (2020). Interaction between KDELR2 and HSP47 as a Key Determinant in Osteogenesis Imperfecta Caused by Bi-allelic Variants in KDELR2. *Am. J. Hum. Genet.* 107, 989–999. doi:10.1016/j.ajhg.2020.09.009

Wang, K., Li, M., and Hakonarson, H. (2010). ANNOVAR: Functional Annotation of Genetic Variants from High-Throughput Sequencing Data. *Nucleic Acids Res.* 38, e164. doi:10.1093/nar/gkq603

Xi, L., Zhang, H., and Zhang, Z.-L. (2021). Clinical and Genetic Analysis in 185 Chinese Probands of Osteogenesis Imperfecta. *J. Bone Miner Metab.* 39, 416–422. doi:10.1007/s00774-020-01163-5

Yang, L., Tsang, K. Y., Tang, H. C., Chan, D., and Cheah, K. S. E. (2014). Hypertrophic Chondrocytes Can Become Osteoblasts and Osteocytes in Endochondral Bone Formation. *Proc. Natl. Acad. Sci.* 111, 12097–12102. doi:10.1073/pnas.1302703111

Zeitlin, L., Rauch, F., Plotkin, H., and Glorieux, F. H. (2003). Height and Weight Development during Four Years of Therapy with Cyclical Intravenous Pamidronate in Children and Adolescents with Osteogenesis Imperfecta Types I, III, and IV. *Pediatrics* 111, 1030–1036. doi:10.1542/peds.111.5.1030

Zhang, X., Yang, M., Lin, L., Chen, P., Ma, K. T., Zhou, C. Y., et al. (2006). Runx2 Overexpression Enhances Osteoblastic Differentiation and Mineralization in Adipose - Derived Stem Cells *In Vitro* and *In Vivo*. *Calcif Tissue Int.* 79, 169–178. doi:10.1007/s00223-006-0083-6

Zhang, H., Yue, H., Wang, C., Hu, W., Gu, J., He, J., et al. (2016). Clinical Characteristics and the Identification of Novel Mutations of COL1A1 and COL1A2 in 61 Chinese Patients with Osteogenesis Imperfecta. *Mol. Med. Rep.* 14, 4918–4926. doi:10.3892/mmr.2016.5835

Zhytnik, L., Maasalu, K., Pashenko, A., Khmyzov, S., Reimann, E., Prans, E., et al. (2019). COL1A1/2 Pathogenic Variants and Phenotype Characteristics in Ukrainian Osteogenesis Imperfecta Patients. *Front. Genet.* 10, 722. doi:10.3389/fgene.2019.00722

Zhytnik, L., Maasalu, K., Reimand, T., Duy, B. H., Kõks, S., and Märtson, A. (2020). Inter- and Intrafamilial Phenotypic Variability in Individuals with Collagen-Related Osteogenesis Imperfecta. *Clin. Transl. Sci.* 13, 960–971. doi:10.1111/cts.12783

Zolezzi, F., Forlino, A., Mottes, M., Valli, M., Sensi, A., Calzolari, E., et al. (1995). A 931 + 2T → C Transition in One COL1A2 Allele Causes Exon 16 Skipping in PROα2(I) mRNA and Produces Moderately Severe OI. *Hum. Mutat.* 6, 268–271. doi:10.1002/humu.1380060315

Conflict of Interest: The authors declare that the research was conducted in the absence of any commercial or financial relationships that could be construed as a potential conflict of interest.

Publisher's Note: All claims expressed in this article are solely those of the authors and do not necessarily represent those of their affiliated organizations, or those of the publisher, the editors and the reviewers. Any product that may be evaluated in this article, or claim that may be made by its manufacturer, is not guaranteed or endorsed by the publisher.

frontiers in Genetics

ORIGINAL RESEARCH
published: 17 February 2022
doi: 10.3389/fgene.2022.792183

Identification of a Novel Missense Mutation of the *PHEX* Gene in a Large Chinese Family with X-Linked Hypophosphataemia

Yanting Yang[1,2,3†], *Yuanda Wang*[4†], *Ying Shen*[5], *Mohan Liu*[4], *Siyu Dai*[1,2,3], *Xiaodong Wang*[1,3*] *and Hongqian Liu*[1,2,3*]

[1]Department of Obstetrics and Gynecology, West China Second University Hospital, Sichuan University, Chengdu, China, [2]Medical Genetics Department/Prenatal Diagnostic Center, West China Second University Hospital, Sichuan University, Chengdu, China, [3]Key Laboratory of Birth Defects and Related Diseases of Women and Children, Ministry of Education, Sichuan University, Chengdu, China, [4]State Key Laboratory of Biotherapy and Cancer Center, Sichuan University, Chengdu, China, [5]Department of Obstetrics/Gynecology, Joint Laboratory of Reproductive Medicine (SCU-CUHK), Key Laboratory of Obstetric, Gynecologic and Pediatric Diseases and Birth Defects of Ministry of Education, West China Second University Hospital, Sichuan University, Chengdu, China

OPEN ACCESS

Edited by:
Yi Zhang,
Central South University, China

Reviewed by:
Wenhao Zhou,
Fudan University, China
Katja Stange,
Leibniz Institute for Farm Animal Biology (FBN), Germany

***Correspondence:**
Xiaodong Wang
wangxd_scu@sina.com
Hongqian Liu
hongqian.liu@163.com

[†]*These authors have contributed equally to this work*

Specialty section:
This article was submitted to Genetics of Common and Rare Diseases, a section of the journal Frontiers in Genetics

Received: *09 October 2021*
Accepted: *18 January 2022*
Published: *17 February 2022*

Citation:
Yang Y, Wang Y, Shen Y, Liu M, Dai S, Wang X and Liu H (2022) Identification of a Novel Missense Mutation of the PHEX Gene in a Large Chinese Family with X-Linked Hypophosphataemia. Front. Genet. 13:792183. doi: 10.3389/fgene.2022.792183

X-linked hypophosphataemia (XLH) is an X-linked dominant rare disease that refers to the most common hereditary hypophosphatemia (HH) caused by mutations in the phosphate-regulating endopeptidase homolog X-linked gene (*PHEX*; OMIM: * 300550). However, mutations that have already been reported cannot account for all cases of XLH. Extensive genetic analysis can thus be helpful for arriving at the diagnosis of XLH. Herein, we identified a novel heterozygous mutation of *PHEX* (NM_000444.5: c.1768G > A) in a large Chinese family with XLH by whole-exome sequencing (WES). In addition, the negative effect of this mutation in *PHEX* was confirmed by both bioinformatics analysis and *in vitro* experimentation. The three-dimensional protein-model analysis predicted that this mutation might impair normal zinc binding. Immunofluorescence staining, qPCR, and western blotting analysis confirmed that the mutation we detected attenuated PHEX protein expression. The heterozygous mutation of *PHEX* (NM_000444.5: c.1768G > A) identified in this study by genetic and functional experiments constitutes a novel genetic cause of XLH, but further study will be required to expand its use in clinical and molecular diagnoses of XLH.

Keywords: X-linked hypophosphatamia (XLH), phosphate-regulating endopeptidase homolog X-linked gene (PHEX), whole-exome sequencing (WES), gene mutations, functional experiments

INTRODUCTION

Hereditary hypophosphataemia (HH) is a type of congenital disease of the phosphate-regulating homeostatic system, including phosphate-metabolism disorder and decreased renal tubular phosphate reabsorption. Thus, HH can cause rickets and osteomalacia in hypophosphataemic rickets (HR) (Carpenter, 2012). HR can be classified as FGF23-associated and non-associated, and HR is also subdivided into several forms, including X-linked hypophosphataemia (XLH), autosomal dominant hypophosphataemic rickets (ADHR), autosomal recessive hypophosphataemia (ARHR), and hereditary hypophosphataemic rickets with hypercalciuria (HHRH). Among these, X-linked hypophosphataemia (XLH) is considered the most common form of FGF23-related, inherited HR

(Marcucci and Brandi, 2021; Quarles, 2012). XLH is an X-linked dominant monogenic rare disease caused by mutations in the phosphate-regulating endopeptidase homolog X-linked gene (*PHEX*; OMIM:* 300550), with an incidence of 3.9/100,000 live births and a prevalence ranging from 1.7/100,000 children to 4.8/100,000 individuals (children and adults) (Beck-Nielsen et al., 2009; Endo et al., 2015; Rafaelsen et al., 2016). The representative features of this disease are hypophosphataemia, diminished synthesis of active vitamin D (1,25 $[OH]_2$ vitamin D), rickets, osteomalacia, odontomalacia, and disproportionately short stature (Haffner et al., 2019).

Individuals affected by XLH present a prominent bowing of the legs and short stature at a very early age, and up to 2/3 of children with XLH require surgical intervention (Gizard et al., 2017; Kocaoglu et al., 2011; Matsubara et al., 2008; Sharkey et al., 2015). As for affected adults, bone deformity, enthesopathy, dental abscesses, arthritis, and severe osteomalacia limit quality of life and require medical treatment for an entire lifetime (Sharkey et al., 2015). However, no studies have suggested that XLH is involved in the life expectancy of the affected individuals. The standardized treatment promotes growth, reduces bone pain, and improves dental health, eventually correcting leg deformities (Sochett et al., 2004). Early treatment augurs superior outcomes (Biosse Duplan et al., 2017; Connor et al., 2015; Mäkitie et al., 2003), and thus making appropriate early and timely diagnosis invaluable. Further, effective prenatal diagnosis of XLH is critical for optimizing a management strategy concerning affected neonates. The diagnosis of XLH depends upon genetic analysis and remains challenging (Haffner et al., 2019). There were 965 mutations of *PHEX* are listed in the Clinvar database (www.ncbi.nlm.nih.gov/clinvar), and approximately 68% of these are pathogenic or likely to be pathogenic. However, current reported mutations cannot account for all XLH cases (Lal et al., 2016; Ma et al., 2015; Zhang et al., 2019; Lin X et al., 2021), and extensive genetic analysis can therefore be helpful in achieving a diagnosis of XLH.

In the present study, we investigated a large Chinese family with XLH and detected a novel missense heterozygous mutation in the *PHEX* gene (NM_000444.5: c.1768G > A) by using whole-exome sequencing (WES), and this mutation was predicted to change glycine to serine at position 590 (p. G590S). We also substantiated the negative effect of this mutation with bioinformatics analysis and *in vitro* experimentation. Our findings broaden the spectrum of pathogenic *PHEX* mutations related to XLH and provide novel molecular evidence to allow the proper diagnosis of XLH.

MATERIALS AND METHODS

Study Participants

The proband, a 32-year-old woman manifested XLH was enrolled at the Medical Genetics/Prenatal Diagnosis Centre of the West China Second University Hospital, Sichuan University, Chengdu, China; and we also recruited all her family members. The control group was comprised of 200 unrelated normal Han Chinese. This study was approved by the Ethical Review Board of West China Second University Hospital, Sichuan University, and informed consent was obtained from each subject or her/his guardian(s) in the case of underaged participants.

Physical and X-ray examinations were performed by specialist physicians and radiologists, respectively, and family history was acquired by doctors from the Genetic Consulting Center. Biomedical and hormonal indices were evaluated at the West China University Hospital and West China Second University Hospital of Sichuan University's Clinical Laboratory Center. The level of electrolyte was detected by the ion-selective electrode (ISE) tests with an electrolyte analyzer (Xun-Da Medical Instrument Corporation). The level of Vit D3 and parathyroid hormone (PTH) was detected by ElectroChemiLuminescence (ECL) technology with Cobas automatic analyzer (Roche) and reagent provided by Roche. As for alkaline phosphatase (ALP), we performed the rate method by automatic chemistry analyzer (Beckman Coulter).

Genetic Studies

WES was executed using patient DNA as follows. We collected genomic DNA from peripheral blood samples using the FitAmp Plasma/Serum DNA Isolation Kit (Epigentek Exon), implemented exon capture by the SureSelect Human All Exon V6 Kit (Agilent), and sequenced DNA through the HiSeq X system (Illumina). ANNOVAR was applied for functional annotation and the 1,000 Genomes Project, HGMD, dbSNP, and ExAC were used to filter the data.

We identified candidate pathogenic variants with respect to the patient via Sanger sequencing of the DNA from the family members as well as the normal controls. PCR reaction was performed using Golden Star T6 Super PCR Mix (TSINGKE) in a thermal cycle with an initial denaturation step of 1 min at 98°C followed by 34 cycles of 98°C for 1 min, 60°C for 15 s, and 72°C for 1 min. At the end of the thermal cycling, the reaction was a final extension at 72°C for 1 min and then immediately placed on ice. PCR reactions were amplified with the ProFlex PCR System (Thermo Fisher). We conducted sequencing of PCR products on an ABI377A DNA sequencer (Applied Biosystems). The primers of *PHEX* (NM_000444.5) we used for PCR were F, 5′ CGAAATACCCATACCAATAAGC 3′; and R, 5′ CATCACAGCAAGACACGGT 3'.

Bioinformatics Analysis

To confirm the conservation of amino acid substitutions in the process of species evolution, the typical protein sequences from several different species were aligned using Clustal Omega (https://www.ebi.ac.uk/Tools/msa/clustalo/) to compare mutated positions with conserved domains. We analyzed these species: Homo sapiens (P78562), *Pan troglodytes* (H2QYE4), *Macaca mulatta* (F7HFQ1), *Canis lupus* (E2RDB0), *Bos taurus* (E1BKS5), *Mus musculus* (P70669), *Rattus norvegicus* (O35812), *Gallus* (E1BR88), *Danio rerio* (A4QP66) and *Xenopus tropicalis* (A0A6I8RG47) from Uniprot (www.uniprot.org). And we got the structure prediction of wild-type of PHEX protein from the Alphafold databased (Jumper et al., 2021; Varadi et al., 2021). The PyMOL Viewer software was used to generate the mutant

PHEX protein and visualize the effects of altered residues on protein-structure models.

Cell Culture and Immunofluorescence Staining

HeLa cells were obtained from the American Type Culture Collection (ATCC®). HeLa cells were grown in DMEM (Thermo Fisher) supplemented with 10% FBS (Gibco) and 1% penicillin-streptomycin (Thermo Fisher) in a humidified 5% CO2 incubator at 37°C. The expression plasmids encoding WT-*PHEX* (His-flag-tagged wild-type human *PHEX*) and mutated-*PHEX* (His-flag-tagged human mutant *PHEX* with c.1768G > A) were constructed by Vigene Biosciences company. HeLa cells were dispensed in a 6-well plastic dish containing 2 ml of fresh DMEM supplemented with 10% FBS and 1% penicillin-streptomycin at passage 3. The cells were then transfected with expressing plasmids using Lipofectamine 3,000 (Invitrogen). And we used pCMS-EGFP plasmid (Vigene Biosciences) as our positive control. For each well of a 6-well dish, 2.5 μg plasmid DNA, 5 μL of P3000 Reagent, 3.75 μL of Lipofectamine 3,000 reagent, and 250 μL of OptiMEM (Gibco) were used. After 6 h, 1 ml of fresh DMEM with 10% FBS and 1% penicillin-streptomycin was added to each well. The intense fluorescence of the GFP tag validates the transfection efficiency. Three independent transfection experiments were performed.

Cell slides with transfected cells were fixed in 4% paraformaldehyde (Sangon Biotech), permeabilized with 0.3% Triton X-100 (Beyotime), and blocked with 5% BSA (Thermo Fisher); the cell-mounted slides were then incubated with primary antibody at 4°C for 12 h. Triton and BSA dissolve in 1xPBS (Thermo Fisher). The primary antibody used was anti-Flag (1:100; ABclonal; mouse). The next day, the slides were washed three times with 1 × PBS, incubated with DyLight 594-labeled secondary antibody (1:800; Thermo Fisher; mouse) for 1 h at 25°C, and then counterstained with 4,6-diamidino-2-phenylindole (DAPI, Sigma-Aldrich) to label nuclei. Images were obtained by a laser scanning confocal microscope (Olympus FV3000). All images were captured under the same setting (brightness:0.00; contract: 0.00; gamma: 1.00). Three independent IF staining were performed.

RNA Extraction and Quantitative Real-Time PCR

We transiently transfected expression plasmids encoding WT-*PHEX* (His-flag-tagged wild-type human *PHEX*) and mutated-*PHEX* (His-flag-tagged human mutant *PHEX* with c.1768G > A) into HeLa cells just as we mentioned previously using Lipofectamine 3,000 (Invitrogen). RNA from cultured HeLa cells was collected after 24 h of transfection. We used 1 ml Trizol (Thermo Fisher) to solubilize the cells for 5 min at room temperature and added 0.2 ml chloroform (Avantor) to promote phase separation for 2–3 min at room temperature. After centrifuging at 10,000 g for 10 min, the upper clear phase was added 0.5 ml isopropanol (Chron Chemicals) for 10 min to precipitate. We collected the precipitated RNA by centrifugation at 10,000 g for 10 min at 4°C. The precipitated RNA was re-extracted by phenol (Chron Chemicals) after resuspension. Finally, the RNA was re-precipitated with 75% ethanol (Rio et al., 2010). And the concentration and purity of the RNA were determined with a NanoDrop 2000 (Thermo Company). In our study, the OD260/OD280 of RNA showed mean values about 1.98.

We performed reverse-transcription to obtain cDNA using Hiscript III Reverse transcriptase (Vazyme), and qPCR was accomplished using Green Premix Ex Taq II (Tli RNase H Plus) (Takara Biomedical Technology) in a StepOnePlus™ Real-Time PCR System with Tower (Applied Biosystems). The PCR conditions were 40 cycles of denaturation at 95°C for 5 s and annealing at 60°C for 30 s. We analyzed results using the $E^{-\Delta\Delta CT}$ method, with the expression of *GAPDH* (NM_001289746.2) serving as a reference gene. Each reaction was repeated three times. The primers for quantitative real-time PCR (qPCR) of *PHEX* (NM_000444.5) were as follows: F, 5′ GAAGCCTTTCTT TTGGGGA 3′; and R, 5′ ATGCCTCTGTTCATCGTGG 3′. And the primers of *GAPDH* (NM_001289746.2) were as follows: F, 5′ ACGGATTTGGTCGTATTGGG 3′; and R, 5′ CGCTCCTGG AAGATGGTGAT 3′. The efficiency of amplification curves was analyzed using LinRegPCR software. Three independent qPCR assays were performed.

Western Blotting Analysis

We transiently transfected expression plasmids encoding WT-*PHEX* (His-flag-tagged wild-type human *PHEX*) and mutated-*PHEX* (His-flag-tagged human mutant *PHEX* with c.1768G > A) into HeLa cells as we mentioned previously by Lipofectamine 3,000 (Invitrogen). Proteins in the cultured HeLa cells were extracted using a universal protein extraction lysis buffer (Bioteke) containing a protease-inhibitor cocktail (Roche). After 30 min of lysis, we performed a centrifuge at 10000 g for 5 min and collected the clear upper layer. Denatured proteins were separated electrophoretically on 10% SDS-PAGE Gel (Epizyme) and transferred to a polyvinylidene difluoride (PVDF) membrane (Millipore) for immunoblot analysis. The primary antibodies that we used were anti-Flag (1:1,000, Abcam; mouse) and anti-GAPDH (1:5,000, Abcam; rabbit). Three independent western blotting analysis were performed.

Statistical Analysis

Statistical analyses were conducted using SPSS 17.0 software. All the data of biomedical and hormonal indices were presented as the means ± SD. Statistical significance between two groups was calculated using a nonparametric test. The level of significance was set at $p < 0.05$. And we used SEM as the error bars.

RESULTS

Characteristics of the Clinical Phenotype

The proband (IV-2) presented to our hospital with short height (143 cm), genu varum, a waddling gait, and obvious family history. The proband's grandmother (II-2), mother (III-2), and elder sister (IV-3) also exhibited these same phenotypes. The

FIGURE 1 | Phenotype and X-ray autoradiographs of the family. **(A)** Clinical phenotype of the affected individuals in the family. The patients present with short stature and obviously bowed legs. **(B)** The radiographs of the lower limbs of the patients show varying degrees of genu varum and osteoarthritis, with osteophytes on the joint margins (indicated by arrows. hips, red; keens, blue; ankles, yellow). **(C)** Patient II-2 exhibits severe joint deformity of both hands and feet due to the lack of earlier treatment.

proband (IV-2) had already given birth to a girl (V-1) who showed leg bowing at a very early stage. And the girl (V-1) died of an unknown cause at 1 year old. The proband's grandmother (II-2) was 80 at the time and showed unexplained rickets during childhood, without receiving any medication. Patient II-2's height was 125 cm, with obvious bowing of her legs. In her young adult years, she performed simple farm work but demonstrated a waddling gait. She gradually manifested difficulty in walking and progressive bone pain. And due to a lack of appropriate treatment, the joints of both her hands and feet showed obvious deformities (**Figure 1C**). The proband's mother (III-2) was at the time 55 years of age and 152 cm tall, and similar to patient II-2 exhibited short stature, genu varum, and difficulty moving; but received oral calcium supplementation at approximately 40 years of age. She can still perform simple tasks with occasional bone pain. The proband's elder sister (IV-3) who achieved a height of 137 cm also showed the aforementioned signs and bore a boy (V-2) who shows no signs of rickets or osteomalacia. Of note, with advances in medicine, both the proband and patient IV-3 received not only oral treatment but also surgical limb correction (tibial osteotomy) during puberty; however, patient IV-3 still shows overt leg bowing (**Figure 1A**). Compared with patient IV-3, the proband manifests a more favorable lower-limb appearance, but still shows a waddling gait (**Figure 1A**). None of our patients showed specific syndromic facial features, and none exhibited dental diseases or complained of recurrent fractures.

TABLE 1 | Clinical and biochemical features of the family under study.

Patient	II-2	III-2	IV-2	IV-3	Reference range
Gender	F	F	F	F	—
Age(y)	78	55	26	33	—
Height (cm)	125	151	143	137	—
Phosphate (mmol/L)	0.681 ± 0.002	0.73 ± 0.004	0.63 ± 0.003	0.72 ± 0.004	0.085–1.51 mmol/L
Calcium (mmol/L)	2.292 ± 0.068	2.183 ± 0.101	2.329 ± 0.135	2.217 ± 0.105	2.11–2.52 mmol/L
Vit D3 (ng/ml)	8.067 ± 0.569	13.793±	16.797 ± 0.166	8.730 ± 0.115	30–100 ng/ml
ALP (U/L)	173.320 ± 5.457	118.10 ± 8.805	120.013 ± 8.993	93.857 ± 6.692	35–100 mmol/L
PTH (ng/L)	50.579 ± 2.384	18.093 ± 1.500	11.08 ± 1.037	14.836 ± 0.646	1.60–6.90 pmol/L

ALP, alkaline phosphatase; PTH, parathyroid hormone.

To investigate the cause of their symptoms, the patients underwent X-ray examinations. The results revealed short stature with varying degrees of genu varum (**Figure 1B**). The radiographs also showed varying degrees of osteoarthritis—with the osteophytes on the joint margins included in the hips, knees, and ankles. These results are consistent with typical radiographic features in adults with XLH (**Figure 1B**). Due to the lack of early treatment, patient II-2's radiograph shows severe osteoarthritis in both hips, knees, and ankles, with obviously narrowed articular cavities (**Figure 1B**). Biochemical tests depicted a low level of serum phosphate in all patients, and in patient II-2, patient III-2, and in the proband (VI-2), this was combined with elevated alkaline phosphatase (ALP); the level of serum parathyroid hormone (PTH) was concomitantly above normal in all patients (**Table 1**). These results were consistent with the diagnosis of XLH. In contrast to rickets, which was secondary to vitamin D or calcium deficiency, all the patients exhibited normal concentrations of calcium and vitamin D3 (**Table 1**). Based on these findings, these patients were diagnosed with XLH. However, we nevertheless recommend genetic analysis, particularly with respect to a mutation in *PHEX* (Haffner et al., 2019).

Identification of a Heterozygous c.1768G > A Mutation of *PHEX* in Patients With X-Linked Hypophosphataemia

To elucidate the genetic cause of HH in this family, we performed WES on all affected individuals. We removed variants if the following conditions were met: (a) the minor allele frequency was greater than or equal to 1% in ExAC Browser, gnomAD, or the 1,000 Genome Projects—considering that pathogenic variants that cause XLH are rare in humans; (b) the variant was not predicted to be deleterious by SIFT, PolyPhen-2, or MutationTaster tools; and (c) the variant was in noncoding exons, 3′- or 5′-untranslated regions, or intronic sequences—except for canonical splice sites. Surprisingly, a heterozygous mutation in *PHEX* (NM_000444.5: c.1768G > A) was screened, which is the known causative gene for XLH. To confirm the mutation's distribution in this family, we assessed this mutation in all family members by Sanger sequencing, including four patients and six unaffected members (**Figure 2A**). All patients harbored this mutation, while other members were identified as wild type (**Figure 2B**). Furthermore, we did not find this mutation in 200 normal controls, which also supported that this mutation might be the genetic cause of this family.

The Heterozygous c.1768G > A Mutation of *PHEX* Impairs Its Expression

For a deeper appreciation of the mutation that we identified in *PHEX*, we performed a relative bioinformatics analysis. Protein-conservation analysis first showed that position 590 was highly conserved among many species (**Figure 3A**), suggesting that this region might be vital for protein function. Based on the structure prediction of wild-type PHEX from the Alphafold database (Jumper et al., 2021; Varadi et al., 2021), we generated three-dimensional protein models of the mutant protein. This single nucleotide mutation was predicted to change the glycine to serine at position 590. Importantly, the glycine in the wild-type protein was predicted to form two polar contacts, whereas the changed serine in the variant was predicted to form three contacts with surrounding residues—adding one with histidine (p.584) (a putative zinc-binding site (Rowe et al., 2005)) (**Figure 3B**). We assumed that the altered polar contact of the putative zinc-binding site may thus lead to abnormal zinc binding.

To further elucidate the damaging effects of *PHEX* mutation on its expression, the WT-*PHEX* (His-flag-tagged wild-type human *PHEX*) and mutated-*PHEX* (His-flag-tagged human mutant *PHEX* with c.1768G > A) plasmids were transiently transfected into HeLa cells respectively. Analysis of immunofluorescence staining showed that PHEX was visibly expressed in the plasma membrane of HeLa cells transfected with WT-*PHEX* plasmid, while PHEX staining was only marginally detectable in the plasma membrane of cells that overexpressed mutated-*PHEX* plasmid (**Figure 3C**). To investigate this mutation affection in detail, we transfected plasmid in HeLa cells and collected RNA. Through qPCR detection, our results show a sharply attenuated mRNA level of the mutation compared to the wild type (**Figure 3D**). We also demonstrated the mutation's potential deleteriousness by using western blotting analysis and uncovered consistently reduced expression of the protein (**Figure 3E**).

Thus, the novel heterozygous mutation in *PHEX* (NM_000444.5: c.1768G > A) causing the impaired function of PHEX protein might be associated with the abnormal protein structure of zinc binding and the decreased transcription level. These data together strongly suggest that the novel heterozygous mutation c.1768G > A in *PHEX* might be the genetic cause of XLH in this family.

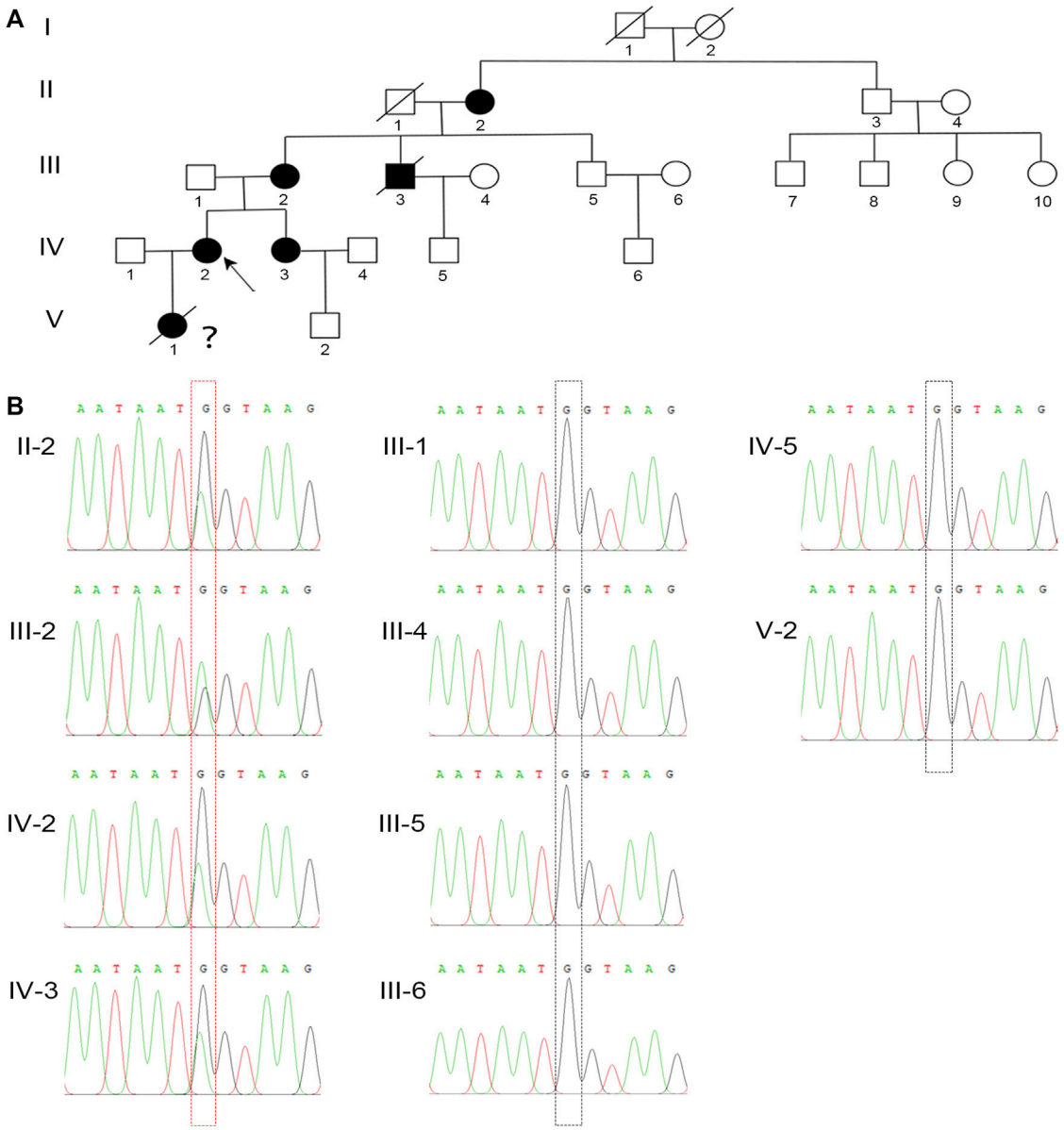

FIGURE 2 | A novel missense mutation in *PHEX* was detected in the XLH family. **(A)** The family pedigree of this XLH family. The black circles and square show the affected individuals with XLH, and the proband is indicated by the black arrow. Because of the lack of clinical and genetic analyses, the diagnosis and genotype of V-1 are uncertain, which is indicated by a question mark. **(B)** Sanger sequencing confirmed a heterozygous G-to-A transversion at nucleotide c.1768 (red dotted box) of the *PHEX* gene in all XLH patients in this family, while the unaffected individuals were identified as wild type (black dotted box).

DISCUSSION

XLH—an X-linked dominant monogenic disorder—is the most common form of hereditary hypophosphataemia, representing approximately 80% of all hypophosphataemic rickets (Guven et al., 2017; Holm et al., 2001; Ruppe et al., 2011). In our study, we identified a novel heterozygous mutation in *PHEX* (NM_000444.6 c.1768G > A) in a large Chinese family. This missense mutation was predicted to cause an abnormal polar contact with a putative zinc-binding site, thus might cause abnormal zinc binding by PHEX protein (Jumper et al., 2021; Varadi et al., 2021). Meanwhile, western blotting showed that this novel mutation resulted in the diminished expression of PHEX. Therefore, we suggested that this heterozygous mutation we found in *PHEX* (NM_000444.6 c.1768G > A) might be the genetic cause of XLH in this family.

In previous studies, 50% of the missense mutations in the *PHEX* have been suggested to be associated with protein trafficking/localization (Sabbagh et al., 2003). Some researchers supposed that these missense mutations cause misfolding and retention of the mutant PHEX protein in the endoplasmic reticulum (ER) resulting from the unsuccessful PHEX protein

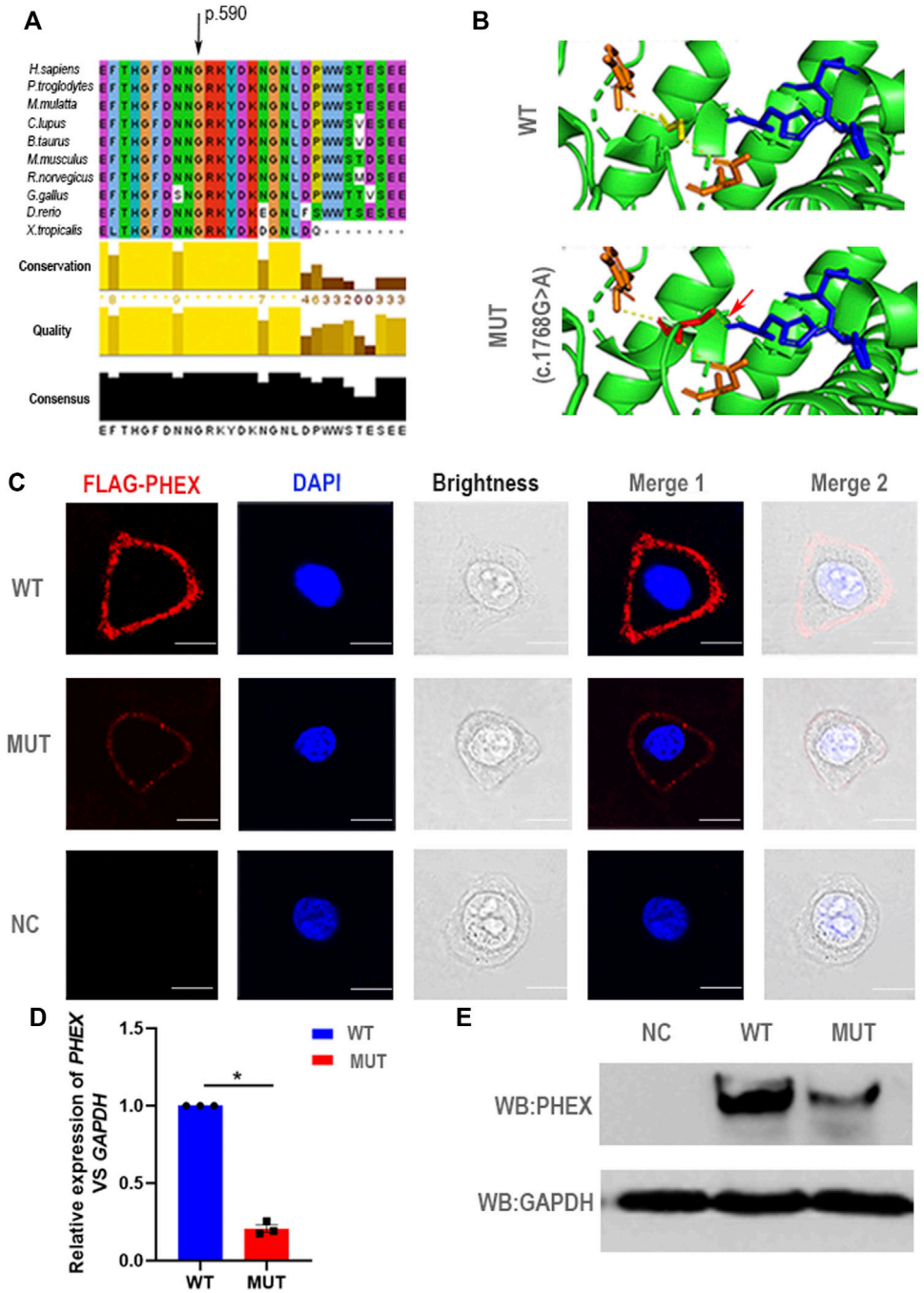

FIGURE 3 | Negative effect of the novel mutation in *PHEX*. **(A)** The mutant position we detected is highly conserved among many species. **(B)** Structural illustration of the missense mutation in *PHEX*. The mutation site in the wild-type PHEX protein model (WT) and mutant PHEX protein model (MUT) are shown as sticks and highlighted in yellow and red. The interrelated putative zinc-binding sites are also represented by sticks and colored in blue. The polar contacts of the target residues are shown as yellow dashed lines, and relative amino acids are shown as orange sticks. In the wild-type protein, Gly590 forms two polar contacts predicted by PyMOL; while in the mutant protein, Ser590 forms three polar contacts due to the addition of one polar contact with His584 that was deemed to be a zinc-binding site predicted by PyMOL. **(C)** The immunofluorescent distribution of PHEX protein. The decline expression level of PHEX protein was noted using immunofluorescence staining of HeLa cells transfected with mutant-*PHEX* plasmid compared to cells transfected with WT-*PHEX* plasmid (red, FLAG-PHEX; blue, DAPI). Scale bars represent 10 μm. Three independent experiments were performed. **(D)** Using qPCR, we observed that *PHEX* mRNA expression levels in the cultured HeLa cells transfected with mutant-*PHEX* plasmid were sharply attenuated compared to the cells transfected with WT-*PHEX* plasmid. (nonparametric test; $*p < 0.05$; error bars, s.e.m.). Three independent experiments were performed. **(E)** The western blotting results showed that PHEX protein was scarcely detectable in HeLa cells transfected with mutant-*PHEX* plasmid compared with the cells transfected with WT-*PHEX* plasmid. Three independent experiments were performed.

trafficking/localization. In our study, we also found a novel missense mutation in *PHEX* (NM_000444.6 c.1768G > A). However, we detected this missense mutation could reduce the PHEX expression, and did not change the localization of PHEX protein in HeLa cells. According to the mutant three-dimensional protein model predicted by PyMOL, this mutation causes an abnormal polar contact with a putative zinc-binding site without misfolding and retention (Jumper et al., 2021; Varadi et al., 2021). While the mechanism needs more study in the future.

In 1995, a phosphate-regulating gene with sequence identity like endopeptidases (*PHEX*) was for the first time described as the direct genetic cause of XLH (The HYP Consortium 1995). *PHEX* encodes a cell-surface-bound protein-cleavage enzyme PHEX that consists of a short amino terminal cytoplasmic domain, a single transmembrane domain, and a large extracellular domain containing a zinc-binding motif and conserved cysteine residues (Sabbagh et al., 2001). Due to a sequence identity similar to that of the neutral endopeptidases, PHEX is regarded as a regulating factor in phosphate homeostasis (Amatschek et al., 2010). The deletion of *PHEX* contributed to the enhanced secretion of fibroblast growth factor 23 (FGF23) in mice (Hyp mouse), thus occupying a critical role in the complicated secretory network, further affecting the regulation of systemic phosphate homeostasis and vitamin D metabolism (Itoh and Ornitz, 2008; Liu Z et al., 2006). The excessive level of FGF23 noted in hypophosphataemia was then shown to suppress 1,25-dihydroxyvitamin D levels and induce rickets or osteomalacia in humans and mice (Bai et al., 2004; Fukumoto and Yamashita., 2002; Shimada et al., 2001,2005).

Inactivating mutations of *PHEX* results in increased circulating and intact FGF23, which ultimately causes HH disorders and defections in bone mineralization in humans and other mammals (Bai et al., 2016; Liu T et al., 2006; Murali et al., 2016; Quarles, 2008; Quarles, 2012; Yuan et al., 2008). Unfortunately, because of the situation of COVID-19, our patients reject to come to our hospital again. We didn't get complete the FGF-23 levels in our patients. But functions of FGF23 have been elaborated clearly, with studies illustrating the resorptive regulation of phosphate and the production as well as catabolism of 1,25-dihydroxyvitamin D and the expression of α-Klotho; the latter is an anti-aging hormone that principally acts on the kidney (Liu T et al., 2006; Quarles, 2008; Quarles, 2012; Yuan et al., 2008). Although these functions reflect the plethora of manifestations of XLH, the molecular mechanisms underlying the mutations in *PHEX* that lead to the elevated secretion of FGF23 and the inherent functions of PHEX are still unclear. PHEX is hypothesized to be the protease responsible for the cleavage and corresponding inactivation of FGF23 due to its high sequence identity relative to other endopeptidases. And while some investigators have shown that FGF-23 is a PHEX substrate (Bowe et al., 2001; Campos et al., 2003), others suggest that FGF23 is not a direct PHEX substrate and cannot demonstrate PHEX-dependent cleavage of FGF-23 *in vitro* (Guo et al., 2001; Liu et al., 2003; Quarles and Drezner, 2001). In fact, an animal study indicated that *Phex* mutations led to elevated FGF-23 levels due to increased transcription of the *Fgf23* gene in osteoblasts and osteocytes (Quarles and Drezner, 2001). Thus, one hypothesis posits the existence of an intermediate pathway between PHEX and FGF-23 that augments FGF-23 levels, leading to phosphaturia and hypophosphataemia; but this assertion requires further study.

Besides, the diagnosis of XLH remains challenging. Previous reports show that XLH, ADHR, and ARHR possess similar clinical features and even reflect similar biochemical characteristics. While the genetic causes of XLH (*PHEX*), ADHR (*FGF23*), and ARHR (*DMP1* and *ENPP1*) have already been clearly described, there remain vast differences in their respective inheritance patterns and underlying pathogenesis (Liu T et al., 2006; Quarles, 2008; Quarles, 2012; Rafaelsen et al., 2016; Yuan et al., 2008). In addition, the physical manifestations may also be misdiagnosed as metaphyseal dysplasia, nutritional rickets, or physiological bowing (Carpenter et al., 2011). Therefore, it is necessary to clinically differentiate the disease cause before commencing treatment and genetic counseling, and genetic analysis is essential for the proper diagnosis of XLH (Saito et al., 2009). As soon as the diagnosis is established, it is recommended to initiate a combination of oral phosphorus (phosphate salts) and active vitamin D (calcitriol or alfacalcidol) for the treatment of children with XLH (Haffner et al., 2019). For symptomatic adults, the clinical recommendation is also the combination of oral treatment to reduce the incidence of osteomalacia and its consequences, and to improve dental health (Haffner et al., 2019); as increased calciuria and even nephrocalcinosis are reported in 30–70% of patients undergoing conventional treatment (Eddy et al., 1997; Goodyer et al., 1987; Keskin et al., 2015). Examples of conventional treatment are the orthopedic procedures usually used to correct deformities and to treat pathological fractures; and surgery is still associated with a high risk for recurrence of limb deformities, particularly prior to puberty (Gizard et al., 2017). Based upon the adverse effects tied to current treatment—and although favorable outcomes can result from appropriate early intervention—affected patients still confront clinical problems even with formal treatment. Thus, timely diagnosis and prenatal diagnosis are extremely valuable.

CONCLUSIONS

In summary, although the specific mechanisms underlying mutations in *PHEX* that resulted in XLH still require further exploration, our findings expand the genetic and molecular evidence with respect to proper clinical and prenatal diagnosis of XLH. We also acknowledge that genetic analysis can play a critical role in XLH diagnosis and prognosis, thus providing additional beneficial knowledge related to genetic counseling.

DATA AVAILABILITY STATEMENT

The datasets for this article are not publicly available due to concerns regarding participant/patient anonymity. Requests to access the datasets should be directed to the corresponding authors.

ETHICS STATEMENT

The studies involving human participants were reviewed and approved by the Ethical Review Board of West China Second University Hospital, Sichuan University. Written informed consent to participate in this study was provided by the participants' legal guardian/next of kin. Written informed consent was obtained from the individual(s) for the publication of any potentially identifiable images or data included in this article.

AUTHOR CONTRIBUTIONS

HL and XW designed and supervised the study experiments. YY wrote the first article draft and performed Immunofluorescence staining, qPCR, and western blotting analysis. YW performed the protein-conservation analysis and three-dimensional protein-model analysis. YS, ML, SD collected data and conducted the clinical evaluations. All authors revised and approved the article.

FUNDING

This work was supported by the Science and Technology Department of Sichuan Province (2021YFS0207) and the Health Commission of Sichuan Province (20PJ073).

ACKNOWLEDGMENTS

We thank the patient and her family for their interest and cooperation.

REFERENCES

Amatschek, S., Haller, M., and Oberbauer, R. (2010). Renal Phosphate Handling in Human - what Can We Learn from Hereditary Hypophosphataemias. *Eur. J. Clin. Invest.* 40 (6), 552–560. doi:10.1111/j.1365-2362.2010.02286.x

Bai, X., Miao, D., Li, J., Goltzman, D., and Karaplis, A. C. (2004). Transgenic Mice Overexpressing Human Fibroblast Growth Factor 23 (R176q) Delineate a Putative Role for Parathyroid Hormone in Renal Phosphate Wasting Disorders. *Endocrinology* 145 (11), 5269–5279. doi:10.1210/en.2004-0233

Bai, X., Miao, D., Xiao, S., Qiu, D., St-Arnaud, R., Petkovich, M., et al. (2016). Cyp24 Inhibition as a Therapeutic Target in Fgf23-Mediated Renal Phosphate Wasting Disorders. *J. Clin. Invest.* 126 (2), 667–680. doi:10.1172/JCI81928

Beck-Nielsen, S. S., Brock-Jacobsen, B., Gram, J., Brixen, K., and Jensen, T. K. (2009). Incidence and Prevalence of Nutritional and Hereditary Rickets in Southern denmark. *Eur. J. Endocrinol.* 160 (3), 491–497. doi:10.1530/EJE-08-0818

Biosse Duplan, M., Coyac, B. R., Bardet, C., Zadikian, C., Rothenbuhler, A., Kamenicky, P., et al. (2017). Phosphate and Vitamin D Prevent Periodontitis in X-Linked Hypophosphatemia. *J. Dent. Res.* 96 (4), 388–395. doi:10.1177/0022034516677528

Bowe, A. E., Finnegan, R., Jan De Beur, S. M., Cho, J., Levine, M. A., Kumar, R., et al. (2001). Fgf-23 Inhibits Renal Tubular Phosphate Transport and Is a Phex Substrate. *Biochem. Biophysical Res. Commun.* 284 (4), 977–981. doi:10.1006/bbrc.2001.5084

Campos, M., Couture, C., Hirata, I. Y., Juliano, M. A., Loisel, T. P., Crine, P., et al. (2003). Human Recombinant Endopeptidase Phex Has a Strict S1' Specificity for Acidic Residues and Cleaves Peptides Derived from Fibroblast Growth Factor-23 and Matrix Extracellular phosphoglycoproteinResearch Support, Non-U.S. Gov't]. *[Journal Articlebiochem. J.* 373 (Pt 1), 271–279. doi:10.1042/BJ20030287

Carpenter, T. O., Imel, E. A., Holm, I. A., Jan De Beur, S. M., and Insogna, K. L. (2011). A Clinician's Guide to X-Linked Hypophosphatemia. *J. Bone Miner. Res.* 26 (7), 1381–1388. doi:10.1002/jbmr.340

Carpenter, T. O. (2012). The Expanding Family of Hypophosphatemic Syndromes. *J. Bone Miner. Metab.* 30 (1), 1–9. doi:10.1007/s00774-011-0340-2

Connor, J., Olear, E. A., Insogna, K. L., Katz, L., Baker, S., Kaur, R., et al. (2015). Conventional Therapy in Adults with X-Linked Hypophosphatemia: Effects on Enthesopathy and Dental Disease. *J. Clin. Endocrinol. Metab.* 100 (10), 3625–3632. doi:10.1210/JC.2015-2199

Eddy, M. C., McAlister, W. H., and Whyte, M. P. (1997). X-linked Hypophosphatemia: Normal Renal Function Despite Medullary Nephrocalcinosis 25 Years after Transient Vitamin D2-Induced Renal Azotemia. *Bone* 21 (6), 515–520. doi:10.1016/S8756-3282(97)00199-3

Endo, I., Fukumoto, S., Ozono, K., Namba, N., Inoue, D., Okazaki, R., et al. (2015). Nationwide Survey of Fibroblast Growth Factor 23 (Fgf23)-related Hypophosphatemic Diseases in japan: Prevalence, Biochemical Data and Treatment. *Endocr. J.* 62 (9), 811–816. doi:10.1507/endocrj.EJ15-0275

Fukumoto, S., and Yamashita, T. (2002). Fibroblast Growth Factor-23 Is the Phosphaturic Factor in Tumor-Induced Osteomalacia and May Be Phosphatonin. *Curr. Opin. Nephrol. Hypertens.* 11 (4), 385–389. doi:10.1097/00041552-200207000-00003

Gizard, A., Rothenbuhler, A., Pejin, Z., Finidori, G., Glorion, C., de Billy, B., et al. (2017). Outcomes of Orthopedic Surgery in a Cohort of 49 Patients with X-Linked Hypophosphatemic Rickets (Xlhr). *Endocr. Connections* 6 (8), 566–573. doi:10.1530/EC-17-0154

Goodyer, P. R., Kronick, J. B., Jequier, S., Reade, T. M., and Scriver, C. R. (1987). Nephrocalcinosis and its Relationship to Treatment of Hereditary Rickets. *J. Pediatr.* 111 (5), 700–704. doi:10.1016/s0022-3476(87)80245-7

Guo, R., Liu, S., Spurney, R. F., and Quarles, L. D. (2001). Analysis of Recombinant Phex: an Endopeptidase in Search of a substrate[Journal Article; Research Support. *Am. J. Physiology-Endocrinology Metab.* 281 (4), E837–E847.doi:10.1152/ajpendo.2001.281.4.e837

Guven, A., Al-Rijjal, R. A., BinEssa, H. A., Dogan, D., Kor, Y., Zou, M., et al. (2017). Mutational Analysis ofPHEX,FGF23andCLCN5in Patients with Hypophosphataemic Rickets. *Clin. Endocrinol.* 87 (1), 103–112. doi:10.1111/cen.13347

Haffner, D., Emma, F., Eastwood, D. M., Duplan, M. B., Bacchetta, J., Schnabel, D., et al. (2019). Clinical Practice Recommendations for the Diagnosis and Management of X-Linked Hypophosphataemia. *Nat. Rev. Nephrol.* 15 (7), 435–455. doi:10.1038/s41581-019-0152-5

Holm, I. A., Nelson, A. E., Robinson, B. G., Mason, R. S., Marsh, D. J., Cowell, C. T., et al. (2001). Mutational Analysis and Genotype-Phenotype Correlation of the Phex Gene in X-Linked Hypophosphatemic Rickets. *J. Clin. Endocrinol. Metab.* 86 (8), 3889–3899. doi:10.1210/jcem.86.8.7761

Itoh, N., and Ornitz, D. M. (2008). Functional Evolutionary History of the Mousefgf Gene Family. *Dev. Dyn.* 237 (1), 18–27. doi:10.1002/dvdy.21388

Jumper, J., Evans, R., Pritzel, A., Green, T., Figurnov, M., Ronneberger, O., et al. (2021). Highly Accurate Protein Structure Prediction with AlphaFold. *Nature* 596 (7873), 583–589. doi:10.1038/s41586-021-03819-2

Keskin, M., Savaş-Erdeve, Ş., Sağsak, E., Çetinkaya, S., and Aycan, Z. (2015). Risk Factors Affecting the Development of Nephrocalcinosis, the Most Common Complication of Hypophosphatemic Rickets. *J. Pediatr. Endocrinol. Metab.* 28 (11-12). doi:10.1515/jpem-2014-0447

Kocaoglu, M., Bilen, F. E., Sen, C., Eralp, L., and Balci, H. I. (2011). Combined Technique for the Correction of Lower-Limb Deformities Resulting from Metabolic Bone Disease. *The J. Bone Jt. Surg. Br. volumeBritish* 93-B (1), 52–56. doi:10.1302/0301-620x.93b1.24788

Lal, D., Neubauer, B. A., Toliat, M. R., Altmüller, J., Thiele, H., Nürnberg, P., et al. (2016). Increased Probability of Co-occurrence of Two Rare Diseases in Consanguineous Families and Resolution of a Complex Phenotype by Next Generation Sequencing. *PLoS One* 11 (1), e0146040. doi:10.1371/journal.pone.0146040

Lin, X., Li, S., Zhang, Z., and Yue, H. (2021). Clinical and Genetic Characteristics of 153 Chinese Patients with X-Linked Hypophosphatemia. *Front. Cel Dev. Biol.* 9, 617738. doi:10.3389/fcell.2021.617738

Liu, S., Guo, R., Simpson, L. G., Xiao, Z.-S., Burnham, C. E., and Quarles, L. D. (2003). Regulation of Fibroblastic Growth Factor 23 Expression but Not Degradation by Phex. *J. Biol. Chem.* 278 (39), 37419–37426. doi:10.1074/jbc.M304544200

Liu, S., Tang, W., Zhou, J., Stubbs, J. R., Luo, Q., Pi, M., et al. (2006). Fibroblast Growth Factor 23 Is a Counter-regulatory Phosphaturic Hormone for Vitamin D. *Jasn* 17 (5), 1305–1315. doi:10.1681/ASN.2005111185

Liu, S., Zhou, J., Tang, W., Jiang, X., Rowe, D. W., and Quarles, L. D. (2006). Pathogenic Role of Fgf23 in Hyp Mice. *Am. J. Physiology-Endocrinology Metab.* 291 (1), E38–E49. doi:10.1152/ajpendo.00008.2006

Ma, S. L., Vega-Warner, V., Gillies, C., Sampson, M. G., Kher, V., Sethi, S. K., et al. (2015). Whole Exome Sequencing Reveals Novel Phex Splice Site Mutations in Patients with Hypophosphatemic Rickets. *PLoS One* 10 (6), e0130729. doi:10.1371/journal.pone.0130729

Marcucci, G., and Brandi, M. L. (2021). Congenital Conditions of Hypophosphatemia Expressed in Adults. *Calcif Tissue Int.* 108 (1), 91–103. doi:10.1007/s00223-020-00695-2

Matsubara, H., Tsuchiya, H., Kabata, T., Sakurakichi, K., Watanabe, K., and Tomita, K. (2008). Deformity Correction for Vitamin D-Resistant Hypophosphatemic Rickets of Adults. *Arch. Orthop. Trauma Surg.* 128 (10), 1137–1143. doi:10.1007/s00402-007-0548-8

Mäkitie, O., Doria, A., Kooh, S. W., Cole, W. G., Daneman, A., and Sochett, E. (2003). Early Treatment Improves Growth and Biochemical and Radiographic Outcome in X-Linked Hypophosphatemic Rickets. *J. Clin. Endocrinol. Metab.* 88 (8), 3591–3597. doi:10.1210/jc.2003-030036

Murali, S. K., Andrukhova, O., Clinkenbeard, E. L., White, K. E., and Erben, R. G. (2016). Excessive Osteocytic Fgf23 Secretion Contributes to Pyrophosphate Accumulation and Mineralization Defect in Hyp Mice. *Plos Biol.* 14 (4), e1002427. doi:10.1371/journal.pbio.1002427

Quarles, L. D., and Drezner, M. K. (2001). Pathophysiology of X-Linked Hypophosphatemia, Tumor-Induced Osteomalacia, and Autosomal Dominant Hypophosphatemia: A PerPHEXing Problem. *J. Clin. Endocrinol. Metab.* 86 (2), 494–496. doi:10.1210/jcem.86.2.7302

Quarles, L. D., (2008). Endocrine Functions of Bone in mineral Metabolism regulationResearch Support. *[Journal Articlej. Clin. Invest.* 118 (12), 3820–3828. doi:10.1172/JCI36479

Quarles, L. D. (2012). Skeletal Secretion of FGF-23 Regulates Phosphate and Vitamin D Metabolism. *Nat. Rev. Endocrinol.* 8 (5), 276–286. doi:10.1038/nrendo.2011.218

Rafaelsen, S., Johansson, S., Ræder, H., and Bjerknes, R. (2016). Hereditary Hypophosphatemia in norway: a Retrospective Population-Based Study of Genotypes, Phenotypes, and Treatment complicationsResearch Support, Non-U.S. Gov't]. *[Journal Articleeur. J. Endocrinol.* 174 (2), 125–136. doi:10.1530/EJE-15-0515

Rio, D. C., Ares, M., Jr, Hannon, G. J., and Nilsen, T. W. (2010). Purification of RNA Using TRIzol (TRI Reagent). *Cold Spring Harb Protoc.* 2010 (6), pdb.doi:10.1101/pdb.prot5439

Rowe, P. S. N., Garrett, I. R., Schwarz, P. M., Carnes, D. L., Lafer, E. M., Mundy, G. R., et al. (2005). Surface Plasmon Resonance (SPR) Confirms that MEPE Binds to PHEX via the MEPE-ASARM Motif: a Model for Impaired Mineralization in X-Linked Rickets (HYP). *Bone* 36 (1), 33–46. doi:10.1016/j.bone.2004.09.015

Ruppe, M. D., Brosnan, P. G., Au, K. S., Tran, P. X., Dominguez, B. W., and Northrup, H. (2011). Mutational Analysis of Phex, Fgf23 and Dmp1 in a Cohort of Patients with Hypophosphatemic Rickets. *Clin. Endocrinol.* 74 (3), 312–318. doi:10.1111/j.1365-2265.2010.03919.x

Sabbagh, Y., Boileau, G., Campos, M., Carmona, A. K., and Tenenhouse, H. S. (2003). Structure and Function of Disease-Causing Missense Mutations in the *PHEX* Gene. *J.Clin.Endocr.Metab.* 88 (5), 2213–2222. doi:10.1210/jc.2002-021809

Sabbagh, Y., Boileau, G., DesGroseillers, L., and Tenenhouse, H. S. (2001). Disease-causing Missense Mutations in the Phex Gene Interfere with Membrane Targeting of the Recombinant proteinResearch Support, Non-U.S. Gov't]. *[Journal Articlehum. Mol. Genet.* 10 (15), 1539–1546. doi:10.1093/hmg/10.15.1539

Saito, T., Nishii, Y., Yasuda, T., Ito, N., Suzuki, H., Igarashi, T., et al. (2009). Familial Hypophosphatemic Rickets Caused by a Large Deletion in Phex Gene. *Eur. J. Endocrinol.* 161 (4), 647–651. doi:10.1530/EJE-09-0261

Sharkey, M. S., Grunseich, K., and Carpenter, T. O. (2015). Contemporary Medical and Surgical Management of X-Linked Hypophosphatemic Rickets. *J. Am. Acad. Orthopaedic Surgeons* 23 (7), 433–442. doi:10.5435/JAAOS-D-14-00082

Shimada, T., Mizutani, S., Muto, T., Yoneya, T., Hino, R., Takeda, S., et al. (2001). Cloning and Characterization of Fgf23 as a Causative Factor of Tumor-Induced Osteomalacia. *Proc. Natl. Acad. Sci.* 98 (11), 6500–6505. doi:10.1073/pnas.101545198

Shimada, T., Yamazaki, Y., Takahashi, M., Hasegawa, H., Urakawa, I., Oshima, T., et al. (2005). Vitamin D Receptor-independent Fgf23 Actions in Regulating Phosphate and Vitamin D Metabolism. *Am. J. Physiology-Renal Physiol.* 289 (5), F1088–F1095. doi:10.1152/ajprenal.00474.2004

Sochett, E., Doria, A. S., Henriques, F., Kooh, S. W., Daneman, A., and Mäkitie, O. (2004). Growth and Metabolic Control during Puberty in Girls with X-Linked Hypophosphataemic Rickets. *Horm. Res. Paediatr.* 61 (5), 252–256. doi:10.1159/000077401

The HYP Consortium (1995). A Gene (PEX) with Homologies to Endopeptidases Is Mutated in Patients with X-Linked Hypophosphatemic Rickets. The HYP Consortium. *Nat. Genet.* 11 (2), 130–136. doi:10.1038/ng1095-130

Varadi, M., Anyango, S., Deshpande, M., Nair, S., Natassia, C., Yordanova, G., et al. (2021). AlphaFold Protein Structure Database: Massively Expanding the Structural Coverage of Protein-Sequence Space with High-Accuracy Models. *Nucleic Acids Res.* 50, D439–D444. doi:10.1093/nar/gkab1061

Yuan, B., Takaiwa, M., Clemens, T. L., Feng, J. Q., Kumar, R., Rowe, P. S., et al. (2008). Aberrant Phex Function in Osteoblasts and Osteocytes Alone Underlies Murine X-Linked hypophosphatemia[Journal Article; Research Support. *J. Clin. Invest.* 118 (2), 722–734. doi:10.1172/JCI32702

Zhang, C., Zhao, Z., Sun, Y., Xu, L., JiaJue, R., Cui, L., et al. (2019). Clinical and Genetic Analysis in a Large Chinese Cohort of Patients with X-Linked Hypophosphatemia. *Bone* 121, 212–220. doi:10.1016/j.bone.2019.01.021

Conflict of Interest: The authors declare that the research was conducted in the absence of any commercial or financial relationships that could be construed as a potential conflict of interest.

Publisher's Note: All claims expressed in this article are solely those of the authors and do not necessarily represent those of their affiliated organizations, or those of the publisher, the editors and the reviewers. Any product that may be evaluated in this article, or claim that may be made by its manufacturer, is not guaranteed or endorsed by the publisher.

frontiers in Genetics

ORIGINAL RESEARCH
published: 10 March 2022
doi: 10.3389/fgene.2022.804202

Identification of Novel *FBN2* Variants in a Cohort of Congenital Contractural Arachnodactyly

Liying Sun[1†], Yingzhao Huang[2,3,4†], Sen Zhao[2,3,4†], Wenyao Zhong[1†], Jile Shi[2,3,4], Yang Guo[1], Junhui Zhao[1], Ge Xiong[1], Yuehan Yin[1], Zefu Chen[2,3,4], Nan Zhang[1], Zongxuan Zhao[1], Qingyang Li[1], Dan Chen[1], Yuchen Niu[3,5], Xiaoxin Li[3,5], Guixing Qiu[2,3,4], Zhihong Wu[3,4,5], Terry Jianguo Zhang[2,3,4], Wen Tian[1]* and Nan Wu[2,3,4]**

[1]Department of Hand Surgery, Clinical and Research Center for Congenital Hand Deformities and Rare Diseases, Beijing Jishuitan Hospital, Beijing, China, [2]Department of Orthopedic Surgery, State Key Laboratory of Complex Severe and Rare Diseases, Peking Union Medical College Hospital, Peking Union Medical College and Chinese Academy of Medical Sciences, Beijing, China, [3]Beijing Key Laboratory for Genetic Research of Skeletal Deformity, Beijing, China, [4]Key Laboratory of Big Data for Spinal Deformities, Chinese Academy of Medical Sciences, Beijing, China, [5]State Key Laboratory of Complex Severe and Rare Diseases, Medical Research Center, Peking Union Medical College Hospital, Peking Union Medical College and Chinese Academy of Medical Sciences, Beijing, China

OPEN ACCESS

Edited by:
Long Guo,
RIKEN Center for Integrative Medical Sciences, Japan

Reviewed by:
Bert Callewaert,
Ghent University, Belgium
Sacha Jensen,
James Cook University, Australia

***Correspondence:**
Terry Jianguo Zhang
jgzhang_pumch@yahoo.com
Wen Tian
wentianJST@163.com
Nan Wu
dr.wunan@pumch.cn

[†]These authors have contributed equally to this work

Specialty section:
This article was submitted to Genetics of Common and Rare Diseases, a section of the journal Frontiers in Genetics

Received: 29 October 2021
Accepted: 08 February 2022
Published: 10 March 2022

Citation:
Sun L, Huang Y, Zhao S, Zhong W, Shi J, Guo Y, Zhao J, Xiong G, Yin Y, Chen Z, Zhang N, Zhao Z, Li Q, Chen D, Niu Y, Li X, Qiu G, Wu Z, Zhang TJ, Tian W and Wu N (2022) Identification of Novel FBN2 Variants in a Cohort of Congenital Contractural Arachnodactyly. Front. Genet. 13:804202. doi: 10.3389/fgene.2022.804202

Congenital contractural arachnodactyly (CCA) is a rare autosomal dominant disorder of connective tissue characterized by crumpled ears, arachnodactyly, camptodactyly, large joint contracture, and kyphoscoliosis. The nature course of CCA has not been well-described. We aim to decipher the genetic and phenotypic spectrum of CCA. The cohort was enrolled in Beijing Jishuitan Hospital and Peking Union Medical College Hospital, Beijing, China, based on Deciphering disorders Involving Scoliosis and COmorbidities (DISCO) study (http://www.discostudy.org/). Exome sequencing was performed on patients' blood DNA. A recent published CCA scoring system was validated in our cohort. Seven novel variants and three previously reported *FBN2* variants were identified through exome sequencing. Two variants outside of the neonatal region of *FBN2* gene were found. The phenotypes were comparable between patients in our cohort and previous literature, with arachnodactyly, camptodactyly and large joints contractures found in almost all patients. All patients eligible for analysis were successfully classified into likely CCA based on the CCA scoring system. Furthermore, we found a double disease-causing heterozygous variant of *FBN2* and *ANKRD11* in a patient with blended phenotypes consisting of CCA and KBG syndrome. The identification of seven novel variants broadens the mutational and phenotypic spectrum of CCA and may provide implications for genetic counseling and clinical management.

Keywords: FBN2 (fibrillin-2), congenital contractural arachnodactyly, arthrogryposis, novel variants, clinical genetics, musculo-skeletal diseases

INTRODUCTION

Congenital contractural arachnodactyly (CCA), also known as Beals syndrome, is an autosomal dominantly inherited connective tissue disorder with an unknown prevalence (Putnam et al., 1995). The clinical manifestations of CCA primarily include arachnodactyly, congenital joint contractures, crumpled ears, kyphoscoliosis, chest deformity, dolichostenomelia, muscle hypoplasia, micrognathia

and high arched palate (Guo et al., 2016; Meerschaut et al., 2019). CCA is caused by variants in fibrillin-2 (*FBN2*) gene. Fibrinllin-2 is an integral component of elastin fibers in extracellular matrix (ECM), which provides supporting structure for tissues and scaffolds for physiological processes (Olivieri et al., 2010). Fibrillin-2 mediates signaling molecules on cell surfaces, including transforming growth factor β(TGF-β), bone morphogenetic proteins (BMPs), integrins and controls ECM formation and remodeling. Pathogenic variants in *FBN2* may weaken microfibril structure or disrupt binding capability, subsequently weaken the elastic fiber and perturbate ECM-mediated signaling, which leads to the anomalies of CCA (Ratnapriya et al., 2014).

Thus far, only 91 variants in *FBN2* gene associated with CCA have been described, as listed in the Human Genome Mutation Database (HGMD). Most of these variants cluster in a hotspot region, which is known as neonatal region, spanning from exon 23 to exon 35 (Meerschaut et al., 2019), which encodes the calcium-binding epidermal growth factor-like (cbEGF) domains. However, a limited number of variants outside the neonatal region has also been reported (Callewaert et al., 2009).

Recently, a clinical scoring system for CCA was developed to classify patients into likely CCA or unlikely CCA, which was based on the presence or absence of the ten main clinical features of this disorder (Meerschaut et al., 2019). Developing a scoring system is particularly important due to the phenotype overlap between CCA and other connective tissue disorders like Marfan syndrome and type VI collagenopathies (Also named as Bethlem myopathy) (Bamshad et al., 1996). However, this scoring system has not been tested in independent cohort and the genotype-phenotype correlation of CCA is still elusive.

In this study, we identified ten pathogenic *FBN2* variants in 27 CCA patients from ten families, of which seven are novel variants. We provide their clinical manifestations and speculate variants' impact on protein function based on variant location. Furthermore, we validated the clinical utility of a newly developed scoring system for CCA (Meerschaut et al., 2019).

MATERIALS AND METHODS

Participants

We included ten families diagnosed with CCA and carrying pathogenic *FBN2* variant from Beijing Jishuitan Hospital and Peking Union Medical College Hospital based on the Deciphering disorders Involving Scoliosis and COmorbidities (DISCO) study (http://www.discostudy.org/) (Tian et al., 2020; Sun et al., 2021). Informed consent was obtained from all patients or their guardians. This study was approved by the institutional review board at Beijing Jishuitan Hospital and Peking Union Medical College Hospital.

Genetic Testing

As a part of DISCO study, peripheral blood DNA from probands and available familial members were prepared into Illumina paired-end libraries and underwent whole-exome capture with the Agilent V5, followed by sequencing on the Illumina HiSeq 4,000 platform (Illumina, San Diego, CA, United States). In-house-developed Peking Union Medical college hospital Pipeline (PUMP) was used for variant calling and annotation (Zhao et al., 2020; Chen et al., 2021; Sun et al., 2021).

Variant-encoding amplicons were amplified by PCR from genomic DNA obtained from subjects and purified using an Axygen AP-GX-50 kit (lot no. 05915KE1) and conducted Sanger sequencing on an ABI3730XL instrument.

ES Data Interpretation

Rare variants with minor allele frequencies less than 0.01 in 1,000 Genomes (October 2013), Genome Aggregation Database (gnomAD, https://gnomad.broadinstitute.org), the Exome Aggregation Consortium (ExAC; http://exac.broadinstitute.org), and the in-house database of DISCO study (>8,394 exomes) were extracted. Besides variants in *FBN2* gene, we also examined other variants according to American College of Medical Genetics and Genomics (ACMG) guidelines (Richards et al., 2015), The prediction of mutational effect was performed using Combined Annotation Dependent Depletion (CADD, https://cadd.gs.washington.edu/) (Rentzsch et al., 2019), Sorting Intolerant From Tolerant (SIFT, http://sift.jcvi.org/) (Ng and Henikoff, 2003), and PolyPhen-2 (http://genetics.bwh.harvard.edu/pph2/) (Adzhubei et al., 2013).

CCA Clinical Score Calculation

We calculated the CCA clinical score of each affected individual based on their recorded phenotypes (Meerschaut et al., 2019). This scoring system was proposed to classify patients into likely CCA or unlikely CCA using phenotype-based scores. The scores were calculated based on the presence or absence of ten phenotypes. Four phenotypes were allotted for three points, including crumpled ears, arachnodactyly, camptodactyly and contractures of large joints. Two phenotypes were allotted for two points, including pectus deformity and dolichostenomelia. Four phenotypes were allotted for one point, including kyphoscoliosis, muscle hypoplasia, highly arched palate and micrognathia. A total score $\geq$7 and <7 indicated this patient was likely CCA or unlikely CCA, respectively. Only those with all the required phenotypes recorded were subjected for calculation.

RESULTS

Clinical Presentation of the Ten Families

This study included 10 unrelated families with a total of 27 cases affected with CCA (**Figure 1**). Eight of the families have more than one affected individual. Median age at admission was 4.95 years. Arachnodactyly (27/27, 100%), crumpled ears (26/27, 96.3%), camptodactyly (26/27, 96.3%), and muscle hypoplasia (22/26, 85%) were observed in almost all recruited cases (**Table 1**). More than half patients (16/25, 64%) presented with contracture of large joints, including elbow, wrist, knee, ankle, and shoulder. 54% patients (13/24) present with kyphosis or scoliosis; 29% patients (7/24) presented with pectus deformity,

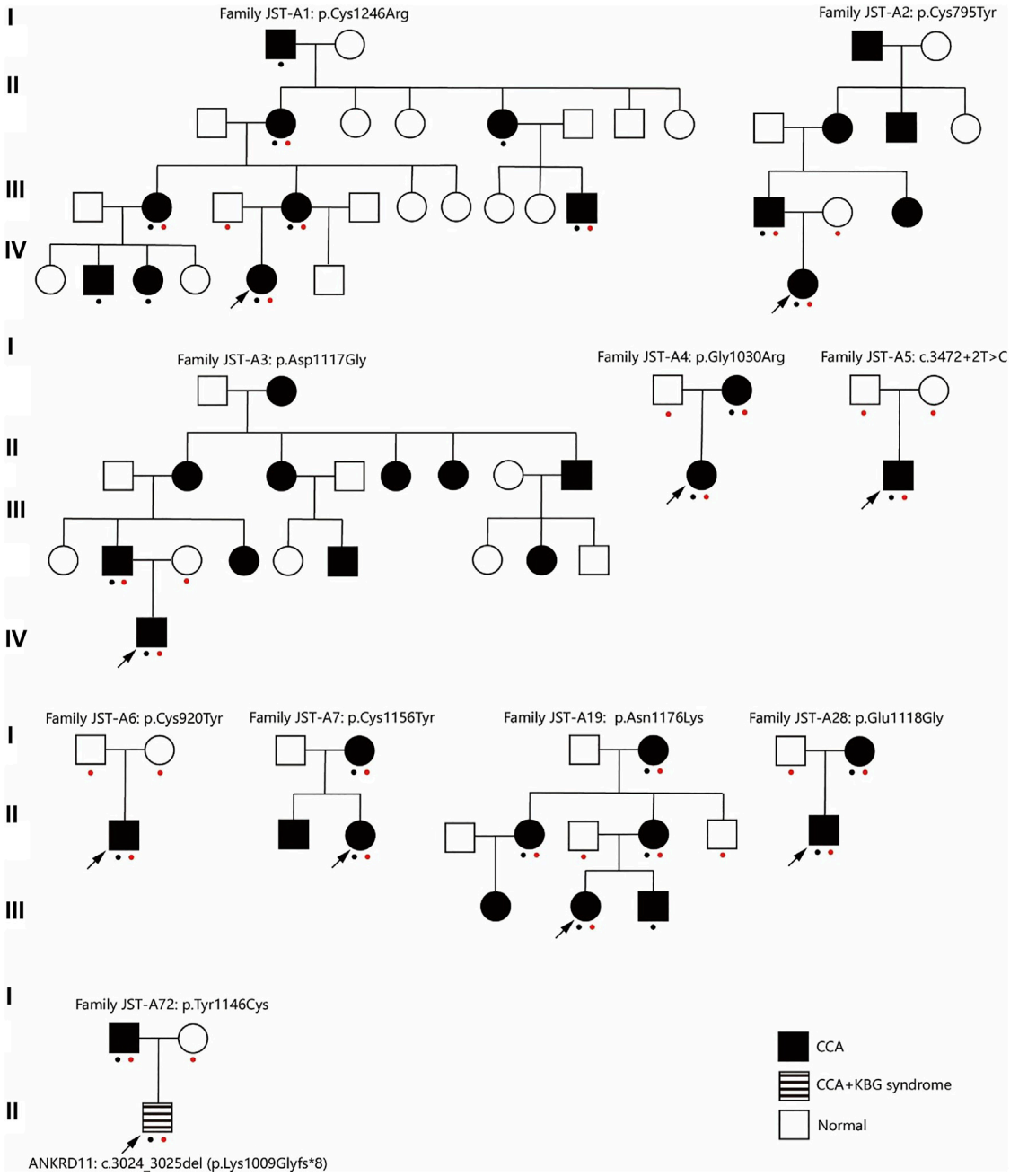

FIGURE 1 | Pedigree of ten families. A red dot indicates this individual underwent genetic test (Sanger sequencing or exome sequencing). A black dot indicates this individual underwent phenotypes assessment. CCA, Congenital contractural arachnodactyly.

including four patients with pectus carinatum and three patients with pectus excavatum; 74% patients (17/23) presented with high arched palate and 71% patients (17/24) presented with micrognathia; 33% patients (9/27) presented with pes planus (**Table1**); Two patients presented with genu varus and no patient presented with dolichostenomelia. Besides characteristic features of CCA, one patient presented with cryptorchidism, global developmental delay, atrial septal defect, bulbous nose, and broad eyebrow.

Identification of *FBN2* Variants

After ES and bioinformatic analyses, ten different *FBN2* variants were identified from the ten families (**Table 2**). Two variants were validated to be *de novo* (Family JST-A5 and JST-A6) and eight variants were segregated with the phenotype. Of the ten variants, three have been previously reported, i.e. p.Tyr1146Cys, c.3472+2T>C and p.Asn1176Lys (Gupta et al., 2002; Callewaert et al., 2009). The remaining seven variants are all novel, i.e. p. Cys1246Arg, p. Glu1118Gly,

TABLE 1 | Summary of patients' phenotypes in our cohort and in the literature.

Phenotype	Our cohort	Literature
Crumpled ears	26/27 (96.3%)	37/45 (82%)
Arachnodactyly	27/27 (100%)	44/48 (92%)
Camptodactyly	26/27 (96.3%)	46/49 (94%)
Pectus deformity	7/24 (29%)	15/30 (50%)
Dolichostenomelia	0/20 (0%)	7/21 (33%)
Muscle hypoplasia	22/26 (85%)	17/24 (71%)
Large joints contracture	16/25 (64%)	37/45 (82%)
Micrognathia	17/24 (71%)	8/17 (41%)
Highly arched palate	17/23 (74%)	17/31 (55%)
Kyphoscoliosis	13/24 (54%)	31/43 (72%)

p. Cys795Tyr, p. Asp1117Gly, p. Gly1030Arg, p. Cys920Tyr and p. Cys1156Tyr. All ten variants are evolutionary conserved and are absent from population controls.

Eight out of ten variants were found in the neonatal region (exon 24-32) of the *FBN2* gene. Among them, six variants alter the highly conserved cbEGF-like domain (p.Tyr1146Cys, p. Asp1117Gly, p. Glu1118Gly, p. Cys1156Tyr, p. Asn1176Lys, and p. Cys1246Arg) (**Figure 2**). One variant alters the TB domain (p.Gly1030Arg). One *de novo* splicing variant was identified (c.3472+2T > C), which has been verified to leading to an exon 26 skip (Gupta et al., 2002). Two variants were found outside the neonatal region of the *FBN2* gene (p.Cys795Tyr and p.

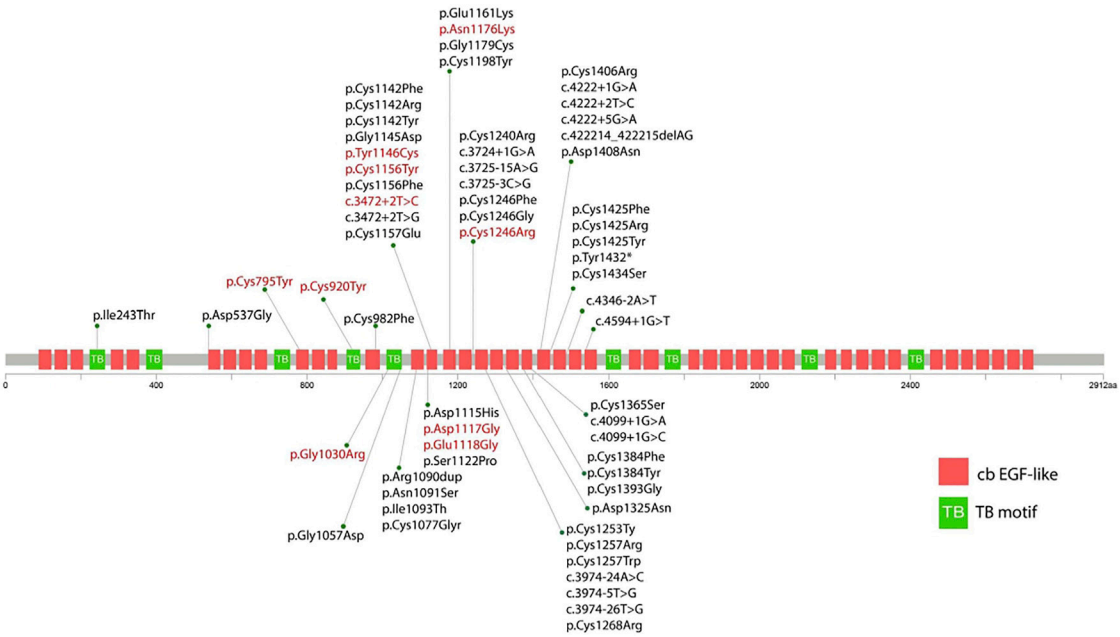

FIGURE 2 | Schematic diagram showing the position of the identified variants in relation to the structural domains of the fibrillin-2 protein. The red variant indicates the variant reported in this study. The black variant indicates the variant reported in previous literature.

TABLE 2 | Summary of identified *FBN2* and *ANKRD11* variants.

Family ID	Gene	Nucleotide change	Protein change	Origin	ACMG Classification
Family JST-A1	*FBN2*	c.3736T > C	p.Cys1246Arg	M	LP
Family JST-A2	*FBN2*	c.2384G > A	p.Cys795Tyr	Pa	LP
Family JST-A3	*FBN2*	c.3350A > G	p.Asp1117Gly	Pa	LP
Family JST-A4	*FBN2*	c.3088G > A	p.Gly1030Arg	M	LP
Family JST-A5	*FBN2*	c.3472+2T > C	p.?	*de novo*	P
Family JST-A6	*FBN2*	c.2759G > A	p.Cys920Tyr	*de novo*	P
Family JST-A7	*FBN2*	c.3467G > A	p.Cys1156Tyr	M	LP
Family JST-A19	*FBN2*	c.3528C > A	p.Asn1176Lys	M	LP
Family JST-A28	*FBN2*	c.3353A > G	p.Glu1118Gly	M	LP
Family JST-A72	*FBN2*	c.3437A > G	p.Tyr1146Cys	Pa	LP
	ANKRD11	c.3024_3025del	p.Lys1009Glyfs*8	*de novo*	P

M, maternal; Pa, paternal; P, pathogenic; LP, likely pathogenic.

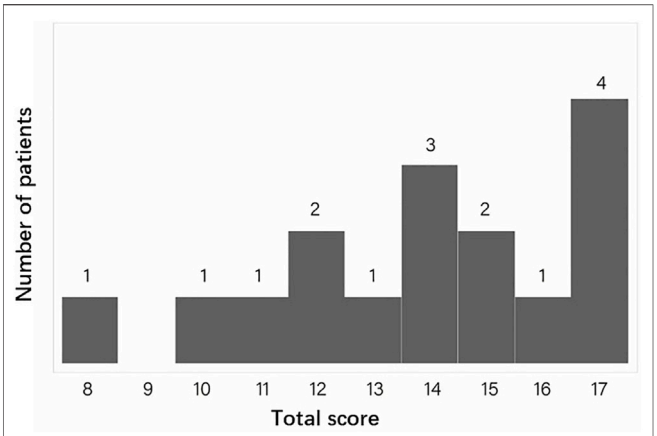

FIGURE 3 | The distribution of the total CCA clinical scores for all eligible patients. The X ray indicates the total score. The Y ray indicates the number of patients.

Cys920Tyr). The p. Cys920Tyr variant would affect the second hybrid domain and the p. Cys795Tyr would affect the cbEGF7 domain, respectively.

Dual Diagnosis

Through interpretation of the ES data, we identified one patient with dual molecular diagnosis. Patient DISCO-JST A72 was a 5 months old boy born to nonconsanguineous northern Han parents. His father presented with typical features of CCA (crumpled ears, camptodactyly, arachnodactyly and dolichostenomelia), while his mother is healthy. At 5 months old, he presented with crumpled ears, camptodactyly, arachnodactyly, global developmental delay, short stature, cryptorchidism, intellectual disability, global developmental delay, atrial septal defect (3.5 mm), bulbous nose, and broad eyebrow. ES of this family reviewed a *de novo* heterozygous *ANKRD11* variant c.3024_3025del (p.Lys1009Glyfs*8) in addition to the heterozygous *FBN2* variant c.3437A > G (p.Tyr1146Cys) inherited from his affected father. The *ANKRD11* frameshift variant is previously unreported and predicted to result in protein truncation or nonsense medicated decay. Loss-of-function of *ANKRD11* gene is a known disease-causing mechanism (Kim et al., 2020). *ANKRD11* is the only known causative gene of KBG syndrome, which is characterized by macrodontia, craniofacial findings, short stature, multiple skeletal anomalies including vertebrae and limbs, neurologic involvement including global developmental delay, seizures, and intellectual disability (Goldenberg et al., 2016). The clinical diagnostic criteria of KBG syndrome included four features macrodontia of upper central permanent incisors, characteristic facial anomalies, hand anomalies, neurologic involvement, significantly delayed bone age, costo-vertebral anomalies, postnatal short stature, and a first degree relative with KBG. For this patient, we observed a remarkable blended phenotype. For global developmental delay, cryptorchidism, intellectual disability, atrial septal defect (3.5 mm), bulbous nose, and broad eyebrow, we considered these phenotypes to be part of KBG syndrome; while crumpled ears, camptodactyly and arachnodactyly are characteristic features of CCA.

Validation of the CCA Scoring System

We calculated the diagnostic score for CCA in our *FBN2*-positive CCA patients. Totally, 16 patients with sufficient phenotype data were eligible for analysis. **Figure 3** gives an overview of the distribution of the total scores calculated for each CCA patient. The minimal, median and maximum score is 8, 14 and 17. All patients' CCA score is ≥ 7, which indicates all patients are successfully classified into likely CCA by the CCA scoring system. For the rest of 11 patients with insufficient clinical data, the clinical score of these patients are still ≥7.

DISCUSSION

In this study, we investigated 10 families with 27 patients diagnosed with CCA, based on their clinical and molecular profiles. We identified seven novel variants and three previously reported variants in *FBN2* gene. Additionally, we reported an individual with dual molecular diagnosis of CCA and KBG syndrome.

FBN2 encodes a 2912-amino acids extracellular matrix protein related to the elasticity of the tissue, which includes nine TB motifs, and 46 cbEGF domains (Davis and Summers, 2012). Each EGF-like domain contains six conserved cysteine residues to support its native folding. Six conserved cysteine residues form three disulfide bridges to maintain protein stability (Davis and Summers, 2012). In the present study, we found that c.2384G > A (p.Cys795Tyr), c.2759G > A (p.Cys920Tyr), c.3437A > G (p.Tyr1146Cys), c.3467G > A (p.Cys1156Tyr), and c.3736T > C (p.Cys1246Arg) alter or produce cysteine residues in the cbEGF domain, which would potentially disrupt the disulfide bond and therefore impair the nature folding of fibrillin-2. This is considered as the major mechanism underlying the pathogenesis of CCA (Guo et al., 2016; Xu et al., 2020).

Nine out of ten variants reported in this study are missense variants, which is consistent with previous findings that nearly all currently reported human *FBN2* pathogenic variants lead to single amino acids substitutions or in-frame exon deletions or duplications. This observation strongly suggests that gain-of-function is the key mechanism underlying the pathogenesis of CCA. This might explain why *fbn2* null mice does not phenocopy human CCA (Shi et al., 2013; Sengle et al., 2015).

In our cohort, we detected only two pathogenic variant [c.2384G > A (p.Cys795Tyr) and c.2759G > A (p.Cys920Tyr)] located outside the neonatal region. There are only three variants outside the neonatal region have been previously reported to lead to CCA (Liu et al., 2019; Renner et al., 2019). Totally, only ~8% CCA was caused by variants outside the neonatal region, which proves from another side of the substantial contribution of the neonatal region to the CCA phenotype. The pathogenicity of these two variants were supported by *in silico* predictions of pathogenicity, the absence of this variant from population controls, and segregation analysis.

We found one case with a blended phenotype consisting of CCA and KBG syndrome. Dual diagnoses in Mendelian disorders with complex phenotypes are being increasingly recognized. Coexisting diseases result in blended clinical phenotypes and poses challenge in diagnosis and management (Posey et al., 2017). One study have found 4.9% of cases suspected of having Mendelian disorders had multiple molecular diagnoses (Posey et al., 2017). Therefore, when phenotypes cannot be completely explained by one detected variant, additional genetic and clinical assessment should be considered. Interestingly, patients with CCA typically presented with tall stature, while KBG syndrome usually resulted in postnatal short stature. In this case, the patient has remarkable short stature.

Review of the phenotype data of CCA probands from literature and our cohort reveals a basically comparable phenotype. For example, external ear malformations like crumpled ears, which are a major characteristic of CCA, were found in 96.3% and 82% patients in our cohort or in the literature, respectively. The high prevalence of crumpled ears in CCA patients suggest it is particularly important in the differential diagnosis of connective tissue disorder. Interestingly, we found no patients in our cohort presented with dolichostenomelia. While in previous reports, 7/21 (33%) patients presented with dolichostenomelia (Fisher's exact test, $p = 0.0005$). Additionally, we found no patients in our cohort presented with cardiovascular anomalies like aortic root dilation. Our findings suggest phenotype heterogeneity of CCA may exists in different populations.

Genotype-phenotype correlation analysis in this study and previous studies revealed no significant associations. Recently, mutational burden has been recognized has a key contributor to the molecular diagnosis of some patients with arthrogryposis through accumulation of multiple deleterious variants (Pehlivan et al., 2019). Multilocus variants might also contribute to the genotype-phenotype correlation and intrafamilial variability in CCA. Fibrillins-2 polymerize extracellularly and form microfibrils with many proteins, e.g., latent transforming growth factor beta binding proteins (LTBPs) and microfibril-associated proteins (MFAPs). The complex binding interactions between these molecules indicate variants in different genes could modify CCA phenotype. Further analysis of large samples would possibly provide insights into the genotype-phenotype correlation in CCA.

The newly developed clinical scoring system for CCA successfully classified all patients in this study into likely CCA, even in patients with insufficient clinical data, indicating the excellent sensitivity of this scoring system. However, we didn't test the specificity of this scoring system due to lack of comprehensive clinical data of possibly misdiagnosed syndromes like Marfan syndrome. Marfan syndrome usually presented with cardiovascular, skeletal and ophthalmological manifestations (Bitterman and Sponseller, 2017). The overlapping phenotypes mainly include scoliosis, pectus deformity and cardiovascular deformity. In this scoring system, these overlapping phenotypes like kyphoscoliosis and pectus deformity were allotted for three points in total. While large joints contractures, camptodactyly, ear malformation, and arachnodactyly are usually absent in Marfan syndrome, which were allotted for three points each. Thus, we can speculate this scoring system would likely diagnose a Marfan syndrome patient into "unlikely CCA". Nevertheless, more data are needed to validate the specificity of this scoring system.

Intrafamilial heterogeneity has been noted in some families with CCA. This phenomenon has also been observed in our cohort and showed by the CCA clinical score. In the family JST-A1 with eight patients eligible for analysis, the highest, lowest and median CCA clinical score was 17, 8 and 13, respectively. The intrafamilial variation in this large family was moderate and all patients were classified into "likely CCA".

In conclusion, we report seven novel and three previously reported *FBN2* mutations in 27 patients from ten families with CCA. Our report enriches the mutational spectrum of *FBN2* and validate the novel CCA scoring system.

DATA AVAILABILITY STATEMENT

The datasets presented in this study can be found in online repositories. The names of the repository/repositories and accession number(s) can be found below: <https://data.mendeley.com/drafts/cxgcj3s8t3, Mendeley.

ETHICS STATEMENT

The studies involving human participants were reviewed and approved by the ethics committee at Beijing Jishuitan Hospital (201808-09), and Peking Union Medical College Hospital (JS-098). Written informed consent to participate in this study was provided by the participants' legal guardian/next of kin. Written informed consent was obtained from the individual(s), and minor(s)' legal guardian/next of kin, for the publication of any potentially identifiable images or data included in this article.

AUTHOR CONTRIBUTIONS

Conceptualization: WT, ZW, TJZ and NW. Cohort enrollment: LS, YG, ZZ, QL, YY, NZ, DC, GX, WZ and YH. Funding acquisition: NW, ZW, WT and TJZ. Experiments: ZC, XL, YN, JS and YH. Genetic data analysis: YH, LS, SZ, WZ, ZY, XL and NW. Bioinformatic analysis: SZ, and ZC. Writing—review and editing: TJZ, GQ, NW and ZW. Data interpretation: WT, ZW, TJZ and NW. Writing original draft: YH, LS, SZ, WZ, YG, GX, WT and NW.

FUNDING

This research was funded in part by the National Key Research and Development Program of China (2016YFC0901500), Center for Rare Diseases Research, Chinese Academy of Medical Sciences,

Beijing, China (2016ZX310174-4), Beijing JST Research Funding (ZR-201907, ZR-201911 and 2019-YJ03), Beijing Jishuitan Hospital Nova Program (XKXX201818), National Natural Science Foundation of China (81822030, 82072391, 81672123, 81972037, 81772299, 81930068, 81772301, and 81972132), Non-profit Central Research Institute Fund of Chinese Academy of Medical Sciences (No. 2019PT320025), Beijing Natural Science Foundation (JQ20032 and 7191007), Tsinghua University-Peking Union Medical College Hospital Initiative Scientific Research Program, CAMS Initiative Fund for Medical Sciences (2016-I2M-3-003, 2016-I2M-2-006 and 2017-I2M-2-001).

ACKNOWLEDGMENTS

We thank the families who participated in this research.

SUPPLEMENTARY MATERIAL

The Supplementary Material for this article can be found online at: https://www.frontiersin.org/articles/10.3389/fgene.2022.804202/full#supplementary-material

REFERENCES

Adzhubei, I., Jordan, D. M., and Sunyaev, S. R. (2013). Predicting Functional Effect of Human Missense Mutations Using PolyPhen-2. *Curr. Protoc. Hum. Genet.* 76. doi:10.1002/0471142905.hg0720s76

Bamshad, M., Jorde, L. B., and Carey, J. C. (1996). A Revised and Extended Classification of the Distal Arthrogryposes. *Am. J. Med. Genet.* 65, 277–281. doi:10.1002/(sici)1096-8628(19961111)65:4<277::aid-ajmg6>3.0.co;2-m

Bitterman, A. D., and Sponseller, P. D. (2017). Marfan Syndrome. *J. Am. Acad. Orthopaedic Surgeons* 25, 603–609. doi:10.5435/JAAOS-D-16-00143

Callewaert, B. L., Loeys, B. L., Ficcadenti, A., Vermeer, S., Landgren, M., Kroes, H. Y., et al. (2009). Comprehensive Clinical and Molecular Assessment of 32 Probands with Congenital Contractural Arachnodactyly: Report of 14 Novel Mutations and Review of the Literature. *Hum. Mutat.* 30, 334–341. doi:10.1002/humu.20854

Chen, N., Zhao, S., Jolly, A., Wang, L., Pan, H., Yuan, J., et al. (2021). Perturbations of Genes Essential for Müllerian Duct and Wölffian Duct Development in Mayer-Rokitansky-Küster-Hauser Syndrome. *Am. J. Hum. Genet.* 108, 337–345. doi:10.1016/j.ajhg.2020.12.014

Davis, M. R., and Summers, K. M. (2012). Structure and Function of the Mammalian Fibrillin Gene Family: Implications for Human Connective Tissue Diseases. *Mol. Genet. Metab.* 107, 635–647. doi:10.1016/j.ymgme.2012.07.023

Goldenberg, A., Riccardi, F., Tessier, A., Pfundt, R., Busa, T., Cacciagli, P., et al. (2016). Clinical and Molecular Findings in 39 Patients with KBG Syndrome Caused by Deletion or Mutation ofANKRD11. *Am. J. Med. Genet.* 170, 2847–2859. doi:10.1002/ajmg.a.37878

Guo, X., Song, C., Shi, Y., Li, H., Meng, W., Yuan, Q., et al. (2016). Whole Exome Sequencing Identifies a Novel Missense FBN2 Mutation Co-segregating in a Four-Generation Chinese Family with Congenital Contractural Arachnodactyly. *BMC Med. Genet.* 17, 91. doi:10.1186/s12881-016-0355-6

Gupta, P. A., Putnam, E. A., Carmical, S. G., Kaitila, I., Steinmann, B., Child, A., et al. (2002). Ten novelFBN2mutations in Congenital Contractural Arachnodactyly: Delineation of the Molecular Pathogenesis and Clinical Phenotype. *Hum. Mutat.* 19, 39–48. doi:10.1002/humu.10017

Kim, S. J., Yang, A., Park, J. S., Kwon, D. G., Lee, J.-S., Kwon, Y. S., et al. (2020). Two Novel Mutations of ANKRD11 Gene and Wide Clinical Spectrum in KBG Syndrome: Case Reports and Literature Review. *Front. Genet.* 11, 579805. doi:10.3389/fgene.2020.579805

Liu, H., Tsui, Y., Wang, J., Su, C., Zheng, R., Shao, Y., et al. (2019). Establishment of a Beals Syndrome Patient-Derived Human Induced Pluripotent Stem Cell Line HELPi001-A. *Stem Cel Res.* 40, 101535. doi:10.1016/j.scr.2019.101535

Meerschaut, I., De Coninck, S., Steyaert, W., Barnicoat, A., Bayat, A., Benedicenti, F., et al. (2020). A Clinical Scoring System for Congenital Contractural Arachnodactyly. *Genet. Med.* 22, 124–131. doi:10.1038/s41436-019-0609-8

Ng, P. C., and Henikoff, S. (2003). SIFT: Predicting Amino Acid Changes that Affect Protein Function. *Nucleic Acids Res.* 31, 3812–3814. doi:10.1093/nar/gkg509

Olivieri, J., Smaldone, S., and Ramirez, F. (2010). Fibrillin Assemblies: Extracellular Determinants of Tissue Formation and Fibrosis. *Fibrogenesis Tissue Repair* 3, 24. doi:10.1186/1755-1536-3-24

Pehlivan, D., Bayram, Y., Gunes, N., Coban Akdemir, Z., Shukla, A., Bierhals, T., et al. (2019). The Genomics of Arthrogryposis, a Complex Trait: Candidate Genes and Further Evidence for Oligogenic Inheritance. *Am. J. Hum. Genet.* 105, 132–150. doi:10.1016/j.ajhg.2019.05.015

Posey, J. E., Harel, T., Liu, P., Rosenfeld, J. A., James, R. A., Coban Akdemir, Z. H., et al. (2017). Resolution of Disease Phenotypes Resulting from Multilocus Genomic Variation. *N. Engl. J. Med.* 376, 21–31. doi:10.1056/NEJMoa1516767

Putnam, E. A., Zhang, H., Ramirez, F., and Milewicz, D. M. (1995). Fibrillin-2 (FBN2) Mutations Result in the Marfan-like Disorder, Congenital Contractural Arachnodactyly. *Nat. Genet.* 11, 456–458. doi:10.1038/ng1295-456

Ratnapriya, R., Zhan, X., Fariss, R. N., Branham, K. E., Zipprer, D., Chakarova, C. F., et al. (2014). Rare and Common Variants in Extracellular Matrix Gene Fibrillin 2 (FBN2) Are Associated with Macular Degeneration. *Hum. Mol. Genet.* 23, 5827–5837. doi:10.1093/hmg/ddu276

Renner, S., Schüler, H., Alawi, M., Kolbe, V., Rybczynski, M., Woitschach, R., et al. (2019). Next-generation Sequencing of 32 Genes Associated with Hereditary Aortopathies and Related Disorders of Connective Tissue in a Cohort of 199 Patients. *Genet. Med.* 21, 1832–1841. doi:10.1038/s41436-019-0435-z

Rentzsch, P., Witten, D., Cooper, G. M., Shendure, J., and Kircher, M. (2019). CADD: Predicting the Deleteriousness of Variants throughout the Human Genome. *Nucleic Acids Res.* 47, D886–D894. doi:10.1093/nar/gky1016

Richards, S., Aziz, N., Bale, S., Bick, D., Das, S., Gastier-Foster, J., et al. (2015). Standards and Guidelines for the Interpretation of Sequence Variants: a Joint Consensus Recommendation of the American College of Medical Genetics and Genomics and the Association for Molecular Pathology. *Genet. Med.* 17, 405–424. doi:10.1038/gim.2015.30

Sengle, G., Carlberg, V., Tufa, S. F., Charbonneau, N. L., Smaldone, S., Carlson, E. J., et al. (2015). Abnormal Activation of BMP Signaling Causes Myopathy in Fbn2 Null Mice. *Plos Genet.* 11, e1005340. doi:10.1371/journal.pgen.1005340

Shi, Y., Tu, Y., Mecham, R. P., and Bassnett, S. (2013). Ocular Phenotype ofFbn2-Null Mice. *Invest. Ophthalmol. Vis. Sci.* 54, 7163–7173. doi:10.1167/iovs.13-12687

Sun, L., Huang, Y., Zhao, S., Zhao, J., Yan, Z., Guo, Y., et al. (2021). Deciphering the Mutational Signature of Congenital Limb Malformations. *Mol. Ther. - Nucleic Acids* 24, 961–970. doi:10.1016/j.omtn.2021.04.012

Tian, W., Huang, Y., Sun, L., Guo, Y., Zhao, S., Lin, M., et al. (2020). Phenotypic and Genetic Spectrum of Isolated Macrodactyly: Somatic Mosaicism of PIK3CA and AKT1 Oncogenic Variants. *Orphanet J. Rare Dis.* 15, 288. doi:10.1186/s13023-020-01572-9

Xu, P., Li, R., Huang, S., Sun, M., Liu, J., Niu, Y., et al. (2020). A Novel Splicing Mutation in the FBN2 Gene in a Family with Congenital Contractural Arachnodactyly. *Front. Genet.* 11, 143. doi:10.3389/fgene.2020.00143

Zhao, S., Zhang, Y., Chen, W., Li, W., Wang, S., Wang, L., et al. (2020). Diagnostic Yield and Clinical Impact of Exome Sequencing in Early-Onset Scoliosis (EOS). *J. Med. Genet.* 58, 41–47. doi:10.1136/jmedgenet-2019-106823

Conflict of Interest: The authors declare that the research was conducted in the absence of any commercial or financial relationships that could be construed as a potential conflict of interest.

Publisher's Note: All claims expressed in this article are solely those of the authors and do not necessarily represent those of their affiliated organizations, or those of the publisher, the editors and the reviewers. Any product that may be evaluated in this article, or claim that may be made by its manufacturer, is not guaranteed or endorsed by the publisher.

frontiers in Genetics

ORIGINAL RESEARCH
published: 16 March 2022
doi: 10.3389/fgene.2022.823861

Novel Loss-of-Function Mutations in *NPR2* Cause Acromesomelic Dysplasia, Maroteaux Type

Jing Wu[1†], Mengru Wang[2†], Zhouyang Jiao[3], Binghua Dou[1], Bo Li[4], Jianjiang Zhang[1], Haohao Zhang[5], Yue Sun[6], Xin Tu[2], Xiangdong Kong[6] and Ying Bai[6*]*

[1]Department of Pediatrics, First Affiliated Hospital of Zhengzhou University, Zhengzhou, China, [2]Key Laboratory of Molecular Biophysics of the Ministry of Education, College of Life Science and Technology and Center for Human Genome Research, Huazhong University of Science and Technology, Wuhan, China, [3]Department of Vascular and Endovascular Surgery, First Affiliated Hospital of Zhengzhou University, Zhengzhou, China, [4]Department of Physiology and Neurobiology, School of Basic Medical Sciences, Zhengzhou University, Zhengzhou, China, [5]Department of Endocrinology, First Affiliated Hospital of Zhengzhou University, Zhengzhou, China, [6]Genetic and Prenatal Diagnosis Center, Department of Obstetrics and Gynecology, First Affiliated Hospital of Zhengzhou University, Zhengzhou, China

OPEN ACCESS

Edited by:
Long Guo,
RIKEN Center for Integrative Medical Sciences, Japan

Reviewed by:
Asmat Ullah,
Shaheed Zulfiqar Ali Bhutto Medical University (SZABMU), Pakistan
Mohammed Faruq,
Council of Scientific and Industrial Research (CSIR), India
Furhan Iqbal,
Bahauddin Zakariya University, Pakistan

***Correspondence:**
Ying Bai
fccbaiy2@zzu.edu.cn
Xiangdong Kong
kongxd@263.net

†These authors share first authorship

Specialty section:
This article was submitted to Genetics of Common and Rare Diseases, a section of the journal Frontiers in Genetics

Received: *28 November 2021*
Accepted: *18 February 2022*
Published: *16 March 2022*

Citation:
Wu J, Wang M, Jiao Z, Dou B, Li B, Zhang J, Zhang H, Sun Y, Tu X, Kong X and Bai Y (2022) Novel Loss-of-Function Mutations in NPR2 Cause Acromesomelic Dysplasia, Maroteaux Type. Front. Genet. 13:823861. doi: 10.3389/fgene.2022.823861

Acromesomelic dysplasia, Maroteaux type (AMDM) is a rare skeletal dysplasia characterized by severe disproportionate short stature, short hands and feet, normal intelligence, and facial dysmorphism. Homozygous or compound heterozygous mutations in the natriuretic peptide receptor 2 (*NPR2*) gene produce growth-restricted phenotypes. The current study was designed to identify and characterize *NPR2* loss-of-function mutations in patients with AMDM and to explore therapeutic responses to recombinant growth hormone (rhGH). *NPR2* was sequenced in two Chinese patients with AMDM via next generation sequencing, and in silico structural analysis or transcript analysis of two novel variants was performed to examine putative protein changes. rhGH treatment was started for patient 1. Three *NPR2* mutations were identified in two unrelated cases: two compound heterozygous mutations c.1112G>A p.(Arg371Gln) and c.2887+2T>C in patient 1 and a homozygous mutation c.329G>A p.(Arg110His) in patient 2, yielding distinct phenotypes. RNA extracted from peripheral blood cells of patient 1 showed alternatively spliced transcripts not present in control cells. Homology modeling analyses suggested that the c.1112G>A p.(Arg371Gln) mutation disrupted the binding of NPR-B homodimer to its ligand (C-type natriuretic peptide) in the extracellular domain as a result of global allosteric effects on homodimer formation. Thus, c.2887+2T>C and c.1112G>A p.(Arg371Gln) in *NPR2* were loss-of-function mutations. Furthermore, rhGH therapy in patient 1 increased the patient's height by 0.6SDS over 15 months without adversely affecting the trunk-leg proportion. The short-term growth-promoting effect was equivalent to that reported for idiopathic short stature. Overall, our findings broadened the genotypic spectrum of *NPR2* mutations in individuals with AMDM and provided insights into the efficacy of rhGH in these patients.

Keywords: acromesomelic dysplasia, maroteaux type, natriuretic peptide receptor 2, loss-of-function mutation, growth hormone therapy, genotype analysis

1 INTRODUCTION

Acromesomelic dysplasia is a heterogeneous group of rare chondrocyte dysfunctions affecting the distal and middle segments of the extremities. Acromesomelic dysplasia occurs in isolated abnormal bone growth and skeletal morphology and is associated with genital and neurological disorders (Mustafa et al., 2020; Khan et al., 2016). To date, five types of acromesomelic dysplasia, i.e., acromesomelic dysplasia, Maroteaux type (AMDM, OMIM #602875); Grebe dysplasia (OMIM #200700) (Umair et al., 2017; Ullah et al., 2018); fibular hypoplasia andcomplex brachydactyly type (Du pan, OMIM #228900)) (Mortier et al., 2019); acromesomelic dysplasia Osebold-Remondini type (OMIM #112910) (Osebold et al., 1985; Ullah et al., 2018); and another recently discovered novel type (OMIM #609441) (Díaz-González et al., 2022), have been identified. These diseases are distinct entities because of their unique features and have been shown to be caused by four genes, namely, natriuretic peptide receptor 2 (*NPR2*), growth and differentiation factor-5, bone morphogenetic protein receptor-1b, protein kinase cGMP-dependent type II, showing autosomal recessive inheritance. Among disease types, the Osebold-Remondini type has not yet been genetically mapped. However, diagnosis is generally made using clinical, radiological, and genetic information.

Specific mutations in *NPR2*, mapped to chromosome 9p13.3, have been identified in patients with AMDM. NPR-B, encoded by *NPR2*, contains four functional domains: an extracellular ligand-binding domain (ECD), a transmembrane domain, an intracellular kinase homology domain, and a guanylyl cyclase domain at the C-terminus (Potter and Hunter, 2001). Physiologically active NPR-B is a homodimer that catalyzes the formation of cGMP from GTP upon binding its ligand, C-type natriuretic peptide (CNP). The CNP/NPR2 signaling pathway is crucial for endochondral ossification, functioning to promote cartilage homeostasis and the proliferation and differentiation of osteoblasts and osteoclasts (Langenickel et al., 2004).

NPR2 mutations cause broad-spectrum phenotypic variability. All affected individuals with AMDM carry a homozygous or compound heterozygous loss-of-function mutation. Heterozygous loss-of-function mutations in *NPR2* are associated with idiopathic short stature without skeletal dysplasia. They are also found in individuals with disproportionate short stature with skeletal anomalies, similar to those observed in SHOX negative-Léri-Weill dyschondrosteosis. However, no individuals have presented with Madelung deformity (Hisado-Oliva et al., 2015). By contrast, gain-of-function mutations in *NPR2* cause tall stature with mild scoliosis or overgrowth syndrome (epiphyseal chondrodysplasia, Miura type).

Here, we report two other AMDM cases of Chinese origin caused by compound heterozygous or homozygous loss-of-function mutations in *NPR2*, identified through whole-exome sequencing analysis. We evaluated the genotype-phenotype correlations in these patients and showed that the two novel mutations resulted in loss of function of *NPR2* based on structural and transcript analyses. Recombinant growth hormone (rhGH) treatment was administered to a 40-month-old affected child for more than 1 year.

2 MATERIALS AND METHODS

2.1 Patients

The two patients and their family members provided written informed consent to participate in this study, and the study was approved by the Ethics Committee of Scientific Research and Clinical Trial of the First Affiliated Hospital of Zhengzhou University (approval no.2019-KY-401). Clinical information was extracted from medical records. All patients fulfilled the following diagnostic criteria: disproportional short stature, defined as a sitting height to height ratio greater than 2 standard deviation scores (SDSs) above the mean for the corresponding age and sex. Conventional laboratory tests could not explain the etiology of short stature. Laboratory examinations of patient 1 after rhGH therapy were performed before and after treatment, including serum alkaline phosphatase (AP), insulin-like growth factor (IGF)-1, total procollagen type 1 amino-terminal propeptide (P1NP), β-crosslaps, and osteocalein.

2.2 Whole-Exome sequencing and Targeted Next-Generation Sequencing

Genomic DNA was isolated from the peripheral blood of the probands of the two families using a DNA extraction kit (Omega, CA, United States). For patient 1, proband-only WES was performed and enriched for exonic sequences using an Agilent SureSelect XT Human All Exon 50 Mb kit (Santa Clara, CA, United States). For patient 2, targeted NGS using a genetic skeletal disease panel (including 225 genes; **Supplementary Table S1**) was performed by a commercial company (MyGenostics, Inc., Beijing, China). The quality of the library was assessed using Qubit 4.0 (Thermo Fisher Scientific Inc., USA). Paired-end sequencing was performed using an Illumina sequencing platform (Illumina, San Diego, CA, United States). After sequencing, data processing and variant annotation were performed using standard analyses (Li et al., 2021). High-quality reads were mapped to the human reference genome GRC37/hg19. Small variants were identified using Genome Analysis Toolkit version 3.8 (McKenna et al., 2010). For recessive model analyses, variants with a minor allele frequency of less than 0.01 in dbSNP138, 1000 Genomes, ExAC, and gnomAD databases were selected. Exonic and splice-site variants of 225 skeletal dysplasia related genes were collected for further analyses. The pathogenicity of variations was analyzed according to American College of Medical Genetics and Genomics (ACMG) guidelines (Richards et al., 2015).

2.3 Sanger Sequencing

Variants in *NPR2* were confirmed by Sanger sequencing, and paired primers were designed using Genetool software

(**Supplementary Table S2**). Polymerase chain reaction (PCR) amplification with each primer set was carried out, and PCR products were sequenced on a 3130xl Genetic Analyzer (Applied Biosystems, Foster City, CA, United States). The data were analyzed using Chromas (Techne).

2.4 Reverse Transcription-PCR

Whole-blood RNA was extracted using TRIzol (Invitrogen, Carlsbad, CA, United States) and reverse transcribed using a HiScript II 1st Strand cDNA Synthesis Kit (Vazyme Biotech Co.,Ltd., Nan jing, China). cDNA sequences of *NPR2* from exons 15–22 were amplified by PCR, subcloned using a KOD FX Polymerase Kit (TOYOBO), and Sanger sequenced.

2.5 Bioinformatics Analysis

The pathogenicity of the identified variants was assessed using Varcards (http://varcards.biols.ac.cn/) and Pubvar (https://www.pubvar.com/) using various tools, including the Rare Exome Variant Ensemble Learner, Sorting Intolerant from Tolerant, Likelihood Ratio Test, Combined Annotation Dependent Depletion, Polymorphism Phenotyping V2, and MutationTaster. Genetic variants in *NPR2* were retrieved from the ClinVar and professional HGMD databases. Alignments were made of *NPR2* from *Homo sapiens*, mice, rhesus monkeys, dogs, and elephants to identify amino acid conservation at novel missense mutation sites.

2.6 Homology Modeling and Molecular Dynamics Simulation

The ECD of HsNPR2 was modeled as follows. First, the template for modeling was retrieved from the Protein Database (PDB; http://www.rcsb.org); using the Basic Local Alignment Search Tool (BLAST). The wild-type ECD (ECD^{wt}) of HsNPR2 (amino acids:17–421) was modeled on the NPR-A crystal structure (PDB entry 1DP4). Subsequent modeling was performed using the MODELLER program, and discrete optimized protein energy (DOPE) scores in terms of spatial restraints of amino acids were ranked to assess model quality. On the basis of DOPE scores, the best quality model was selected and the model quality was then monitored using the SAVES (services.mbi.ucla.edu/SAVES/) and ProSAweb validation servers (https://prosa.services.came.sbg.ac.at/prosa.php) (Ramachandran et al., 1963). The homomeric structure of ECD^{wt} was generated using the GalaxyWeb server (http://galaxy.seoklab.org/cgi-bin/submit. cgi?type = HOMOMER). The mutant ECD (ECD^{371Q}) was generated by inputting the corresponding mutant amino acid sequences of ECD in the same analysis process as described above.

Homodimers of ECD^{wt}/ECD^{371Q} were subjected to MD simulations for structural refinement. MD simulations were performed with the TIP3P water model using the Gromacs 2021 package, and the topology of the protein structure was generated by CHARMm36ff parameterization (Irfanullah et al., 2018). Additionally, 0.1 M NaCl was added to neutralize the system, and energy minimization was performed using the steepest descent algorithm (at a maximum force of 10 kJ/mol) to avoid steric clash. Each system was heated at 300 K using the V-rescale method (Bussi et al., 2007), and pressure was equilibrated at 1.0 bar using a Parrinello-Rahman barostat (Parrinello and Rahman, 1981). Finally, the MD simulation for each homodimer was run for 100 ns. The coordinates of the refined structures were extracted from the final trajectory frame. The MD refined models of homology ECD were validated using the SAVES and ProSAweb validation servers and were exported into Discovery Studio 2016 for further analyses. Comparative analyses were performed to determine the structural variations between ECD^{wt} and ECD^{371Q}.

2.7 Ligand Preparation and Molecular Docking

The CNP model was extracted from the NPR-C crystal (PDB entry 1jdp) using PyMOL (Rootsi et al., 2004). We used the HPEPDOCK server to perform molecular docking of CNP with the MD refined model of homology ECD^{wt} and ECD^{371Q} based on the hierarchical algorithm (Zhou et al., 2018). The HPEPDOCK webserver is available at http://huanglab.phys.hust.edu.cn/hpepdock/.

3 RESULTS

3.1 Clinical Features

Patient 1 was a girl who presented with short stature and small stubby fingers (**Figure 1**; **Supplementary Table S3**), which were noticed at 6 months of age. She was born by cesarean section after 37 weeks of gestation as the second child of healthy, nonconsanguineous parents. Her birth weight was 2,800 g, and her birth length was 50 cm. At 3 years and 4 months of age, her sitting height to standing height ratio was 0.575. Her psychomotor development, intelligence, and cognitive development were normal. Physical examination revealed noticeably short upper and lower extremities, brachydactylic fingers and toes (**Figures 1B,C**), apparent prominent forehead, long face, short and broad nose, pronounced shortening, and slightly bowed forearm. The radiological manifestations were compatible with AMDM (**Figures 1F–K**). Her parents and siblings had proportionate bodies without small hands, feet, or extremities.

Patient 2 was a 31-year-old woman who presented with disproportionate acromesomelic dysplasia (**Figure 1**; **Supplementary Table S3**). Her arm span was 108 cm, and her arm span to height ratio was 0.86. Her sitting height was 75.7 cm, with a sitting to standing height ratio of 0.6. Her upper and lower segments were measured at 59.5 and 66 cm, respectively, with an upper to lower segment ratio of 0.9. Her head circumference was 52.5 cm. Her foot span was 17 cm, and her hand span was 10 cm. Prominent forehead, long face, low-set ears, high-arched palate, short neck, torticollis with normal forward and backward head movement, uneven shoulder with the left side relatively higher, bilateral short broad thumbs and

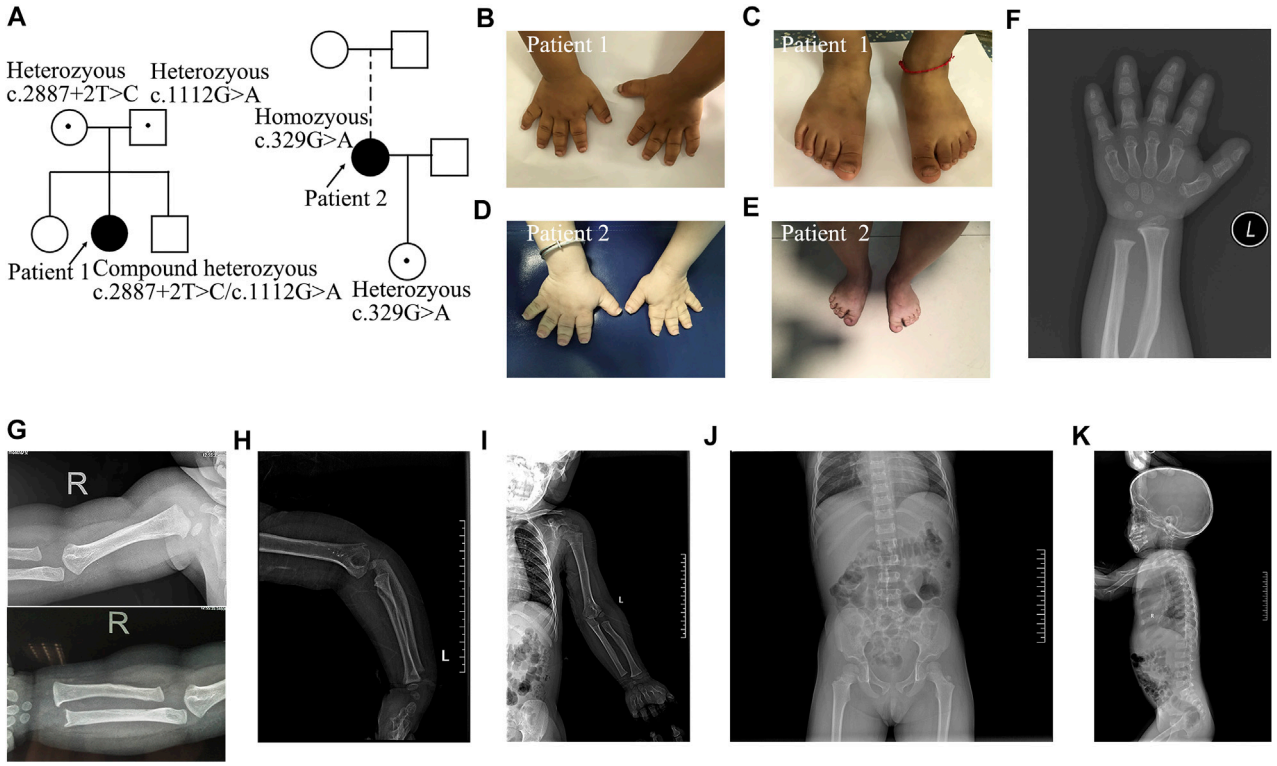

FIGURE 1 | Pedigrees and images of two patients with Acromesomelic Dysplasia Maroteaux Type. **(A)** Pedigree of two families containing patient 1 and 2; **(B,C)** small hands and feet in patient 1; **(D,E)** patient 2 with loose and redundant skin on fingers and feet; **(F)** short and dysplastic metacarpals and phalanges in patient 1; **(G-I)** The humerus and radius are curved, besides, osteophyte existed in both distal ulna and lateral epicondylar humeri in patient 1. There was no dislocation of the radial head. There were no missing or fused bones; **(J,K)** Mild scoliosis and irregular anterior wedging of vertebral bodies in patient 1.

toes, large halluces, and loose and redundant skin on the hands were noted (**Figures 1D,E**). She did not show clinical evidence of Madelung deformity, scoliosis, brachydactyly, and clinodactyly. She refused further imaging examination. Her menarche occurred at 15 years of age. Her 5-year 11-month-old daughter presented with proportionate dwarfism. Both the proband and her daughter had normal intelligence, hearing, and speech.

3.2 rhGH Treatment and Related Laboratory Measurements in Patient 1

Patient 1 was treated with rhGH (from 0.35 mg/kg/week at initial treatment to 0.47 mg/kg/week, using daily subcutaneous injections). Subsequently, her growth velocity improved by 10.4 cm after 15 months of rhGH treatment, with a height gain of +0.6 SDS (**Figure 2**). There were no considerable adverse effects and no clinical deterioration of skeletal deformities. The association of height gain with steady increases in serum IGF-1 and P1NP levels following initiation of GH treatment and dose increases was observed in the patient, but no obvious changes in serum AP, N-MID, and β-crosslap levels were observed during rhGH treatment (**Supplementary Table S4**).

3.3 Genetic Analysis

Using whole-exome sequencing of patient 1, we identified two single nucleotide variants in *NPR2* (NM_003995.3): c.1112G>A p.(Arg371Gln) and c.2887+2T>C (**Figure 3A**; **Supplementary Figures S1, S2**). Sanger sequencing showed that the c.1112G>A variant was inherited from the mother, whereas the c.2887+2T>C variant was inherited from the father. Analysis of sequencing data from patient 2 revealed a homozygous missense mutation, c.329G>A p.(Arg110His), in exon 1 of *NPR2* (**Figure 3B**; **Supplementary Figure S3**). Sanger sequencing showed that her daughter was heterozygous for the mutation. Three variants were respectively classified as "likely pathogenic variant" (PM1+PM2_supporting + PM3+PP3+PP4, PVS1+PM2_supporting + PP3+PP4 and PS1+ PM2_supporting + PP3+PP4).

Patient 2 was adopted and her biological paternal samples were not available. The results showed that the two families segregated AMDM in an autosomal recessive manner. The missense variants [c.1112G>A p.(Arg371Gln) and c.329G>A p.(Arg110His)] were predicted to be pathogenic or deleterious using various online tools (**Supplementary Table S5**). The amino acids Arg371 and Arg110 were completely conserved among mammals, including rhesus monkeys, mice, dogs, and elephants (**Figure 3C**).

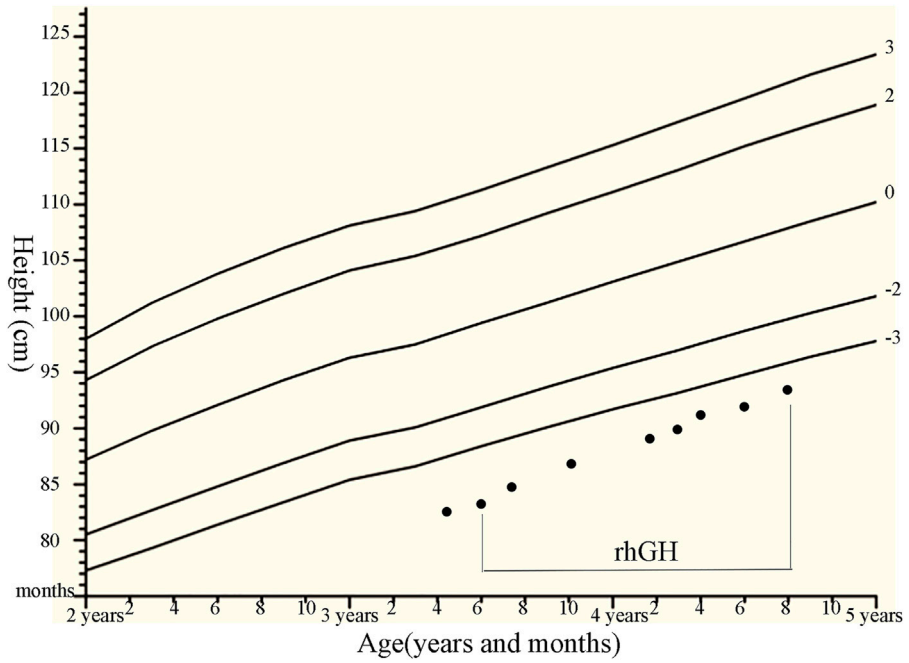

FIGURE 2 | Growth chart of the patients with compound heterozygous NPR2 mutations (c.1112G>A and c.2887+2T>C) with the rhGH therapies. We plotted the height on standardized growth charts for Chinese children and adolescents aged 0–18 years (Li et al., 2009), and evaluate rhGH treatment efficacy for our patient.

3.4 Multiple Forms of Aberrant Splicing for the Splice Mutation c.2887+2T>C

We showed that the RNA of patient 1 was aberrantly spliced and lacked partial exon 20 (c.2888-2944), exon 19 (c.2713-2887), or exons 17–19 (c.2520-2877; **Figure 4**; **Supplementary Figure S4**). The transcript generated from the skipping of exon 19 was out-of-frame and was predicted to produce a truncated protein of about 101 kDa [p.(Asp901GlyfsX9)]. By contrast, the transcript generated from the partial skipping of exon 20 lacked 19 amino acids [p.(Gly963 to Gly981)]. The transcript generated from skipping of exons 17–19 was also out-of-frame and was translated into a truncated protein [p.(His840GlnfsX31)].

3.5 Structural and Functional Analysis of the Novel Missense Mutation p.(Arg371Gln)

To test whether the p.(Arg371Gln) missense mutation influenced the binding capacity of CNP to NPR-B, we derived three-dimensional homology models of the ECD of NPR-B (**Figure 5**). A PDB library BLAST search was performed to identify the appropriate template for the NPR-B ECD domain. PDB entry 1DP4 (59.6% similarity with ECD) was selected as the template for homology modeling. The model having the lowest DOPE score (−49087.96) was selected for further exploration. After stereochemical validation and Z-score analysis, minor deviation around the mutation site was intuitively observed by superimposition of the monomer model of ECD^{wt} and ECD^{371Q} (**Figures 5A–C**). The homomeric structures of ECD, produced by the GalaxyWeb server, were subjected to MD simulation for initial structural refinement (**Supplementary Figures S5, S6**). The last frame of the trajectory was selected for further analysis of the coordinates of the MD refined homology ECD domain. The stereochemical validation of the MD refined homology ECD revealed that approximately 89.4% of residues occupied the most favored region in the Ramachandran plot (**Figure 5D**). Z-score (−8.5) analysis using the ProSAweb server demonstrated that the quality was sufficient for subsequent analyses (**Figure 5H**). Upon superimposition between the homodimers of ECD^{wt} and ECD^{371Q}, we observed that the CNP binding site of ECD^{371Q} was constricted and may result in a reduction in CNP binding (**Figures 5E–G**). In addition, analysis of the molecular interactions between homodimers indicated one hydrogen bond interaction between Try78 and Arg110 in ECD^{wt}, three hydrogen bond interactions between Asp86 and His114, and more π-cation interactions in ECD^{371Q} (**Figures 5I,J**; **Table 1**).

Next, we performed molecular docking studies between CNP and homodimers (ECD^{wt} and ECD^{371Q}, **Figures 5K,L**) using the HPEPDOCK server. Compared with the wild-type homodimers of NPR-B, molecular interactions of CNP with mutated homodimers of NPR-B were reduced by one hydrogen bond interaction and one salt bridge interaction (**Table 2**), suggesting that ECD^{371Q} homodimers of NPR-B weakened the binding of CNP to the mutated homodimers of NPR-B.

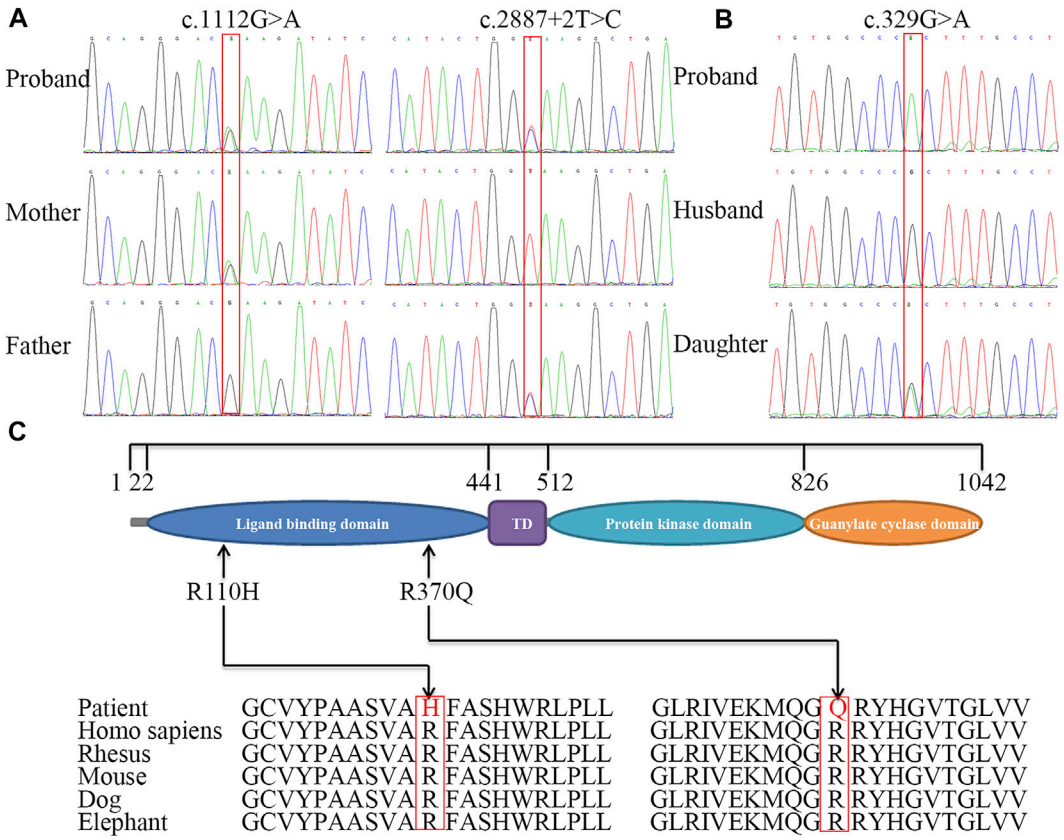

FIGURE 3 | Sequence analysis of *NPR2* gene and conservation analysis of missense mutations. Partial DNA sequence of three variants including c.1112G>A and splice donor site variant identified in family 1, mother and father are carriers for above mentioned mutation **(A)**, and missense homozygous mutation c.329G>A identified in patient 2, her daughter is carrier for the same mutation **(B)**. The structure of *NPR2* and the position of mutations **(C)**. The different geometric shapes with different colors on amino acid (aa) sequence denote the four distinct functional regions respectively. Its amino acid substitution in two patients were both highly conservative substitution.

4 DISCUSSION

In the current study, we performed clinical and molecular evaluations of two Chinese patients with AMDM exhibiting the phenotype of short stature and characteristic shortening of the middle and distal segments of the limbs. For Chinese patients, only one patient with AMDM has been reported. WES analysis revealed the novel compound heterozygous mutations c.2887+2T>C and c.1112G>A p.(Arg371Gln) in *NPR2* in patient 1. In addition, a homozygous missense mutation c.329G>A p.(Arg110His) was found in patient 2, which was recently reported (Simsek-Kiper et al., 2021). The pathogenicity of the two novel mutations (c.2887+2T>C, c.1112G>A) was confirmed by segregation analysis, transcript analysis, and in silico analysis. Heterozygous *NPR2* mutations with dominant-negative effects have been first observed in patients with idiopathic short stature (Bartels et al., 2004). Our finding that heterozygous carriers of variants (c.1112G>A, c.2887+2T>C, c.329G>A) also had a subtler proportionate short stature suggested that heterozygous mutations caused haploinsufficiency or topology modification of *NPR2*, which resulted in the loss of height potential.

Most AMDM-related *NPR2* mutations are hypothesized to cause disease by impairing trafficking to the plasma membrane, altering CNP ligand binding affinity, or inhibiting the activity of NPR-B. Recently, Irfanullah et al. suggested that the missense mutation p.(Leu314Arg) allosterically affects the binding of NPR-B homodimer to CNP (Irfanullah et al., 2018). The novel missense variant p.(Arg371Gln) identified in patient 1 was positioned in the CNP-ligand binding domain. In silico modeling analysis showed that inter-residual molecular interactions of the mutant structure were enhanced compared with that in the wild-type owing to enhanced hydrogen bond formation between Asp86 of one monomer and His114 of the other monomer. Our modeling results were consistent with the speculation that the mutation disrupted the CNP binding site in the extracellular domain as a result of the global allosteric effects of the homodimer. The splice mutation c.2887+2T>C identified in patient 1 was located in intron 19 of *NPR2*. An RNA/cDNA study was performed to analyze the consequences of c.2887+2T>C, which resulted in three aberrantly spliced transcripts in patient 1. The main transcript, lacking exon 19, was predicted to produce a truncated protein lacking a large proportion of the guanylate cyclase domain. Therefore, this

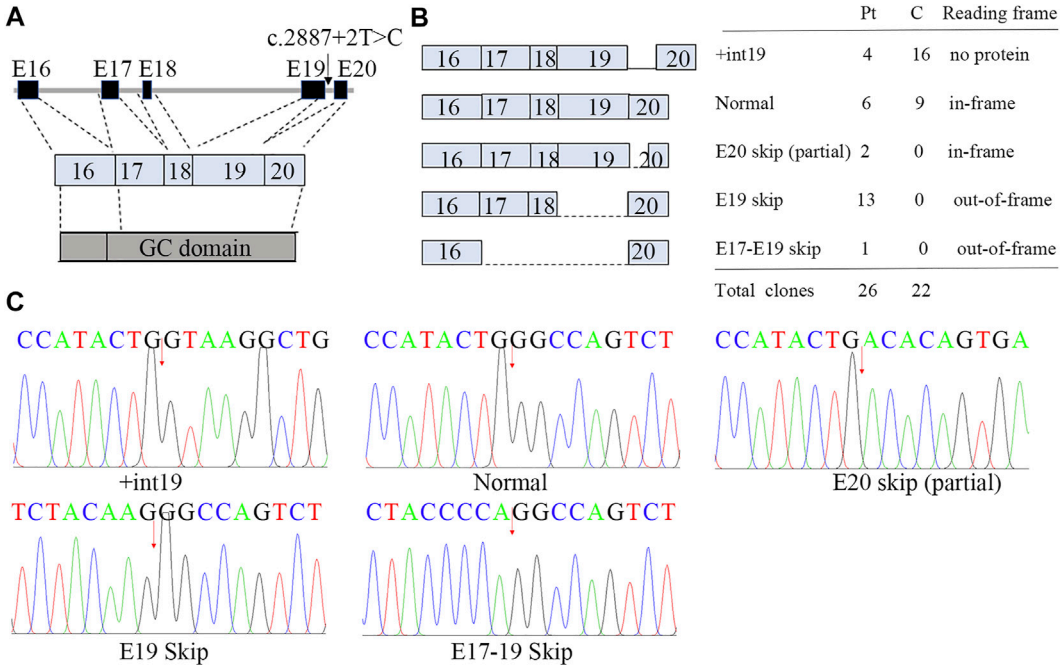

FIGURE 4 | Aberrant splicing of c.2887+2T>C. **(A)** Genomic architecture of *NPR2* gene through exons 16 to 20. **(B)** Subcloning of the RT-PCR product demonstrated multiple forms of aberrant splicing. The table shows the number of clones. **(C)** cDNA sequencing of breakpoint in *NPR2*. The possible breakpoints are indicated with arrows.

mutation is likely to cause disease by suppressing the activity of NPR-B. Subcellular localization studies have shown that the mutation p.(Arg110Cys) in *NPR2*, identified in a Japanese family showing the phenotype of short stature, is defective in cellular trafficking from the endoplasmic reticulum to the Golgi apparatus (Jacob et al., 2018). We hypothesize that the reported missense mutation p.(Arg110His) may cause AMDM by impairing trafficking to the plasma membrane.

Evaluation of typical facial features and radiological data for skeletal involvement will be beneficial to the clinical diagnosis of AMDM. Patient 1 had more striking skeletal dysplasia in the middle and distal extremities than in the trunk. Patient 2 and the reported 9-year-old boy carried the same homozygous mutation c.329G>A in *NPR2* (**Supplementary Table S3**). The above-mentioned boy had mild obstructive sleep apnea, whereas patient 2 did not. No radiological data were available for patient 2. Current information demonstrated that morphological changes in vertebral bodies with age may increase the risk for subsequent development of spinal stenosis (Ain et al., 2019) and obstructive sleep apnea (Huang et al., 2012; Simsek-Kiper et al., 2021), which will seriously influence patient quality of life and should be considered during follow-up. Tricuspid regurgitation was found in patient 1 in our study and mitral valve insufficiency in a 54-year-old female patient and the above-mentioned boy with AMDM (Simsek-Kiper et al., 2021). The co-occurrence of heart valve diseases may be because of the high parental consanguinity rate, which may contribute to heart valve diseases probably related to other gene mutations (Simsek-Kiper et al., 2021). Although NPR-B has already been shown to mediate the effects of aortic valve development and disease in mice (Blaser et al., 2018), the relationship between *NPR2* and heart valve diseases is unclear and should be explored in the future. Patient 2 had a 6-year-old daughter who was conceived without the use of any type of assisted reproductive technology. To date, most reported cases have been in children. No reports have described female fertility in adults affected with AMDM; however, a few other pedigrees have also shown normal fertility in men with the AMDM phenotype (Irfanullah et al., 2018). A distinct *NPR2*-knockout mouse model harboring a 4-bp deletion in exon 3 exhibited dwarfism and female sterility with normal pituitary and uterine function (Geister et al., 2013). The precise contribution of NPR-B to human reproduction is not yet clear.

Few reports have described long-term data in patients with AMDM receiving rhGH treatment. To date, there had been three patients with AMDM who received rhGH treatment, reported in two different studies; however, the therapeutic effects of rhGH treatment were controversial. Arya et al. (2020) found that the final heights of the two patients with AMDM (130.5 and 134 cm, respectively) were significantly greater than the average reported final height (110–120 cm) of patients with AMDM after long-term rhGH treatment (0.525–0.7 mg/kg/week, 8 years). Olney, (2006) have suggested that one patient with AMDM showed poor responses to high-dose rhGH treatment (0.35 mg/kg/week, 1.5–5.5 years of age) owing to resistance to the effects of rhGH. In this study, rhGH therapy improved the linear growth of proband 1 after high-dose GH treatment

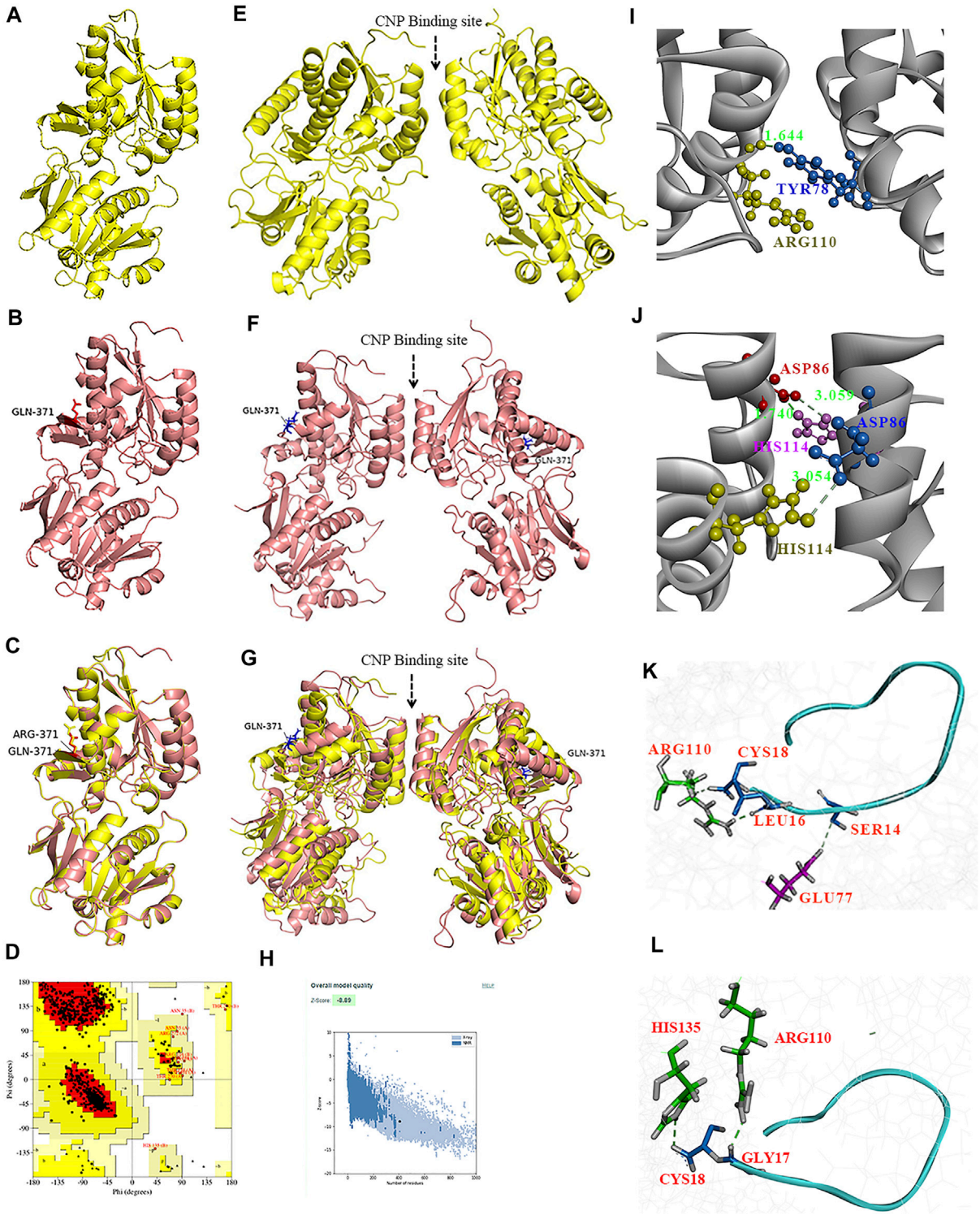

FIGURE 5 | Homology modeling of the wild type and mutant ECD of HsNPR2. A three-dimensional model of the monomer of ECD^{wt} **(A)**, monomer of ECD^{371Q} **(B)**, and the graphic superimposition between the monomer of ECD^{wt} and ECD^{371Q} **(C)**. Validation of the homology ECD domain model of HsNPR2. Residues distribution of the ECD **(D)** in the correspondent regions of Ramachandran plot. Z-score validation of the ECD **(E)**. The MD refined homo-dimer of ECD^{wt} **(F)**, the MD refined homo-dimer of ECD^{371Q} **(G)** and the graphic superimposition of the MD refined homology between ECD^{wt} and ECD^{371Q} **(H)**. Comparing to ECD^{wt}, the binding between CNP and the MD refined homodimer of ECD^{371Q} is arrow-pointed in panel. Structural and molecular analyses suggest mutant ECD of NPR2 constricts the CNP binding site due to enhanced polar interactions in the homodimer **(I,J)**. One hydrogen bond formation between Try78 and Arg110 in the ECD^{wt} **(I)** and three hydrogen bonds formation between D86 and H114 **(J)**. By comparison to ECD^{wt} **(K)** of NPR2, lessened molecular interactions observed on the ligand CNP to the homodimer of and ECD^{mt} **(L)**.

TABLE 1 | Molecular interactions between the MD refined ECD homo-dimer of NPR2.

MD refined ECD homo-dimer of NPR2	Hydrogen bonds		π-cation interactions	
	Chain A	Chain B	Chain A	Chain B
Wild type	R110	Y78	R110	Y78
			H135	Y78
			F111	L82
			H114	L79
			H114	L82
			L82	F111
			V85	F111
			L82	H114
Mutant (R371Q)	D86	H114	H110	Y78
	H114	D86	Y78	R110
	D86	H114	L82	H114
			Y78	R110
			F111	L82
			F111	V85
			H114	L82
			V85	F111
			L71	H114

Amino acid residues are denoted by single letter symbols i.e.D = Asp, E = Glu, F=Phe, H=His, L = Leu,R = Arg, V=Val, Y = Tyr.

(0.35 mg/kg/week, 3.4–5 years of age). In these three GH-responsive patients with AMDM including those in the current study, IGF-1 levels were within or below the lower limit of the normal range but increased steadily during rhGH treatment. In addition, strikingly lower IGF-1 levels were found in NPR2-knockout mice than in wild-type littermates (Olney, 2006). The mechanism described below may partly explain how rhGH treatment improves bone growth disturbance in patients with AMDM. rhGH restores plasma IGF-1 levels (Binder et al., 2005; Wagner et al., 2021) and sensitivity to IGF-I in local distinct cell lines or to its autocrine/paracrine action (Lebl et al., 2001). IGF-1 further inhibits the p38 mitogen-activated protein kinase cascade (Studer et al., 2004) and promotes high extracellular signal-regulated kinase/p38 activity ratios favoring chondrocyte proliferation (Hutchison, 2012). Notably, rhGH treatment has already been shown to have positive effects on height improvement in AMDM and many other types of skeletal dysplasia (Camtosun et al., 2019; Levy-Shraga et al., 2020; Cetin et al., 2018; Sarafoglou et al., 2010; Utsumi et al., 2017). Additional studies are needed in other individuals with AMDM to determine whether rhGH treatment is effective.

To date, 71 pathogenic mutations in *NPR2* have been shown to be associated with AMDM based on an inclusive review of the literature (Mustafa et al., 2020; Simsek-Kiper et al., 2021) (including the two current cases) and two databases (Human Gene Mutation Database and Leiden Open Variation Database; **Supplementary Table S6**; **Supplementary Figure S7**), including 39 missense mutations, 15 nonsense mutations, six splicing mutations, 10 deletions, and one insertion. Biallelic mutations in *NPR2* that underlie AMDM are found throughout the entire length, except for in exons 9 and 18. Exons 1 (14/71, 19.72%), 6 (6/71, 8.45%), and 19 (9/71, 12.68%) had higher point mutation frequencies than any of the other exons. Biallelic mutations in *NPR2* that underlie AMDM are found throughout the entire length, except for in exons 9 and 18. These identified variants were mainly located in the extracellular CNP-binding domain (47.9%) and intracellular guanylyl cyclase domain (28.2%). Almost all families show unique *NPR2* variants, suggesting a high proportion of segregation through families. It is difficult to identify the genotype-phenotype correlations of distinct mutations in different functional regions of NPR-B or even in the same functional region.

There were some limitations to our study. First, because the biological parents of patient 2 were unavailable, clinical phenotypes and segregation analysis could not be performed in this study. Second, owing to the absence of previous clinical records, we could not describe the developmental data of patient 2 in this study. Third, it may still be important to investigate the molecular effect of these mutations in *NPR2 in vitro* in the future. Therefore, further studies and randomized controlled trials with more patients are needed to confirm the effects of rhGH therapy on final height in patients with AMDM.

In conclusion, clinical and molecular evaluations produced three different variants in *NPR2* in two families from China, manifesting the variable clinical features of AMDM. The identified novel mutations, c.2887+2T>C and p. Arg371Gln, exerted dominant-negative effects, reducing the activity of NPR-B and the binding affinity of NPR-B to CNP. Our findings indicated that the two novel mutations were loss-of-function mutations. Relatively short-term high-dose rhGH treatment significantly increased the height SDS of patient 1. Further studies and randomized controlled trials with more patients are needed to confirm the effects of rhGH therapy on final height in patients with AMDM.

TABLE 2 | Molecular interactions between CNP and the MD refined ECD homo-dimer of NPR2.

MD refined ECD homo-dimer of NPR2	Hydrogen bonds			Salt bridges interactions		
	CNP	Chain A	Chain B	CNP	Chain A	Chain B
Wild type	L16	R110		K6	E77	
	C18	R110		R9		D134
	S14		E77			
Mutant (R371Q)	G17	R110		R9		E185
	C18	H135				

Amino acid residues are denoted by single letter symbols i.e C=Cys, D = Asp, E = Glu, G = Gly, H=His, L = Leu, K = Lys, R = Arg, S=Ser.

DATA AVAILABILITY STATEMENT

The datasets for this article are not publicly available due to concerns regarding participant/patient anonymity. Requests to access the datasets should be directed to the corresponding authors.

ETHICS STATEMENT

The studies involving human participants were reviewed and approved by the Ethics Committee of Scientific Research and Clinical Trial of The First Affiliated Hospital of Zhengzhou University (2019-KY-401). Written informed consent to participate in this study was provided by the participants' legal guardian/next of kin. Written informed consent was obtained from the individual(s), and minor(s)' legal guardian/next of kin, for the publication of any potentially identifiable images or data included in this article.

AUTHOR CONTRIBUTIONS

JW and YB designed the study, performed data analysis, and wrote the manuscript. MW and ZJ had performed lab experiments and transcriptome analysis. BD, BL, JZ, HZ, YS, and XK collected the blood samples and clinical data, and performed protein structure analysis. XK and XT had revised the manuscript. All authors contributed to data interpretation, approved the final, and submitted version of the manuscript.

FUNDING

This work was supported by the National Natural Science Foundation of China (No. 81300685 to JW, No. 81501851 to YB, and No. U1904137 to HZ) and the Natural Science Foundation of Henan Province (No. 202300410470 to JW).

ACKNOWLEDGMENTS

We thank all the family members for their generous participation. We sincerely thank the cooperation of patient's families.

SUPPLEMENTARY MATERIAL

The Supplementary Material for this article can be found online at: https://www.frontiersin.org/articles/10.3389/fgene.2022.823861/full#supplementary-material

REFERENCES

Ain, N. U., Iqbal, M., Valta, H., Emerling, C. A., Ahmed, S., Makitie, O., et al. (2019). Novel Variants in Natriuretic Peptide Receptor 2 in Unrelated Patients with Acromesomelic Dysplasia Type Maroteaux. *Eur. J. Med. Genet.* 62 (9), 103554. doi:10.1016/j.ejmg.2018.10.006

Arya, V. B., Raj, M., Younes, M., Chapman, S., Irving, M., Kapoor, R. R., et al. (2020). Acromesomelic Dysplasia, Type Maroteaux: Impact of Long-Term (8 Years) High-Dose Growth Hormone Treatment on Growth Velocity and Final Height in 2 Siblings. *Horm. Res. Paediatr.* 93 (5), 335–342. doi:10.1159/000511874

Bartels, C. F., Bükülmez, H., Padayatti, P., Rhee, D. K., van Ravenswaaij-Arts, C., Pauli, R. M., et al. (2004). Mutations in the Transmembrane Natriuretic Peptide Receptor NPR-B Impair Skeletal Growth and Cause Acromesomelic Dysplasia, Type Maroteaux. *Am. J. Hum. Genet.* 75 (1), 27–34. doi:10.1086/422013

Binder, G., Neuer, K., Ranke, M. B., and Wittekindt, N. E. (2005). PTPN11 Mutations Are Associated with Mild Growth Hormone Resistance in Individuals with Noonan Syndrome. *J. Clin. Endocrinol. Metab.* 90 (9), 5377–5381. doi:10.1210/jc.2005-0995

Blaser, M. C., Wei, K., Adams, R. L. E., Zhou, Y.-Q., Caruso, L.-l., Mirzaei, Z., et al. (2018). Deficiency of Natriuretic Peptide Receptor 2 Promotes Bicuspid Aortic Valves, Aortic Valve Disease, Left Ventricular Dysfunction, and Ascending Aortic Dilatations in Mice. *Circ. Res.* 122 (3), 405–416. doi:10.1161/CIRCRESAHA.117.311194

Bussi, G., Donadio, D., and Parrinello, M. (2007). Canonical Sampling through Velocity Rescaling. *J. Chem. Phys.* 126 (1), 014101. doi:10.1063/1.2408420

Çamtosun, E., Akıncı, A., Demiral, E., Tekedereli, İ., and Sığırcı, A. (2019). A Case of Cleidocranial Dysplasia with a Novel Mutation and Growth Velocity Gain with Growth Hormone Treatment. *Jcrpe* 11 (3), 301–305. doi:10.4274/jcrpe.galenos.2018.2018.0211

Çetin, T., Şıklar, Z., Kocaay, P., and Berberoğlu, M. (2018). Evaluation of the Efficacy of Long-Term Growth Hormone Theraphy in Patients with Hypochondroplasıa. *Jcrpe* 10 (4), 373–376. doi:10.4274/jcrpe.0043

Díaz-González, F., Wadhwa, S., Rodriguez-Zabala, M., Kumar, S., Aza-Carmona, M., Sentchordi-Montané, L., et al. (2022). Biallelic cGMP-dependent Type II Protein Kinase Gene (PRKG2) Variants Cause a Novel Acromesomelic Dysplasia. *J. Med. Genet.* 59 (1), 28–38. doi:10.1136/jmedgenet-2020-107177

Geister, K. A., Brinkmeier, M. L., Hsieh, M., Faust, S. M., Karolyi, I. J., Perosky, J. E., et al. (2013). A Novel Loss-Of-Function Mutation in Npr2 Clarifies Primary Role in Female Reproduction and Reveals a Potential Therapy for Acromesomelic Dysplasia, Maroteaux Type. *Hum. Mol. Genet.* 22 (2), 345–357. doi:10.1093/hmg/dds432

Hisado-Oliva, A., Garre-Vázquez, A. I., Santaolalla-Caballero, F., Belinchón, A., Barreda-Bonis, A. C., Vasques, G. A., et al. (2015). HeterozygousNPR2Mutations Cause Disproportionate Short Stature, Similar to Léri-Weill Dyschondrosteosis. *J. Clin. Endocrinol. Metab.* 100 (8), E1133–E1142. doi:10.1210/jc.2015-1612

Huang, P.-C., Chang, J.-H., Shen, M.-L., and Chen, K.-B. (2012). Management of General Anesthesia for a Patient with Maroteaux Type Acromesomelic Dysplasia Complicated with Obstructive Sleep Apnea Syndrome and Hereditary Myopathy. *J. Anesth.* 26 (4), 640–641. doi:10.1007/s00540-012-1389-3

Hutchison, M. R. (2012). BDNF Alters ERK/p38 MAPK Activity Ratios to Promote Differentiation in Growth Plate Chondrocytes. *Mol. Endocrinol.* 26 (8), 1406–1416. doi:10.1210/me.2012-1063

Irfanullah, A., Zeb, A., Shinwari, N., Shah, K., Gilani, S. Z. T., Khan, S., et al. (2018). Molecular and In Silico Analyses Validates Pathogenicity of Homozygous Mutations in the NPR2 Gene Underlying Variable Phenotypes of Acromesomelic Dysplasia, Type Maroteaux. *Int. J. Biochem. Cel Biol.* 102, 76–86. doi:10.1016/j.biocel.2018.07.004

Jacob, M., Menon, S., Botti, C., and Marshall, I. (20182018). Heterozygous NPR2 Mutation in Two Family Members with Short Stature and Skeletal Dysplasia. *Case Rep. Endocrinol.* 2018, 1–4. doi:10.1155/2018/7658496

Khan, S., Basit, S., Khan, M. A., Muhammad, N., and Ahmad, W. (2016). Genetics of Human Isolated Acromesomelic Dysplasia. *Eur. J. Med. Genet.* 59 (4), 198–203. doi:10.1016/j.ejmg.2016.02.011

Langenickel, T., Buttgereit, J., Pagel, I., Dietz, R., Willenbrock, R., and Bader, M. (2004). Forced Homodimerization by Site-Directed Mutagenesis Alters

Guanylyl Cyclase Activity of Natriuretic Peptide Receptor B. *Hypertension* 43 (2), 460–465. doi:10.1161/01.HYP.0000110907.33263.0b

Lebl, J., Průhová, S., Zapletalová, M., and Pechová, fnm. (2001). IGF-I Resistance and Turner's Syndrome. *J. Pediatr. Endocrinol. Metab.* 14 (1), 37–41. doi:10.1515/jpem.2001.14.1.37

Levy-Shraga, Y., Modan-Moses, D., Wientroub, S., Ovadia, D., and Zeitlin, L. (2020). The Effect of Growth Hormone Treatment in a Child with Tricho-Rhino-Phalangeal Syndrome: A Case Report and Review of the Literature. *Eur. J. Med. Genet.* 63 (4), 103830. doi:10.1016/j.ejmg.2019.103830

Li, H., Ji, C. Y., Zong, X. N., and Zhang, Y. Q. (2009). Height and Weight Standardized Growth Charts for Chinese Children and Adolescents Aged 0 to 18 Years. *Zhonghua Er Ke Za Zhi* 47 (7), 487–492.

Li, Q., Chen, Z., Xiong, H., Li, R., Yu, C., Meng, J., et al. (2021). Novel Partial Exon 51 Deletion in the Duchenne Muscular Dystrophy Gene Identified via Whole Exome Sequencing and Long-Read Whole-Genome Sequencing. *Front. Genet.* 12, 762987. doi:10.3389/fgene.2021.762987

Mortier, G. R., Cohn, D. H., Cormier-Daire, V., Hall, C., Krakow, D., Mundlos, S., et al. (2019). Nosology and Classification of Genetic Skeletal Disorders: 2019 Revision. *Am. J. Med. Genet.* 179 (12), 2393–2419. doi:10.1002/ajmg.a.61366

Mustafa, S., Akhtar, Z., Latif, M., Hassan, M., Faisal, M., and Iqbal, F. (2020). A Novel Nonsense Mutation in NPR2 Gene Causing Acromesomelic Dysplasia, Type Maroteaux in a Consanguineous Family in Southern Punjab (Pakistan). *Genes Genom* 42 (8), 847–854. doi:10.1007/s13258-020-00955-3

Olney, R. C. (2006). C-type Natriuretic Peptide in Growth: A New Paradigm. *Growth Horm. IGF Res.* 16 (Suppl. A), 6–14. doi:10.1016/j.ghir.2006.03.016

Osebold, W. R., Lester, E. L., Remondini, D. J., Spranger, J. W., Opitz, J. M., and Reynolds, J. F. (1985). An Autosomal Dominant Syndrome of Short Stature with Mesomelic Shortness of Limbs, Abnormal Carpal and Tarsal Bones, Hypoplastic Middle Phalanges, and Bipartite Calcanei. *Am. J. Med. Genet.* 22 (4), 791–809. doi:10.1002/ajmg.1320220414

Parrinello, M., and Rahman, A. (1981). Polymorphic Transitions in Single Crystals: A New Molecular Dynamics Method. *J. Appl. Phys.* 52 (12), 7182–7190. doi:10.1063/1.328693

Potter, L. R., and Hunter, T. (2001). Guanylyl Cyclase-Linked Natriuretic Peptide Receptors: Structure and Regulation. *J. Biol. Chem.* 276 (9), 6057–6060. doi:10.1074/jbc.R000033200

Ramachandran, G. N., Ramakrishnan, C., and Sasisekharan, V. (1963). Stereochemistry of Polypeptide Chain Configurations. *J. Mol. Biol.* 7, 95–99. doi:10.1016/s0022-2836(63)80023-6

Richards, S., Aziz, N., Bale, S., Bick, D., Das, S., Gastier-Foster, J., et al. (2015). Standards and Guidelines for the Interpretation of Sequence Variants: A Joint Consensus Recommendation of the American College of Medical Genetics and Genomics and the Association for Molecular Pathology. *Genet. Med.* 17 (5), 405–424. doi:10.1038/gim.2015.30

Rootsi, S., Kivisild, T., Benuzzi, G., Help, H., Bermisheva, M., Kutuev, I., et al. (2004). Phylogeography of Y-Chromosome Haplogroup I Reveals Distinct Domains of Prehistoric Gene Flow in Europe. *Am. J. Hum. Genet.* 75 (1), 128–137. doi:10.1086/422196

Sarafoglou, K., Moassesfar, S., and Miller, B. (2010). Improved Growth and Bone mineral Density in Type I Trichorhinophalangeal Syndrome in Response to Growth Hormone Therapy. *Clin. Genet.* 78 (6), 591–593. doi:10.1111/j.1399-0004.2010.01434.x

Simsek-Kiper, P. O., Urel-Demir, G., Taskiran, E. Z., Arslan, U. E., Nur, B., Mihci, E., et al. (2021). Further Defining the Clinical and Molecular Spectrum of Acromesomelic Dysplasia Type Maroteaux: A Turkish Tertiary center Experience. *J. Hum. Genet.* 66 (6), 585–596. doi:10.1038/s10038-020-00871-0

Studer, R. K., Bergman, R., Stubbs, T., and Decker, K. (2004). Chondrocyte Response to Growth Factors Is Modulated by P38 Mitogen-Activated Protein Kinase Inhibition. *Arthritis Res. Ther.* 6 (1), R56–R64. doi:10.1186/ar1022

Ullah, A., Umair, M., Muhammad, D., Bilal, M., Lee, K., Leal, S. M., et al. (2018). A Novel Homozygous Variant in BMPR1B Underlies Acromesomelic Dysplasia Hunter-Thompson Type. *Ann. Hum. Genet.* 82 (3), 129–134. doi:10.1111/ahg.12233

Umair, M., Rafique, A., Ullah, A., Ahmad, F., Ali, R. H., Nasir, A., et al. (2017). Novel Homozygous Sequence Variants in the GDF5 Gene Underlie Acromesomelic Dysplasia Type-Grebe in Consanguineous Families. *Congenit. Anom.* 57 (2), 45–51. doi:10.1111/cga.12187

Utsumi, T., Okada, S., Izawa, K., Honda, Y., Nishimura, G., Nishikomori, R., et al. (2017). A Case with Spondyloenchondrodysplasia Treated with Growth Hormone. *Front. Endocrinol.* 8, 157. doi:10.3389/fendo.2017.00157

Wagner, B. M., Robinson, J. W., Lin, Y.-W., Lee, Y.-C., Kaci, N., Legeai-Mallet, L., et al. (2021). Prevention of Guanylyl Cyclase-B Dephosphorylation Rescues Achondroplastic Dwarfism. *JCI Insight* 6 (9). doi:10.1172/jci.insight.147832

Zhou, P., Moon, J. E., Mericq, V., Potter, L. R., Warman, M. L., Hirschhorn, J. N., et al. (2018). HPEPDOCK: A Web Server for Blind Peptide-Protein Docking Based on a Hierarchical Algorithm. *Nucleic Acids Res.* 46 (W1), W443–W450. doi:10.1093/nar/gky357

Conflict of Interest: The authors declare that the research was conducted in the absence of any commercial or financial relationships that could be construed as a potential conflict of interest.

Publisher's Note: All claims expressed in this article are solely those of the authors and do not necessarily represent those of their affiliated organizations, or those of the publisher, the editors, and the reviewers. Any product that may be evaluated in this article, or claim that may be made by its manufacturer, is not guaranteed or endorsed by the publisher.

frontiers | Frontiers in Genetics

ORIGINAL RESEARCH
published: 05 April 2022
doi: 10.3389/fgene.2022.827560

A Novel Mutation c.3392G>T of *COL2A1* Causes Spondyloepiphyseal Dysplasia Congenital by Affecting Pre-mRNA Splicing

*Lihong Fan[1], Longfei Ji[2], Yuqing Xu[3], Guosong Shen[1], Kefeng Tang[1], Zhi Li[1], Sisi Ye[1] and Xueping Shen[1]**

[1]Center of Prenatal Diagnosis, Huzhou Maternity & Child Health Care Hospital, Huzhou, China, [2]Department of Clinical Laboratory, The First People's Hospital of Huzhou, Huzhou, China, [3]Department of Reproductive Genetics, Women's Hospital, School of Medicine Zhejiang University, Hangzhou, China

Spondyloepiphyseal dysplasia congenital (SEDC) is a rare chondrodysplasia caused by dominant pathogenic variants in *COL2A1*. Here, we detected a novel variant c.3392G > T (NM_001844.4) of *COL2A1* in a Chinese family with SEDC by targeted next-generation sequencing. To confirm the pathogenicity of the variant, we generated an appropriate minigene construct based on HeLa and HEK293T cell lines. Splicing assay indicated that the mutated minigene led to aberrant splicing of *COL2A1* pre-mRNA and produced an alternatively spliced transcript with a skipping of partial exon 48, which generated a predicted in-frame deletion of 15 amino acids (p. Gly1131_Pro1145del) in the COL2A1 protein. Due to the pathogenicity of the variation, we performed prenatal diagnosis on the proband's wife, which indicated that the fetus carried the same mutation.

Keywords: spondyloepiphyseal dysplasia congenital, *COL2A1*, next-generation sequencing, minigene, in-frame deletion, prenatal diagnosis

OPEN ACCESS

Edited by:
Yi Zhang,
Central South University, China

Reviewed by:
May Thandar Aung-Htut,
Murdoch University, Australia
Xuexiu Zheng,
Gwangju Institute of Science and Technology, South Korea
Junjiang Fu,
Southwest Medical University, China

****Correspondence:***
Xueping Shen
xp050204@163.com

Specialty section:
This article was submitted to Genetics of Common and Rare Diseases, a section of the journal Frontiers in Genetics

Received: *02 December 2021*
Accepted: *22 March 2022*
Published: *05 April 2022*

Citation:
Fan L, Ji L, Xu Y, Shen G, Tang K, Li Z, Ye S and Shen X (2022) A Novel Mutation c.3392G>T of COL2A1 Causes Spondyloepiphyseal Dysplasia Congenital by Affecting Pre-mRNA Splicing. Front. Genet. 13:827560. doi: 10.3389/fgene.2022.827560

INTRODUCTION

Spondyloepiphyseal dysplasia congenital (SEDC) is a rare genetic disorder characterized by a short trunk, cervical spine subluxation, scoliosis, coxa vara, kyphosis, and metaphyseal changes (Xiong et al., 2018). Patients may also show extra-skeletal abnormalities such as myopia, hearing loss, and cleft palate (Deng et al., 2016; Zheng et al., 2020). The various mutations in the *COL2A1* gene, which contains 57 exons are the genetic cause of SEDC (Anderson et al., 1990; Nishimura et al., 2005).

Until today, according to HGMD (professional 2020.4), at least 130 different *COL2A1* mutations have been reported to be causally associated with SEDC. Most of these reported mutations were analyzed primarily at the genomic level (Dasa et al., 2019; Zheng et al., 2020). Only in a few studies have the effects of mutations been confirmed at both DNA and RNA levels (Bruni et al., 2021). A major concern is that we may detect many genomic DNA (gDNA) substitutions of unknown significance, and their pathogenicity is sometimes in urgent need of accurate assessment, especially when prenatal diagnosis and genetic counseling are required. A considerable number of studies have shown that exonic single-nucleotide variants can affect RNA splicing (Inoue et al., 2020; Wang et al., 2020). The most effective way to identify splicing alterations is to analyze the mRNA extracted from the patients' relevant tissue. But in fact, this type of sample is not always available. In addition, it is often uneasy to analyze mRNA due to its instability and low expression level in peripheral leukocytes.

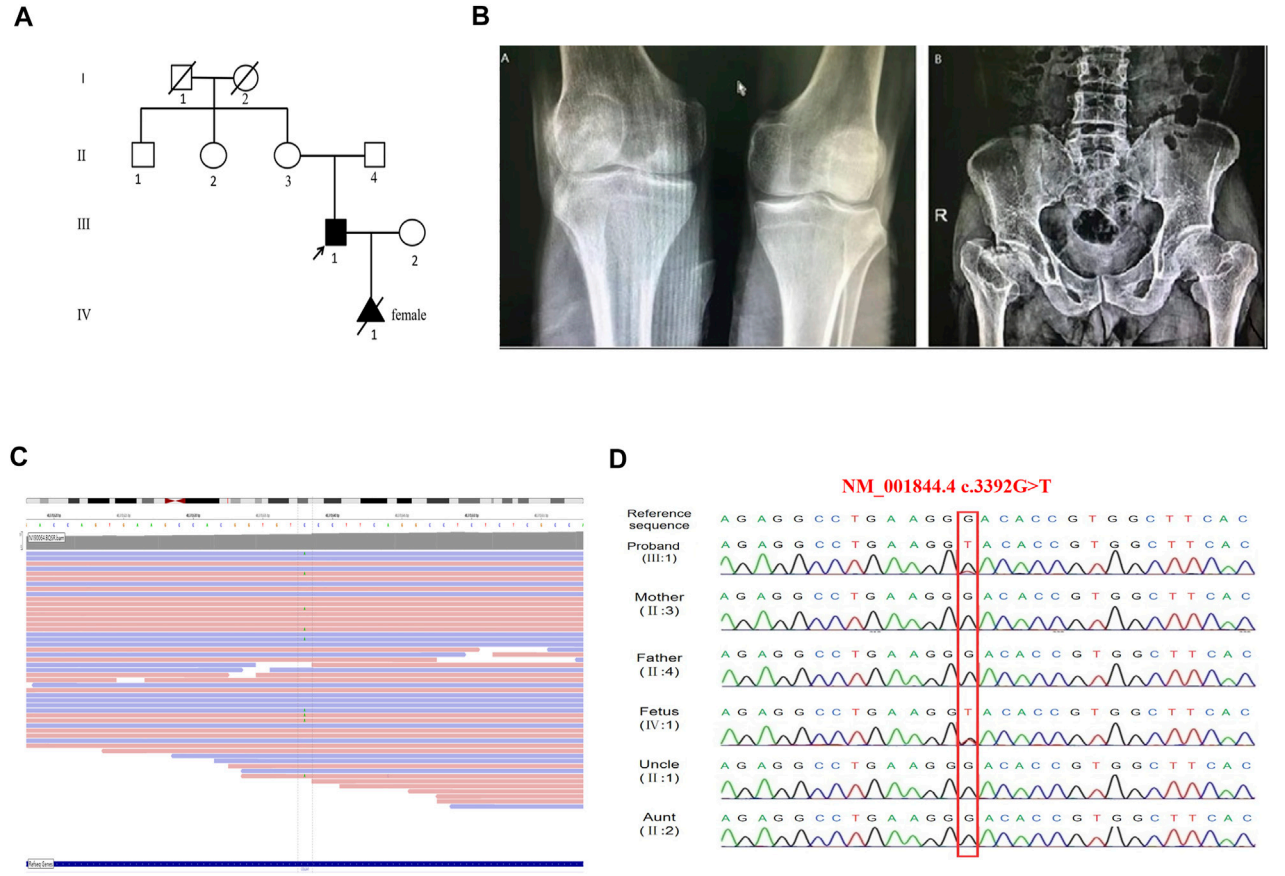

FIGURE 1 | Feature of the proband and the *COL2A1* mutation in this family. **(A)** The pedigree of the proband. **(B)** Radiographs of the proband. The lower femur and the upper tibia are flattened and narrowed (left panel), the bilateral femoral heads are flattened, and the femoral neck is shortened (right panel). **(C)** Screenshot of the Integrative Genomics Viewer. Alternative alleles at *COL2A1* c.3392 position are marked. The total depth of sequencing coverage at this position was 44 reads. The allele frequency was 20% of tatal depth corresponding to the ref/alt was 35/9, suggesting mosaicism. **(D)** The Targeted next-generation sequencing and Sanger sequencing showed the proband and fetus carring the same mutation of c.3392G > T.

Now minigene analysis has emerged as an alternative method to preliminarily assess whether a particular variant affects pre-mRNA splicing (Putscher et al., 2021).

In this study, we detected a novel variant in an SEDC family and further analyzed its pathogenicity by generating an appropriate minigene construct, followed by prenatal diagnosis and genetic counseling.

PATIENTS AND METHODS

Case Presentation

The proband (III 1, **Figure 1A**) was a 36 years old man, with a height of 143 cm. He had an abnormal gait when he was 1 year old and then X-ray films showed hip dislocation (data not shown). Growth was markedly tardy from 13 years old and the pain in the hip appeared since the age of 25 years old, especially after long-distance walking. His eyesight, hearing, and intelligence were normal. X-ray films revealed flattened bilateral femoral heads, shortened femoral neck, flattened and narrowed articular surface of the lower femur and upper tibia (**Figure 1B**). His parents were healthy as neither of them displayed any signs of skeletal deformities or extra-skeletal deformities. As the proband's wife was pregnant at the first visit, both the proband's genetic diagnosis and prenatal diagnosis needed to be provided.

The current investigation was approved by the Ethics Committee of Huzhou Maternity & Child Health Care Hospital. All participants were provided their written informed consents.

Targeted Next-Generation Sequencing and Data Analyses

A targeted next-generation sequencing panel was used to capture all exon sequences of 2,740 genes known to be associated with skeletal disorders. The peripheral blood sample of the proband was collected. Genomic DNA was then extracted using a Lab-Aid 820 DNA blood Mini Kit (Zeesan, China). Exome capture was

TABLE 1 | *In silico* analysis of the *COL2A1* variant c.3392G > T.

	Software	Value	Effect		Software	Δ Score	Effect
Missense variant prediction	REVEL	0.980	+	Splicing prediction	SpliceAI	0.98	+
	ClinPred	0.999	+		CBS	0.93	+
	Polyphen2	0.999	+		HSF		+

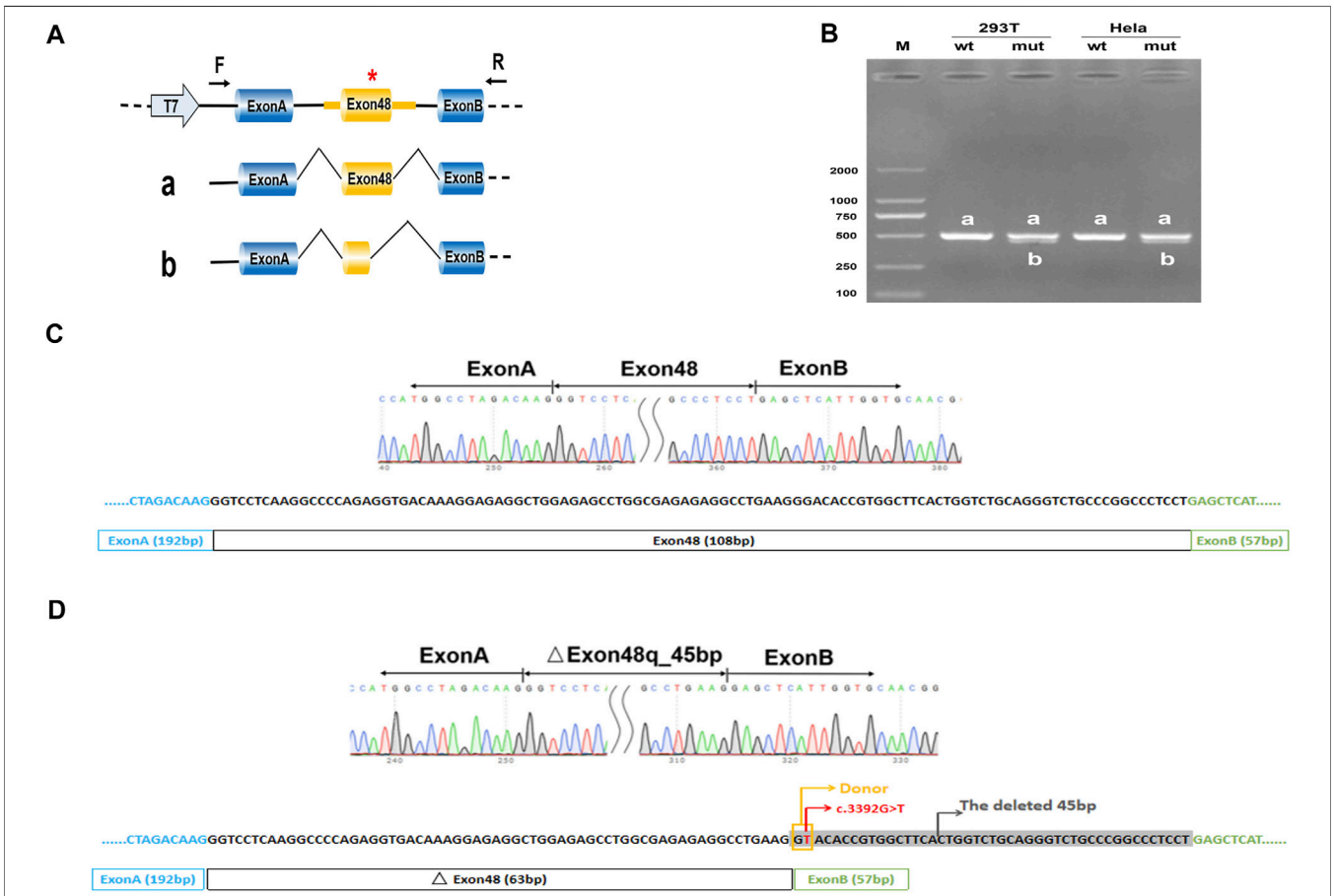

FIGURE 2 | Minigene analysis based on pcDNA3.1-COL2A1-wt/mut recombinant vectors. **(A)**, Schematic illustration of cloned vectors. Red * indicates the mutation position. **(B)** Gel electrophoresis of the RT-PCR products in both 293T and HeLa cell lines. M means the DNA marker. Wild type (wt) exhibited a single band, a (full); mutant type (mut) exhibited double bands, a (full) and b (45 bp deletion). **(C)** Sanger sequencing result of the normal transcript. **(D)** Sanger sequencing result of the transcript with cryptic splicing caused by the mutation. The two bases in the yellow rectangle form a new donor, and the sequences in grey shade represent the missing 45 bases.

performed using SureSelect Human All Exon V6 kit (Agilent Technologies, Santa Clara, CA, United States), followed by sequencing using an Illumina HiSeq2000 system (Illumina, San Diego, CA, United States). Whereafter, multiple database annotations (such as dbSNPs, ESP6500, GnomAD, 1,000 genomes, HGMD, LOVD 3.0, and ClinVar) were performed simultaneously to identify single nucleotide variants (SNVs). Finally, Sanger sequencing was performed to confirm the variant and evaluate the mode of inheritance.

Splicing Prediction

To assess the presumptive effect of this variant on splicing, three different *in silico* prediction tools: SpliceAI (https://spliceailookup.broadinstitute.org/), Human Splicing Finder-Version 3.1 (HSF, http://www.umd.be/HSF3/HSF.shtml), and CBS were used.

Minigene Splicing Assay

To create hybrid minigene constructs we used two vectors including pcMINI and pcDNA3.1, which we developed

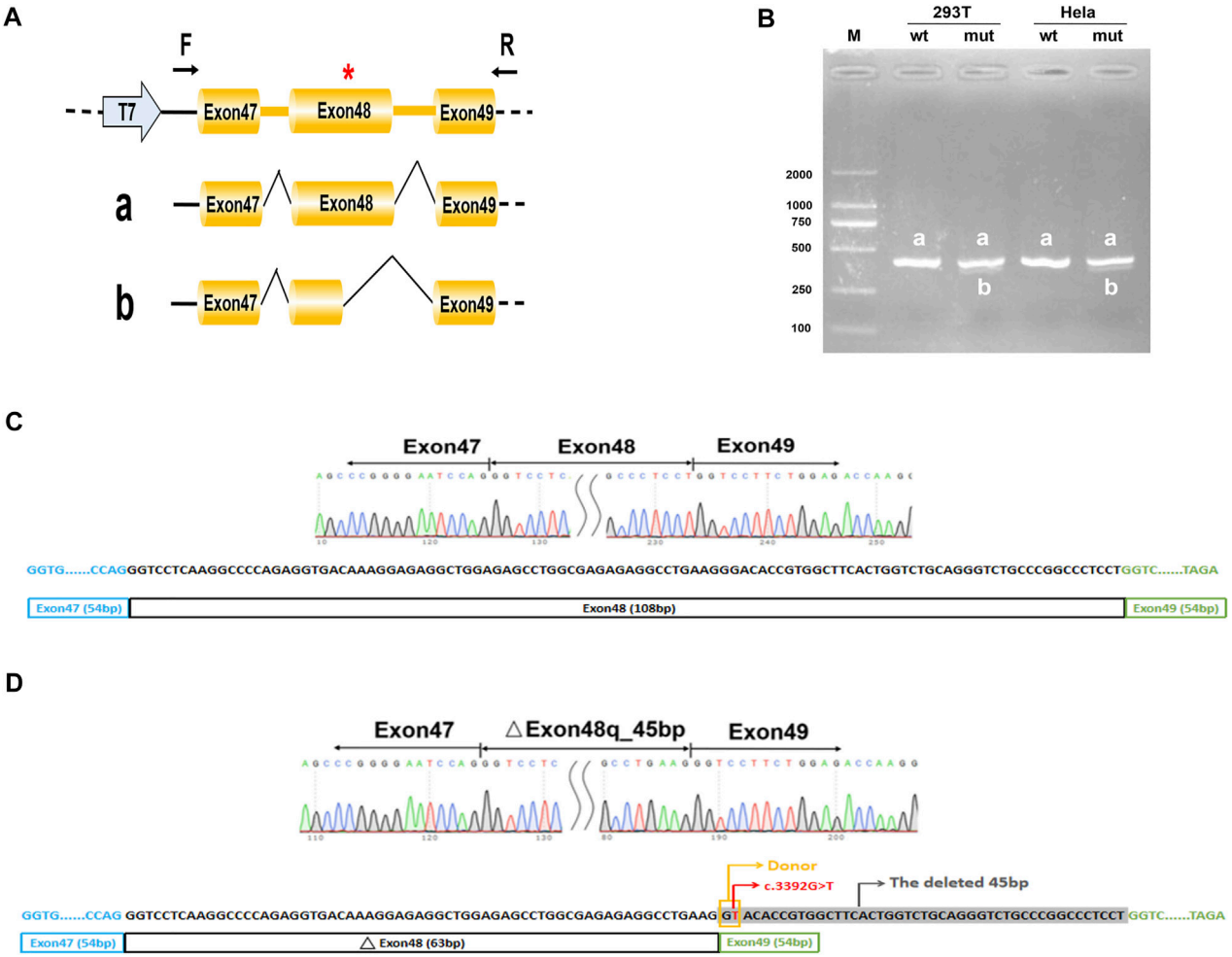

FIGURE 3 | Minigene analysis based on pcMINI-COL2A1-wt/mut recombinant vectors. **(A)**, Schematic illustration of cloned vectors. Red * indicates the mutation position. **(B)** Gel electrophoresis of the RT-PCR products in both 293T and HeLa cell lines. M means the DNA marker. Wild type (wt) exhibited a single band, a (full); mutant type (mut) exhibited double bands, a (full) and b (45 bp deletion). **(C)** Sanger sequencing result of the normal transcript. **(D)** Sanger sequencing result of the transcript with cryptic splicing caused by the mutation. The two bases in the yellow rectangle form a new donor, and the sequences in grey shade represent the missing 45 bases.

previously. Two wild-type fragments, one containing partial intro47 (169bp)-Exon48 (108bp)-partial intro48 (218bp), another containing Exon47 (54bp)-intro47 (182bp)-Exon48 (108bp)-intro48 (244bp)-Exon49 (54bp) were amplified by NEST-PCR. Then we introduced mutations by site-directed mutagenesis using PrimeStar mutagenesis basal kit (Takara Bio Inc.), according to the manufacturer's instructions. The wild-type and mutated amplified products were purified by a gel extraction kit and then respectively cloned into the pcMINI and the pcDNA3.1 expression vector at the KpnI and BamHI restriction sites to generate four minigene constructs: pcMINI-COL2A1-wt/mut, and pcDNA3.1-COL2A1-wt/mut. All the primers are shown in **Supplementary Table S1**.

After plasmid amplification in DH5α competent cells and plasmid extraction (SIMGEN), the sequences and correct orientations of all the recombinant vectors were checked by Sanger sequencing (Macrogen, Madrid, Spain). Then the hybrid minigenes were transfected into HEK293T and HeLa cells using Lipofectamine® 2000 (Thermo Fisher Scientific, Waltham, MA, CA). Total RNA was extracted from cells after 48h using the Trizol reagent (TaKaRa) according to the manufacturer's instructions. Reverse transcription was performed with the Hifair® II 1st Strand cDNA Synthesis SuperMix for qPCR (gDNA digester plus) kit (Yeasen, Shanghai China) according to the manufacturer's instructions. The cDNA was amplified by PCR, then PCR

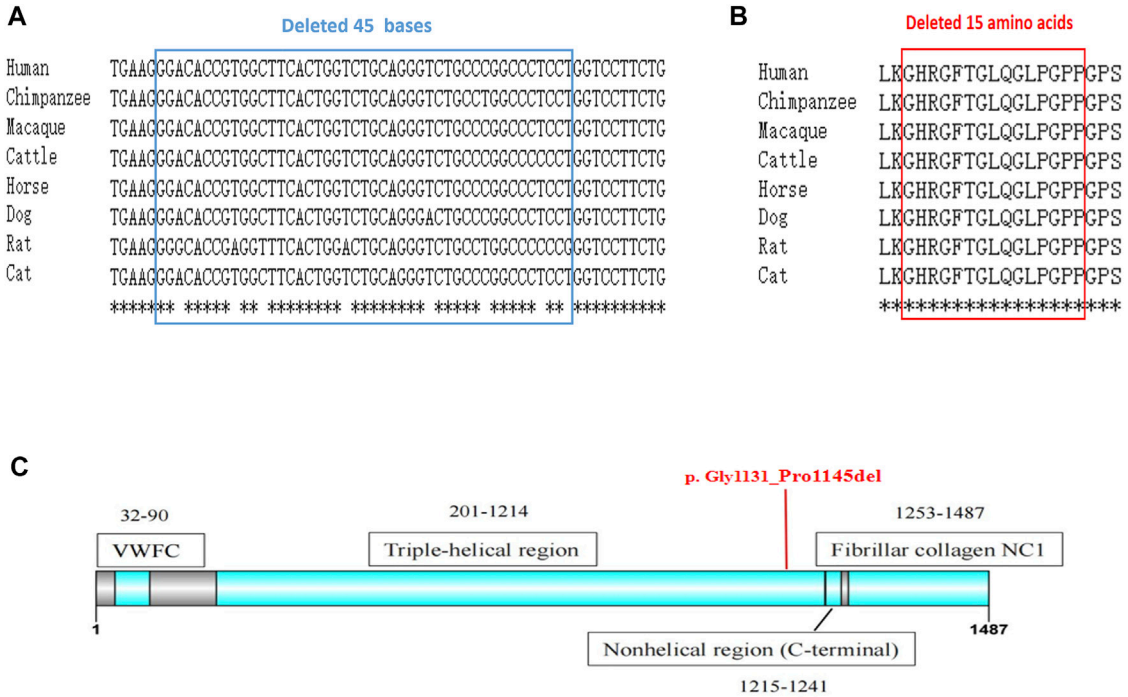

FIGURE 4 | The conservation analysis and location of the mutation. **(A)** Alignment of *COL2A1* DNA sequences from multiple species. The affected bases affected by our novel mutation are highly conserved during evolution. **(B)** Alignment of COL2A1 amino-acid sequences from multiple species., analyzed by Online clustal omega (https://www.ebi.ac.uk/Tools/msa/clustalo/). **(C)** The deleted 15 amino acids locate in the triple helix region of COL2A1. The secondary structure of the protein is obtained from the uniprot database.

products were analyzed by electrophoresis on a 1.5% agarose gel and Sanger sequencing (Macrogen, Madrid, Spain).

Prenatal Diagnosis

Ultrasound-guided amniocentesis was performed at 19^{+2} weeks of gestation to obtain 30 ml of amniotic fluid, 15 ml for cell culture, a necessary step for conventional karyotype analysis, and another 15 ml for DNA extraction, which was performed for Sanger sequencing. The DNA extraction procedure is the same as described above.

RESULTS

Identification and Bioinformatics Prediction of c.3392G > T in *COL2A1*

A novel variant c.3392G > T (NM_001844.4) in exon 48 of *COL2A1* was identified in the proband. A lower-than-expected number of reads supporting the variant suggested possible mosaicism (**Figure 1C**). This variant was not included in the normal population database (dbSNPs, ESP6500, GnomAD, and 1,000 genomes databases) or, as a pathogenic variant, in HGMD (professional 2020.2), LOVD 3.0, and ClinVar databases. Sanger sequencing of the mutation site observed in the proband confirmed the presence of the wild-type sequence in the unaffected parents (**Figure 1D**), thus identifying a *de novo* mutation in the proband. Functional predictions of the missense mutation by REVEL, Polyphen2, and ClinPred are shown in **Table 1**. *In silico* tools, HSF, SpliceAI, and CBS predicted that c.3392G > T may affect *COL2A1* RNA splicing by creating a new donor site. The splicing score is also shown in **Table 1**.

Splicing Analysis of *COL2A1* c.3392G > T in the Minigene

Considering that the variant does not contain the splice acceptor site of exon 48 of *COL2A1*, we generated an appropriate minigene construct to explore the variant's effect (**Figure 2A**, **Figure 3A**). By electrophoresis, the RT-PCR amplification products showed each mutant sample had two bands, one identical to the wild type and one slightly lower than the wild type (**Figures 2B**, **3B**). Sanger sequencing of the long product showed that the wild type sequence came from the normal splicing, whereas the short product revealed a skipping of exon 48, which generated an in-frame deletion of 15 amino acids (p. Gly1131_Pro1145del) in the COL2A1 protein (**Figures 2C**,D, **3C**,D).

A comparison of the amino acid sequences indicates that these lost amino acids were highly evolutionary conserved among different species (**Figures 4A,B**). Moreover, the lost 15 amino acids locate in the triple helix region of COL2A1, predicating it may affect the protein spatial structure (**Figure 4C**). According to the American College of Medical Genetics and Genomics (ACMG) guidelines for interpretation of sequence variants (Richards et al., 2015), we consider this variant to be pathogenic (PS3+PM2_Supporting + PS4_Supporting + PP4+PS2).

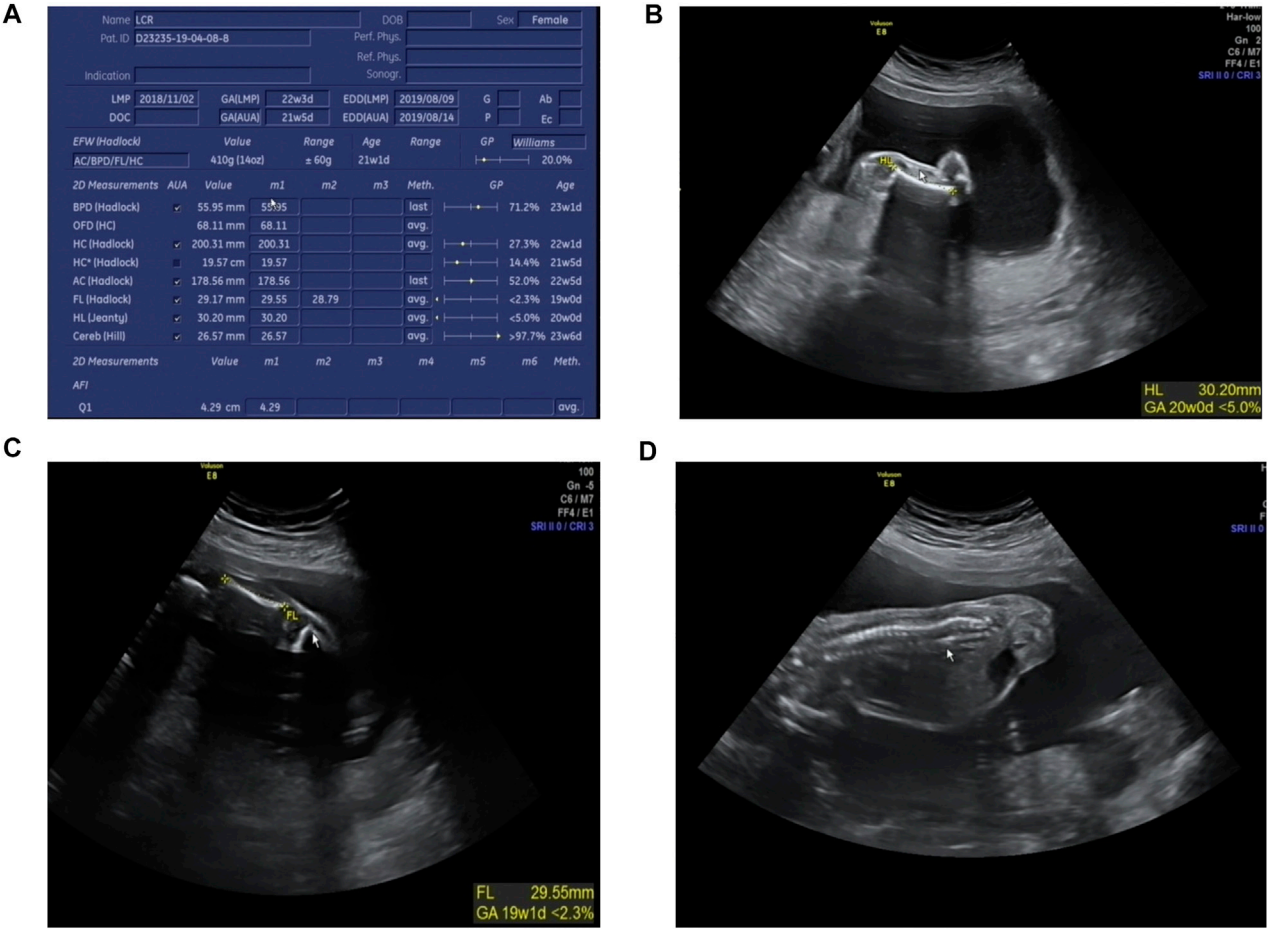

FIGURE 5 | Radiographic features of the fetus (at 22^{+3} weeks' gestation). **(A)** The fetus was generally smaller than the fetus at the same gestational age; **(B)** HL was equivalent to that of fetus at 20 weeks gestation; **(C)** FL was equivalent to that of fetus at 19^{+1} weeks' gestation; **(D)** Fetus scoliosis could be seen.

Prenatal Diagnosis and Genetic Counseling

The karyotype analysis revealed no abnormality. Sanger sequencing revealed that the fetus carried c.3392G > T in the heterozygous state (**Figure 1D**). The ultrasonography showed the fetus with corresponding structural malformations. At 22^{+3} weeks of gestation, head circumference, abdomen circumference, humerus length (HL), and femur length (FL) were at least lower than −2SD compared with the normal fetus at this gestational age (**Figure 5**). The couple chose to terminate the pregnancy due to molecular testing results and bone abnormalities.

DISCUSSION

SEDC is a heterogeneous group of skeletal dysplasias, associated with *COL2A1* mutations. Skeletal abnormalities in patients usually appear at birth and gradually progress (Dasa et al., 2019). Although therapeutic research has made progress in recent years, it is still incurable and may profoundly affect patients' functional ability and quality of life. Prenatal diagnosis and genetic counseling are necessary for families with affected members.

Over the last decade, as gene sequencing has become widely used in clinical practice, thousands of rare variants have been identified. About 50% of these variants are missense variants, whose pathogenicity is generally difficult to assess accurately (Stenson et al., 2009). According to previous studies, approximately 15%–50% of exon single-nucleotide variations can affect protein function by affecting normal pre-mRNA splicing rather than substituting amino acids (Soukarieh et al., 2016; Baralle and Buratti, 2017). If only the DNA is examined, exonic variants far from the classical GT-AG splicing site might easily be misclassified as missense variants. Here, taking into account the patient's typical clinical manifestations and that *in silico* splicing analysis showed the variant c.3392G > T in *COL2A1* had a high probability of disrupting gene splicing, we further conducted a minigene splicing assay. The results showed that the c.3392G > T variant generated a new donor and resulted in cryptic splicing, leading to an in-frame deletion of 15 amino acids in the triple-helical domain, which is considered the most

important domain of COL2A1 (Zhang et al., 2020). According to the previous analysis of the mutation types and phenotypes, non-substitutions (deletions, duplications, delins, and insertions) are more likely to cause mild phenotypes (Zhang et al., 2020). The explanation given is that the non-substitutions may result in significantly abnormal amino acid sequences that are easily recognized and degraded, while the normal allele without variants provide the essential functions of type II collagen to sustain the basic function of cartilage tissue. On the other hand, the size of the in-frame deletion is considered to have a very significant correlation with the severity of the phenotype (Bruni et al., 2021). Variations with missing amino acids equal to or less than 18, which correspond to the number of residues in a turn of the extended left-handed helix formed by each collagen chain in the collagen triple helix, are associated with less severe phenotypes (Gelse et al., 2003). Deletions of more than 18 amino acid residues may form more extended loops, introducing larger structural defects in heterotrimers, while shorter loops might be more easily accommodated, producing fewer irregular protein assemblies (Bruni et al., 2021).

Mosaicism has been previously reported in at least seven families with *COL2A1*-related disease (Winterpacht et al., 1993; Spranger et al., 1994; Forzano et al., 2007; Désir et al., 2012; Nagendran et al., 2012; Yamamoto et al., 2020; Muirhead et al., 2021). In these studies, parents in a somatic mosaic status with the *COL2A1* mutation were clinically unaffected or showed a milder phenotype while offspring with heterozygous mutations tended to show a severe phenotype, the most severe cases even died neonatally (Forzano et al., 2007; Nagendran et al., 2012). Back to our study, the mutation c.3392G > T was detected in the proband at a low level although the sequencing result is not quantitative, and it has been proved as a loss of function variant, which is a common mechanism of *COL2A1*-related disorder. The features observed in the proband were slight, but fully consistent with SEDC, one type of *COL2A1*-related disorder. The fetus carried the heterozygous mutation and showed the key characteristics as early as 22^{+3} weeks. Consequently, we further clarified the genetic cause of SEDC in the family and speculated that the fetus would have more severe symptoms than the proband.

Before molecular defects in SEDC patients were reported, prenatal diagnosis of SEDC relied on ultrasound findings of shortened long bones, short femurs, a narrow chest, increased nuchal translucency, and so on (Patel and Filly, 1995; Chitty et al., 2006). According to previous studies, abnormal ultrasound findings of an SEDC fetus are not obvious until the second trimester of pregnancy. The earliest gestational age at which FL shortening could be detected is 16 weeks (Kirk and Comstock, 1990). In our study, the structural abnormalities of the fetus were first observed at 22^{+3} weeks gestation, which had exceeded the best period for prenatal diagnosis. Hence, for the families affected with SEDC, a prenatal molecular diagnosis should be completed as soon as possible. Obviously, confirmation of the proband's pathogenic variation is a prerequisite for prenatal diagnosis and genetic counseling.

In conclusion, we verified the pathogenicity of the novel *COL2A1* variant c.3392G > T by next-generation sequencing and *in vitro* minigene assay, thus clarifying the cause of SEDC in the subject family and helping to guide for future pregnancy. In addition, our findings emphasize the importance of evaluating the impact of missense variants on pre-mRNA. The minigene assay may be a reliable and easy-to-use tool when a certain mutation is suspected to affect the normal splicing, and to collect the patient's sample again for RNA transcription is impossible, or the mutant gene is not expressed or expressed too low in the blood.

DATA AVAILABILITY STATEMENT

The datasets presented in this study can be found in online repositories. The name of the repository and accession number can be found below: SRA, NCBI; PRJNA817328.

ETHICS STATEMENT

The studies involving human participants were reviewed and approved by the Ethics Committee of Huzhou Maternity and Child Health Care Hospital. The patients/participants provided their written informed consent to participate in this study.

AUTHOR CONTRIBUTIONS

XS designed the study and reviewed the manuscript. LF analyzed the data and wrote the manuscript. KT and GS collected the samples and performed the experiments. LJ and YX conducted the research and analyzed the results. ZL and SY analyzed the radiological results. All authors have read and approved the manuscript.

FUNDING

The work was supported by the Zhejiang medical and health technology program (2021KY1085) and Huzhou science and technology program (2020GY26).

ACKNOWLEDGMENTS

We thank the family for their participation in this study.

SUPPLEMENTARY MATERIAL

The Supplementary Material for this article can be found online at: https://www.frontiersin.org/articles/10.3389/fgene.2022.827560/full#supplementary-material

REFERENCES

Anderson, I. J., Goldberg, R. B., Marion, R. W., Upholt, W. B., and Tsipouras, P. (1990). Spondyloepiphyseal Dysplasia Congenita: Genetic Linkage to Type II Collagen (COL2AI). *Am. J. Hum. Genet.* 46 (5), 896–901.

Baralle, D., and Buratti, E. (2017). RNA Splicing in Human Disease and in the Clinic. *Clin. Sci. (Lond)* 131 (5), 355–368. doi:10.1042/cs20160211

Bruni, V., Spoleti, C. B., La Barbera, A., Dattilo, V., Colao, E., Votino, C., et al. (2021). A Novel Splicing Variant of COL2A1 in a Fetus with Achondrogenesis Type II: Interpretation of Pathogenicity of In-Frame Deletions. *Genes* 12 (9), 1395. doi:10.3390/genes12091395

Chitty, L. S., Tan, A. W. C., Nesbit, D. L., Hall, C. M., and Rodeck, C. H. (2006). Sonographic Diagnosis of SEDC and Double Heterozygote of SEDC and Achondroplasia-A Report of Six Pregnancies. *Prenat. Diagn.* 26 (9), 861–865. doi:10.1002/pd.1525

Dasa, V., Eastwood, J. R. B., Podgorski, M., Park, H., Blackstock, C., Antoshchenko, T., et al. (2019). Exome Sequencing Reveals a Novel COL2A1 Mutation Implicated in Multiple Epiphyseal Dysplasia. *Am. J. Med. Genet.* 179 (4), 534–541. doi:10.1002/ajmg.a.61049

Deng, H., Huang, X., and Yuan, L. (2016). Molecular Genetics of the COL2A1-Related Disorders. *Mutat. Research/Reviews Mutat. Res.* 768, 1–13. doi:10.1016/j.mrrev.2016.02.003

Désir, J., Cassart, M., Donner, C., Coucke, P., Abramowicz, M., and Mortier, G. (2012). Spondyloperipheral Dysplasia as the Mosaic Form of Platyspondylic Lethal Skeletal Dyplasia torrance Type in Mother and Fetus with the sameCOL2A1mutation. *Am. J. Med. Genet.* 158a (8), 1948–1952. doi:10.1002/ajmg.a.35301

Forzano, F., Lituania, M., Viassolo, A., Superti-Furga, V., Wildhardt, G., Zabel, B., et al. (2007). A Familial Case of Achondrogenesis Type II Caused by a dominantCOL2A1 Mutation and "patchy" Expression in the Mosaic Father. *Am. J. Med. Genet.* 143a (23), 2815–2820. doi:10.1002/ajmg.a.32047

Gelse, K., Pöschl, E., and Aigner, T. (2003). Collagens-structure, Function, and Biosynthesis. *Adv. Drug Deliv. Rev.* 55 (12), 1531–1546. doi:10.1016/j.addr.2003.08.002

Inoue, T., Nagano, C., Matsuo, M., Yamamura, T., Sakakibara, N., Horinouchi, T., et al. (2020). Functional Analysis of Suspected Splicing Variants in CLCN5 Gene in Dent Disease 1. *Clin. Exp. Nephrol.* 24 (7), 606–612. doi:10.1007/s10157-020-01876-x

Kirk, J. S., and Comstock, C. H. (1990). Antenatal Sonographic Appearance of Spondyloepiphyseal Dysplasia Congenita. *J. Ultrasound Med.* 9 (3), 173–175. doi:10.7863/jum.1990.9.3.173

Muirhead, K. J., Clause, A. R., Schlachetzki, Z., Dubbs, H., Perry, D. L., Hagelstrom, R. T., et al. (2021). Genome Sequencing Identifies Three Molecular Diagnoses Including a Mosaic Variant in the COL2A1 Gene in an Individual with Pol III-Related Leukodystrophy and Feingold Syndrome. *Cold Spring Harb Mol. Case Stud.* 7 (6), a006143. doi:10.1101/mcs.a006143

Nagendran, S., Richards, A. J., McNinch, A., Sandford, R. N., and Snead, M. P. (2012). Somatic Mosaicism and the Phenotypic Expression of COL2A1 Mutations. *Am. J. Med. Genet.* 158a (5), 1204–1207. doi:10.1002/ajmg.a.35303

Nishimura, G., Haga, N., Kitoh, H., Tanaka, Y., Sonoda, T., Kitamura, M., et al. (2005). The Phenotypic Spectrum ofCOL2A1mutations. *Hum. Mutat.* 26 (1), 36–43. doi:10.1002/humu.20179

Patel, M. D., and Filly, R. A. (1995). Homozygous Achondroplasia: US Distinction between Homozygous, Heterozygous, and Unaffected Fetuses in the Second Trimester. *Radiology* 196 (2), 541–545. doi:10.1148/radiology.196.2.7617874

Putscher, E., Hecker, M., Fitzner, B., Lorenz, P., and Zettl, U. K. (2021). Principles and Practical Considerations for the Analysis of Disease-Associated Alternative Splicing Events Using the Gateway Cloning-Based Minigene Vectors pDESTsplice and pSpliceExpress. *Ijms* 22 (10), 5154. doi:10.3390/ijms22105154

Soukarieh, O., Gaildrat, P., Hamieh, M., Drouet, A., Baert-Desurmont, S., Frébourg, T., et al. (2016). Exonic Splicing Mutations Are More Prevalent Than Currently Estimated and Can Be Predicted by Using In Silico Tools. *Plos Genet.* 12 (1), e1005756. doi:10.1371/journal.pgen.1005756

Spranger, J., Menger, H., Mundlos, S., Winterpacht, A., and Zabel, B. (1994). Kniest Dysplasia Is Caused by Dominant Collagen II (COL2A1) Mutations: Parental Somatic Mosaicism Manifesting as Stickler Phenotype and Mild Spondyloepiphyseal Dysplasia. *Pediatr. Radiol.* 24 (6), 431–435. doi:10.1007/bf02011911

Stenson, P. D., Mort, M., Ball, E. V., Howells, K., Phillips, A. D., Thomas, N. S., et al. (2009). The Human Gene Mutation Database: 2008 Update. *Genome Med.* 1 (1), 13. doi:10.1186/gm13

Wang, S., Wang, Y., Wang, J., Liu, Z., Zhang, R., Shi, X., et al. (2020). Six Exonic Variants in the SLC5A2 Gene Cause Exon Skipping in a Minigene Assay. *Front. Genet.* 11, 585064. doi:10.3389/fgene.2020.585064

Winterpacht, A., Hilbert, M., Schwarze, U., Mundlos, S., Spranger, J., and Zabel, B. U. (1993). Kniest and Stickler Dysplasia Phenotypes Caused by Collagen Type II Gene (COL2A1) Defect. *Nat. Genet.* 3 (4), 323–326. doi:10.1038/ng0493-323

Xiong, Q., Liu, Y., Xue, Y., Liu, S., Wang, J., Li, P., et al. (2018). A Novel De Novo Mutation in COL2A1 Leading to Spondyloepiphyseal Dysplasia Congenita in a Chinese Family. *Hum. Genome* 5, 17059. doi:10.1038/hgv.2017.59

Yamamoto, K., Kubota, T., Takeyari, S., Kitaoka, T., Miyata, K., Nakano, Y., et al. (2020). Parental Somatogonadal COL2A1 Mosaicism Contributes to Intrafamilial Recurrence in a Family with Type 2 Collagenopathy. *Am. J. Med. Genet.* 182 (3), 454–460. doi:10.1002/ajmg.a.61422

Zhang, B., Zhang, Y., Wu, N., Li, J., Liu, H., and Wang, J. (2020). Integrated Analysis ofCOL2A1variant Data and Classification of Type II Collagenopathies. *Clin. Genet.* 97 (3), 383–395. doi:10.1111/cge.13680

Zheng, W. b., Li, L. j., Zhao, D. c., Wang, O., Jiang, Y., Xia, W. b., et al. (2020). Novel Variants in COL2A1 Causing Rare Spondyloepiphyseal Dysplasia Congenita. *Mol. Genet. Genomic Med.* 8 (3), e1139. doi:10.1002/mgg3.1139

Conflict of Interest: The authors declare that the research was conducted in the absence of any commercial or financial relationships that could be construed as a potential conflict of interest.

Publisher's Note: All claims expressed in this article are solely those of the authors and do not necessarily represent those of their affiliated organizations, or those of the publisher, the editors and the reviewers. Any product that may be evaluated in this article, or claim that may be made by its manufacturer, is not guaranteed or endorsed by the publisher.

frontiers | Frontiers in Pediatrics

ORIGINAL RESEARCH
published: 16 May 2022
doi: 10.3389/fped.2022.797978

ZPA Regulatory Sequence Variants in Chinese Patients With Preaxial Polydactyly: Genetic and Clinical Characteristics

Lei Zeng[1], Jie-Yuan Jin[2,3], Fang-Mei Luo[2,3], Yue Sheng[2], Pan-Feng Wu[1,4] and Rong Xiang[1,2,3,4]**

[1] Department of Orthopaedics, Xiangya Hospital, Central South University, Changsha, China, [2] School of Life Sciences, Central South University, Changsha, China, [3] Hunan Key Laboratory of Animal Models for Human Diseases, School of Life Sciences, Central South University, Changsha, China, [4] Hunan Key Laboratory of Medical Genetics, School of Life Sciences, Central South University, Changsha, China

OPEN ACCESS

Edited by:
Rong Qiang,
Northwest Women's and Children's Hospital, China

Reviewed by:
Sajid Malik,
Quaid-i-Azam University, Pakistan
Shuchao Pang,
Jining Medical University, China
Muhammad Umair,
King Abdullah International Medical Research Center (KAIMRC), Saudi Arabia

***Correspondence:**
Pan-Feng Wu
wupanfeng@csu.edu.cn
Rong Xiang
shirlesmile@csu.edu.cn

Specialty section:
This article was submitted to Genetics of Common and Rare Diseases, a section of the journal Frontiers in Pediatrics

Received: *19 October 2021*
Accepted: *29 March 2022*
Published: *16 May 2022*

Citation:
Zeng L, Jin J-Y, Luo F-M, Sheng Y, Wu P-F and Xiang R (2022) ZPA Regulatory Sequence Variants in Chinese Patients With Preaxial Polydactyly: Genetic and Clinical Characteristics. Front. Pediatr. 10:797978. doi: 10.3389/fped.2022.797978

Preaxial polydactyly (PPD) is a common congenital abnormality with an incidence of 0.8–1.4% in Asians, characterized by the presence of extra digit(s) on the preaxial side of the hand or foot. PPD is genetically classified into four subtypes, PPD type I–IV. Variants in six genes/loci [including GLI family zinc finger 3 (*GLI3*), ZPA regulatory sequence (ZRS), and pre-ZRS region] have been identified in PPD cases. Among these loci, ZRS is, perhaps, the most special and well known, but most articles only reported one or a few cases. There is a lack of reports on the ZRS-variant frequency in patients with PPD. In this study, we recruited 167 sporadic or familial cases (including 154 sporadic patients and 13 families) with PPD from Central-South China and identified four ZRS variants in four patients (2.40%, 4/167), including two novel variants (ZRS131A > T/chr7:g.156584439A > T and ZRS474C > G/chr7:g.156584096C > G) and two known variants (ZRS428T > A/chr7:g.156584142T > A and ZRS619C > T/chr7:g.156583951C > T). ZRS131A > T and ZRS428T > A were detected in PPD I cases and ZRS474C > G and ZRS619C > T combinedly acted to cause PPD II. The detectable rate of ZRS variants in PPD I was 1.60% (2/125), while PPD II was significantly higher (9.52%, 2/21). Three bilateral PPD cases harbored ZRS variants (13.64%, 3/22), suggesting that bilateral PPD was more possibly caused by genetic etiologies. This study identified two novel ZRS variants, further confirmed the association between ZRS and PPD I and reported a rare PPD II case resulted from the compound heterozygote of ZRS. This investigation preliminarily evaluated a ZRS variants rate in patients with PPD and described the general picture of PPD in Central-South China.

Keywords: ZRS, preaxial polydactyly type I, preaxial polydactyly type II, enhancer, SHH

INTRODUCTION

Preaxial polydactyly (PPD) is a common congenital abnormality with an incidence of 0.8–1.4% in Asians, characterized by the presence of extra digit(s) on the preaxial side of the hand or foot (1). Severity varies from mere broadening of the distal phalanx with slight bifurcation at the tip to full duplication of the thumb, including the metacarpals (2). PPD is genetically classified into

four subtypes, PPD type I–IV (**Table 1**) (3). PPD I (OMIM 174400) indicates the duplication of one or more of the skeletal components of biphalangeal thumbs, which is the most common subtype in many populations (2). PPD II (OMIM 174500) refers to isolated triphalangeal thumbs or the thumb duplication with triphalangeal components (4). PPD III (174600) is also known as index finger polydactyly. Thumbs of PPD III cases are replaced by one or two index fingers (5). PPD IV (174700) is polysyndactyly of the thumb (6).

Currently, only six genes/loci [*GLI1*, *GLI3*, serine/threonine kinase like domain containing 1 (*STKLD1*), ZPA regulatory sequence (ZRS), pre-ZRS region, and a deletion of 240 kb from the sonic hedgehog signaling molecule (*SHH*) promoter] have been identified in isolated PPD cases and ZRS is, perhaps, the most special and well known (7–12). ZRS, the zone of polarizing activity (ZPA) (located in the posterior region of the limb bud) regulatory sequence, is a limb-specific enhancer of *SHH*, which is located nearly 1 Mb from *SHH* and within intron 5 of *Limb development membrane protein 1 (LMBR1)* (4). ZRS can promote the expression of SHH in ZPA during the limb development. SHH diffuses from ZPA (posterior mesoderm) to anterior region of limb bud and there is no SHH in anterior region. The graded distribution of SHH determines the finger pattern. ZRS variants would alter the expression of SHH and cause limb deformities. ZRS variants and duplications had been shown to cause PPD I, PPD II, Werner mesomelic syndrome (WMS) (OMIM 188770), and other limb deformities (such as mirror-image polydactyly and radial ray deficiency) (12–16). The correlation between PPD and ZRS is definite, but most articles only reported one or a few cases, especially in PPD II cases. There is a lack of reports on the ZRS-variant frequency in patients with PPD.

In this study, we recruited 167 sporadic or familial cases with PPD from Central-South China. We identified four ZRS variants in four PPD cases (4/167, 2.40%), including two novel variants (ZRS131A > T/chr7:g.156584439A > T and ZRS474C > G/chr7:g.156584096C > G) and two known variants (ZRS428T > A/chr7:g.156584142T > A and ZRS619C > T/chr7:g.156583951C > T). This study preliminarily investigated the ZRS variant rate in patients with PPD living in Central-South China, expanded the spectrum of ZRS variants, furthered our understanding of PPD, and contributed to genetic diagnosis and counseling of patients with PPD.

MATERIALS AND METHODS

Patients and Subjects

This study was approved by the Review Board of Xiangya Hospital of Central South University. A total of 167 sporadic or familial PPD cases admitted to the Department of Orthopaedics of Xiangya Hospital were recruited. They were all from Central-South China, especially Hunan province. Almost subjects were preschoolers and informed consent forms were obtained from the patients and their guardians. All the subjects and their guardians consented to participate in this study and to publication of the images. Blood was collected from patients and their blood relations.

Deoxyribonucleic Acid Extraction

Peripheral blood samples were collected from patients and their family members to extract genomic DNA by the DNeasy Blood and Tissue Kit (Qiagen, Valencia, CA, United States).

Variant Screening

The highly conserved 774-bp region of the ZRS (chr7: 156583796-156584569, hg19) was obtained from the National Center for Biotechnology Information (NCBI) database[1] and primers were designed by Integrated DNA Technologies (IDT)[2] (**Table 2**) (17). PCR was operated to amplify the target sequences by CFX384 Touch PCR Amplifier (Bio-Rad, Hercules, CA, United States). PCR product sequences were determined using the ABI 3100 Genetic Analyzer (Thermo Fisher Scientific, Waltham, MA, United States) by Sanger sequencing performed by Boshang Biotechnology Co., Ltd. (Shanghai, China). For patients who were identified ZRS variants, further genetic screening (using PCR and Sanger sequencing) was used to detect whether they harbored pathogenic variants in *GLI3* (NM_000168.6, NP_000159.3), *GLI1* (NM_005269.3, NP_005260.1), *STKLD1* (NM_153710.5, NP_714921.4), or pre-ZRS. Their primer pairs were also designed by IDT (**Table 2**).

Prediction of Pathogenicity

MutationTaster[3] was applied for predicting the pathogenicity of variants. GnomAD[4] was used to annotate the minimum allele frequency (MAF) of variants. ZRS sequences of species from Evgeny et al. (18) were used to compare the conservation of variant sites (18).

RESULTS

We recruited 167 cases with PPD from Central-South China, including 154 sporadic patients and 13 families, named as PPD001–PPD167 depending on the order of recruitment. Among these cases, almost subjects (154/167, 92.22%) were Han Chinese and 148 patients had isolated PPD (**Table 3**). Based on PPD subtypes to divide subjects, 125 patients (74.85%) revealed PPD I, 21 patients (12.57%) had PPD II, and only four cases exhibited PPD III (1/167, 0.60%) or PPD IV (3/167, 1.80%). The rest of PPD subjects (17 cases, 10.18%) presented other organ malformations, such as congenital heart disease, radial ray deficiency, and anal atresia. There were 103 male patients (61.68%) and 64 female patients (38.32%). Most subjects were younger than 3 years old. Except 19 cases without clinical details, the overwhelming majority of PPD I/II was unilateral (109/127, 85.83%), in which PPD, on the right hand, accounted for almost two-thirds (72/109, 66.06%; **Table 3**).

In accordance with the flow diagram (**Figure 1**), we identified four ZRS variants in four patients (PPD003, PPD029, PPD116, and PPD154; **Table 4**). The detectable rate of ZRS variants in PPD

[1]https://www.ncbi.nlm.nih.gov/gene/105804841

[2]http://sg.idtdna.com/Primerquest/Home/Index

[3]http://www.mutationtaster.org/

[4]http://gnomad-sg.org/

TABLE 1 | Classification of PPD and their clinical features and causative genes/loci.

Subtype	OMIM	Clinical features	Heredity	Gene/Locus
PPD I	174400	The duplication of one or more of the	AR	*GLI1*
		skeletal components of biphalangeal thumbs	AR	Serine/threonine kinase like domain containing 1 (*STKLD1*)
			AD	ZRS
PPD II	174500	Isolated triphalangeal thumb or thumb duplication	AD	ZRS
		with a triphalangeal component	AD	pre-ZRS
PPD III	174600	Thumbs replaced by one or two index fingers	–	–
PPD IV	174700	Polysyndactyly of the thumb	AD	GLI family zinc finger 3 (GLI3)

PPD, preaxial polydactyly; AD, autosomal dominant; AR, autosomal recessive.

I was 1.60% (2/125), while PPD II was significantly higher (2/21, 9.52%). Three of these four patients were with bilateral thumbs involvement, occupying 13.64% of bilateral PPD (3/22). None ZRS variant was identified in patients with left PPD, although they were more than one-third total subjects (37.72%, 63/167).

PPD029 Family

The proband of PPD029 (III:1) was a 4-year-old girl, who presented bilateral triphalangeal thumbs (**Figures 2A–C**). She harbored compound heterozygous variants in ZRS (ZRS474C > G/chr7:g.156584096C > G and ZRS619C > T/chr7:g.156583951C > T) without *GLI3*, *GLI1*, *STKLD1*, or pre-ZRS variants (**Figure 2D**). ZRS474C > G was inherited from her father (II:2) and another variant was from her mother (II:3). Other family members without variants or with only one variant were unaffected.

PPD154 Family

The proband of PPD154 (II:1) was a boy with PPD I on the right hand (**Figures 2E–G**). He was admitted to our hospital for operative treatment at his age of 1.5 years. We identified a *de novo* variant in ZRS (ZRS131A > T/chr7:g.156584439A > T) in this patient and did not find suspicious variants in *GLI3*, *GLI1*, *STKLD1*, and pre-ZRS (**Figure 2H**). His parents were unaffected.

PPD003 Family and PPD116 Family

Known ZRS variant (ZRS428T > A/chr7:g.156584142T > A) was identified in two families with PPD II (PDD003) or PPD I (PDD116). Four variants identified in this study were highly evolutionarily conserved and were predicted to be disease-causing by MutationTaster (**Figure 2I** and **Table 4**).

DISCUSSION

Polydactyly is the most common limb malformation in China and PPD is over half (data from National Stocktaking Report on Birth Defect Prevention)[5]. PPD I is the most common subtype and PPD III is rarest (2, 19). In this study, 125 cases (74.85%, 125/167) had PPD I and only one patient (1.80%, 1/167) was diagnosed with PPD III. 17 patients with PPD (10.18%, 17/167) had other organ malformations, including congenital heart disease, radial ray deficiency, and anal atresia. These complications were relatively frequent in patients with PPD. Male patients with PPD are approximately twice as many as female (19). In this study, the proportion of male patients was 61.68% (103/167). This study showed that overwhelming majority of PPD I/II were unilateral (85.83%, 109/127), in which PPD, on the right hand, accounted for almost two-thirds (66.06%, 72/109), consistent with previous studies (19, 20).

In this study, we tested ZRS variants in 167 patients with PPD and identified unique variants (MAF $\leq$ 0.05) in four cases (2.40%, 4/167). The detectable rate of ZRS variants in PPD I was 1.60% (2/125), while PPD II was significantly higher (9.52%, 2/21). Indeed, most known ZRS variants are identified in PPD II cases [data from the human gene mutation database (HGMD)][6]. In this study, three ZRS variants were associated with bilateral PPD and 13.64% bilateral PPD cases (3/22) harbored ZRS variants, suggesting that bilateral PPD was more possibly caused by genetic etiologies. Compared with that no ZRS variant was detected by Xiang et al. (20) in 82 Chinese patients with PPD I/II or Rao et al. (21) in 72 Chinese patients with PPD, our identification was fortunate (20, 21). For the remaining 163 cases, we planned to applied chromosomal microarray analysis (CMA), whole-exon sequencing (WES), and genome-wide association study (GWAS) to detect their genetic etiologies. Furthermore, environmental factors, such as alcohol, are causes of limb deformities (22).

Of these four variants, ZRS131A > T and ZRS474C > G were novel and ZRS428T > A and ZRS619C > T had been reported in patients with PPD II (4, 15). ZRS428T > A was identified in both the patients with PPD I (PPD116) and PPD II (PPD003), suggesting the variability of ZRS428T > A-related clinical phenotypes. ZRS131A > T was identified in a sporadic case with PPD I (PPD154). Generally, ZRS variants are associated with PPD II and ZRS was first linked with PPD I by Xu et al. (12). Our report may be the second case worldwide, further demonstrating the correlation between ZRS and PPD I.

PPD029 was a rare case. We found that the proband harbored the compound heterozygote of ZRS (ZRS474C > G and ZRS619C > T). Given that Jacob et al. (23) reported ZRS variant carriers with minor anomalies and underlined the importance of accurate clinical examination in mild triphalangeal thumb families, we carefully checked the phenotypes of her family members with one ZRS variant and did not find any

[5]https://wenku.so.com/d/8c145f3c9e9b4892c02bf7e70aa83d01

[6]http://www.hgmd.cf.ac.uk/ac/search.php

TABLE 2 | Primer pairs of ZPA regulatory sequence (ZRS), *GLI3*, *GLI1*, *STKLD1*, and pre-ZRS.

Primer	Sequences (5′→3′)	Primer	Sequences (5′→3′)
ZRS 1f	GGAGGTATAACCTCTGGCCAGTG	ZRS 1r	CGCTTCCACCTGGTCAGTCC
ZRS 2f	CCAGAGCGTAGCACACGGTC	ZRS 2r	CAATTTATGGATCATCAGTGGC
ZRS 3f	TCAGGCCTCCATCTTAAAGAG	ZRS 3r	GAAATGGTTATGGATCAGAAAGT
GLI3 1f	GAAAGTTGATGGCTCTGTTGTTT	GLI3 1r	CAGGTGCAAACGCTCAATTC
GLI3 2f	GCTCTCAAAGTTGCTGTGAATG	GLI3 2r	TGGGAAAGAAGTAGGGAAAGTAAG
GLI3 3f	CAGTACCTCACAGAGCTTCATAAC	GLI3 3r	CAGTGAACCCACGAACAGATAG
GLI3 4f	TTCTCATGGAAGAAGCCATAGG	GLI3 4r	CTTTATACACGTCCCGAGTGAG
GLI3 5f	TCTGAGATGCCTCAAGAGAAAC	GLI3 5r	GGGTCTCAGGATGTCCAAAT
GLI3 6f	GCAAGTTGCCAGCTTCTTATC	GLI3 6r	TTTGACCTGCCTCTTGGTATAG
GLI3 7f	TTAGGTCTGCGTGTATGTGTG	GLI3 7r	GACATGGGATGCAGGTTACA
GLI3 8f	TGGTACTGCTCCTTGTTGATG	GLI3 8r	ACTGCCTGTGTTTGCTTCT
GLI3 9f	CCTCCTGTTGTGTCTGATTCTT	GLI3 9r	GTCATAAAGCCCTCTCCAGTTC
GLI3 10f	AGGAAGCATGCATACACAGTTA	GLI3 10r	CATCAGTTTGCACAGCTCTTATG
GLI3 11f	AACTTGGAGGGCGTGTTAG	GLI3 11r	CGGGATAGTTCTTTGTTTCCTTATG
GLI3 12f	TACCTCGTTCTTGTGGGATTTG	GLI3 12r	CTTCTCTGCCTTGACGGTTT
GLI3 13f	ATTGGCTCCCTTTCCTTGAC	GLI3 13r	CAGATGCATGGTCTGATGTAGAA
GLI3 14-1f	TGGTCTCTCCCTTTCTCTGT	GLI3 14-1r	TCAGGCTCATCCTCTCCAT
GLI3 14-2f	CAGCAGTACCGCCTCAAG	GLI3 14-2r	TCGTTCAGGTTGGCATCAG
GLI3 14-3f	CAGTCCCGAAACTTCCACTC	GLI3 14-3r	GCCTTACAGGGCTGTTCAT
GLI3 14-4f	CCCATTCAGTGGAACGAAGT	GLI3 14-4r	GCCCTTGGTAGATGTTGATGT
GLI3 14-5f	AGATGCTTGGGCAGATTAGTG	GLI3 14-5r	GCTGGCGTCTGAAATAGAGAA
GLI3 14-6f	CCATCCGCTGTGCTCTAATC	GLI3 14-6r	TCCGTTGGTTGCAGTCTTT
GLI1 1f	ATTCCGTGGCAGATGTCTTAG	GLI1 1f	CTGGAATGGGAATGGAGGATAC
GLI1 2f	CCCATGCCAGTTTCCTATCTAC	GLI1 2f	CCTCACATCTCCAAGCATCTC
GLI1 3f	CATAGGTTAGGTGCATGGAGAG	GLI1 3r	CTCAGGAAGGATTGGGCTATTT
GLI1 4f	TCAAGCCCTCAAACTACCTAAC	GLI1 4r	CTCAGACTACACTGGTGAATGG
GLI1 5 + 6f	CATCCCATTCACCAGTGTAGTC	GLI1 5 + 6r	GGAAGAGGCAGGAGCAATATC
GLI1 7f	GGAAGACCTGAGATGTGAGATATG	GLI1 7r	GAGAGCCCTGATTTAGGAAGAG
GLI1 8f	TGTGTGTCCTGTTGGAGATTG	GLI1 8r	GTAGGAGGAGGAGTGGTTAAGT
GLI1 9-1f	CTCCATCCTCCTTACTTCCTTTG	GLI1 9-1r	CTTGGGCTCCACTGTAGAAAT
GLI1 9-2f	CCACTCTCCACTCAACAGAAG	GLI1 9-2r	GAATGGATGGGTTGGGAAGTA
GLI1 10f	TGCTTAGCCCTTTCTACACTTAC	GLI1 10r	TGACTTCCTCCTCTCAACCT
GLI1 11-1f	AGGAGGCAGGGTGAAATTTAG	GLI1 11-1r	AGAGTATCAGTAGGTGGGAAGT
GLI1 11-2f	TACCTCCCAACCTCTGTCTAC	GLI1 11-2r	GCCCTATGTGAAGCCCTATTT
GLI1 11-3f	CTACCAGAGTCCCAAGTTTCTG	GLI1 11-3r	GCGATCTGTGATGGATGAGATT
STKLD1 1f	TACGCGGTCGCTACTGAT	STKLD1 1r	CCCACGCCCTCAAATACTC
STKLD1 2f	AGGGATACAGGGTTGTAGAAGA	STKLD1 2r	GATTAGTCTCCGCAAGTGTCAG
STKLD1 3f	GTTGGTTGTGGTTGTGGTAATG	STKLD1 3r	AACTGGTGCTGATGCTCTATC
STKLD1 4f	GTTGGGATGTGTGACAGAGAAG	STKLD1 4r	CCTATGAGACTATGCACCGAAAG
STKLD1 5f	AGAGAGAGGAAGCTGAAGGT	STKLD1 5r	CCTCGAGGCACACATTTAAGA
STKLD1 6f	CAAGATGCAAGGAGAGGATACA	STKLD1 6r	GCTTGAGACCACTTGGAAGA
STKLD1 7f	TTTGTGGAGGAGAGGAGGAT	STKLD1 7r	AGGAGGTCTCTTTGGAGTTTAC
STKLD1 8f	TGGCTCCAGATCAACACAAA	STKLD1 8r	CACTGCTGTCATTATCCTGCTA
STKLD1 9f	GGTCTCTGGGCATTCTTGTAG	STKLD1 9r	GTGCTTGTATTAGGGTGGAGAG
STKLD1 10f	GAGAGACCCTGCCAAATGAA	STKLD1 10r	GTTGGGAGCTATGGAGGATATTT
STKLD1 11f	CATCATCTGTGTGCTCCAAGAC	STKLD1 11r	GCCTCCACGCTGCAATAAA
STKLD1 12f	GACCTAGCGCTAATCCTCATTG	STKLD1 12r	CCTAGAAGATGGCCTAGAAGGT
STKLD1 13f	CATTAGGCCACAGGGATTCA	STKLD1 13r	AGGATGCGACCAGCATTT
STKLD1 14f	GTAGTGGGATGGCAGCTATTG	STKLD1 14r	TGGGCAAGAAGTCCTGAAAC
STKLD1 15-16f	GTTGTCGTTAGCTGGAGGAA	STKLD1 15-16r	ACCTGGCAGATGTAACTGATG

(Continued)

TABLE 2 | (Continued)

Primer	Sequences (5′→3′)	Primer	Sequences (5′→3′)
STKLD1 17f	TTCTTGCATGGTCCTGTTCA	STKLD1 17r	GCCAAATGAGTGGGAAGTTTAAG
STKLD1 18f	CCCACTTAAACTTCCCACTCAT	STKLD1 18r	CAGGAAACTCTTTGGAGAGGTC
pre-ZRS 1f	GGAAGTGCTGCTTAGTGTTAGT	pre-ZRS 1r	GTTCCCATACGCCCAGATTT
pre-ZRS 2f	GCTGTGATACTTCAGCTTCCT	pre-ZRS 2r	GCCATAATTTAGTGCCCTCCTA
pre-ZRS 3f	AAATCTGGGCGTATGGGAAC	pre-ZRS 3r	CCTGGTAGACAGGTACTGTTAGA
pre-ZRS 4f	TGGATCTAGGAGGGCACTAAA	pre-ZRS 4r	CAGAGGCCTGAACTATCAAACA
pre-ZRS 5f	ACATCAGGAGAACTTGTGTAGG	pre-ZRS 5r	CCAACCAAGGGTGAGTAGTT
pre-ZRS 6f	ACTGGCTGTAATACTACTCCAATAC	pre-ZRS 6r	AACAATCTTACTGCCTTTGATGTG

TABLE 3 | Characteristics and clinical phenotypes of all the subjects.

	PPD I	PPD II	PPD III	PPP IV	Others*	Total	PPD with ZRS variants
Age (years)	3.326 ± 0.518	2.730 ± 0.695	0.9	3.400 ± 0.513	6.029 ± 1.904	3.529 ± 0.446	1.750 ± 0.777
Gender	78 M; 47 F	12 M; 9 F	1 M; 0 F	2 M; 1 F	10 M; 7 F	103 M; 64 F	3 M (2.91%); 1 F (1.56%)
Ethnicity (Han)	114	19	1	3	17	154	4
Other ethnicities**	11	2	0	0	0	13	0
Number	125	21	1	3	17	167	4
Proportion	74.85%	12.57%	0.60%	1.80%	10.18%	100.00%	2.40%
Unilateral	32 L; 63 R	5 L; 9 R	0	0	–	37 L; 72 R	0 L (0.00%); 1 R (1.39%)
Bilateral	12	6	1	3	–	22	3 (13.64%)
Cases without details	18	1	0	0	–	19	0
Familial/sporadic	8/117	3/18	0/1	1/2	1/16	13/154	1/3
Isolated/syndromic	125/0	21/0	1/0	1/2	0/17	148/19	4/0
ZRS variants detection rate	1.60%	9.52%	0.00%	0.00%	0.00%	2.40%	–

*PPD, preaxial polydactyly; M, male; F, female; L, left thumb involved; R, right thumb involved. *PPD with multiple organ malformations, such as congenital heart disease, radial ray deficiency, anal atresia. **Other ethnicities include Tujia nationality, Miao nationality, and Hui nationality.*

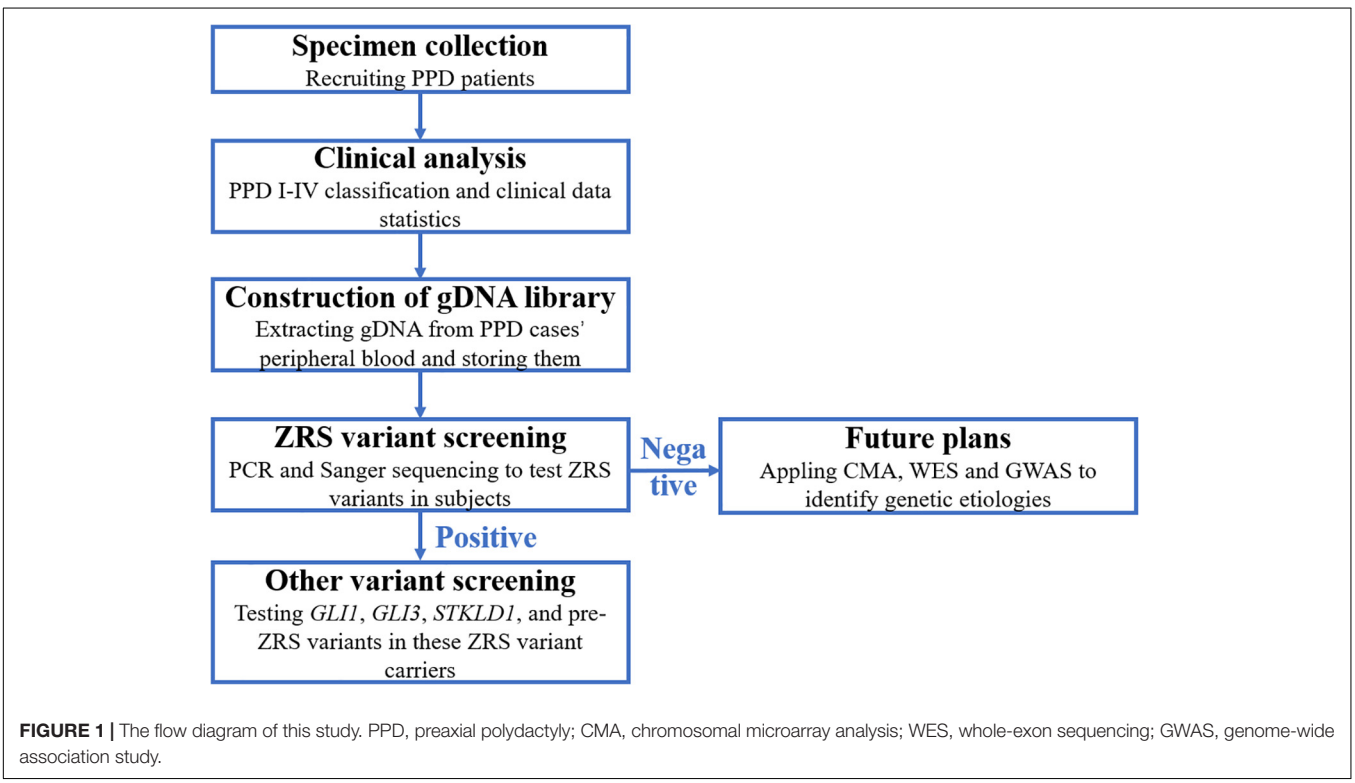

FIGURE 1 | The flow diagram of this study. PPD, preaxial polydactyly; CMA, chromosomal microarray analysis; WES, whole-exon sequencing; GWAS, genome-wide association study.

TABLE 4 | Phenotypes and genotypes of patients with PPD with ZRS variants.

Patient	Age (years)	Gender	Phenotype	ZRS variant	Location (hg19)	MutationTaster	GnomAD
PDD003	1	M	Bilateral PPD with triphalangeal thumb on the right hand	ZRS428T > A	Chr7:156584142	D	0.00006
PDD116	0.5	M	Bilateral PPD I				
PDD029	4	F	Bilateral triphalangeal thumbs	ZRS474C > G	Chr7:156584096	D	–
				ZRS619C > T	Chr7:156583951	D	0.00000
PDD154	1.5	M	PPD I on the right hand	ZRS131A > T	Chr7:156584439	D	–

PPD, preaxial polydactyly; M, male; F, female; D, disease causing.

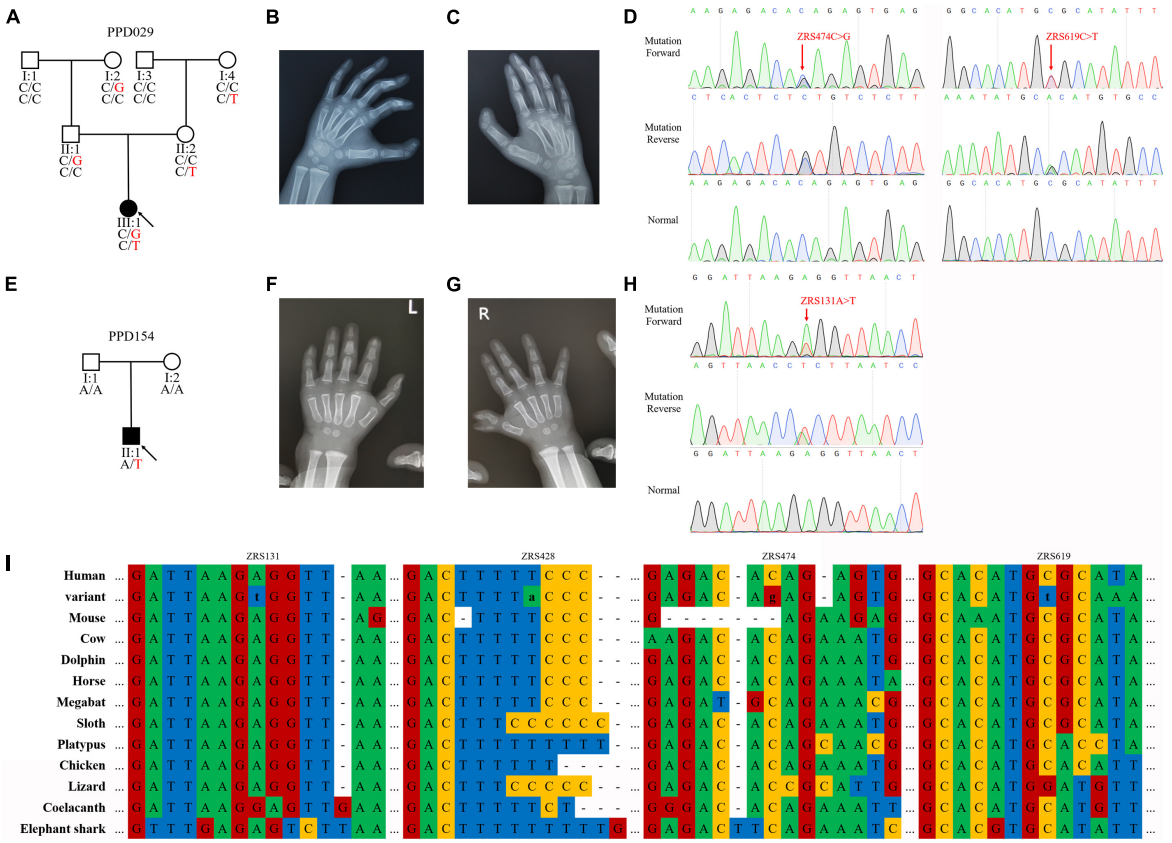

FIGURE 2 | ZPA regulatory sequence (ZRS) variants identified in preaxial polydactyly (PPD) families. **(A,E)** Pedigrees of PPD families (PPD029 and PPD154). "PPD029" and "PPD154" were PPD family numbers. Squares indicate male family members and circles indicate female family members. The black symbols represent the affected members and arrows indicate probands. Genotypes are identified by letters and a slash, with red representing variants. **(B,C,F,G)** Symptoms of patients. PPD029 had bilateral triphalangeal thumbs and PPD154 exhibited PPD I on the right hand. **(D,H)** Sequencing results of ZRS variants using Sanger sequencing. **(I)** Species conservation analysis of mutant base sites in ZRS.

limb defects (cannot completely exclude the possibility of an extremely subtle anomaly) (23). We reasoned that PPD in this family was attributed to combinedly acting by these two variants. PPD II is an autosomal dominant disease and our description indicated that PPD II individuals can be affected with a pattern of autosomal recessive inheritance. A previous study indicated that compared with a heterozygous variant in ZRS (ZRS402C > T), the homozygote led to more severe phenotypes, WMS, manifesting the superimposed effect of ZRS variants and our detection demonstrated again this phenomenon (24). ZRS619C > T had been reported by Mohammad et al. (15) in a Saudi Arabian family presented with variable preaxial deformities of the upper limbs including isolated triphalangeal thumb, PPD, preaxial syndactyly, and absent thumb and radius (15). Some family members suffered from renal agenesis and congenital heart disease. The variant (ZRS619C > T) showed obvious phenotypic heterogeneity in the Saudi Arabian family, whereas the variant was unable to alone trigger PPD in PPD029 family. It suggested that the pathogenicity of ZRS variants may be affected by ethnic difference, individual variation, and/or environmental factor.

ZPA regulatory sequence is a limb-specific enhancer of *SHH*, which induces the expression of SHH within ZPA (25). SHH expends from posterior mesoderm to anterior region of limb buds and lacks within the anterior-proximal. The expression gradient of SHH is crucial in establishing the number and the identity of the digits during anteroposterior patterning of the limb (26). Duplications involved ZRS or gain-of-function variants in ZRS would promote the expression of SHH in ZPA and then trigger the ectopic expression within the anterior region, where proliferation of mesenchymal cells is increased to cause PPD I/II (27). For four ZRS variants identified by us, their biological functions were not clarified and further studies needed to be performed. But, we predicted the pathogenicity of these four ZRS variants and analyzed their conservation. GnomAD showed that these variants were absent from controls or extremely rare. Thus, we highly suspected that these ZRS variants were their genetic etiologies, which should be further investigated.

CONCLUSION

In summary, we recruited 167 sporadic or familial cases with PPD from Central-South China and identified four ZRS variants (ZRS131A > T/chr7:g.156584439A > T, ZRS428T > A/chr7:g.156584142T > A, ZRS474C > G/chr7:g.156584096C > G, and ZRS619C > T/chr7:g.156583951C > T) in four patients with PPD (2.39%). Our description about epidemiological investigation of PPD helped us to understand the general picture of PPD in Central-South China. Our detection of two novel ZRS variants not only enrich the genetic map of PPD, but also contributed to genetic diagnosis and counseling of patients with PPD. Furthermore, we reported two patients with PPD I harboring ZRS variants further supporting the link between ZRS and PPD I and a PPD II case caused by the compound heterozygote in ZRS contributing to our understanding of PPD II and its genetic mechanism.

DATA AVAILABILITY STATEMENT

The original contributions presented in the study are included in the article/supplementary material, further inquiries can be directed to the corresponding authors.

ETHICS STATEMENT

The studies involving human participants were reviewed and approved by the Review Board of Xiangya Hospital of Central South University. Written informed consent to participate in this study was provided by the participants' legal guardian/next of kin. Written informed consent was obtained from the individual(s), and minor(s)' legal guardian/next of kin, for the publication of any potentially identifiable images or data included in this article.

AUTHOR CONTRIBUTIONS

LZ performed the acquisition, analysis, and interpretation of the data. J-YJ contributed to conception and design, carried out the analysis, and interpretation of the data. F-ML and YS carried out the analysis and interpretation of the data. P-FW contributed to conception and design and wrote the original draft. RX revised the draft and finally approved the final version of the manuscript. All authors contributed to the article and approved the submitted version.

FUNDING

This study was supported by the National Science and Technology Major Project of the Ministry of Science and Technology of China (2017ZX10103005-006), the National Natural Science Foundation of China (81970403, 82072194, 82170598, and 82102527), and Provincial Natural Science Foundation of Hunan (2021JJ40968).

ACKNOWLEDGMENTS

We thank the patients and their family members for their participation in this study and all the patient advisers for their assistance in clinical examination and blood specimen collection.

REFERENCES

1. Evanson BJ, Hosseinzadeh P, Riley SA, Burgess RC. Radial Polydactyly and the Incidence of Reoperation Using A New Classification System. *J Pediatr Orthop.* (2016) 36:158–60. doi: 10.1097/BPO.0000000000000395
2. Malik S. Polydactyly: phenotypes, genetics and classification. *Clin Genet.* (2014) 85:203–12. doi: 10.1111/cge.12276
3. Umair M, Ahmad F, Bilal M, Ahmad W, Alfadhel M. Clinical genetics of polydactyly: an updated review. *Front Genet.* (2018) 9:447. doi: 10.3389/fgene.2018.00447
4. Wu PF, Guo S, Fan XF, Fan LL, Jin JY, Tang JY, et al. A Novel ZRS Mutation in a Chinese Patient with Preaxial Polydactyly and Triphalangeal Thumb. *Cytogenet Genome Res.* (2016) 149:171–5. doi: 10.1159/000448820
5. Atasu M. Hereditary index finger polydactyly: phenotypic, radiological, dermatoglyphic, and genetic findings in a large family. *J Med Genet.* (1976) 13:469–76. doi: 10.1136/jmg.13.6.469
6. Al-Qattan MM, Shamseldin HE, Salih MA, Alkuraya FS. GLI3-related polydactyly: a review. *Clin Genet.* (2017) 92:457–66. doi: 10.1111/cge.12952
7. Fujioka H, Ariga T, Horiuchi K, Otsu M, Igawa H, Kawashima K, et al. Molecular analysis of non-syndromic preaxial polydactyly: preaxial polydactyly type-IV and preaxial polydactyly type-I. *Clin Genet.* (2005) 67:429–33. doi: 10.1111/j.1399-0004.2005.00431.x
8. Petit F, Jourdain AS, Holder-Espinasse M, Keren B, Andrieux J, Duterque-Coquillaud M, et al. The disruption of a novel limb cis-regulatory element of SHH is associated with autosomal dominant preaxial polydactyly-hypertrichosis. *Eur J Hum Genet.* (2016) 24:37–43. doi: 10.1038/ejhg.2015.53

9. Potuijt JWP, Baas M, Sukenik-Halevy R, Douben H, Nguyen P, Venter DJ, et al. A point mutation in the pre-ZRS disrupts sonic hedgehog expression in the limb bud and results in triphalangeal thumb-polysyndactyly syndrome. *Genet Med.* (2018) 20:1405–13. doi: 10.1038/gim.2018.18
10. Ullah A, Umair M, Majeed AI, Abdullah, Jan A, Ahmad W. A novel homozygous sequence variant in GLI1 underlies first case of autosomal recessive pre-axial polydactyly. *Clin Genet.* (2019) 95:540–1. doi: 10.1111/cge.13495
11. Umair M, Bilal M, Ali RH, Alhaddad B, Ahmad F, Abdullah, et al. Whole-exome sequencing revealed a nonsense mutation in STKLD1 causing non-syndromic pre-axial polydactyly type A affecting only upper limb. *Clin Genet.* (2019) 96:134–9. doi: 10.1111/cge.13547
12. Xu C, Yang X, Zhou H, Li Y, Xing C, Zhou T, et al. A novel ZRS variant causes preaxial polydactyly type I by increased sonic hedgehog expression in the developing limb bud. *Genet Med.* (2020) 22:189–98. doi: 10.1038/s41436-019-0626-7
13. Lettice LA, Heaney SJ, Purdie LA, Li L, de Beer P, Oostra BA, et al. A long-range Shh enhancer regulates expression in the developing limb and fin and is associated with preaxial polydactyly. *Hum Mol Genet.* (2003) 12:1725–35. doi: 10.1093/hmg/ddg180
14. Wieczorek D, Pawlik B, Li Y, Akarsu NA, Caliebe A, May KJ, et al. A specific mutation in the distant sonic hedgehog (SHH) cis-regulator (ZRS) causes Werner mesomelic syndrome (WMS) while complete ZRS duplications underlie Haas type polysyndactyly and preaxial polydactyly (PPD) with or without triphalangeal thumb. *Hum Mutat.* (2010) 31:81–9. doi: 10.1002/humu.21142
15. Al-Qattan MM, Al Abdulkareem I, Al Haidan Y, Al Balwi M. A novel mutation in the SHH long-range regulator (ZRS) is associated with preaxial polydactyly, triphalangeal thumb, and severe radial ray deficiency. *Am J Med Genet A.* (2012) 158A:2610–5. doi: 10.1002/ajmg.a.35584
16. Vanlerberghe C, Faivre L, Petit F, Fruchart O, Jourdain AS, Clavier F, et al. Intrafamilial variability of ZRS-associated syndrome: characterization of a mosaic ZRS mutation by pyrosequencing. *Clin Genet.* (2015) 88:479–83. doi: 10.1111/cge.12534
17. Gurnett CA, Bowcock AM, Dietz FR, Morcuende JA, Murray JC, Dobbs MB. Two novel point mutations in the long-range SHH enhancer in three families with triphalangeal thumb and preaxial polydactyly. *Am J Med Genet A.* (2007) 143A:27–32. doi: 10.1002/ajmg.a.31563
18. Kvon EZ, Kamneva OK, Melo US, Barozzi I, Osterwalder M, Mannion BJ, et al. Progressive Loss of Function in a Limb Enhancer during Snake Evolution. *Cell.* (2016) 167:633–642e611. doi: 10.1016/j.cell.2016.09.028
19. Xiang Y, Bian J, Wang Z, Xu Y, Fu Q. Clinical study of 459 polydactyly cases in China, 2010 to 2014. *Congenit Anom.* (2016) 56:226–32. doi: 10.1111/cga.12163
20. Xiang Y, Jiang L, Wang B, Xu Y, Cai H, Fu Q. Mutational screening of GLI3, SHH, preZRS, and ZRS in 102 Chinese children with nonsyndromic polydactyly. *Dev Dyn.* (2017) 246:392–402. doi: 10.1002/dvdy.24488
21. Rao C, Chen J, Peng Q, Mo Q, Xia X, Lu X. Mutational Screening of GLI3, SHH, and SHH ZRS in 78 Chinese Children with Nonsyndromic Polydactyly. *Genet Test Mol Biomark.* (2018) 22:577–81. doi: 10.1089/gtmb.2018.0096
22. Pauli RM, Feldman PF. Major limb malformations following intrauterine exposure to ethanol: two additional cases and literature review. *Teratology.* (1986) 33:273–80. doi: 10.1002/tera.1420330304
23. Potuijt JWP, Hoogeboom J, de Graaff E, van Nieuwenhoven CA, Galjaard RJH. Variable expression of subclinical phenotypes instead of reduced penetrance in families with mild triphalangeal thumb phenotypes. *J Med Genet.* (2020) 57:660–3. doi: 10.1136/jmedgenet-2019-106685
24. VanderMeer JE, Lozano R, Sun M, Xue Y, Daentl D, Jabs EW, et al. A novel ZRS mutation leads to preaxial polydactyly type 2 in a heterozygous form and Werner mesomelic syndrome in a homozygous form. *Hum Mutat.* (2014) 35:945–8. doi: 10.1002/humu.22581
25. Al-Qattan MM. Zone of polarizing activity regulatory sequence mutations/duplications with preaxial polydactyly and longitudinal preaxial ray deficiency in the phenotype: a review of human cases, animal models, and insights regarding the pathogenesis. *Biomed Res Int.* (2018) 2018:1573871. doi: 10.1155/2018/1573871
26. Tickle C, Towers M. Sonic Hedgehog Signaling in Limb Development. *Front Cell Dev Biol.* (2017) 5:14. doi: 10.3389/fcell.2017.00014
27. Johnson EJ, Neely DM, Dunn IC, Davey MG. Direct functional consequences of ZRS enhancer mutation combine with secondary long range SHH signalling effects to cause preaxial polydactyly. *Dev Biol.* (2014) 392:209–20. doi: 10.1016/j.ydbio.2014.05.025

Conflict of Interest: The authors declare that the research was conducted in the absence of any commercial or financial relationships that could be construed as a potential conflict of interest.

Publisher's Note: All claims expressed in this article are solely those of the authors and do not necessarily represent those of their affiliated organizations, or those of the publisher, the editors and the reviewers. Any product that may be evaluated in this article, or claim that may be made by its manufacturer, is not guaranteed or endorsed by the publisher.

frontiers | Frontiers in Genetics

CASE REPORT
published: 22 June 2022
doi: 10.3389/fgene.2022.887082

Case Report: Prenatal Diagnosis of Postaxial Polydactyly With Bi-Allelic Variants in Smoothened (SMO)

*Lihong Fan[1], Pengzhen Jin[2], Yeqing Qian[2], Guosong Shen[1], Xueping Shen[1] and Minyue Dong[2,3]**

[1]Center of Prenatal Diagnosis, Huzhou Maternity & Child Health Care Hospital, Huzhou, China, [2]Women's Hospital, School of Medicine Zhejiang University, Hangzhou, China, [3]Key Laboratory of Reproductive Genetics (Zhejiang University), Ministry of Education, Hangzhou, China

Postaxial polydactyly is a common congenital malformation which involves complex genetic factors. This retrospective study analyzed the cytogenetic and molecular results of a Chinese fetus diagnosed with postaxial polydactyly of all four limbs. Fetal karyotyping and chromosomal microarray analysis (CMA) did not find any abnormality while trio whole-exome sequencing (trio-WES) identified bi-allelic variants in smoothened (*SMO*) and (NM_005631.5: c.1219C > G, NP_005622.1: p. Pro407Ala, and NM_005631.5: c.1619C > T, NP_005622.1: p. Ala540Val). Sanger sequencing validated these variants. The mutations are highly conserved across multiple species. In-depth bioinformatics analysis and familial co-segregation implied the compound heterozygous variants as the likely cause of postaxial polydactyly in this fetus. Our findings provided the basis for genetic counseling and will contribute to a better understanding of the complex genetic mechanism that underlies postaxial polydactyly.

Keywords: postaxial polydactyly, whole-exome sequencing, bi-allelic variants, smoothened, genetic counseling

OPEN ACCESS

Edited by:
Long Guo,
RIKEN Center for Integrative Medical Sciences, Japan

Reviewed by:
Asmat Ullah,
University of Copenhagen, Denmark
Sajid Malik,
Quaid-i-Azam University, Pakistan

****Correspondence:***
Minyue Dong
dongmy@zju.edu.cn

Specialty section:
This article was submitted to Genetics of Common and Rare Diseases, a section of the journal Frontiers in Genetics

Received: *01 March 2022*
Accepted: *13 May 2022*
Published: *22 June 2022*

Citation:
Fan L, Jin P, Qian Y, Shen G, Shen X and Dong M (2022) Case Report: Prenatal Diagnosis of Postaxial Polydactyly With Bi-Allelic Variants in Smoothened (SMO). Front. Genet. 13:887082. doi: 10.3389/fgene.2022.887082

INTRODUCTION

Postaxial polydactyly (PAP), characterized by an extra digit at the fifth finger or toe, is one of the most common congenital malformations (Umair et al., 2018). It can be a marker of a wide variety of neurological and systemic abnormities and usually occurs in syndromic types (Verma and El-Harouni, 2015; Chandra et al., 2017). Limb growth in vertebrates is regulated by a complex network of intercellular communication and gene expression. The Sonic hedgehog protein (SHH), one of three mammalian hedgehog (HH) proteins, is expressed in the zone of polarizing activity (ZPA) of the limb bud and those of the notochord and floor plate in the neural tube (Riddle et al., 1993; Johnson et al., 1994; Jessell, 2000; Xavier et al., 2016). There is compelling evidence that the SHH signaling pathway plays an important role in regulating the patterning and growth of the developing limb (Hill et al., 2003; Tickle and Barker, 2013; Chinnaiya et al., 2014; Choudhry et al., 2014). The major components of the SHH pathway include smoothened (SMO), PTCH, and GLI transcription factors. In the absence of ligand binding of SHH, PTCH binds to SMO and inhibits its activity. Here, SUFU binds to the GLI transcription factors, which are subsequently phosphorylated by PKA, CK1, and GSK3β and degraded by the proteasome. Under this condition, GLI is converted to GLIr with the C-terminal domain truncated and enters the nucleus, inhibiting the transcription of downstream target genes (**Figure 1A**). When SHH is present, it binds to the extracellular domain of PTCH and releases its repressive effects on SMO. Freed of PTCH1-mediated suppression, SMO relieves the sequestration by SUFU and phosphorylation from PKA, CK1, and GSK3β, thus stabilizing the GLI

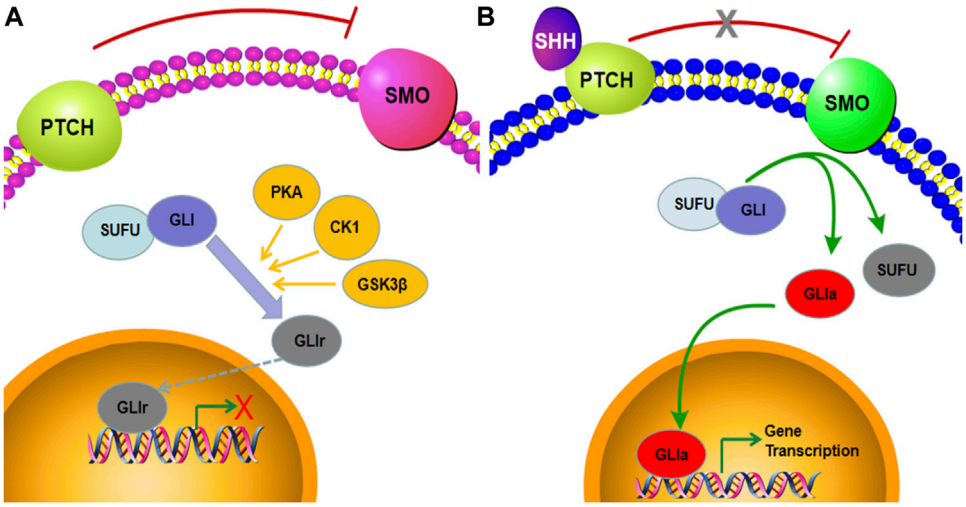

FIGURE 1 | Graphical representation of active and inactive SHH signaling pathways. **(A)** When SHH is absent, the full-length GLI is phosphorylated by PKA, CK1, and GSK3β and proteolytic cleavaged into the GLI repressor, which subsequently suppresses the expression of SHH target genes. **(B)** In the presence of the SHH ligand, SMO inhibits the sequestration by SUFU and phosphorylation by PKA, CK1, and GSK3β, leading to the formation of the GLI activator and ultimately to induction of target gene transcription.

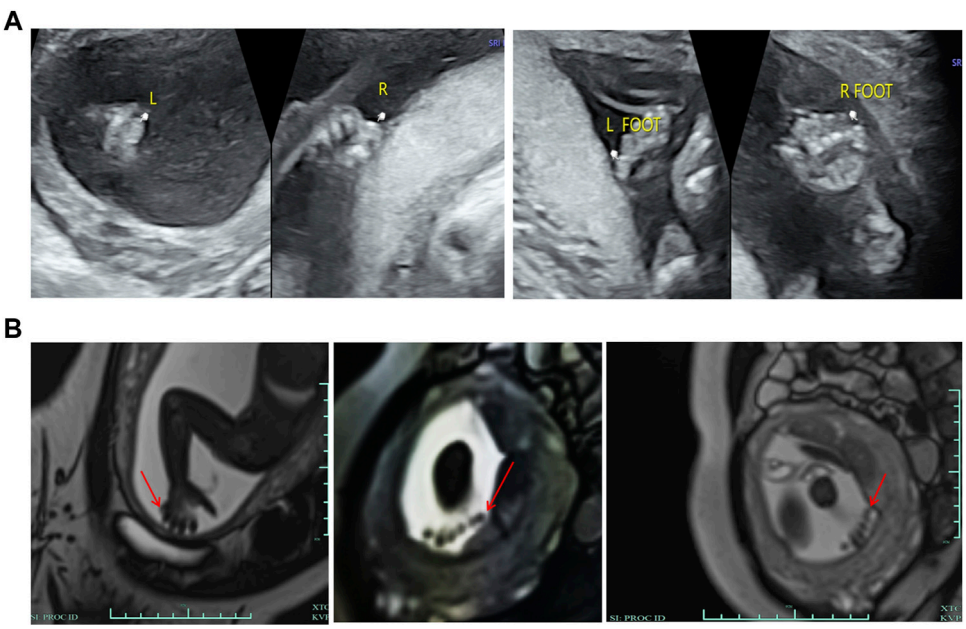

FIGURE 2 | Clinical features of the fetus. **(A)** Ultrasonography showed that there were echoes of the sixth toe on the lateral side of the little toe of both feet and the lateral side of the little finger of both hands, with a size of about 0.6*0.4 cm, and no obvious bony structure in them. **(B)** MRI showed a finger-like signal shadow on the outside of the right little finger, while the number of fingers on the left hand was not clear due to the position of the fetus. Six toe-like signal shadows were seen on both feet.

proteins in their full-length transcriptional activator form. The activated GLI (GLIa) translocates into the nucleus and promotes the transcription of SHH target genes (**Figure 1B**) (Briscoe and Thérond, 2013; Niida et al., 2021; Sigafoos et al., 2021). Here, we observed that the SHH signaling pathway is a highly regulated cascade of extracellular ligands, receptor proteins, cytoplasmic signaling molecules, transcription factors, coregulators, and target genes. Mutations in *SHH*, *PTCH*, *SMO*, and *GLI* can lead to the downregulation of the SHH pathway and ultimately to malformations (Johnson et al., 2014; Le et al., 2020; Yi et al., 2020). Most studies on PAP-related mutations have focused on *GLI*, while few studies, on *SMO* (Zou et al., 2019;

Cao et al., 2020; Xiang et al., 2020; Patel et al., 2021). To the best of our knowledge, no previous study on prenatal diagnosis of *SMO* mutations has been available so far. The present study reported novel bi-allelic variants in *SMO* likely causing the PAP in a fetus.

PATIENTS AND METHODS

Case Presentation

A 29-year-old primigravida woman was referred to our center for further evaluation at 23^{+2} weeks of gestation. First-trimester screening and second-trimester screening for Down syndrome indicated a low risk. Routine prenatal ultrasound scans (US) at 22^{+1} weeks of gestation suggested the PAP of all four limbs (**Figure 2A**). MRI scans subsequently confirmed the result of fetal PAP (**Figure 2B**). The mother denied being exposed to teratogenic agents or irradiation or using nicotine or alcohol during the pregnancy. No family history of neurological disease or congenital malformations was recorded.

The current investigation was approved by the Ethics Committee of Women's Hospital, School of Medicine Zhejiang University. All participants provided their written informed consent.

Amniocentesis

Amniocentesis was performed aseptically under the guidance of ultrasonography at 23^{+2} weeks of gestation. Thirty milliliters of amniotic fluid were obtained, of which 15 mL was for cell culture, while the remaining 15 mL was for DNA extraction.

Karyotype Analysis

Karyotype analysis included the culture of amniocytes in appropriate culture media and G-banded karyotyping at the 320–400 band level.

Chromosomal Microarray Analysis

Genomic DNA was extracted from the amniotic fluid and the peripheral blood of the parents. Then, fetal DNA was analyzed using the CytoScan™ HD whole-genome SNP array (Affymetrix, United States), and data were analyzed by Chromosome Analysis Suite 4.2, according to manufacturers' instructions.

Trio Whole-Exome Sequencing and Sanger Sequencing

Genomic DNA extracted from the amniotic fluid and the peripheral blood of the parents was used for Trio-WES. Exome capture was performed using the SureSelect Human All Exon V4 kit (Agilent Technologies, Santa Clara, CA, United States), followed by sequencing using an Illumina HiSeq2500 system (Illumina, San Diego, CA, United States). After sequencing and filtering out low-quality reads, high-quality reads were compared to the GRCh37/hg19 reference human genome using Sentieon BWA (Sentieon, United States) with the MEM align method, and only the variants located in the coding sequence or splice site regions would be retained. Variant calling was performed using the Genome Analysis Tool Kit (GATK v4.0). Then, the candidate variants, including single-nucleotide variants (SNVs) and indels, were filtered by frequencies on specific databases, including the Human Gene Mutation Database (HGMD), ClinVar database, 1000 Genomes Project, Exome Aggregation Consortium (ExAC), Exome Sequencing Project 6500 (ESP6500), database of single-nucleotide polymorphisms (dbSNP), and Genome Aggregation Database (gnomAD). Mutation sites, known as polymorphic sites, were excluded, and the variants with allele frequency≤1% were retained. We used PolyPhen2, SIFT, Condel, MutationTaster, and phyloP to predict the effect of variants. The interpretation of sequence variants was performed according to the American College of Medical Genetics and Genomics (ACMG) (Richards et al., 2015). Online Clustal Omega (https://www.ebi.ac.uk/Tools/msa/clustalo/) was used to analyze the evolutionarily conserved sequences among species (humans, chimpanzees, macaques, mice, rats, *Sus scrofa*, horses, and *Bos taurus*). Finally, the identified variants were confirmed with Sanger sequencing. Sequences containing the two potential variants were amplified. The primer sequences were designed by Primer3 (http://primer3.ut.ee/), and all the primers are shown in **Supplementary Table S1**. Then, the PCR products were sequenced on the ABI 3500DX, followed by analysis by DNASTAR 5.0 software.

RESULTS

CMA and karyotype analysis did not reveal any abnormalities. However, the trio-WES study identified a compound heterozygote in *SMO* (chr7:128846383, NM_005631.5: c.1219C > G, NP_005622.1: p. Pro407Ala; chr7:128850356, NM_005631.5: c.1619C > T, NP_005622.1: p. Ala540Val) inherited from the mother and father, respectively. Sanger sequencing confirmed the variants and showed that the two compound heterozygous mutations in *SMO* co-segregate with the disorder in this family (**Figure 3A**). The two mutations were absent in the 1000 Genomes, ESP6500, dbSNP144, and ExAC databases, and only the mutation c.1619C > T had a low allele frequency (0.00001989, all heterozygote) observed in gnomAD. The alignment of the amino acid sequences indicates that the two mutant residues were 100% conserved among many species (**Figure 3B**). Moreover, both variants were predicted to be pathogenic by the SIFT, PROVEAN, and MutationTaster tools (**Table 1**). Based on the consistency of genotype–phenotype correlation and the effect of the mutations, we speculated that the compound heterozygous mutations in *SMO* might be responsible for the limb abnormalities in this Chinese family.

Finally, the couple chose to terminate the pregnancy after carefully considering the abnormal ultrasonography findings and trio-WES results.

DISCUSSION

The genetic mechanism underlying polydactyly is highly complex. The SHH pathway is the essential evolutionarily

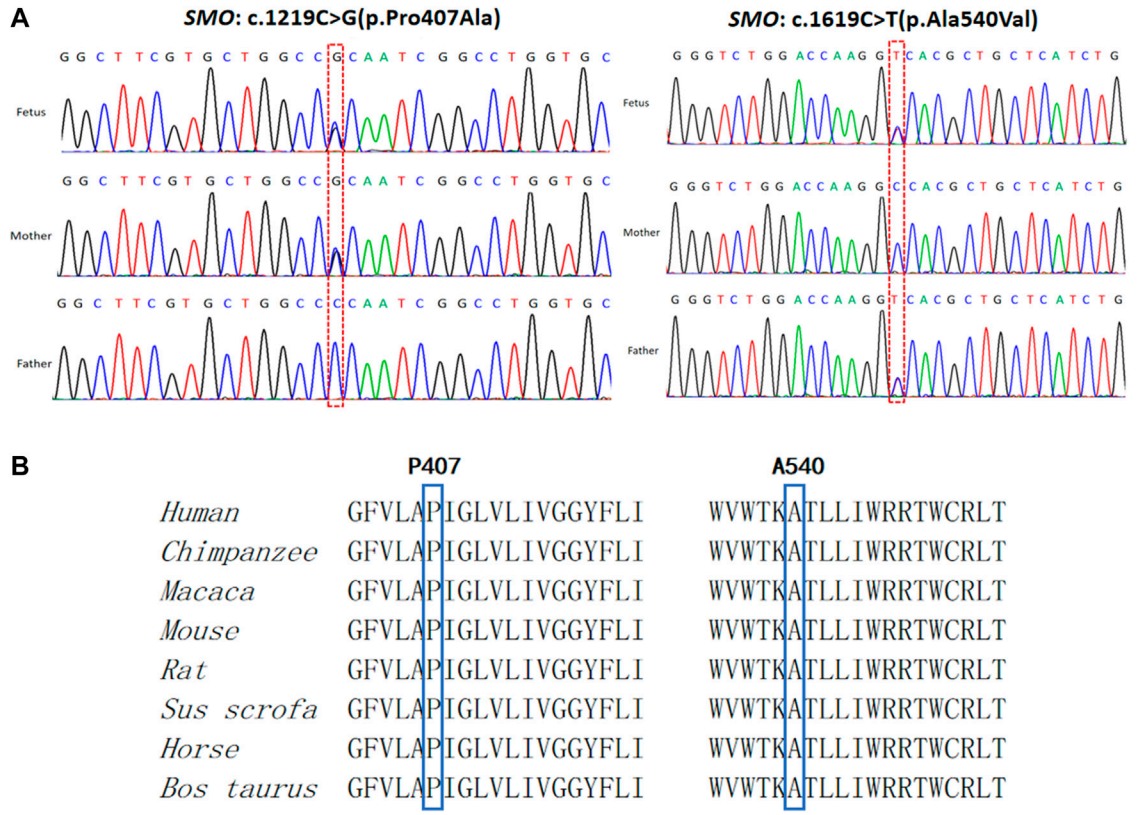

FIGURE 3 | Genetic variations identified in this case. **(A)** Two variants detected in the fetus and parents. **(B)** Conservation of the mutated amino acids (Pro407 and Ala540) across different species.

TABLE 1 | *In silico* analysis of the *SMO* variants c.1219C > G and c.1619C > T.

Variant	MutationTaster	PROVEAN	SIFT
c.1219C > G	Disease-causing	Deleterious	Damaging
c.1619C > T	Disease-causing	Deleterious	Damaging

conserved pathway related to the growth and patterning of the limbs (Patterson et al., 2009; Rahi and Mehan, 2020). SMO, a seven-transmembrane, encoded by *SMO*, is required for active SHH signaling (Zhang et al., 2001; Le et al., 2020). A previous study showed that removing *SMO* from the apical ectodermal ridge resulted in the loss of functional SHH signaling, ultimately leading to disruption of digit patterns and the formation of additional postaxial cartilage contraction (Bouldin et al., 2010).

In the present study, we identified bi-allelic variants in *SMO*, c.1219C > G (p. Pro407Ala), and c.1619C > T (p. Ala540Val) in a Chinese family. The second variant was previously reported in a Han Chinese boy, also in a state of compound heterozygosity (Zhang et al., 2019). It was predicted that this mutation affects the signaling ability of SMO as the alanine residue at position 540 is quite close to the seventh TM domain, which is considered to be the key site for signaling transduction. In addition, the previous study also performed a gene expression analysis and showed a significant decrease in the *SMO* expression in the patient compared with healthy controls. Back to our study, although the mRNA and protein level in the fetus cannot be detected due to the unavailability of the fetus' sample, the pathogenic effect of Pro407Ala and Ala540Val substitution in SMO may be supported by the following points: 1) both loci were quite conserved among different species; 2) *in silico* bioinformatics applications predicted that both mutations are deleterious; 3) *SMO* belongs to recessive genes, and the two mutations co-segregated with the disorder in the family; 4) no other pathogenic variants were detected in the known polydactyly or limb development genes, such as *SHH*, *PTCH*, and *GLI*; and 5) the phenotype of PAP found in the fetus could be explained by *SMO* defects.

We searched the PubMed database to find relevant literature on *SMO* mutations. As a result, we found that the previous studies on *SMO* were limited and focused on activating somatic mutations that caused diseases such as sporadic basal cell carcinoma (BCC), medulloblastoma (MB), and Curry–Jones syndrome (CRJS) (Kool et al., 2014; Twigg et al., 2016; Bisceglia et al., 2020). Germline mutations, leading to developmental disorders, have not been reported until recent years. According to the previous reports, there were, in total, 10 patients with a series of congenital developmental abnormalities caused by *SMO* mutations (Rubino et al., 2018; Zhang et al., 2019; Le et al., 2020; Green et al., 2022). The fact that all the patients had

compound heterozygous variants, while their parents were in a heterozygous state and had no associated phenotype, confirmed that *SMO* belongs to recessive genes. PAP can be observed in nine out of 10 patients, and 100% (9/9) of the patients with PAP also had other symptoms, such as thalamic hamartoma, cystic epilepsy, atrioventricular septal defect (AVSD), and aganglionosis. The most severe case was one who presented AVSD and died at 3 months of age (Le et al., 2020). In addition, all nine cases mentioned previously were diagnosed after birth, and our report on the fetus is to date the only prenatal genetic diagnosis of *SMO* mutations. We speculated that PAP may be the earliest prenatal manifestation and that the fetus may present other related symptoms after birth.

As one of the most common congenital malformations, PAP often appears as a key feature of malformation syndromes, such as Meckel–Gruber syndrome (Turkyilmaz et al., 2021), Bardet–Biedl syndrome (Ullah et al., 2017), and Pallister–Hall syndrome (Yang et al., 2021). According to previous studies, about 8% of bilateral PAP cases are related to a set of other congenital syndromic defects. As is well known, many syndromes have postnatal features that cannot be detected prenatally on ultrasound scans. The fetal phenotype is useful but sometimes limited source of information for the diagnosis of many Mendelian diseases. In prenatal cases with a less severe phenotype or an isolated anomaly, it is always quite difficult for parents to make a decision on continuing or terminating the pregnancy. We believe that prenatal WES is particularly valuable in detecting genetic variants of certain genes that may be critical to human development and helps us predict the postnatal phenotypes associated with the detected genes.

The most important limitation to our study lies in the fact that there is a lack of postpartum assessment and validation of associated malformations, such as thalamic hamartoma, cystic epilepsy, atrioventricular septal defect, and aganglionosis, due to our failure to get the permission for an autopsy. Therefore, it is still uncertain whether the fetus' polydactyly was isolated or syndromic, although no abnormality in organs such as the heart and the brain was indicated by multiple prenatal ultrasounds and MRI. Given the very scarce reporting of occasional mutations, more studies in patients with related phenotypes are urgently needed to describe a full spectrum of *SMO* mutations. Detailed functional experiments are also needed to confirm how these mutations work.

In conclusion, we identified a novel compound heterozygous mutation (c.1219C > G, p. Pro407Ala and c.1619C > T, p. Ala540Val) in the gene *SMO*. There is convincing evidence, although no definite proof, that this mutation is causative for the PAP in the present family. The genetic diagnosis provided evidence for assessing the risk of recurrence and was invaluable for genetic counseling of the couple contemplating future pregnancies.

DATA AVAILABILITY STATEMENT

The datasets for this article are not publicly available due to concerns regarding participant/patient anonymity. Requests to access the datasets should be directed to the corresponding author.

ETHICS STATEMENT

The studies involving human participants were reviewed and approved by the Ethics Committee of Women's Hospital, School of Medicine Zhejiang University. The patients/participants provided their written informed consent to participate in this study. Written informed consent was obtained from the minor(s)' legal guardian/next of kin for the publication of any potentially identifiable images or data included in this article.

AUTHOR CONTRIBUTIONS

MD designed the study and reviewed the manuscript. LF analyzed the data and wrote the manuscript. XS and GS performed the experiments. YQ and PJ collected the data. All authors have read and approved the manuscript.

FUNDING

The work was supported by the Zhejiang medical and health technology program (2021KY1085) and the Huzhou science and technology program (2020GY26).

ACKNOWLEDGMENTS

We thank the family for their participation in this study.

SUPPLEMENTARY MATERIAL

The Supplementary Material for this article can be found online at: https://www.frontiersin.org/articles/10.3389/fgene.2022.887082/full#supplementary-material

REFERENCES

Bisceglia, M., Panniello, G., Galliani, C. A., Centola, M., D'Errico, M. M., Minenna, E., et al. (2020). Metastatic Basal Cell Carcinoma of the Skin: A Comprehensive Literature Review, Including Advances in Molecular Therapeutics. *Adv. Anat. Pathol.* 27 (5), 331–353. doi:10.1097/pap.0000000000000267

Bouldin, C. M., Gritli-Linde, A., Ahn, S., and Harfe, B. D. (2010). Shh Pathway Activation Is Present and Required within the Vertebrate Limb Bud Apical Ectodermal Ridge for Normal Autopod Patterning. *Proc. Natl. Acad. Sci. U.S.A.* 107 (12), 5489–5494. doi:10.1073/pnas.0912818107

Briscoe, J., and Thérond, P. P. (2013). The Mechanisms of Hedgehog Signalling and its Roles in Development and Disease. *Nat. Rev. Mol. Cell Biol.* 14 (7), 416–429. doi:10.1038/nrm3598

Cao, R., Liu, S., Chai, W., and Shen, P. (2020). Polydactyly Patient Carried a Mutation of PTCH1 Which Has Been Identified in Nevoid Basal Cell Nevus Syndrome. *DNA Cell Biol.* 39 (10), 1754–1759. doi:10.1089/dna.2019.5236

Chandra, S., Daryappa, M., Mukheem Mudabbir, M., Pooja, M., and Arivazhagan, A. (2017). Pallister-Hall Syndrome. *J. Pediatr. Neurosci.* 12 (3), 276–279. doi:10.4103/jpn.JPN_101_17

Chinnaiya, K., Tickle, C., and Towers, M. (2014). Sonic Hedgehog-Expressing Cells in the Developing Limb Measure Time by an Intrinsic Cell Cycle Clock. *Nat. Commun.* 5, 4230. doi:10.1038/ncomms5230

Choudhry, Z., Rikani, A. A., Choudhry, A. M., Tariq, S., Zakaria, F., Asghar, M. W., et al. (2014). Sonic Hedgehog Signalling Pathway: a Complex Network. *Ann* 21 (1), 28–31. doi:10.5214/ans.0972.7531.210109

Green, T. E., Schimmel, M., Schubert, S., Lemke, J. R., Bennett, M. F., Hildebrand, M. S., et al. (2022). Bi-allelic SMO Variants in Hypothalamic Hamartoma: a Recessive Cause of Pallister-Hall Syndrome. *Eur. J. Hum. Genet.* 30, 384–388. doi:10.1038/s41431-021-01023-4

Hill, R. E., Heaney, S. J. H., and Lettice, L. A. (2003). Sonic Hedgehog: Restricted Expression and Limb Dysmorphologies. *J. Anat.* 202 (1), 13–20. doi:10.1046/j.1469-7580.2003.00148.x

Jessell, T. M. (2000). Neuronal Specification in the Spinal Cord: Inductive Signals and Transcriptional Codes. *Nat. Rev. Genet.* 1 (1), 20–29. doi:10.1038/35049541

Johnson, E. J., Neely, D. M., Dunn, I. C., and Davey, M. G. (2014). Direct Functional Consequences of ZRS Enhancer Mutation Combine with Secondary Long Range SHH Signalling Effects to Cause Preaxial Polydactyly. *Dev. Biol.* 392 (2), 209–220. doi:10.1016/j.ydbio.2014.05.025

Johnson, R. L., Laufer, E., Riddle, R. D., and Tabin, C. (1994). Ectopic Expression of Sonic Hedgehog Alters Dorsal-Ventral Patterning of Somites. *Cell* 79 (7), 1165–1173. doi:10.1016/0092-8674(94)90008-6

Kool, M., Jones, D. T. W., Jäger, N., Northcott, P. A., Pugh, T. J., Hovestadt, V., et al. (2014). Genome Sequencing of SHH Medulloblastoma Predicts Genotype-Related Response to Smoothened Inhibition. *Cancer Cell* 25 (3), 393–405. doi:10.1016/j.ccr.2014.02.004

Le, T.-L., Sribudiani, Y., Dong, X., Huber, C., Kois, C., Baujat, G., et al. (2020). Bi-allelic Variations of SMO in Humans Cause a Broad Spectrum of Developmental Anomalies Due to Abnormal Hedgehog Signaling. *Am. J. Hum. Genet.* 106 (6), 779–792. doi:10.1016/j.ajhg.2020.04.010

Niida, Y., Togi, S., and Ura, H. (2021). Molecular Bases of Human Malformation Syndromes Involving the SHH Pathway: GLIA/R Balance and Cardinal Phenotypes. *Ijms* 22 (23), 13060. doi:10.3390/ijms222313060

Patel, R., Singh, S. K., Bhattacharya, V., and Ali, A. (2021). Novel GLI3 Pathogenic Variants in Complex Pre- and Postaxial Polysyndactyly and Greig Cephalopolysyndactyly Syndrome. *Am. J. Med. Genet.* 185 (1), 97–104. doi:10.1002/ajmg.a.61919

Patterson, V. L., Damrau, C., Paudyal, A., Reeve, B., Grimes, D. T., Stewart, M. E., et al. (2009). Mouse Hitchhiker Mutants Have Spina Bifida, Dorso-Ventral Patterning Defects and Polydactyly: Identification of Tulp3 as a Novel Negative Regulator of the Sonic Hedgehog Pathway. *Hum. Mol. Genet.* 18 (10), 1719–1739. doi:10.1093/hmg/ddp075

Rahi, S., and Mehan, S. (2020). Understanding Abnormal SMO-SHH Signaling in Autism Spectrum Disorder: Potential Drug Target and Therapeutic Goals. *Cell Mol. Neurobiol.* 42, 931–953. doi:10.1007/s10571-020-01010-1

Richards, S., Aziz, N., Bale, S., Bick, D., Das, S., Gastier-Foster, J., et al. (2015). Standards and Guidelines for the Interpretation of Sequence Variants: a Joint Consensus Recommendation of the American College of Medical Genetics and Genomics and the Association for Molecular Pathology. *Genet. Med.* 17 (5), 405–424. doi:10.1038/gim.2015.30

Riddle, R. D., Johnson, R. L., Laufer, E., and Tabin, C. (1993). Sonic Hedgehog Mediates the Polarizing Activity of the ZPA. *Cell* 75 (7), 1401–1416. doi:10.1016/0092-8674(93)90626-2

Rubino, S., Qian, J., Pinheiro-Neto, C. D., Kenning, T. J., and Adamo, M. A. (2019). A Familial Syndrome of Hypothalamic Hamartomas, Polydactyly, and SMO Mutations: a Clinical Report of 2 Cases. *J. Neurosurg. Pediatr.* 23 (1), 98–103. doi:10.3171/2018.7.Peds18292

Sigafoos, A. N., Paradise, B. D., and Fernandez-Zapico, M. E. (2021). Hedgehog/GLI Signaling Pathway: Transduction, Regulation, and Implications for Disease. *Cancers* 13 (14), 3410. doi:10.3390/cancers13143410

Tickle, C., and Barker, H. (2013). The Sonic Hedgehog Gradient in the Developing Limb. *WIREs Dev. Biol.* 2 (2), 275–290. doi:10.1002/wdev.70

Turkyilmaz, A., Geckinli, B. B., Alavanda, C., Arslan Ates, E., Buyukbayrak, E. E., Eren, S. F., et al. (2021). Meckel-Gruber Syndrome: Clinical and Molecular Genetic Profiles in Two Fetuses and Review of the Current Literature. *Genet. Test. Mol. Biomarkers* 25 (6), 445–451. doi:10.1089/gtmb.2020.0311

Twigg, S. R. F., Hufnagel, R. B., Miller, K. A., Zhou, Y., McGowan, S. J., Taylor, J., et al. (2016). A Recurrent Mosaic Mutation in SMO , Encoding the Hedgehog Signal Transducer Smoothened, Is the Major Cause of Curry-Jones Syndrome. *Am. J. Hum. Genet.* 98 (6), 1256–1265. doi:10.1016/j.ajhg.2016.04.007

Ullah, A., Umair, M., Yousaf, M., Khan, S. A., Nazim-Ud-Din, M., Shah, K., et al. (2017). Sequence Variants in Four Genes Underlying Bardet-Biedl Syndrome in Consanguineous Families. *Mol. Vis.* 23, 482–494.

Umair, M., Ahmad, F., Bilal, M., Ahmad, W., and Alfadhel, M. (2018). Clinical Genetics of Polydactyly: An Updated Review. *Front. Genet.* 9, 447. doi:10.3389/fgene.2018.00447

Verma, P. K., and El-Harouni, A. A. (2015). Review of Literature: Genes Related to Postaxial Polydactyly. *Front. Pediatr.* 3, 8. doi:10.3389/fped.2015.00008

Xavier, G. M., Seppala, M., Barrell, W., Birjandi, A. A., Geoghegan, F., and Cobourne, M. T. (2016). Hedgehog Receptor Function during Craniofacial Development. *Dev. Biol.* 415 (2), 198–215. doi:10.1016/j.ydbio.2016.02.009

Xiang, Y., Li, X., Zhan, Z., Feng, J., Cai, H., Li, Y., et al. (2020). A Novel Nonsense GLI3 Variant Is Associated with Polydactyly and Syndactyly in a Family by Blocking the Sonic Hedgehog Signaling Pathway. *Front. Genet.* 11, 542004. doi:10.3389/fgene.2020.542004

Yang, Y., Shen, F., Jing, X.-P., Zhang, N., Xu, S.-Y., Li, D.-D., et al. (2021). Case Report: Whole-Exome Sequencing of Hypothalamic Hamartoma from an Infant with Pallister-Hall Syndrome Revealed Novel De Novo Mutation in the GLI3. *Front. Surg.* 8, 734757. doi:10.3389/fsurg.2021.734757

Yi, X., Yuan, X., Xie, H., Chen, X., and Zhu, Y. (2020). A Familial Sonic Hedgehog (SHH) Stop-Gain Mutation Associated with Agenesis of the Corpus Callosum, Mild Intellectual Disability and Facial Dysmorphism. *Brain Dev.* 42 (10), 771–774. doi:10.1016/j.braindev.2020.07.004

Zhang, J., Li, Y., Fan, Y., Wu, D., and Xu, J. (2019). Compound Heterozygous Mutations in SMO Associated with Anterior Segment Dysgenesis and Morning Glory Syndrome. *Gene* 713, 143973. doi:10.1016/j.gene.2019.143973

Zhang, X. M., Ramalho-Santos, M., and McMahon, A. P. (2001). Smoothened Mutants Reveal Redundant Roles for Shh and Ihh Signaling Including Regulation of L/R Asymmetry by the Mouse Node. *Cell* 105 (6), 781–792. doi:10.1016/s0092-8674(01)00385-3

Zou, Q., Tian, Z., Zheng, J., Zhi, X., Du, X., Shu, J., et al. (2019). A Novel Missense in GLI3 Possibly Affecting One of the Zinc Finger Domains May Lead to Postaxial Synpolydactyly: Case Report. *BMC Med. Genet.* 20 (1), 174. doi:10.1186/s12881-019-0889-5

Conflict of Interest: The authors declare that the research was conducted in the absence of any commercial or financial relationships that could be construed as a potential conflict of interest.

Publisher's Note: All claims expressed in this article are solely those of the authors and do not necessarily represent those of their affiliated organizations, or those of the publisher, the editors, and the reviewers. Any product that may be evaluated in this article, or claim that may be made by its manufacturer, is not guaranteed or endorsed by the publisher.

frontiers | Frontiers in Genetics

ORIGINAL RESEARCH
published: 24 June 2022
doi: 10.3389/fgene.2022.938814

A Null Mutation of *TNFRSF11A* Causes Dysosteosclerosis, Not Osteopetrosis

Tarık Kırkgöz[1], Behzat Özkan[1], Filiz Hazan[2], Sezer Acar[1], Özlem Nalbantoğlu[1], Beyhan Özkaya[1], Melike Ataseven Kulalı[3], Semra Gürsoy[4], Shiro Ikegawa[5] and Long Guo[5]**

[1]Division of Pediatric Endocrinology, Dr. Behçet Uz Children's Education and Research Hospital, Izmir, Turkey, [2]Department of Medical Genetics, Dr. Behçet Uz Children's Education and Research Hospital, Izmir, Turkey, [3]Division of Pediatric Genetics, School of Medicine, Afyon Kocatepe University, Afyonkarahisar, Turkey, [4]Division of Pediatric Genetics, Dr. Behçet Uz Children's Education and Research Hospital, Izmir, Turkey, [5]Laboratory for Bone and Joint Diseases, RIKEN Center for Integrative Medical Sciences, Tokyo, Japan

Dysosteosclerosis (DOS) is a rare sclerosing bone dysplasia characterized by unique osteosclerosis of the long tubular bones and platyspondyly. DOS is inherited in an autosomal recessive manner and is genetically and clinically heterogeneous. To date, four individuals with DOS who have five different *TNFRSF11A* mutations have been reported. Based on their data, it is hypothesized that mutations producing aberrant mutant RANK proteins (missense or truncated or elongated) cause DOS, while null mutations lead to osteopetrosis, autosomal recessive 7 (OPTB7). Herein, we present the fifth case of *TNFRSF11A*-associated DOS with a novel homozygous frame-shift mutation (c.19_31del; p.[Arg7CysfsTer172]). The mutation is predicted to cause nonsense mutation-mediated mRNA decay (NMD) in all RANK isoform transcripts, resulting in totally null allele. Our findings suggest genotype-phenotype relationship in *TNFRSF11A*-associated OPTB7 and DOS remains unclear, and that the deficiency of *TNFRSF11A* functions might cause DOS, rather than osteopetrosis. More data are necessary to understand the phenotypic spectrum caused by *TNFRSF11A* mutations.

Keywords: TNFRSF11A/TNR11/RANK, dysosteosclerosis, sclerosing bone dysplasia, osteopetrosis, mutation

OPEN ACCESS

Edited by:
Cristina Sobacchi,
National Research Council (CNR), Italy

Reviewed by:
Mario Abinun,
Newcastle University, United Kingdom
Stuart Ralston,
University of Edinburgh,
United Kingdom

****Correspondence:***
Sezer Acar
dr.acarsezer@gmail.com
Long Guo
longguo601@gmail.com

Specialty section:
This article was submitted to Genetics of Common and Rare Diseases, a section of the journal Frontiers in Genetics

Received: *08 May 2022*
Accepted: *06 June 2022*
Published: *24 June 2022*

Citation:
Kırkgöz T, Özkan B, Hazan F, Acar S, Nalbantoğlu Ö, Özkaya B, Kulalı MA, Gürsoy S, Ikegawa S and Guo L (2022) A Null Mutation of TNFRSF11A Causes Dysosteosclerosis, Not Osteopetrosis. Front. Genet. 13:938814. doi: 10.3389/fgene.2022.938814

INTRODUCTION

Dysosteosclerosis (DOS) is a rare form of dense bone disease characterized by osteosclerosis and platyspondyly (Spranger et al., 1968). Its features are short stature, recurrent fractures, optic atrophy, cranial nerve palsy, developmental delay, flattened fingernails, skin related complications, and failure of tooth eruption (MIM %224300). Irregular osteosclerosis, flattened diffusely dense vertebral bodies, sclerotic skull, radiolucent sub-metaphyseal portions of the long tubular bones with sclerotic diaphysis are radiological features of DOS (Houston et al., 1978; Elçioglu et al., 2002; Whyte et al., 2010; Guo et al., 2018). Moreover, metaphyseal osteosclerosis and platyspondyly are the characteristic and important guiding findings in differentiating DOS from other types of sclerosing bone dysplasia (Howaldt et al., 2019).

DOS is inherited in an autosomal recessive manner and is genetically and clinically heterogeneous. Four disease genes for DOS have been described to date (Campeau et al., 2012; Guo et al., 2018; Guo et al., 2019; Howaldt et al., 2019; Uludağ Alkaya et al., 2021). *SLC29A3* (solute carrier family 29 member 3) was the first identified gene, followed by *TNSFR11A* (tumor necrosis factor receptor superfamily member 11a; also known as RANK (receptor activator of nuclear factor kappa B)), *TCIRG1* (T cell immune regulator 1) and *CSF1R* (colony stimulating factor 1 receptor)

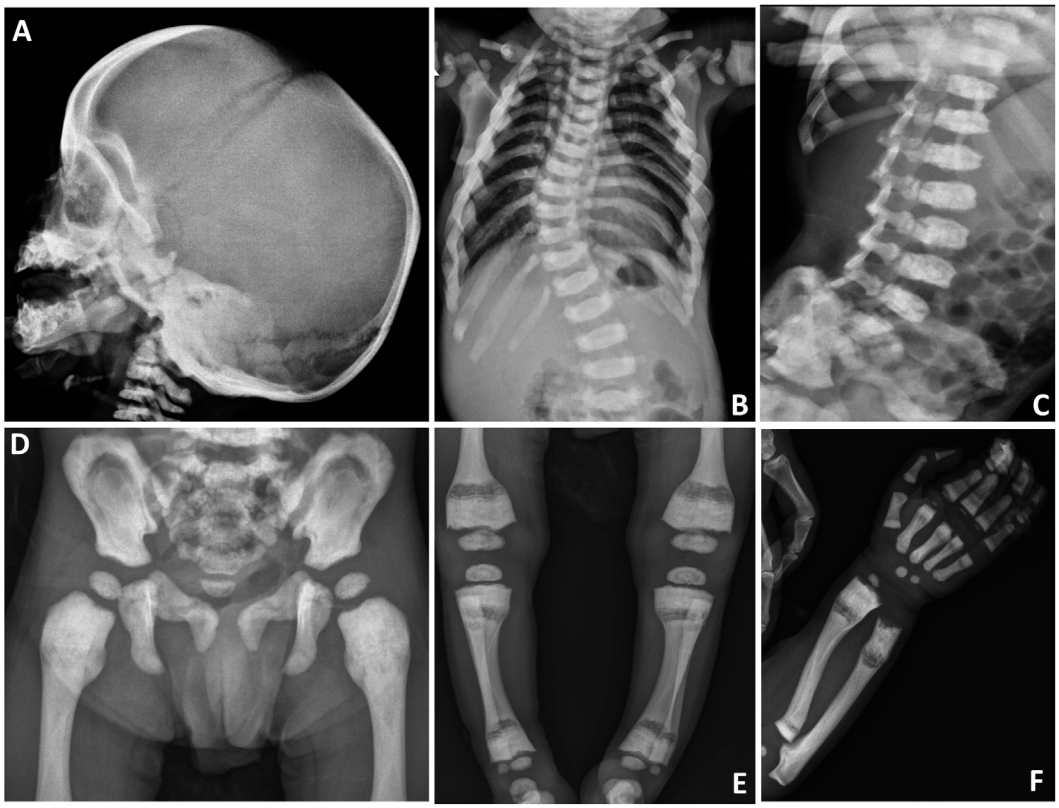

FIGURE 1 | Skeletal survey of the patient. **(A)** Sclerosis of the craniofacial bones, especially at the skull base. **(B)** Scoliosis at the thoracic level. **(C)** Plate irregularities and mildly reduced height of the vertebral corpus (platyspondyly). **(D)** Sclerosis at the pelvic bones, especially in the iliac bodies. **(E)** Radiolucency at the metadiaphyseal junction and sclerosis at the end of long bones. **(F)** Sclerosis of the radius, ulna, metacarpal bones, and proximal phalanges. Radiolucency at the metadiaphyseal junction of radius and ulna is also noted.

(Campeau et al., 2012; Guo et al., 2018; Guo et al., 2019; Howaldt et al., 2019; Uludağ Alkaya et al., 2021). Notably, *TNSFR11A* and *TCIRG1* mutations are also reported in osteopetrosis, autosomal recessive 7 (OPTB7) and osteopetrosis, autosomal recessive 1 (OPTB1), respectively (Frattini et al., 2000; Guerrini et al., 2008; Pangrazio et al., 2012).

To date, four DOS individuals with five different *TNFRSF11A* mutations (2 missense/nonsense, 2 splice-site, 1 deletion) have been reported (Guo et al., 2018; Xue et al., 2019; Xue et al., 2020; Xue et al., 2021a; Xue et al., 2021b). According to the previous hypothesis for genotype-phenotype relationship, aberrant mutant RANK proteins (missense or truncated or elongated) cause DOS, while null mutations lead to OPTB7 (Guo et al., 2018; Xue et al., 2019; Xue et al., 2020; Xue et al., 2021a). Herein, we present the fifth case of *TNFRSF11A*-associated DOS in a 19-month-old boy, in whom we identified a novel homozygous mutation in *TNFRSF11A* (c.19_31del; p.[Arg7CysfsTer172]). Unlike the previously reported DOS mutations, the mutation is predicted to cause nonsense mutation-mediated mRNA decay (NMD) in all RANK isoform transcripts, which leads us to re-consider the phenotype and genotype relationship of the *TNFRSF11A* mutation.

MATERIALS AND METHODS

Case Report

A 19-month-old boy was consulted to pediatric endocrinology unit for hypocalcemia and short stature. He was the third baby to healthy consanguineous Turkish parents who had healthy boys and two abortions. Family history was unremarkable with no affected family members. The prenatal course was uneventful. The proband was born at term by normal Cesarean section with a birth weight of 3,200 g (+0.02 standard deviation score (SDS)). He had a history of hypocalcemic convulsion at day 4, and was treated with intravenous calcium and vitamin D supplementation. The patient was discharged to home with phenobarbital therapy at day 14. From 4th month, he was hospitalized three times due to lower respiratory tract infection.

On the physical examination at age 19 months, his height, weight and head circumference were at −3.1, −2.7, and +0.2 SDSs, respectively. Midface hypoplasia, edematous eyelids, down slanting palpebral fissures, long eyelashes, long philtrum, high arched palate, low set ears, and micrognathia were detected. A prominent forehead, open anterior fontanelle (4 × 4 cm), pectus carinatum, café-au-lait spot (4 × 3 cm) on anterior thorax, and bowing of femora and ulnae were noticed. Ophthalmological

examination revealed optic atrophy and horizontal nystagmus. Moderate delay in developmental milestones was observed.

On biochemical evaluation, serum calcium was 7.4 mg/dl (Normal (N): 9.0–11), phosphorus was 4.4 mg/dl (N: 4–6.5), ALP was 84 U/L (N: 116–450), albumin was 4.1 g/L (N: 3.5-5.5), PTH was 102.3 ng/L (N: 15–88), and 25-OH vitamin D was 27 µg/L (N: 30–100). Liver-kidney function tests, thyroid function tests and ions were normal. Skeletal survey showed diffuse osteosclerosis of the craniofacial, axial and appendicular skeletons, especially in diaphyseal areas of the long tubular bones (**Figures 1A,D–F**). In the evaluation of the vertebral structures, end plate irregularities, mildly reduced height (platyspondyly) and thoracic and lumbar scoliosis were observed (**Figures 1B,C**). Pelvic bones showed sclerosis, especially in the iliac bodies (**Figure 1D**). Calcium replacement (50 mg/kg/day) and maintenance dose vitamin D (400 U/day) treatments were started, and the calcium value was normalized within a week. After normalization of serum calcium level, the treatment was discontinued and biochemical parameters remained normal in the follow-up. After his clinical improvement at age 21 months, he was discharged to follow up in the outpatient clinic.

One month after the discharge, he was hospitalized to the pediatric intensive care unit of another hospital with complaints of fever, cough, vomiting, and weight loss. In the initial evaluation, lower respiratory tract infection and sepsis were considered and appropriate fluid and antibiotic therapy was initiated. When respiratory findings worsened and respiratory acidosis became evident, he was intubated and connected to a mechanical ventilator. Cranial magnetic resonance imaging revealed severe hydrocephalus and therefore a ventro-peritoneal shunt was inserted. Despite the treatments, his clinical condition deteriorated and he died after 4 months of follow-up in the pediatric intensive care unit at age 26 months.

Targeted Sequencing

After written informed consents, blood samples were obtained from the patient, parents, and brothers. Genomic DNA was extracted from leukocytes using the MagPurix kit (Zinexts Life Science Corp., New Taipei City 235, Taiwan), according to manufacturer's instructions. For the molecular genetic evaluation, a Custom Target Capture-based Osteopetrosis gene panel (Celemix Inc., Seoul, Korea), which was designed according to the before-2018 ENMC classification was used.

PCR and Sanger Sequencing

The variant identified by the targeted sequencing was confirmed by Sanger sequencing. The region of genome including the mutations was amplified by PCR and sequenced both strands. Exon-specific Sanger sequencing was performed using 5′-GAGCTTGGGCACCACCTG-3′ and 5′-TCCGCTCCCCAAAACTCC-3′ primers on Applied Biosystems 3500 Genetic Analyzer. The sequences were evaluated by two different sequencing programs; i.e., CLC Genomics Workbench 3 sequencing program (Qiagen) and Chromas lite Software (Technelysium, South Brisbane QLD, Australia).

Variant Evaluation

The variant was evaluated by dbSNP (http://www.ncbi.nlm.nih.gov/projects/SNP/), 1000 genomes (http://www.1000genomes.org/), ExAC (http://exac.broadinstitute.org/), gnomAD (http://gnomad.broadinstitute.org/), ESP6500 (http://evs.gs.washington.edu/EVS/), Human Gene Mutation Database (HGMD; http://portal.biobase-international.com/hgmd/pro/start.php), and Mutation Taster (http://mutationtaster.org).

RESULTS AND DISCUSSION

By the target sequence, a novel homozygous frameshift variant (NM_003839.3: c.19_31del; p.Arg7CysfsTer172) in *TNFRSF11A* was detected. The variant was confirmed by Sanger sequencing (**Figure 2**). The parents were both heterozygous for the variant (**Figure 2**). This variant was interpreted as "Likely Pathogenic" according to American College of Medical Genetics criteria (ACGM) (Richards et al., 2015). This variant did not exist in any available databases including dbSNP, 1000 genomes, ExAC, gnomAD, ESP6500, and HGMD. According to an *in silico* analysis with Mutation Taster, this variant was predicted to affect signal peptide and protein structure, and causes NMD.

DOS and OPTB7 are inherited as autosomal recessive traits and are clinically very similar. However, they can be differentiated by the remarkable radiological features of DOS, including platyspondyly and enlarged lower metaphyseal parts of tubular bones with punctate densities and radiolucency (Spranger et al., 1968; Houston et al., 1978; Elçioglu et al., 2002; Whyte et al., 2010; Guo et al., 2018). OPTB7 is caused by loss-of-function mutations of *TNFRSF11A*, which are missense mutations or deleterious mutations leading to NMD (Guerrini et al., 2008; Pangrazio et al., 2012; Xue et al., 2021b). *TNFRSF11A*-associated DOS is caused by splice-site or frameshift mutations which are capable of producing concurrent truncated or long RANK proteins (**Table 1**). Five *TNFRSF11A* isoforms encoding five different proteins have been identified (**Figure 3**). It has been speculated that the clinical difference of DOS and OPTB7 may relate to the different effects of *TNFRSF11A* mutations in different *TNFRSF11A* isoform transcripts (Guo et al., 2018). The variants identified in the first three reported cases of *TNFRSF11A*-associated DOS cause NMD in some transcript isoforms, while simultaneously producing truncated or elongated RANK proteins in the remaining transcript isoforms according to the results of RT-PCR for the patient-derived cells and the exon trapping assay for cell lines (Guo et al., 2018; Xue et al., 2019; Xue et al., 2020). The functions of these truncated or elongated RANK proteins remain unclear. In a mutant mouse model with a nine-amino-acid insertion in *Tnfrsf11a*, the homozygotes develop osteopetrosis while the heterozygotes show osteolytic lesions. The abnormal RANK proteins in the mutant mice accumulated in Golgi apparatus and increased osteoclastogenesis by activating the unfolded protein response (Alonso et al., 2021). The findings suggest that the truncated or elongated RANK proteins generated in the first three cases of *TNFRSF11A*-associated DOS probably results in gain-of-function, which would be associated with the DOS phenotype.

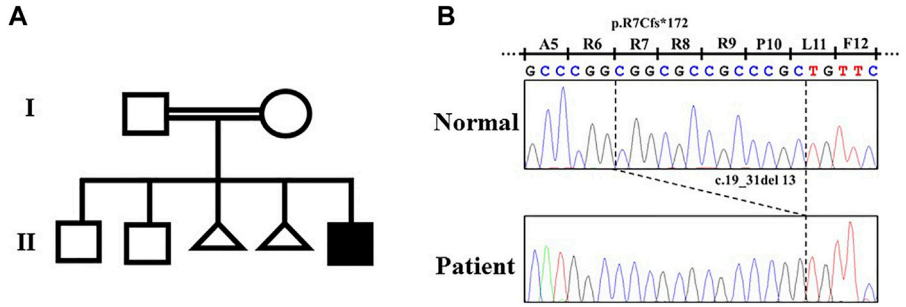

FIGURE 2 | Pedigree of the family with dysosteosclerosis and the *TNFRSF11A* variant. **(A)** Pedigree. **(B)** Electropherograms of the Sanger sequence analysis.

TABLE 1 | Clinical and radiographic findings of *TNFRSF11A*-associated dysosteosclerosis.

	Case				
	1[sta]	2[ndb]	3[rdc]	4[thd]	5[the]
Mutation[f]					
Allele 1 (mutant protein)	c.616+3A > G (p.N174Kfs*31)	c.784G > T (p.E262_Q279del)	c.1664del (p.S555Cfs*12)	c.385C > T (p.R129C)	c.19_31del (none)
Allele 2 (mutant protein)	c.616+3A > G (p.N174Kfs*31)	c.784G > T (p.E262_Q279del)	c.414_427 + 7del (none)	c.385C > T (p.R129C)	c.19_31del (none)
Clinical data					
Age at onset	3 years	17 years	8 months	13 months	19 months
Height [cm]	150 (–1.98 SD)	159.8 (–1.90 SD)	81 (–3.7 SD)	115 (–7.35 SD)	70.5 (–3.1 SD)
Cranial nerve palsy	–	–	+	+	+
Hydrocephaly	–	–	–	+	+
Hepatosplenomegaly	–	–	–	+	–
Hypogammaglobinemia	–	–	–	–	–
Mandibular or maxillary osteomyelitis	–	+	–	+	–
Anemia	–	+	NA	+	–
Thrombocytopenia	–	NA	NA	+	–
Extramedullary hematopoiesis	–	–	–	+	–
Indication for HSCT	–	–	+	–	–
Radiographic data					
Platyspondyly	+	+ mild	+ mild	+	+ mild
Concaved vertebrae at posterior thirds	+	+	-	-	-
Radiolucency of widened submetaphyseal portions of the tubular bones	+	+	+	+	+

HSCT, hematopoietic stem cell transplantation; NA, not available.
[a]*Guo et al. J Hum Genet 2018.*
[b]*Xue et al. J Bone Miner Res 2019.*
[c]*Xue et al. J Hum Genet 2020.*
[d]*Xue et al. J Hum Genet 2021.*
[e]*This study.*
[f]*Mutations are named according to NM_003839.3; The longest mutant proteins among the isoforms are listed.*

However, in the fourth case, a single amino acid substitution in *TNFRSF11A* was identified, suggesting that phenotype-genotype association is not easily predictable in *TNFRSF11A*-related bone diseases (**Table 1**) (Xue et al., 2021a).

The variant we identified in this study leads to frameshift and premature termination in exon 6 (**Figure 3**), thus being predicted to be a null mutation due to NMD. Contrary to the previous hypothesis, the clinical findings of our patient were quite compatible with DOS, while the variant causes NMD in all transcript isoforms (**Figure 3**). These conflicting findings suggest that the relationship between genotype and phenotype in *TNFRSF11A*-associated DOS cases is complicated and further studies are needed. It would also be interesting to explore the similar issue further for *TCRIG1* (Howaldt et al., 2019).

Our study reports the first case of DOS caused by *TNFRSF11A* null mutations, which are previously considered to cause OPTB7. We re-evaluated the

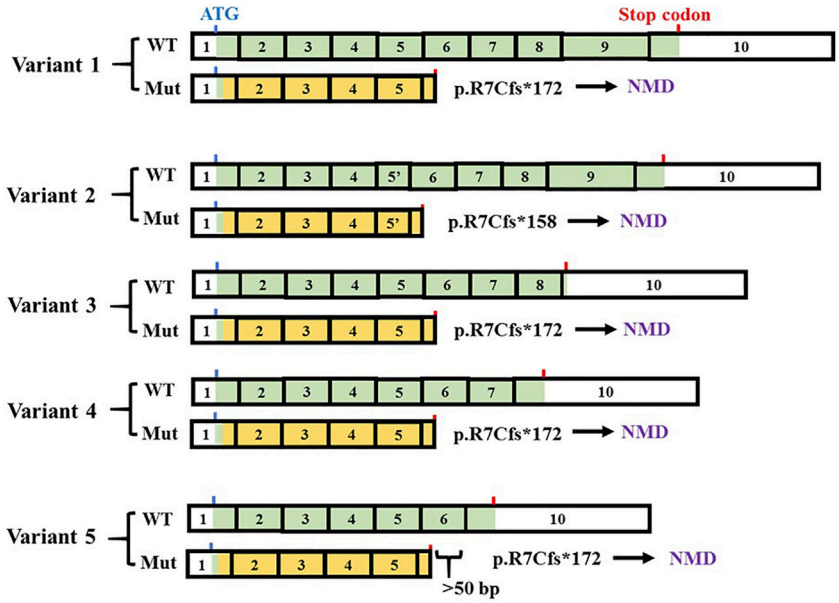

FIGURE 3 | TNFRSF11A isoforms and the effect of the variant (c.19_31del). Five variant transcripts are in NCBI database (variant 1: NM_003839.3; variant 2: NM_001278268.1, variant 3: NM_001270949.1, variant 4: NM_001270950.1, variant 5: NM_001270951.1). The exons are numbered based on the longest variant (variant 1). The changed parts of coding sequence are labeled in orange. The positions of the first ATG and the stop codons were indicated by blue and red bars, respectively. c.19_31del produces no transcripts due to nonsense mutation-mediated mRNA decay (NMD).

TABLE 2 | Patients with null mutations of *TNFRSF11A*.

Reference	Patient	Mutation		Position of New stop codon[b]	Isoform[c]					X-ray
		Nucleotide[a]	Type		1	2	3	4	5	
Guerrini et al.	P1	Allele 1 = 2: c.838G > T	Nonsense	exon 9	–	–	WT	WT	WT	NA
Am J Hum Genet 2008	P2	Allele 1 = 2: c.1301G > A	Nonsense	exon 9	–	–	WT	WT	WT	NA
Pangrazio et al. J Bone Miner Res 2012	P3	Allele 1: c.247G > T	Nonsense	exon 3	–	–	–	–	–	NA
		Allele 2: c.372C > A	Nonsense	exon 4	–	–	–	–	–	
	P4	Allele 1 = 2: c.328dupC	Frame-shift	exon 4	–	–	–	–	–	NA
Xu et al. BMC Surg 2021	P5	Allele 1 = 2: c.1196C > G	Nonsense	exon 9	–	–	WT	WT	WT	A
Silveira et al. Am J Med Genet C 2021	P6	Allele 1 = 2: c.1371_1372delTG	Nonsense	exon 9	–	–	WT	WT	WT	NA
This study	P7	Allele 1 = 2: c.19_31del	Frame-shift	exon 6	–	–	–	–	–	A

[a]*Mutations are named according to NM_003839.3; the longest transcript corresponding to isoform 1.*
[b]*Exon 10 is the last exon (NM_003839.3).*
[c]*indicates that no isoform is expected to be produced due to the nonsense mutation mediated RNA decay.*
WT, wild type; NA, not publicly available; A, publicly available.

phenotypes of the OPTB7 patients with null mutations. Until now, six patients carrying seven mutations causing NMD in all or some of the transcripts have been reported (**Table 2**) (Guerrini et al., 2008; Pangrazio et al., 2012; Silveira et al., 2021; Xu et al., 2021). Their radiographic data critical to differentiate DOS are not publicly available, except for a case reported by (Xu et al., 2021). Its skeletal phenotype is more compatible with the diagnosis of DOS rather than OP, since the platyspondyly with concaved vertebrae at posterior thirds and the radiolucency of widened sub-metaphyseal portions of the tubular bones are evident (Xu et al., 2021). Based on the findings on the case and our case, it could be hypothesized that the deficient *TNFRSF11A* functions causes a broad phenotypic spectrum covering DOS and OP. The remaining RANK function of the *TNFRSF11A* mutations may be an important factor that decides the radiographic features of the patients.

The previous four cases of TNFRSF11A-associated DOS show that the skeletal phenotypes are heterogeneous even if all cases meet the criteria of DOS. Generally, the young cases (Case 3 and 4) had a clear radiolucent band in the sub-metaphyseal region of tubular bones, which was widely splayed and sclerotic (Xue et al., 2020; Xue et al., 2021a). In contrast, the radiolucency in the enlarged lower metaphyseal parts was diffuse in the older cases (Case 1 and 2) (Guo et al., 2018; Xue et al., 2019). Moreover, although platyspondyly were

found in all cases, concaved vertebrae at posterior thirds were present only in the older cases (**Table 1**) (Guo et al., 2018; Xue et al., 2019). In this study, our patient at age 19 months showed similarities to the previous young cases in both spinal and sub-metaphyseal changes (**Figures 1C,E**; **Table 1**). These results suggest the phenotypes of *TNFRSF11A*-associated DOS considerably evolve with age and form a continuous phenotypic spectrum. Long-term observation would contribute to the understanding of the evolving phenotypes.

In conclusion, our findings indicate that we are still far from establishing a genotype-phenotype relationship in *TNFRSF11A*-associated OPTB7 and DOS. Detailed and continuous evaluation on the radiographic data remains necessary to elucidate the phenotypic spectrum caused by *TNFRSF11A* mutations.

DATA AVAILABILITY STATEMENT

The datasets presented in this article are not readily available because study participants did not give full consent for releasing individual genomic data publicly. Requests to access the datasets should be directed to the corresponding authors.

ETHICS STATEMENT

The studies involving human participants were reviewed and approved by the Ethical Committee of RIKEN. Written informed consent to participate in this study was provided by the participants' legal guardian/next of kin.

AUTHOR CONTRIBUTIONS

The study was designed by SA and LG. The draft was written by TK, SI, and LG. The patient samples and the clinical information were collected and summarized by BO, FH, SA, ON, BO, MK, and SI. The experiments were performed by TK, SG, and BO. The data were analyzed by SA, SI, and LG. All authors revised the manuscript and approved the final version.

FUNDING

This study is supported by the grants from the Japan Society for the Promotion of Science (SI, No. 18H02932 and 22H03207), the Japan Agency For Medical Research and Development (SI, No. 20bm0804006h0 and 20ek0109486h), the Japanese Society for Bone and Mineral Research (LG, the JSBMR Rising Stars Grant), and the Suzuken Memorial Foundation (LG).

ACKNOWLEDGMENTS

We would like to thank the patient and the family for participating in this study.

REFERENCES

Alonso, N., Wani, S., Rose, L., Van't Hof, R. J., Ralston, S. H., and Albagha, O. M. E. (2021). Insertion Mutation in Tnfrsf11a Causes a Paget's Disease-like Phenotype in Heterozygous Mice and Osteopetrosis in Homozygous Mice. *J Bone & Mineral Res* 36, 1376–1386. doi:10.1002/jbmr.4288

Campeau, P. M., Lu, J. T., Sule, G., Jiang, M.-M., Bae, Y., Madan, S., et al. (2012). Whole-exome Sequencing Identifies Mutations in the Nucleoside Transporter Gene SLC29A3 in Dysosteosclerosis, a Form of Osteopetrosis. *Hum. Mol. Genet.* 21, 4904–4909. doi:10.1093/hmg/dds326

Elçioglu, N. H., Vellodi, A., and Hall, C. M. (2002). Dysosteosclerosis: a Report of Three New Cases and Evolution of the Radiological Findings. *J. Med. Genet.* 39, 603–607. doi:10.1136/jmg.39.8.603

Frattini, A., Orchard, P. J., Sobacchi, C., Giliani, S., Abinun, M., Mattsson, J. P., et al. (2000). Defects in TCIRG1 Subunit of the Vacuolar Proton Pump Are Responsible for a Subset of Human Autosomal Recessive Osteopetrosis. *Nat. Genet.* 25, 343–346. doi:10.1038/77131

Guerrini, M. M., Sobacchi, C., Cassani, B., Abinun, M., Kilic, S. S., Pangrazio, A., et al. (2008). Human Osteoclast-Poor Osteopetrosis with Hypogammaglobulinemia Due to TNFRSF11A (RANK) Mutations. *Am. J. Hum. Genet.* 83, 64–76. doi:10.1016/j.ajhg.2008.06.015

Guo, L., Bertola, D. R., Takanohashi, A., Saito, A., Segawa, Y., Yokota, T., et al. (2019). Bi-Allelic CSF1R Mutations Cause Skeletal Dysplasia of Dysosteosclerosis-Pyle Disease Spectrum and Degenerative Encephalopathy with Brain Malformation. *Am. J. Hum. Genet.* 104, 925–935. doi:10.1016/j.ajhg.2019.03.004

Guo, L., Elcioglu, N. H., Karalar, O. K., Topkar, M. O., Wang, Z., Sakamoto, Y., et al. (2018). Dysosteosclerosis Is Also Caused by TNFRSF11A Mutation. *J. Hum. Genet.* 63, 769–774. doi:10.1038/s10038-018-0447-6

Houston, C., Gerrard, J., and Ives, E. (1978). Dysosteosclerosis. *Am. J. Roentgenol.* 130, 988–991. doi:10.2214/ajr.130.5.988

Howaldt, A., Nampoothiri, S., Quell, L.-M., Ozden, A., Fischer-Zirnsak, B., Collet, C., et al. (2019). Sclerosing Bone Dysplasias with Hallmarks of Dysosteosclerosis in Four Patients Carrying Mutations in SLC29A3 and TCIRG1. *Bone* 120, 495–503. doi:10.1016/j.bone.2018.12.002

Pangrazio, A., Cassani, B., Guerrini, M. M., Crockett, J. C., Marrella, V., Zammataro, L., et al. (2012). RANK-dependent Autosomal Recessive Osteopetrosis: Characterization of Five New Cases with Novel Mutations. *J. Bone Min. Res.* 27, 342–351. doi:10.1002/jbmr.559

Richards, S., Aziz, N., Bale, S., Bick, D., Das, S., Gastier-Foster, J., et al. (2015). Standards and Guidelines for the Interpretation of Sequence Variants: a Joint Consensus Recommendation of the American College of Medical Genetics and Genomics and the Association for Molecular Pathology. *Genet. Med.* 17, 405–424. doi:10.1038/gim.2015.30

Silveira, K. C., Kanazawa, T. Y., Silveira, C., Lacarrubba-Flores, M. D. J., Carvalho, B. S., and Cavalcanti, D. P. (2021). Molecular Diagnosis in a Cohort of 114 Patients with Rare Skeletal Dysplasias. *Am. J. Med. Genet.* 187, 396–408. doi:10.1002/ajmg.c.31937

Spranger, J., Albrecht, C., Rohwedder, H.-J., and Wiedemann, H.-R. (1968). Die Dysosteosklerose - eine Sonderform der generalisierten Osteosklerose. *Fortschr Röntgenstr* 109, 504–512. doi:10.1055/s-0029-1228480

Uludağ Alkaya, D., Akpınar, E., Bilguvar, K., and Tüysüz, B. (2021). Resolution of Sclerotic Lesions of Dysosteosclerosis Due to Biallelic SLC29A3 Variant in a Turkish Girl. *Am. J. Med. Genet. A* 185, 2271–2277. doi:10.1002/ajmg.a.62198

Whyte, M. P., Wenkert, D., McAlister, W. H., Novack, D. V., Nenninger, A. R., Zhang, X., et al. (2010). Dysosteosclerosis Presents as an "Osteoclast-Poor" Form of Osteopetrosis: Comprehensive Investigation of a 3-Year-Old Girl and Literature Review. *J. Bone Min. Res.* 25, 2527–2539. doi:10.1002/jbmr.131

Xu, Y., Yu, X., and Huang, M. (2021). A Novel Mutation in TNFRSF11A Gene Causes Pediatric Osteopetrosis: Case Report. *BMC Surg.* 21, 269. doi:10.1186/s12893-021-01266-4

Xue, J.-Y., Ikegawa, S., and Guo, L. (2021). Genetic Disorders Associated with the RANKL/OPG/RANK Pathway. *J. Bone Min. Metab.* 39, 45–53. doi:10.1007/s00774-020-01148-4

Xue, J.-Y., Simsek-Kiper, P. O., Utine, G. E., Yan, L., Wang, Z., Taskiran, E. Z., et al. (2021). Expanding the Phenotypic Spectrum of TNFRSF11A-Associated Dysosteosclerosis: a Case with Intracranial Extramedullary Hematopoiesis. *J. Hum. Genet.* 66, 607–611. doi:10.1038/s10038-020-00891-w

Xue, J. Y., Wang, Z., Smithson, S. F., Burren, C. P., Matsumoto, N., Nishimura, G., et al. (2020). The Third Case of TNFRSF11A-Associated Dysosteosclerosis with a Mutation Producing Elongating Proteins. *J. Hum. Genet.* 9, 1–7. doi:10.1038/s10038-020-00831-8

Xue, J. y., Wang, Z., Shinagawa, S., Ohashi, H., Otomo, N., Elcioglu, N. H., et al. (2019). TNFRSF11A -Associated Dysosteosclerosis: A Report of the Second Case and Characterization of the Phenotypic Spectrum. *J. Bone Min. Res.* 34, 1873–1879. doi:10.1002/jbmr.3805

Conflict of Interest: The authors declare that the research was conducted in the absence of any commercial or financial relationships that could be construed as a potential conflict of interest.

Publisher's Note: All claims expressed in this article are solely those of the authors and do not necessarily represent those of their affiliated organizations, or those of the publisher, the editors and the reviewers. Any product that may be evaluated in this article, or claim that may be made by its manufacturer, is not guaranteed or endorsed by the publisher.

frontiers | Frontiers in Pediatrics

ORIGINAL RESEARCH
published: 14 July 2022
doi: 10.3389/fped.2022.888923

FGD1 Variant Associated With Aarskog–Scott Syndrome

Yilin Zhu[1†], Qingqing Chen[1†], Haiyan Lin[2], Huifei Lu[1], Yangbin Qu[1], Qingfeng Yan[1,3,4] and Chunlin Wang[1]*

[1] Department of Pediatrics, The First Affiliated Hospital, College of Medicine, Zhejiang University, Hangzhou, China, [2] Department of Pediatrics, The First People's Hospital of Wenling, Taizhou, China, [3] College of Life Sciences, Zhejiang University, Hangzhou, China, [4] Key Laboratory for Cell and Gene Engineering of Zhejiang Province, Hangzhou, China

Background: Aarskog–Scott syndrome, a rare X-linked genetic disorder, is identified by combined clinical manifestations of short stature, facial, skeletal, and genital anomalies. Annually, two or three new cases are diagnosed with Aarskog–Scott syndrome, which is associated with *FGD1* variants. However, there is no specific treatment for Aarskog–Scott syndrome due to its unclear mechanism.

Methods: Clinical data were collected when the patient first visited the hospital. Trio whole-exome sequencing and Sanger sequencing were performed for the genetic cause of disease. To evaluate the pathogenicity of the variants *in vitro*, stable cell lines were constructed using lentivirus infection in 143B cell. Furthermore, Western blot was used to verify the expression of signaling pathway-related proteins, and the transcription levels of osteogenic-related genes were verified by luciferase reporter gene assay.

Results: A 7-year-old boy was manifested with facial abnormalities, intellectual disability, and short stature (−3.98 SDS) while the growth hormone level of stimulation test was normal. Trio whole-exome sequencing and Sanger sequencing identified a variant (c.1270A>G, p.Asn424Asp) in *FGD1* gene. The Asn424 residue was highly conserved and the hydrogen bond in the FGD1 variant protein has changed, which led to decrease in the interaction with CDC42 protein. *In vitro* study showed that the Asn424Asp variant significantly decreased the transcription levels of *OCN, COL1A1,* and ALP *activity*, and it activated the phosphorylation of JNK1.

Conclusion: Molecular biological mechanisms between abnormal expression of *FGD1*and Aarskog–Scott syndrome remain poorly understood. In our study, c.1270A>G variant of *FGD1* resulted in Aarskog–Scott syndrome, and the analysis of pathogenicity supports the deleterious effect of the variant. Furthermore, we demonstrated the weakened affinity of the mutant FGD1 and CDC42. Decreased expression of osteogenic-related gene and abnormal activation of JNK1 were also shown in this work.

Keywords: *FGD1*, short stature, Aarskog-Scott syndrome, CDC42, JNK1

OPEN ACCESS

Edited by:
Long Guo,
RIKEN Center for Integrative Medical Sciences, Japan

Reviewed by:
Reza Jabal,
Albert Einstein College of Medicine, United States
Claudia Gonzaga-Jauregui,
Universidad Nacional Autónoma de México, Mexico

***Correspondence:**
Chunlin Wang
hzwangcl@zju.edu.cn

†These authors share first authorship

Specialty section:
This article was submitted to Genetics of Common and Rare Diseases, a section of the journal Frontiers in Pediatrics

Received: *03 March 2022*
Accepted: *31 May 2022*
Published: *14 July 2022*

Citation:
Zhu Y, Chen Q, Lin H, Lu H, Qu Y, Yan Q and Wang C (2022) FGD1 Variant Associated With Aarskog–Scott Syndrome. Front. Pediatr. 10:888923. doi: 10.3389/fped.2022.888923

INTRODUCTION

Aarskog–Scott syndrome (AAS, OMIM 305400), also termed as faciogenital dysplasia, is a male-predominant X-linked developmental disorder. It is rare, having a population prevalence of 1/25,000 or less (1). Children with AAS have heterogeneous clinical manifestations. Short stature, craniofacial, genital, and skeletal anomalies are the classically

characteristic combination (2). With respect to short stature, the most common symptom in the disease; it is disproportionate, with an increased upper-to-lower segment ratio and shortened distal extremities (3, 4). Abnormalities emerge when children with this condition are 2–4 years old, with a delayed peak of pubertal growth spurt (5). There are individual differences in the growth hormone (GH) treatment for AAS due to the normal level of GH. However, previous studies have shown that GH therapy can promote growth in children with AAS (3). Therefore, the study of pathogenic mechanisms is desirable and would be expected to help in the formulation of more effective treatment regimes. So far, only one causal gene, *FGD1,* has been identified, but the relationship between aberrant expression of *FGD1* and AAS remains unclear.

The *FGD1* gene (faciogenital dysplasia 1, OMIM 300546), located at Xp11.21, encodes the RhoGEF and PH domain-containing protein 1 (6). The FGD1 protein is made up of a proline-rich region, Dbl homology (DH), and pleckstrin homology (PH) domains, a FYVE-finger domain, and a second PH domain (PH2) from the N-terminus to the C-terminus (7). As a member of the guanine nucleotide exchange factor family, the FGD1 protein specifically binds to cell division cycle 42 (CDC42), a member of the Ras homology (Rho) family of GTPase protein (8, 9). The binding of CDC42 to the DH domain of FGD1 catalyzes the exchange from GDP-bound (inactive) to GTP-bound (active) forms, which leads to the activation of the downstream signal pathway (10, 11). FGD1/CDC42 has been reported to be involved in numerous signaling pathways, including the actin cytoskeleton organization, cell polarization, vesicular trafficking, cell cycle progression, and gene expression (12–14). Furthermore, current research suggests that FGD1 may be a critical regulator of events modulating extracellular matrix, which is already known as an important factor in skeletal formation (15, 16).

In this report, detailed clinical and molecular genetic analysis using whole-exome sequencing (WES) technology was performed on a Chinese child with AAS. Gene sequencing revealed a variant in the *FGD1* gene c.1270A>G (p. Asn424Asp). Coincidentally, a boy, also diagnosed with AAS, has the same mutation site and has been previously reported in a case report (17). To verify the pathogenicity of the variant, we performed a series of experiments *in vitro*.

MATERIALS AND METHODS

Subjects

The study was authorized by the Ethics Committee of The First Affiliated Hospital, Zhejiang University, China, which followed the Declaration of Helsinki principles. Written and informed consent was obtained from the proband's parents for publication of this case.

Clinical Evaluation

A detailed clinical evaluation was collected at the time of diagnosis, including medical history and clinical presentations. Physical examination, laboratory and radiological imaging tests were recorded, as well as magnetic resonance imaging (MRI).

Cytogenetic and Molecular Studies

Whole-exome sequencing of a proband–parent trio was used to search for the causative gene. The genomic DNA of the proband and his family members was isolated from peripheral blood samples using a TaKaRa blood genome DNA extraction kit (TaKaRa, USA). A total amount of 3 μg DNA was used for exome capture with the SureSelect Human All Exon V6 kit (Agilent Technologies), and then the prepared target libraries were sequenced on Illumina HiSeq X Ten (Illumina, San Diego, CA, USA) at an average depth of 100×, according to the instructions of the manufacturer. Whereafter, the results of Sanger sequencing were analyzed using Chromas Lite v2.01 (Technelysium Pty Ltd, Tewantin, QLD, Australia). The description of the Sanger sequencing variant detected in the *FGD1* gene was made on the basis of the NCBI entry NG_008054.1 (NM_004463.3). The description of the variant was conducted according to the Human Genome Variation Society sequence variant nomenclature (18).

Conservative and Pathogenicity Analysis of the Variant

The protein sequences of FGD1 in different vertebrate species were downloaded from the UniProt Knowledge Database (https://www.uniprot.org/). A multiple-sequence alignment was created using the ClustalX program (ftp://ftp-igbmc.u-strasbg.fr/pub/ClustalX/). Results from Sequence alignment were displayed online using ConSurf (http://consurf.tau.ac.il/) (19). The variant pathogenicity predictors were carried out by the webserver PREDICT-SNP (https://loschmidt.chemi.muni.cz/predictsnp1/) (20).

Variant Classification

The pathogenicity of the variant was classified according to the classification of the latest version of ACMG (American College of Medical Genetics and Genomics) (21). The findings were divided into five categories, namely, (1) pathogenic, (2) likely pathogenic, (3) uncertain significance, (4) likely benign, and (5) benign.

Homologous Modeling of Human FGD1

The 3D structure of the FGD1 protein globally was generated by Threading ASSEmbly Refinement (I-TASSER) (https://zhanglab.ccmb.med.umich.edu/I-TASSER/) (22) due to the lack of an existing experimental structure. The UniProt database was the source for attaining the amino acid sequence of wildtype human FGD1. Meanwhile, the local structural, stability, and flexibility analysis of mutant FGD1 was predicted by the online server Dynamut (http://biosig.unimelb.edu.au/dynamut/) (23). The structures of the protein were rendered in PyMOL 2.4 for analysis and illustration.

Lentivirus Infection

The full-length cDNA fragment of human *FGD1*, excluding the stop codon, was subcloned into a pCDH vector for expression. A 3×FLAG tag was added to the C-terminal of pCDH-*FGD1*. An In-Fusion HD Cloning kit (TakaRa, USA) was used to construct

the mutational pCDH-*FGD1*. Transfection was done using three plasmid systems, including packaging plasmid (psPAX2), envelope plasmid (pMDG2), and the pCDH plasmid containing *FGD1*-WT-cDNA or *FGD1*-mut-cDNA. The three plasmids were co-transfected at a ratio of 5:3:2 into HEK-293T cells, and the medium was collected after 48 h. Subsequently, the virus supernatant was added into 143B cells after being filtered. After 24 h, the stably transfected cells were selected with a suitable concentration of 6 μg/ml puromycin.

Dual-Luciferase Reporter Gene Assays

Analogously, the plasmids of pGL4-OCN-Luc and pGL4-COL1A1-Luc were constructed by ligating promoter sequences of *OCN* and *COL1A1* into the pGL4.48 vector (Promega, USA). Prior to transient transfection, 143B cells were plated into 24-well-plates at a confluency of 70–80%. The reconstructed reporter plasmids and helper plasmid pGL4.74 [hRluc/TK] (Promega, USA) were co-transfected at a ratio of 50:1 (a total of 500 ng DNA) by using Lipofectamine™ 3,000 transfection reagent (Thermo Fisher, USA). Culture medium was replaced with fresh medium 8 h later. The Dual-Glo® Luciferase Assay System (Promega, Cat# 2920) was performed 48 h after transfection.

Measurement of Protein Interaction in Cells

NanoLuc® Binary Technology (NanoBiT) (Promega, Cat# N2014), a novel technology that was used to analyze the interacted relation in proteins. It contains two complementary subunits, LgBiT (18 kDa) and SmBiT (3.6 kDa). *FGD1*-LgBiT-C (or *FGD1*-mut-LgBiT-C) and CDC42-SmBit-N were constructed, as well as the confluency of HEK-293T cells in 24-well reached at ∼70–80% before transfection. The transfected method was the same as above, except the ratio of DNA was 1:1. Then, 48 h after transfection, the luciferin was measured by a Multimode Plate Reader VICTOR Nivo (ND-1000, Thermo Fisher) after the addition of the diluted substrate.

Cell Culture

HEK-293T, 143B cell lines were cultured in 60 mm cell culture dish, which was added with 4 ml HG-DMEM (Gibco) supplemented with 10% fetal bovine serum. In addition, the CO_2 cell culture incubator was set to 37°C and 5% CO_2. The cells were passaged when cell confluence reached 90%.

Western Blotting

A total protein Extraction Kit (Abcam) was used to extract the proteins from cells according to instructions, and protein quantification was conducted by bicinchoninic acid assay. The supernatant was resolved on 10% SDS-PAGE and transferred from the gel to polyvinylidene difluoride later. The membranes were then incubated in TBS-5% skim milk for 1 h at room temperature. The first antibodies were incubated overnight at 4°C, and the secondary antibody was incubated for 2 h at room temperature. The primary antibodies included p-JNK1 (1:1,000, CST), GADPH (1:2,000, ABclonal), FGD1 (1:2,000, ABclonal), and T-JNK1 (1:1000, CST). The second antibodies, goat anti-mouse/rabbit IgG, were purchased from Abcam.

Alkaline Phosphatase (ALP) Activity Assay

The ALP activity of stable transfected cell lines which was cultured with osteogenic medium (Stemcell, Canada) was tested by an ALP activity assay (Beyotime, Shanghai, China). Cells in 24-well-plates were collected and no protease inhibitor cocktail lysis buffer was used for lysis. Then, 50 μl/well-Supernatant protein was fully mixed in the 96-well-plate with the substrate of 50 μl/well of *p*-nitrophenol. After incubation at 37°C for 30 min and adding 100 μl of stop solution, the absorbance of the mixture was detected at 405 nm (BioTek, USA).

Statistical Analysis

All the statistical analyses were performed by *t*-test (two-tailed, unpaired) in the GraphPad Prism 8 program. ImageJ was used to handle and process the Western blotting images. All the experiments were repeated at least three times independently. It was considered significant that the *p*-value was lower than 0.05 ($^{*}p < 0.05$, $^{**}p < 0.01$, $^{***}p < 0.001$).

RESULTS

Clinical Evaluation

The proband, a 7-year-old boy of healthy non-consanguineous parents, was referred to our hospital complaining of growth retardation for 6 years. He was born at full term by spontaneous vaginal delivery with a birth weight of 3.75 kg. His weight was 17.8 kg (−2.0 SDS) and height 105.7 cm (−3.98 SDS). The proband had short stature (HP:0004322), facial abnormalities, including triangular face (HP:0000325), long philtrum (HP:0000343), low-set ears (HP:0000369), and short nose (HP:0003196) (**Figure 1A**). Wechsler Intelligence Scale for Children Test revealed intellectual disability (HP:0001249) (IQ = 70). The peak-stimulated GH level of the stimulation tests was 13.57 ng/ml, and the bone age was about 3 years and 8 months (Greulich–Pyle method) (**Figure 1B**). Additionally, there were no abnormalities in the functions of the thyroid, liver, gonad, adrenal gland, blood glucose, or electrolytes. Further imaging examination (pituitary MRI and spinal X-ray) showed nothing unremarkable. Notably, his family members were all short: his father's height was 160 cm (−2.08 SDS), his mother's height was 150 cm (−1.96 SDS), his elder adult sister's height was 153 cm (−1.41 SDS), and his maternal grandfather's height was 150 cm (−3.72 SDS). However, they were physically healthy without intellectual disability and other malformations.

A Missense Mutation in *FGD1* Was Identified as the Causal Variant

The proband (III-2) (**Figure 1C**) had severe short stature, intellectual disability, and facial abnormalities, all of which suggested a genetic factor and necessitated genetic testing. To determine the proband's genetic etiology, trio-WES and Sanger sequencing were performed on the proband and his parents. Peripheral blood samples were collected and genomic DNA was extracted subsequently. The WES analysis of the patient revealed 35,224 variants in the exome region. Among these, a total of 33,250 (94.39%) single-nucleotide polymorphism (SNP) loci and 1,974 indel variations were identified. Next, 24,356 SNPs and

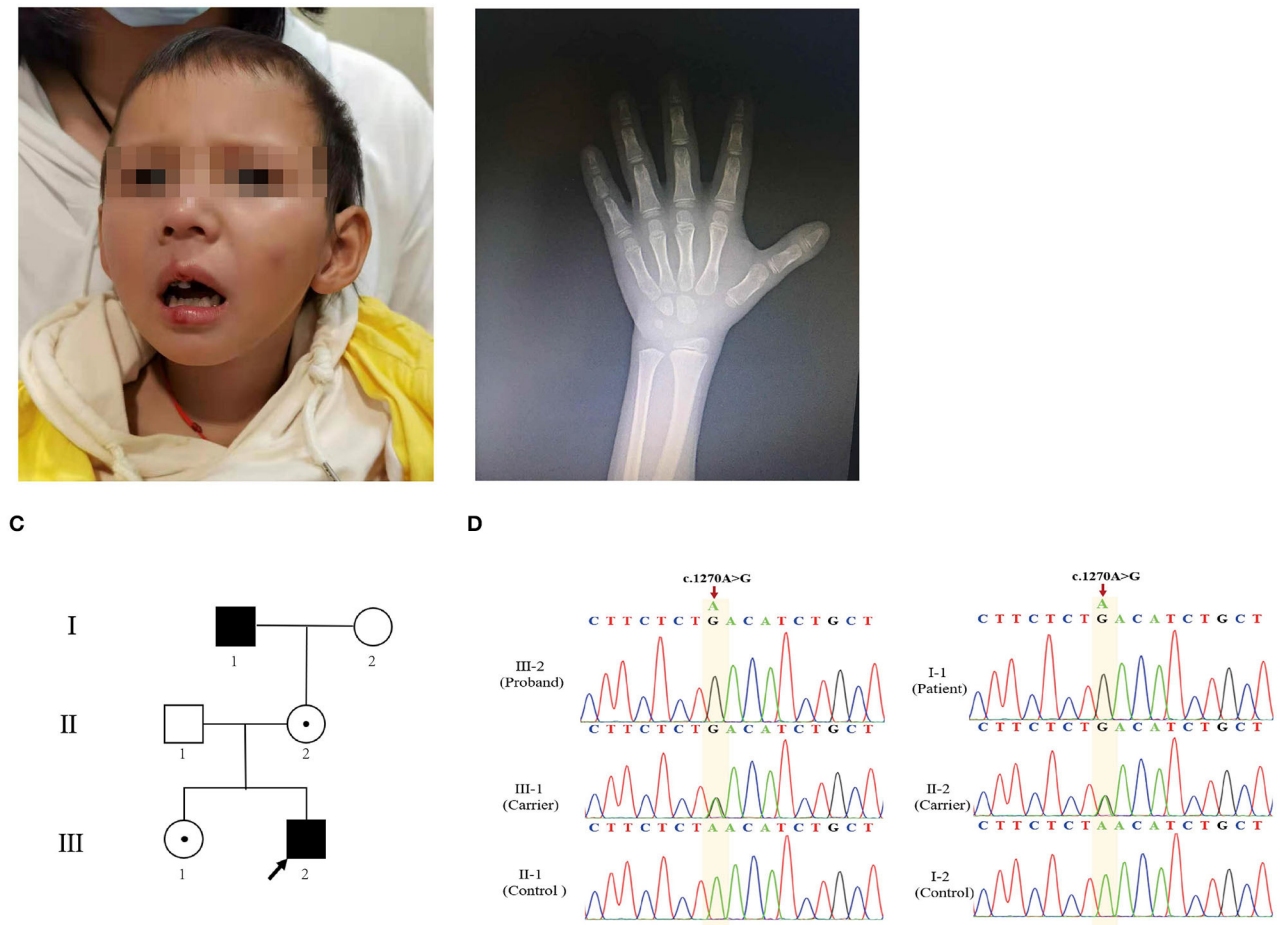

FIGURE 1 | Clinical characteristics of the proband. **(A)** Image of the proband. Facial abnormalities included triangular face, long philtrum, low-set ears, and short nose. **(B)** Hand X-ray of the patient. **(C)** The pedigree analysis and pedigree symbols. The squares and circles refer to males and females, respectively, and the arrow indicates the proband. A filled symbol represents a person affected with AAS, and the center of the black spot circle indicates carrier status. **(D)** Sanger sequencing chromatogram demonstrates mutation from affected individuals and heterozygous variant from unaffected family members.

1,010 InDels were screened out, which were potentially affecting coding sequences (i.e., non-synonymous, nonsense, or located in the canonical splice-site region). A total of 162 SNPs and 8 InDels were deleterious mutations according to the PROVEAN, SIFT, PolyPhen-2, MutationTaster, and protein structure prediction software. We then screened 22 SNPs and 3 InDels based on genetic patterns. Then, 11 corresponding SNPs were filtered out based on the minor allele frequency of SNPs when <0.01 was used to exclude common mutations based on the 1000G_ALL database (http://www.internationalgenome.org/) (**Supplementary Table S1**). Based on the clinical manifestation and heredity pattern, *FGD1* (chrX: 54,494,287 in GRCh37, c.1270A>G, p.Asn424Asp) was considered as the most relevant candidate gene for the proband (**Supplementary Figure S1A**). Because of the X-linked recessive inheritance pattern associated with the *FGD1* gene and the proband's maternal grandfather (I-1) having severe short stature, Sanger sequencing was used to confirm whether the proband's other family members carried the same mutation. The results indicated that the proband's variant came from his maternal grandfather (I-1). Both of them were hemizygous males. His mother (II-2) and sister (III-1) were both carriers (**Figure 1D**). This variant was classified as likely pathogenic according to the variant guidelines of the ACMG (PM1, PM2, PP1, PP3). Additionally, the mutation was predicted to be pathogenic by PredictSNP (score 0.65), PolyPhen-1 (score 0.67), PhD-SNP (score 0.86), SIFT (score 0.53), and SNAP (score 0.72) (**Supplementary Figure S1B**).

Sequence Conservation and Three-Dimensional Structure of FGD1

The mutation site of the FGD1 protein (p. Asn424Asp) was located in the DH domain (**Figure 2A**). To identify the importance of the position in the domain, we compared FGD1 protein sequences in 58 vertebrates. **Figure 2B** shows

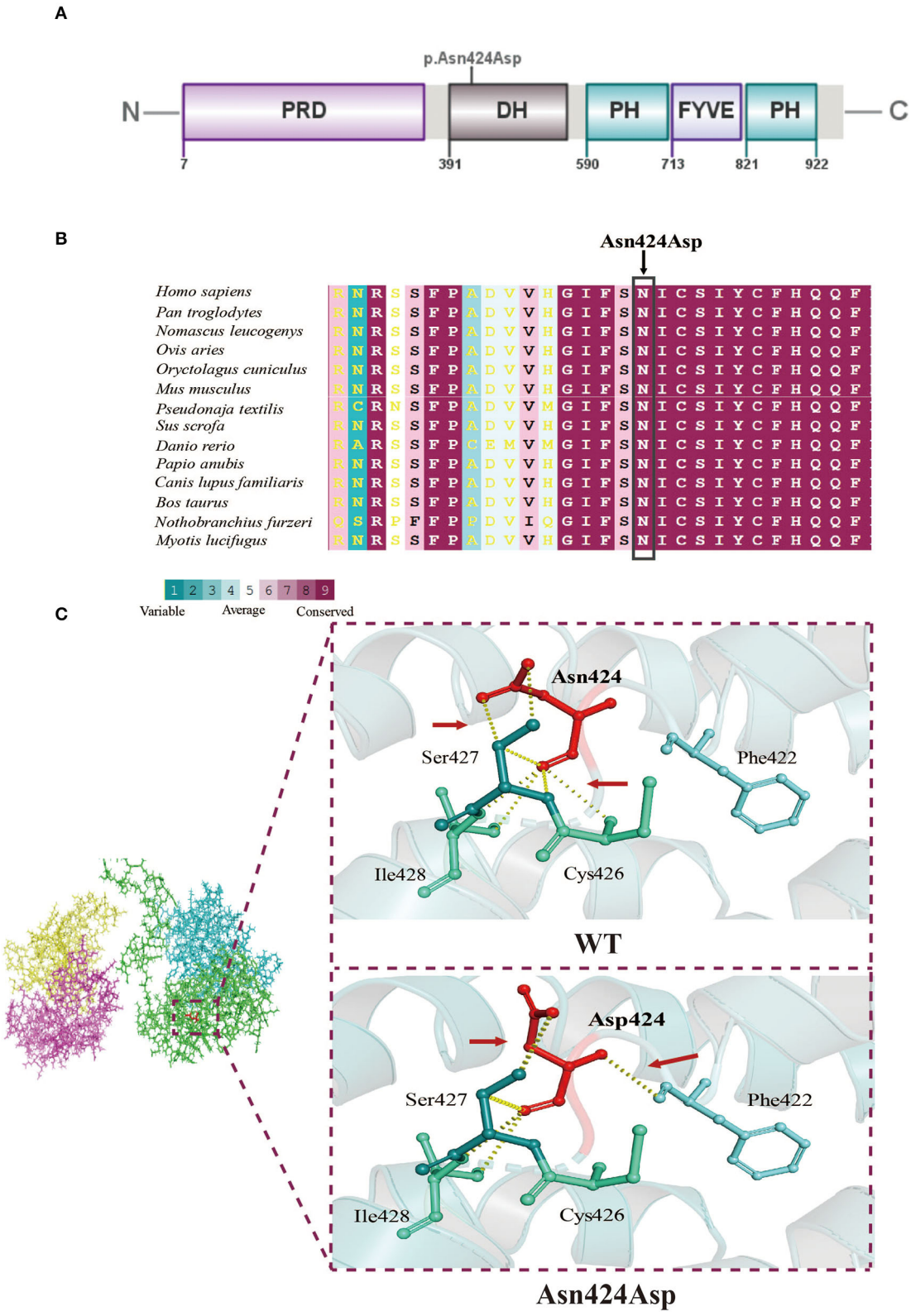

FIGURE 2 | Molecular analysis. **(A)** A schematic diagram showing the location of the mutation site. **(B)** Interspecific conservation analysis of the p.Asn424Asp mutation in FGD1, highlighted by the box. **(C)** Three-dimensional structure model of the local structural changes between wildtype and mutant FGD1 protein, as predicted by Dynamut. Red arrows represent the difference in hydrogen between the wildtype and mutant.

a comparison of FGD1 protein sequences in representative species, including *Homo sapiens, Pan troglodytes, Ovis aries, Oryctolagus cuniculus, Mus musculus, Pseudonaja textilis, Sus scrofa, Danio rerio, Papio anubis, Canis lupus familiaris, Bos taurus, Nothobranchius furzeri,* and *Myotis lucifugus*. The conservation of the variant position in FGD1 was conservatively scored using ConSurf, which indicated that the residues at site Asn424 of FGD1 were highly conserved through the represented vertebrates.

The biological function of a protein is determined by the secondary structure of the protein. Three-dimensional structural modeling of both normal and mutant FGD1 proteins in order to exhibit the consequences of the N424D mutation on the tertiary or quaternary structure of the FGD1 protein was done (**Figure 2C**). Typically, the oxygen atom and nitrogen atom of Asn (p.424) are held together with the nitrogen atom of Cys (p.426) and the carbon atom of Ser (p.427) by hydrogen bonds. The p.Asn424Asp variant would not only disrupt the hydrogen bonds but also build a new association with Phe (p.422), which resulted in structural changes inevitably.

FGD1^{N424D} Variant Upregulates p-JNK1

It is generally accepted that FGD1 is a highly specific CDC42 guanine exchange factor, and the binding domain is located in DH, similar to the mutational domain (24). To clarify the effect of the variant on combinative activity, we examined the mutant FGD1 protein-binding ability of CDC42 according to the schematic diagram (**Figure 3A**). This finding indicated that mutations in the *FGD1* gene led to a significant decrease in the binding capacity of CDC42 (**Figure 3B**). Activated-CDC42 activates multiple downstream signaling pathways by interacting with effector proteins. JNK1, which is downstream of CDC42, is known to be associated with bone development (25). To further determine the downstream pathways, the expression level of

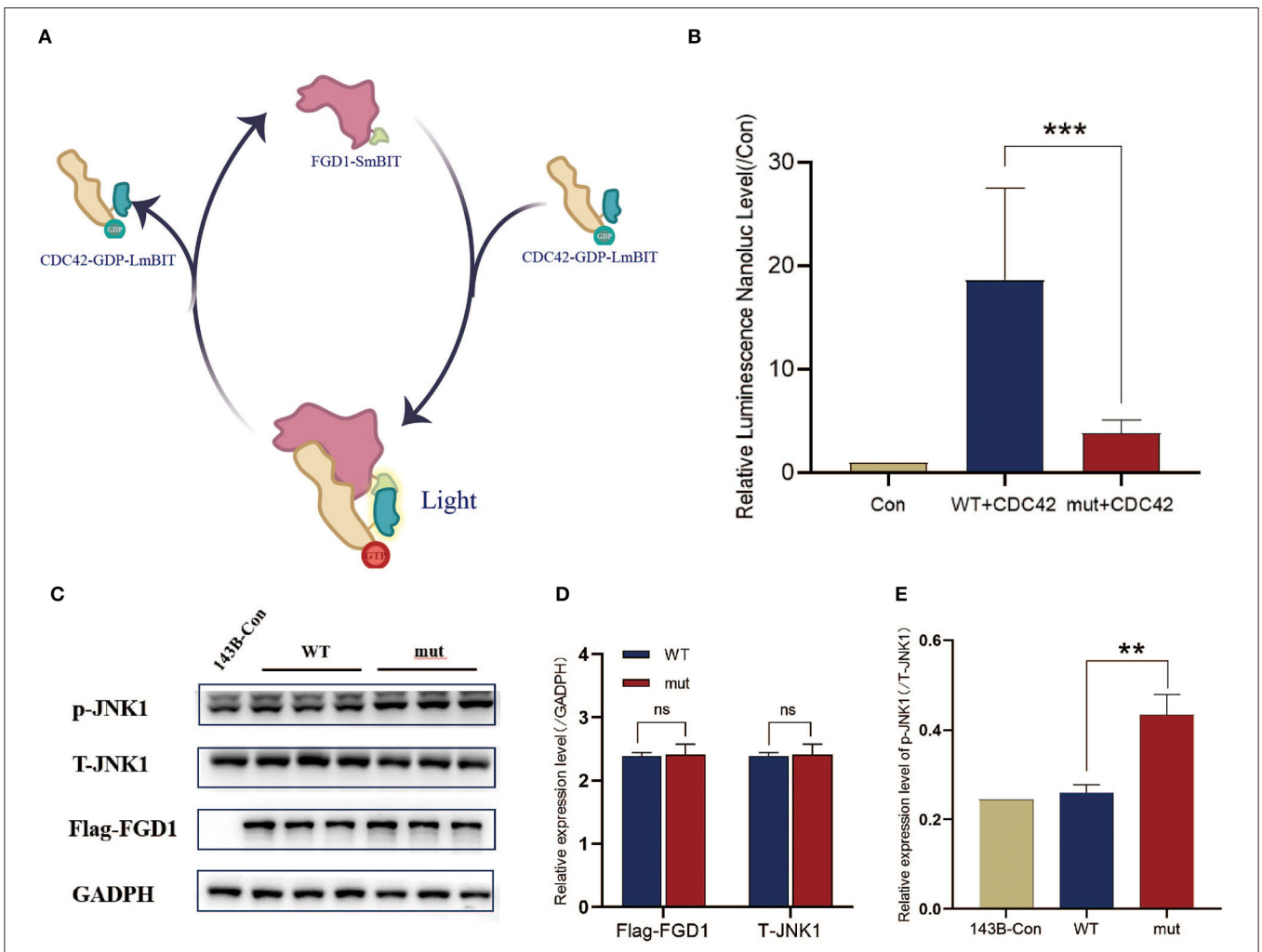

FIGURE 3 | The interaction of the variant of FGD1 and CDC42 has been decreased, which might be contributing to the increase of p-JNK1. **(A)** Schematic diagram of interaction between FGD1 protein and CDC42 protein by NanoLuc® Binary Technology. **(B)** To facilitate the comparison, luciferase values were normalized to Control values (100%), histogram and bar chart represent the relative value of FGD1-CDC42 binding capacity. **(C)** Western blotting analysis of Flag-FGD1, p-JNK1, and T-JNK1 in 143B cell lines. **(D,E)** Quantified analysis of Western blotting of Flag-FGD1, p-JNK1, and T-JNK1 in 143B cell lines. $^{**}p < 0.01$, and $^{***}p < 0.001$.

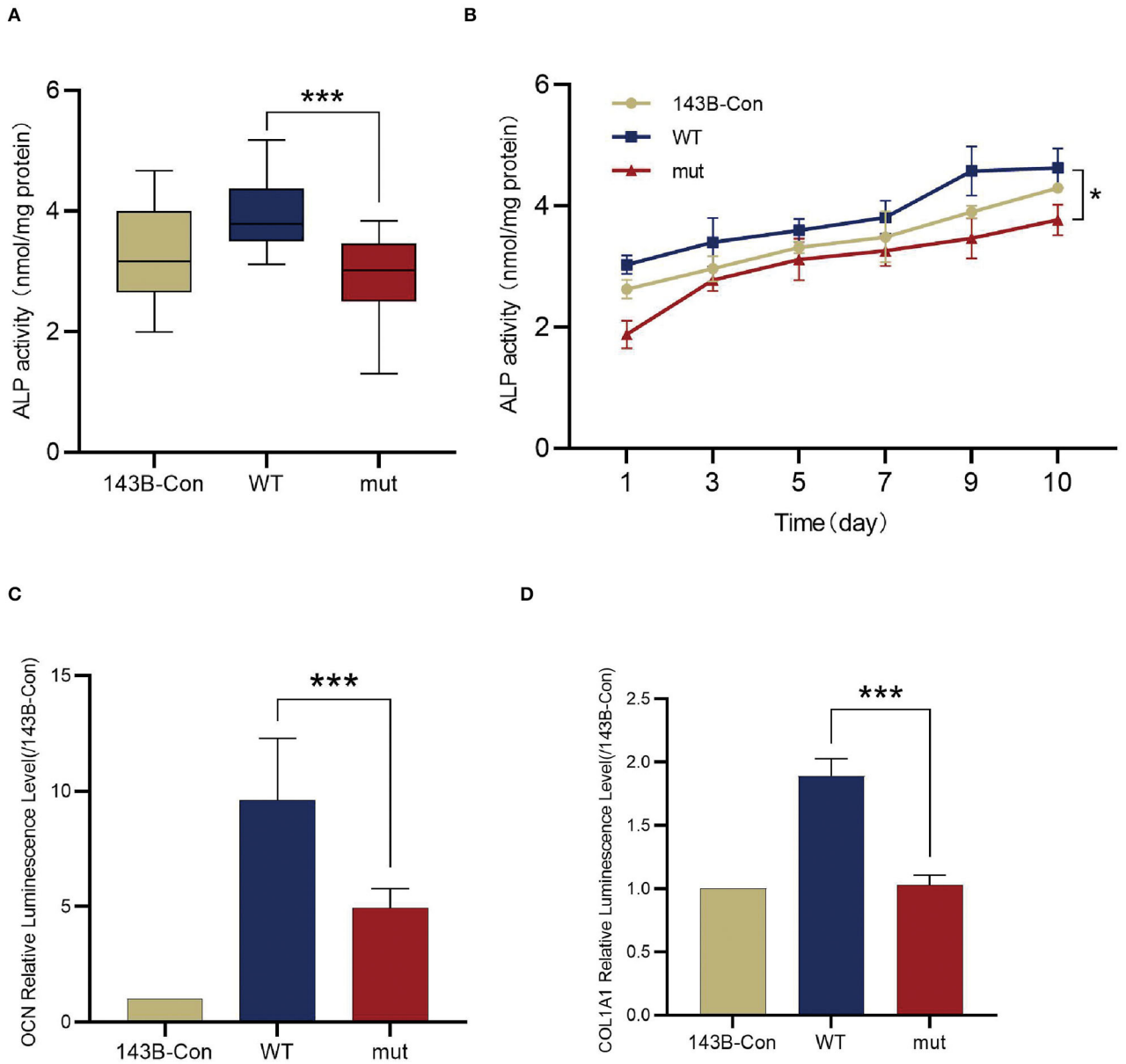

FIGURE 4 | Comparison of the osteogenic differentiations between wildtype 143B and mutant 143B. **(A)** ALP activity determined by ALP activity assay. **(B)** ALP activity was measured every other day for 10 days since stable cell lines cultured with osteogenic medium. **(C)** The transcription of *OCN* was evaluated by dual luciferase reporter gene assay. **(D)** The transcription of *COL1A1* were evaluated by dual luciferase reporter gene assay. ***$p < 0.001$.

JNK1 and phosphorylated JNK1(The 183/Tyr 185) was measured by Western blotting. The results showed a significantly higher level of phosphor-JNK1 in the FGD1 mutant group (1.109 ± 0.0614 vs. 0.8800 ± 0.02828, $t = 11.93$, $p < 0.01$), while the total cellular level of JNK1 remained the same in the wildtype and mutant groups (**Figures 3C–E**).

The *FGD1* Variant Inhibits the Activity of ALP and Downregulates *OCN* and *COL1A1*

To determine the influence of the *FGD1* variant in skeletal development, $FGD1^{wt}$ and $FGD1^{N424D}$ overexpression was performed in a human osteosarcoma cell line, 143B. For the osteogenic makers, the transcriptional level of *OCN*, *COL1A1*, and ALP activity was detected (**Figures 4A–D**). Cell lysates were used for ALP activity measurement by an ALP activity assay kit. We examined the ALP activity in 143B-WT and 143B-mut, and the result demonstrated that the mutant has an obvious decrease in ALP activity compared with the wildtype (2.887 ± 0.7146 vs. 3.947 ± 0.5884, $t = 6.564$, $p < 0.001$) (**Figure 4A**). For dynamic changes of ALP, test data were collected for 10 consecutive days since the cell lines cultured with osteogenic medium. The results showed the ALP activity of the groups rose

first, then gradually went steady, but the mutant group was below throughout (**Figure 4B**). In addition, the transcription level of *OCN* and *COL1A1* was analyzed by dual-luciferase reporter gene assays. *OCN* and *COL1A1* promoter luciferase plasmids were expressed in stable cell lines. Compared with the wildtype group in expression of *OCN*, the mutant group significantly decreased (4.937 ± 0.8401 vs. 9.616 ± 2.677, $t = 4.124$, $p < 0.001$). Corresponding to this, the level of *COL1A1* transcription was significantly lower in the *FGD1* mutation group compared with the wildtype group (1.027 ± 0.07944 vs. 1.892 ± 0.1351, $t = 11.03$, $p < 0.001$) (**Figures 4C,D**).

DISCUSSION

In this study, we described a 7-year-old boy with AAS in a Chinese family exhibiting severe short stature, facial abnormalities, and intellectual disability. WES and Sanger sequencing confirmed the disease-causing mutation in *FGD1* (c.1270A>G). As a consequence of a wide variety of clinical features, a clinical suspicion of AAS was reliant on fulfilling a few primary and secondary criteria according to Teebi presented in 1993 (26). The diversity of clinical manifestations means that AAS is still difficult to diagnose and requires differential diagnosis, such as Robinow syndrome, Noonan syndrome, and SHORT syndrome. Therefore, this highlights the importance of genetic testing. Among the appearance characteristics of the boy, short stature, short nose, and long philtrum matched primary criteria, low-set ears belonged to the additional, and only triangular face was slightly different from the common feature of round face (26–28). Compared with the typical clinical presentation of affected patients, the boy did not have genital hypoplasia (shawl scrotum) and skeletal anomalies (short/broad hands). Despite the boy meeting a few diagnostic criteria, AAS remained unclear. It can be hard to distinguish between other disorders according to these clinical manifestations alone (1). Based on the genetic testing report, clinical manifestations, and family history (maternal grandfather with severe short stature), the boy was diagnosed with AAS caused by the *FGD1* variant. Furthermore, stubby metacarpals, bilateral swollen testicles, and inguinal hernia were reported previously in a patient with AAS who carried the same variant, in addition to short stature and facial abnormalities (17). However, while the boy in our study had intellectual disability, the other patient who carried the same variant only had mildly delayed motor development (walking at the age of 15 months).

In the boy's family, his maternal grandfather with severe short stature was also diagnosed as AAS, carrying the same *FGD1* variant. His maternal grandfather did not have facial abnormalities and intellectual disability, which could be due to clinical heterogeneity. However, milder manifestations could also be related to the increasing age (29). Intriguingly, his mother and sister also carried the same *FGD1* variant, who only presented with mild short stature. This was also observed in other female carriers (2, 17, 30). Alternatively, clinical phenotypes of female patients with AAS, in general, seemed relatively mild, which may be associated with X chromosome inactivation (31, 32).

Associated intellectual disability appears to be rare. Only few independent studies have been reported. However, no direct evidence was given to the correlation between AAS and intellectual disability (33–36). Aside from the *FGD1* gene, 4 of the 11 corresponding SNPs sites were associated with intellectual disability (**Supplementary Table S1**). However, they were unable to explain all of the boy's clinical manifestations by analyzing clinical presentation and genetic pattern. For example, the *CCDC41* gene variants would be present in nephronophthisis (37); *LSS* gene variants can result in alopecia (38); *LTBP3* gene variants are characterized by hypoplastic amelogenesis imperfecta (39); *NTRK1* gene variants have been found to cause congenital insensitivity to pain (40).

In this study, consistent with the clinical phenotype, pathogenicity assay, structural modeling, and conservation analysis show the deleterious effects. Clinical and molecular evidence indicated the pathogenicity of the c.1270A>G variant in *FGD1*. However, how *FGD1* variants result in the phenotype of skeletal anomalies remains unclarified. We presented the evidence that the mutation in *FGD1* weakened the interaction with CDC42 and tend to impair catalytic role. Consistent with the previous study showing negative mutants of CDC42 inhibit CDC42 signaling and suppressed osteogenesis, our study manifests the attenuated CDC42 signaling in skeletal dysplasia (41). Although dysregulation of the FGD1/CDC42 signaling pathway is suspected to be associated with skeletal defects in AAS, whether the downstream signaling molecules and the mechanism of mutations in *FGD1* might influence bone development remain to be elucidated (42). It is well-known that CDC42 regulates MAPK signaling pathways, including P38, ERK, and JNK, that might have an important impact on numerous cellular activities. Studies on the function of P38 and ERK in bone development were popular compared to JNK. Nevertheless, increasing number of research suggests that JNKs are critical mediators of osteoblast activity (43, 44). In mammals, JNK1, JNK2, and JNK3 are three distinct genes that encode JNKs. Among them, JNK1 and JNK2 are distributed widely in most cell types, whereas JNK3 is limited to the brain and testes (45). In regulating cell activities in particular cell cycle and apoptosis, active-CDC42 positively regulates p-JNK while during some cell life activities, such as hepatocyte differentiation, the inhibition of CDC42 activity leads to upregulate p-JNK (46). Similarly, our study showed decreased affinity of FGD1 and CDC42 promoted JNK1 phosphorylation. Therefore, we deduce that the variant of *FGD1* influences bone development *via* the increase in phosphorylation-JNK1. However, whether it is a direct or an indirect effect awaits further experiments.

To further explore the downstream characterization of molecular changes that adversely affect the formation of multiple skeletal structures, the follow-up experiments were performed. RUNX2 is an essential transcription factor involved in mesenchymal progenitors toward the osteogenic lineage (47). No significant discrepancies of RUNX2 were detected in the literature, which demonstrated that p-JNK1 did not affect the expression of RUNX2, but further decreased its transcriptional activity (25). Therefore, some osteogenic markers, the target genes of *RUNX2*, have been detected in our study.

ALP, an early marker for osteogenic differentiation, is widely recognized to represent the degree of osteogenic differentiation (48). As shown here, the mutation in *FGD1* led to decreased ALP activity compared to wildtype. Furthermore, osteogenic induction medium enhanced the ALP activity increase gradually to a stable level, but the activity of ALP in the mutant set is consistently lower than the others. The previous literature illustrated that the mutation in the *ALP* gene could result in skeletal disorder, including short stature (49). Besides, COL1A1 and OCN are largely considered as the maturation state markers or transcription factors of osteoblasts. Our cellular experiments confirmed that the variant identified in *FGD1* that contributed to the reduced transcription level of *COL1A1* and *OCN* plays the key role in skeletal development. Damian et al. reported that the mutations in *COL1A1* affect bone growth by bone deformities, and this was in line with the subsequent studies, which showed the evidence of a cumulative affected on short stature caused by mutations in *COL1A1* (50, 51). Similarly, downregulated *OCN* often occurs in the mechanism studies of idiopathic short stature (52–54).

CONCLUSION

We reported a patient with AAS due to the c.1270A>G variant in *FGD1* gene predicted to be pathogenic by bioinformatics programs. Additionally, we found that the variant weakened the interaction with CDC42 and decreased the expression of osteogenic-related genes through abnormal activation of JNK1 *in vitro*.

DATA AVAILABILITY STATEMENT

The datasets for this article are not publicly available due to concerns regarding participant/patient anonymity. Requests to access the datasets should be directed to the corresponding author.

ETHICS STATEMENT

The studies involving human participants were reviewed and approved by Clinical Research Ethics Committee of The First Affiliated Hospital, College of Medicine, Zhejiang University. Written informed consent to participate in this study was provided by the participants' legal guardian/next of kin. Written informed consent was obtained from the individual(s), and minor(s)' legal guardian/next of kin, for the publication of any potentially identifiable images or data included in this article.

AUTHOR CONTRIBUTIONS

YZ and QC wrote the manuscript together. HLi provided the clinical data. YZ, QC, HLu, and YQ participated in the experiment. QY and CW contributed to conception and design of the study. All authors contributed to manuscript revision, read, and approved the submitted version.

SUPPLEMENTARY MATERIAL

The Supplementary Material for this article can be found online at: https://www.frontiersin.org/articles/10.3389/fped.2022.888923/full#supplementary-material

Supplementary Figure S1 | Genetic diagnosis. **(A)** A schematic showing the filtering procedure of variants obtained by whole-exome sequencing. The number indicates the number of variants passed for each step. **(B)** Pathogenic assay for $FGD1^{N424D}$ variant.

Supplementary Table S1 | The 11 corresponding SNPs. OMIM, Online Mendelian Inheritance in Man; ACMG, American College of Medical Genetics and Genomics.

REFERENCES

1. Orrico A, Galli L, Clayton-Smith J, Fryns JP. Clinical utility gene card for: Aarskog-Scott Syndrome (*faciogenital dysplasia*) - update 2015. *Eu J Human Gen: EJHG*. (2015) 23:558. doi: 10.1038/ejhg.2014.178
2. Hamzeh AR, Saif F, Nair P, Binjab AJ, Mohamed M, Al-Ali MT, et al. A novel, putatively null, FGD1 variant leading to Aarskog-Scott syndrome in a family from UAE. *BMC Pediatr.* (2017) 17:31. doi: 10.1186/s12887-017-0781-4
3. Darendeliler F, Larsson P, Neyzi O, Price AD, Hagenäs L, Sipilä I, et al. Growth hormone treatment in Aarskog syndrome: analysis of the KIGS (Pharmacia international growth database) data. *J Pediat Endocrinol Metabol: JPEM.* (2003) 16:1137–42. doi: 10.1515/JPEM.2003.16.8.1137
4. Duncan PA, Klein RM, Wilmot PL, Shapiro LR. Addditional features of the Aarskog syndrome. *J Pediatr.* (1977) 91:769–70. doi: 10.1016/S0022-3476(77)81038-X
5. Shalev SA, Chervinski E, Weiner E, Mazor G, Friez MJ, Schwartz CE. Clinical variation of Aarskog syndrome in a large family with 2189delA in the FGD1 gene. *Am J Med Gen Part A*. (2006) 140:162–5. doi: 10.1002/ajmg.a.31033
6. Wang Q, Chen P, Liu J, Lou J, Liu Y, Yuan H. Xp11. 22 duplications in four unrelated Chinese families: delineating the genotype-phenotype relationship for HSD17B10 and FGD1 BMC. *Med Genom.* (2020) 13:66. doi: 10.1186/s12920-020-0728-8
7. Aten E, Sun Y, Almomani R, Santen GW, Messemaker T, Maas SM, et al. Exome sequencing identifies a branch point variant in Aarskog-Scott syndrome. *Hum Mutat.* (2013) 34:430–4. doi: 10.1002/humu.22252
8. Zheng Y, Fischer DJ, Santos MF, Tigyi G, Pasteris NG, Gorski JL, et al. The faciogenital dysplasia gene product FGD1 functions as a Cdc42Hs-specific guanine-nucleotide exchange factor. *J Biol Chem.* (1996) 271:33169–72. doi: 10.1074/jbc.271.52.33169
9. Pasteris NG, Cadle A, Logie LJ, Porteous ME, Schwartz CE, Stevenson RE, et al. Isolation and characterization of the faciogenital dysplasia (Aarskog-Scott syndrome) gene: a putative Rho/Rac guanine nucleotide exchange factor. *Cell.* (1994) 79:669–78. doi: 10.1016/0092-8674(94)90552-5
10. Xiao XH, Lv LC, Duan J, Wu YM, He SJ, Hu ZZ, et al. Regulating Cdc42 and its signaling pathways in cancer: small molecules and MicroRNA as new treatment candidates. *Molecules.* (2018) 23:787. doi: 10.3390/molecules23040787
11. Cotteret S, Chernoff J. The evolutionary history of effectors downstream of Cdc42 and Rac. *Genome Biol.* (2002) 3:0002. doi: 10.1186/gb-2002-3-2-reviews0002
12. Rincon S, Coll PM, Perez P. Spatial regulation of Cdc42 during cytokinesis. *Cell cycle (Georgetown, Tex).* (2007) 6:1687–91. doi: 10.4161/cc.6.14.4481
13. Etienne-Manneville S. Cdc42–the centre of polarity. *J Cell Sci.* (2004) 117:1291–300. doi: 10.1242/jcs.01115
14. Cerione RA. Cdc42: new roads to travel. *Trends Cell Biol.* (2004) 14:127–32. doi: 10.1016/j.tcb.2004.01.008
15. Genot E, Daubon T, Sorrentino V, Buccione R. FGD1 as a central regulator of extracellular matrix remodelling–lessons from faciogenital dysplasia. *J Cell Sci.* (2012) 125:3265–70. doi: 10.1242/jcs.093419

16. Wu W, Jing D, Meng Z, Hu B, Zhong B, Deng X, et al. FGD1 promotes tumor progression and regulates tumor immune response in osteosarcoma via inhibiting PTEN activity. *Theranostics.* (2020) 10:2859–71. doi: 10.7150/thno.41279
17. Ge Y, Li N, Wang Z, Wang J, Cai H. Novel variant in the FGD1 gene causing Aarskog-Scott syndrome. *Exp Ther Med.* (2017) 13:2623–8. doi: 10.3892/etm.2017.4301
18. den Dunnen JT, Dalgleish R, Maglott DR, Hart RK, Greenblatt MS, McGowan-Jordan J, et al. HGVS recommendations for the description of sequence variants: 2016 update. *Hum Mutat.* (2016) 37:564–9. doi: 10.1002/humu.22981
19. Ashkenazy H, Abadi S, Martz E, Chay O, Mayrose I, Pupko T, et al. ConSurf 2016: an improved methodology to estimate and visualize evolutionary conservation in macromolecules. *Nucleic Acids Res.* (2016) 44:W344–50. doi: 10.1093/nar/gkw408
20. Bendl J, Stourac J, Salanda O, Pavelka A, Wieben ED, Zendulka J, et al. PredictSNP: robust and accurate consensus classifier for prediction of disease-related mutations. *PLoS Comput Biol.* (2014) 10:e1003440. doi: 10.1371/journal.pcbi.1003440
21. Li MM, Datto M, Duncavage EJ, Kulkarni S, Lindeman NI, Roy S, et al. Standards and guidelines for the interpretation and reporting of sequence variants in cancer: a joint consensus recommendation of the association for molecular pathology, American society of clinical oncology, and college of American pathologists. *J Mol Diagnos: JMD.* (2017) 19:4–23. doi: 10.1016/j.jmoldx.2016.10.002
22. Roy A, Kucukural A, Zhang Y, I-TASSER. a unified platform for automated protein structure and function prediction. *Nat Protoc.* (2010) 5:725–38. doi: 10.1038/nprot.2010.5
23. Rodrigues CH, Pires DE, Ascher DB. DynaMut: predicting the impact of mutations on protein conformation, flexibility and stability. *Nucleic Acids Res.* (2018) 46:W350–w5. doi: 10.1093/nar/gky300
24. Zagryazhskaya-Masson A, Monteiro P, Macé AS, Castagnino A, Ferrari R, Infante E, et al. Intersection of TKS5 and FGD1/CDC42 signaling cascades directs the formation of invadopodia. J cell biology. 2020;219. doi: 10.1083/jcb.201910132
25. Huang YF, Lin JJ, Lin CH, Su Y, Hung SC. c-Jun N-terminal kinase 1 negatively regulates osteoblastic differentiation induced by BMP2 via phosphorylation of Runx2 at Ser104. *J Bone Mineral Res: Off J Am Soc Bone Min Res.* (2012) 27:1093–105. doi: 10.1002/jbmr.1548
26. Teebi AS, Rucquoi JK, Meyn MS. Aarskog syndrome: report of a family with review and discussion of nosology. *Am J Med Genet.* (1993) 46:501–9. doi: 10.1002/ajmg.1320460508
27. Jabalameli MR, Ignacio B, Julio M, Ignacio B, Reuben JP, Sarah E, et al. Aarskog-Scott syndrome: phenotypic and genetic heterogeneity. *AIMS Genetics.* (2016) 3:49–59. doi: 10.3934/genet.2016.1.49
28. Zanetti Drumond V, Sousa Salgado L, Sousa Salgado C, Oliveira VAL, de Assis EM, Campos Ribeiro M, et al. The prevalence of clinical features in patients with Aarskog-scott syndrome and assessment of genotype-phenotype correlation: a systematic review. *Genet Res.* (2021) 2021:6652957. doi: 10.1155/2021/6652957
29. Fryns JP. Aarskog syndrome: the changing phenotype with age. *Am J Med Genet.* (1992) 43:420–7. doi: 10.1002/ajmg.1320430164
30. Altincik A, Kaname T, Demir K, Böber E, A. novel mutation in a mother and a son with Aarskog-Scott syndrome. *J Ped Endocrinol Metabol: JPEM.* (2013) 26:385–8. doi: 10.1515/jpem-2012-0233
31. Galupa R, Heard E. X-chromosome inactivation: new insights into cis and trans regulation. *Curr Opin Genet Dev.* (2015) 31:57–66. doi: 10.1016/j.gde.2015.04.002
32. Orrico A, Galli L, Obregon MG, de Castro Perez MF, Falciani M, Sorrentino V. Unusually severe expression of craniofacial features in Aarskog-Scott syndrome due to a novel truncating mutation of the FGD1 gene. *Am J Med genetics Part A.* (2007) 143a:58–63. doi: 10.1002/ajmg.a.31562
33. Logie LJ, Porteous ME. Intelligence and development in Aarskog syndrome. *Arch Dis Child.* (1998) 79:359–60. doi: 10.1136/adc.79.4.359
34. Pérez-Coria M, Lugo-Trampe JJ, Zamudio-Osuna M, Rodríguez-Sánchez IP, Lugo-Trampe A. de la Fuente-Cortez B, et al. Identification of novel mutations in Mexican patients with Aarskog-Scott syndrome. *Mol Gen Genom Med.* (2015) 3:197–202. doi: 10.1002/mgg3.132
35. Verhoeven WM, Egger JI, Hoogeboom AJ. X-linked Aarskog syndrome: report on a novel FGD1 gene mutation. Executive dysfunction as part of the behavioural phenotype. *Gen Couns.* (2012) 23:157–67. doi: 10.1016/S0924-9338(12)74868-X
36. Orrico A, Galli L, Buoni S, Hayek G, Luchetti A, Lorenzini S, et al. Attention-deficit/hyperactivity disorder (ADHD) and variable clinical expression of Aarskog-Scott syndrome due to a novel FGD1 gene mutation (R408Q). *Am J Med Gen Part A.* (2005) 135:99–102. doi: 10.1002/ajmg.a.30700
37. Failler M, Gee HY, Krug P, Joo K, Halbritter J, Belkacem L, et al. Mutations of CEP83 cause infantile nephronophthisis and intellectual disability. *Am J Hum Genet.* (2014) 94:905–14. doi: 10.1016/j.ajhg.2014.05.002
38. Besnard T, Sloboda N, Goldenberg A, Küry S, Cogné B, Breheret F, et al. Biallelic pathogenic variants in the lanosterol synthase gene LSS involved in the cholesterol biosynthesis cause alopecia with intellectual disability, a rare recessive neuroectodermal syndrome. *Gen Med: Off J Am Coll Med Gen.* (2019) 21:2025–35. doi: 10.1038/s41436-019-0445-x
39. Huckert M, Stoetzel C, Morkmued S, Laugel-Haushalter V, Geoffroy V, Muller J, et al. Mutations in the latent TGF-beta binding protein 3 (LTBP3) gene cause brachyolmia with amelogenesis imperfecta. *Hum Mol Genet.* (2015) 24:3038–49. doi: 10.1093/hmg/ddv053
40. Echaniz-Laguna A, Altuzarra C, Verloes A, De La Banda MGG, Quijano-Roy S, Tudorache RA, et al. NTRK1 gene-related congenital insensitivity to pain with anhidrosis: a nationwide multicenter retrospective study. *Neurogenetics.* (2021) 22:333–41. doi: 10.1007/s10048-021-00668-z
41. Gao L, Gorski JL, Chen CS. The Cdc42 guanine nucleotide exchange factor FGD1 regulates osteogenesis in human mesenchymal stem cells. *Am J Pathol.* (2011) 178:969–74. doi: 10.1016/j.ajpath.2010.11.051
42. Gorski JL, Estrada L, Hu C, Liu Z. Skeletal-specific expression of Fgd1 during bone formation and skeletal defects in faciogenital dysplasia (FGDY; Aarskog syndrome). *Develop Dynamics: Off Pub Am Assoc Anatom.* (2000) 218:573–86. 10.1002/1097-0177(2000)9999:9999<::AID-DVDY1015>3.0.CO;2-F
43. Xu R, Zhang C, Shin DY, Kim JM, Lalani S, Li N, et al. c-Jun N-Terminal Kinases (JNKs) are critical mediators of osteoblast activity *in vivo*. *J Bone Min Res: Off J Am Soc Bone Min Res.* (2017) 32:1811–5. doi: 10.1002/jbmr.3184
44. Weston CR, Davis RJ. The JNK signal transduction pathway. *Curr Opin Cell Biol.* (2007) 19:142–9. doi: 10.1016/j.ceb.2007.02.001
45. Zhou B, Chu M, Xu S, Chen X, Liu Y, Wang Z, et al. Hsa-let-7c-5p augments enterovirus 71 replication through viral subversion of cell signaling in rhabdomyosarcoma cells. *Cell Biosci.* (2017) 7:7. doi: 10.1186/s13578-017-0135-9
46. Li Z, Tian Y, Qu L, Mao J, Zhong H. AAV-Mig-6 increase the efficacy of TAE in VX2 rabbit model, is associated with JNK mediated autophagy. *J Cancer.* (2019) 10:1060–9. doi: 10.7150/jca.27418
47. Chan WCW, Tan Z, To MKT, Chan D. Regulation and Role of Transcription Factors in Osteogenesis. International journal of molecular sciences. (2021) 22:5445. doi: 10.3390/ijms22115445
48. Rosenberg M, Shilo D, Galperin L, Capucha T, Tarabieh K, Rachmiel A, et al. Bone morphogenic protein 2-loaded porous silicon carriers for osteoinductive implants. *Pharmaceutics.* (2019) 11:602. doi: 10.3390/pharmaceutics11110602
49. Cui Y, Zhang Y, Fu D, Liu X, Wei H. [Analysis of ALPL gene variant in a patient with infantile hypophosphatasia]. *Zhonghua Yi Xue Yi Chuan Xue Za Zhi.* (2021) 38:481–4. doi: 10.3760/cma.j.cn511374-20200414-00267
50. Rauch D, Robinson ME, Seiltgens C, Sutton VR, Lee B, Glorieux F, et al. Assessment of longitudinal bone growth in osteogenesis imperfecta using metacarpophalangeal pattern profiles. *Bone.* (2020) 140:115547. doi: 10.1016/j.bone.2020.115547
51. Ye X, Fang D, He Y, Yan H, Qiu W, Sun Y. Dual diagnosis of osteogenesis imperfecta (OI) and short stature and advanced bone age with or without early-onset osteoarthritis and/or osteochondritis dissecans (SSOAOD) reveals a cumulative effect on stature caused by mutations in COL1A1 and ACAN genes. *Eur J Med Genet.* (2020) 63:104074. doi: 10.1016/j.ejmg.2020.104074
52. Liu X, Du Z, Yi X, Sheng T, Yuan J, Jia J. Circular RNA circANAPC2 mediates the impairment of endochondral ossification by miR-874-3p/SMAD3 signalling pathway in idiopathic short stature. *J Cell Mol Med.* (2021) 25:3408–26. doi: 10.1111/jcmm.16419

53. Ishikawa M, Williams GL, Ikeuchi T, Sakai K, Fukumoto S, Yamada Y. Pannexin 3 and connexin 43 modulate skeletal development through their distinct functions and expression patterns. *J Cell Sci.* (2016) 129:1018–30. doi: 10.1242/jcs.176883
54. Lin KL, Chou CH, Hsieh SC, Hwa SY, Lee MT, Wang FF. Transcriptional upregulation of DDR2 by ATF4 facilitates osteoblastic differentiation through p38 MAPK-mediated Runx2 activation. *J Bone Min Res: Off J Am Soc Bone Min Res.* (2010) 25:2489–503. doi: 10.1002/jbmr.159

Conflict of Interest: The authors declare that the research was conducted in the absence of any commercial or financial relationships that could be construed as a potential conflict of interest.

Publisher's Note: All claims expressed in this article are solely those of the authors and do not necessarily represent those of their affiliated organizations, or those of the publisher, the editors and the reviewers. Any product that may be evaluated in this article, or claim that may be made by its manufacturer, is not guaranteed or endorsed by the publisher.

frontiers | Frontiers in Genetics

TYPE Original Research
PUBLISHED 31 August 2022
DOI 10.3389/fgene.2022.960504

OPEN ACCESS

EDITED BY
Rong Qiang,
Northwest Women's and Children's Hospital, China

REVIEWED BY
Asmat Ullah,
University of Copenhagen, Denmark
Chao Xu,
Shandong Provincial Hospital, China
Sajid Malik,
Quaid-i-Azam University, Pakistan

*CORRESPONDENCE
Shanshan Li,
lissane0508@126.com
Zhenlin Zhang,
zhangzl@sjtu.edu.cn

SPECIALTY SECTION
This article was submitted to Genetics of Common and Rare Diseases, a section of the journal Frontiers in Genetics

RECEIVED 03 June 2022
ACCEPTED 01 August 2022
PUBLISHED 31 August 2022

CITATION
Lv S, Zhao J, Liu L, Wang C, Yue H, Zhang H, Li S and Zhang Z (2022), Exploring and expanding the phenotype and genotype diversity in seven Chinese families with spondylo-epi-metaphyseal dysplasia.
Front. Genet. 13:960504.
doi: 10.3389/fgene.2022.960504

Exploring and expanding the phenotype and genotype diversity in seven Chinese families with spondylo-epi-metaphyseal dysplasia

Shanshan Lv, Jiao Zhao, Li Liu, Chun Wang, Hua Yue, Hao Zhang, Shanshan Li* and Zhenlin Zhang*

[1]Shanghai Clinical Research Center of Bone Diseases, Department of Osteoporosis and Bone Diseases, Shanghai Jiao Tong University Affiliated Sixth People's Hospital, Shanghai, China

Spondylo-epi-metaphyseal dysplasia (SEMD) is a heterogeneous group of disorders with different modes of inheritance and is characterized by disproportionate or proportionate short stature. To date, more than 30 disease-causing genes have been identified, and different types of SEMD exhibit greatly overlapping clinical features, which usually complicate the diagnosis. This study was performed to expand the clinical and molecular spectrum of SEMD among Chinese subjects and to explore their potential phenotype–genotype relations. We enrolled seven families including 11 affected patients with SEMD, and their clinical, radiographic, and genetic data were carefully analyzed. All the seven probands showed different degrees of short stature, and each of them exhibited additional specific skeletal manifestations; four probands had extraosseous manifestations. X-rays of the seven probands showed common features of SEMD, including vertebral deformities, irregular shape of the epiphysis, and disorganization of the metaphysis. Seven variants were identified in *TRPV4* (c.694C> T, p.Arg232Cys), *COL2A1* (c.654 + 1G > C; c.3266_3268del, p.Gly1089del), *CCN6* (c.396 T> G, p.Cys132Trp; c.721 T>C, p.Cys241Arg), SBDS (c.258 + 2T> C), and *ACAN* (c.1508C> A, p.Thr503Lys) genes, and two of them were novel. Two families with *TRPV4* variants showed considerable intrafamily and interfamily heterogeneities. In addition, we reported one case of SEMD with a severe phenotype caused by *ACAN* gene mutation. Our study expands the phenotype and genetic spectrum of SEMD and provides evidence for the phenotype–genotype relations, aiding future molecular and clinical diagnosis as well as procreative management of SEMD.

KEYWORDS

spondylo-epi-metaphyseal dysplasia, phenotype-genotype relation, TRPV4, COL2A1, CCN6, SBDS, ACAN

Introduction

Spondylo-epi-metaphyseal dysplasia (SEMD) is a heterogeneous genetic disorder, involving vertebral, epiphyseal, and metaphyseal dysplasia, and is diagnosed based on clinical phenotype, radiographic examination, and molecular sequencing. The primary clinical feature is a different degree of short stature (may present with short limbs or short trunk), combined with specific orthopedic symptoms (such as developmental coxa vara and scoliosis). Epiphyseal dysplasia usually leads to early-onset osteoarthritis, mostly in weight-bearing joints (Briggs et al., 1995). Odontoid hypoplasia causes atlantoaxial instability with severe spinal compression problems (Miyoshi et al., 2004). Radiological features included platyspondyly, vertebral body irregularity, destruction of articular cartilage, and dysplasia of epiphysis and metaphysis (Spranger, 1989).

This category of diseases is usually given the nomenclature according to the site name of manifest radiographic abnormalities (Alanay and Lachman, 2011; Mortier et al., 2019) (Figure 1), including spondyloepiphyseal dysplasia (SED), spondylometaphyseal dysplasia (SMD), spondylo-epi-metaphyseal dysplasia (SEMD), metaphyseal dysplasia (MD), and epiphyseal dysplasia (ED). With the in-depth study, SEMD is further classified according to specific clinical manifestations. For example, SED with different clinical manifestations can be divided into spondyloepiphyseal dysplasia congenita (SEDC, OMIM# 183900), spondyloepiphyseal dysplasia-Kimberley type (SED-KT, OMIM# 608361), and spondyloepiphyseal dysplasia-Maroteaux type (SED-MT, OMIM# 184095).

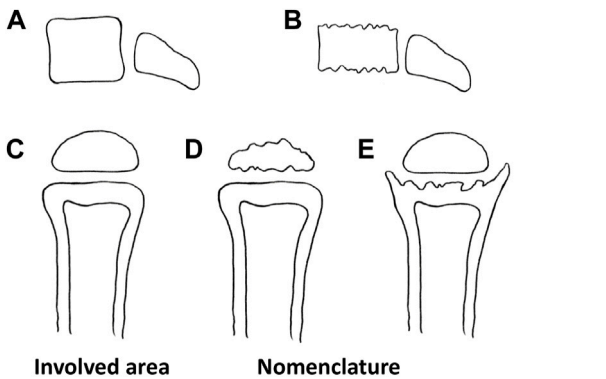

FIGURE 1
Nomenclature according to the involved area name of dysplasia. A + D: epiphyseal dysplasia, A + E: metaphyseal dysplasia, B + D: spondyloepiphyseal dysplasia, B + E: spondylometaphyseal dysplasia, and B + D + E: spondylo-epi-metaphyseal dysplasia.

So far, more than 30 pathogenic genes have been identified to cause SEMD. These disease-causing genes are involved in encoding various types and functions of proteins (Cormier-Daire, 2008). It is difficult to define them as a common signal pathway among all the SEMD. In such clinical and genetic heterogeneous diseases, different gene–disease associations and overlapping clinical characteristics of different genes complicate the differential diagnosis. According to the nosology and classification of genetic skeletal disorders 2019 revision, groups 10–13 are classified as spondylo-epi-metaphyseal abnormalities, but these diseases still exist in other groups (Mortier et al., 2019). The more common SEMD were *COL2A1*-related dysplasia and pseudoachondroplasia (OMIM# 177170).

At present, most of the reports of SEMD are single case reports, and there are few studies focusing on exploring the phenotype of SEMD caused by different disease-causing genes. We reported seven families with SEMD caused by *TRPV4*, *COL2A1*, *CCN6*, *SBDS*, and *ACAN* genes in order to explore the relationship between phenotype and genotype of them. Several studies have reported the phenotype–genotype relations of skeletal disorders caused by *COL2A1*, *COMP*, and *CCN6* genes (Barat-Houari et al., 2016a; Madhuri et al., 2016; Liang et al., 2021), but we still need more families to prove it, especially Chinese families. Therefore, we summarized the clinical manifestations, radiological data, and molecular features of patients with SEMD, hoping to improve our understanding of Chinese families with SEMD.

Methods

Patients with clinical assessment

Seven non-consanguineous families (11 affected individuals) with features of spinal, epiphyseal, and metaphyseal dysplasia participated in this study from 2014–2020. Clinical data were collected, including basic information, family history, age of onset, physical examinations [included height, weight, arm, span, upper/lower segment (U/L) ratio, and standard deviation score (SDS) (Li, 2009)], and skeletal and other system manifestations. Radiographs of the spine, pelvises, and affected joints were taken. Laboratory examinations including liver and kidney functions, blood routine, and bone turnover markers were collected. The study was reviewed and approved by the Ethics Committee of the Shanghai Jiao Tong University Affiliated Sixth People's Hospital and conducted in accordance with the Declaration of Helsinki. Informed written consents were obtained from all study participants or their legal guardians.

Targeted exome sequencing

Peripheral blood samples were collected in EDTA tubes from seven probands and 20 available family members. Informed consent was obtained from all 27 participants before the genetic analysis. The QuickGene DNA whole blood kits (Kurabo Industries Ltd., Osaka, Japan) and the Nucleic Acid Isolation System (QuickGene-610L; Autogen, Inc., Holliston, MA, United States) were used to extract genomic DNA. We used the TES to detect candidate genes of seven probands' DNA samples. TES was performed using the Agilent SureSelect (SureSelect Reagent Kit; Agilent Technologies, CA, United States) target enrichment kit, which consisted of 322 pathogenic genes known to cause skeletal disease (Lv et al., 2021). Sequencing was performed on the Illumina Hiseq platform using paired-end 150-bp reads.

Evaluation of variants

We prioritized the variants that were known to cause disease in the Human Gene Mutation Database (HGMD) or other databases. The variants had lower allele frequency (< 0.001) in healthy control population databases (dbSNP, 1,000 Genomes, ESP6500, and gnomAD). The conservation and pathogenicity of variants were predicted by in silico tools (UniProt, Mutation Taster, Polyphen2, SIFT, and Human Splicing Finder). The pathogenicity of variants was also determined through appraisal of patients' clinical phenotypes and scientific literature studies. The interpretation criteria of variants consisted of the American College of Medical Genetics and Genomics (ACMG) practice guidelines (Richards et al., 2015). Sanger sequencing was used to validate the candidate variants in all family members. Novel variants were recognized by using the Human Gene Mutation Database (HGMD) and ClinVar (Landrum et al., 2018; Stenson et al., 2020).

Results

This study included 11 patients derived from seven unrelated families who suffered from spinal, epiphyseal, and metaphyseal abnormalities. They are all of Han nationality from eastern Asia. Also, the ratio of females to males was 2/5, with 2 females and 5 males. The mean age of onset occurred at 4.9 ± 4.7 years. Detailed clinical characteristics of seven probands are shown in Table 1. Two families had an obvious positive family history, and the specific pedigrees of these seven families are shown in Figure 2.

TRPV4-related skeletal dysplasia (OMIM# 605427)

In family 1, proband 1 (II-1) was an 8.6-year-old girl with normal pregnancy, delivery, and family history. Her height was 125 cm (−1.1 SDS), and her arm span was 118 cm. She came to medical attention at the age of 8 when her mother noticed her scoliosis. Physical examinations revealed mild scoliosis, increased lumbar lordosis, and normal gait. She had myopia and normal hearing and intelligence. X-rays demonstrated mild scoliosis, ovoid vertebral bodies, rough edges of the vertebral bodies, and disorganization of the metaphysis (Figure 3).

Family 2 included three affected individuals, but their clinical phenotypes were highly variable. The 13-year-old boy proband 2 (III-1) was 155.4 cm (−0.5 SDS) tall. Since the age of 10, there was a significant kyphosis in his lumbar without low back pain and joint movement limitation. Physical examinations revealed severe lumbar lordosis and fourth metatarsal dysplasia. His father (II-1, 35 years old) had mild contracture of the distal joints of both hands and hallux valgus deformity of both feet since the age of 10 and difficulty in walking now. His brother (III-1, 7 years old) did not show any abnormalities. Their heights were within the normal range; his father was 172 cm tall, and his brother was 123.5 cm tall. X-rays of the spine and pelvis in proband 2 showed rough edges of the vertebral bodies, lumbar lordosis, disorganization of the metaphysis, and shortening of the femoral neck. X-rays of the spine, pelvis, and feet of his father manifested scoliosis, depression of the anterior edge of vertebral bodies, flattening of the acetabular roof, shortening of the femoral neck, stenosis of joint spaces, and hallux valgus deformity (Figure 3). However, his brother's X-ray showed a mild irregularity in the shape of the vertebral bodies.

COL2A1-related skeletal dysplasia Spondyloepiphyseal dysplasia congenita (OMIM# 183900)

In family 3, proband 3 (II-1) was a 9-year-old boy, with a height of 110 cm (−5.6 SDS). At 33 weeks of gestation, his mother's color doppler ultrasound showed that the fetal femur was shortened by 1 cm. He had visible thoracic abnormalities (pectus excavatum) at birth, learned to walk at the age of 2, and underwent thoracic correction surgery at the age of 3. Since he was 6 years old, he had hip stiffness with pain and limited mobility. At present, he has been unable to straighten his waist. Physical examinations showed that both maxillary lateral incisors were absent. X-rays showed scoliosis, platyspondyly, flattening and irregularity of the acetabular roof, femoral head necrosis, and disappearance of the femoral neck (Figure 4).

TABLE 1 Clinical characteristics of seven probands with SEMD.

Patient	Gender	Age (y)	Age at onset	Weight (kg)	Height (cm)	SDS	Arm span	U/L	Muscle weakness	Osteoarthropathy	Joint contractures	Skeletal phenotype	Extraosseous phenotype	Diagnosis
P1	F	8.6	8	21	125	−1.1	118	63/62	No	No	No	Scoliosis	Myopia	Hereditary motor and sensory neuropathy
P2	M	13	10	41	155.4	−0.5	156	76/79.4	No	No	No	Lumbar lordosis, fourth metatarsal dysplasia (unusual feature)	No	Hereditary motor and sensory neuropathy
P3	M	8.7	0	37	101	−5.6	100	48/53	No	No	Yes	Severe short stature, pectus excavatum, scoliosis, and hip pain and stiffness	Tooth dysplasia	Spondyloepiphyseal dysplasia congenita
P4	M	29	0	40	146	−4.4	139	70/76	No	Yes	Yes	Severe short stature, enlargement extension of the fingers, elbows, knees, and ankles, and joint pain and stiffness	Retinal detachment and cataract	Kniest dysplasia
P5	F	14.6	10	44	154.9	−0.8	—	—	Yes	Yes	Yes	Enlargement extension of the fingers, elbows, knees, and ankles and joint pain and stiffness	No	Progressive pseudorheumatoid dysplasia
P6	M	11.8	6	39	116	−4.8	116	52/64	No	No	No	Severe short stature and joint pain	Mild intellectual disability and tooth dysplasia	Shwachman–Bodian–Diamond syndrome
P7	M	48	0	52	148	−4.0	135	—	No	Yes	No	Severe short stature, brachydactyly (unusual feature), clubfoot, and joint pain and stiffness	No	Spondyloepiphyseal dysplasia

P, probands; M, male; F, female; SDS, standard deviation score; U/L, upper /lower part of the body.

10.3389/fgene.2022.960504

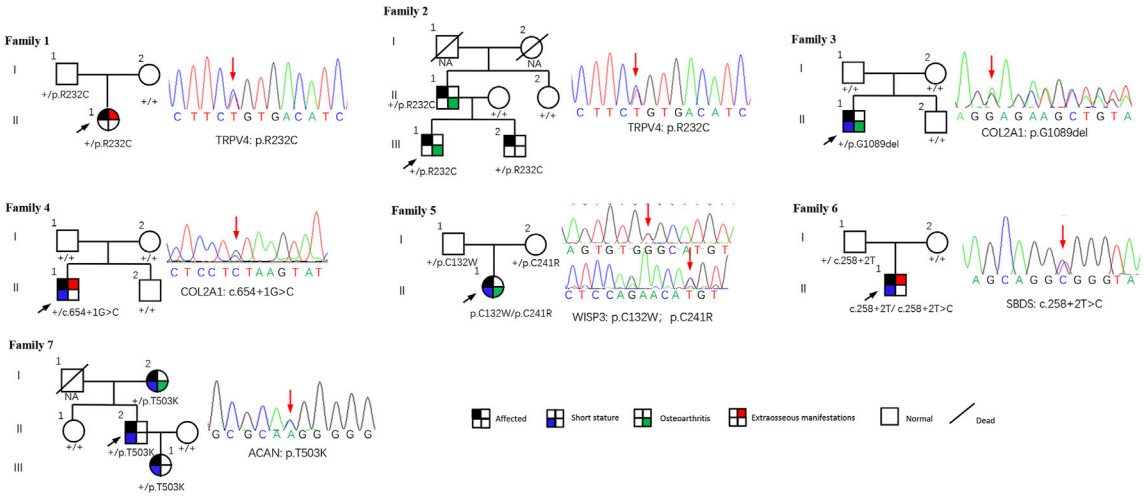

FIGURE 2
Pedigrees of seven families with SEMD. Almost all accessible family members were sequenced and examined. Mutations are shown below each subject, and the corresponding sequence diagrams are displayed next to the pedigrees. Circles and squares indicate females and males, respectively. Arrows identify the proband in the families. Slashes indicate deceased individuals.

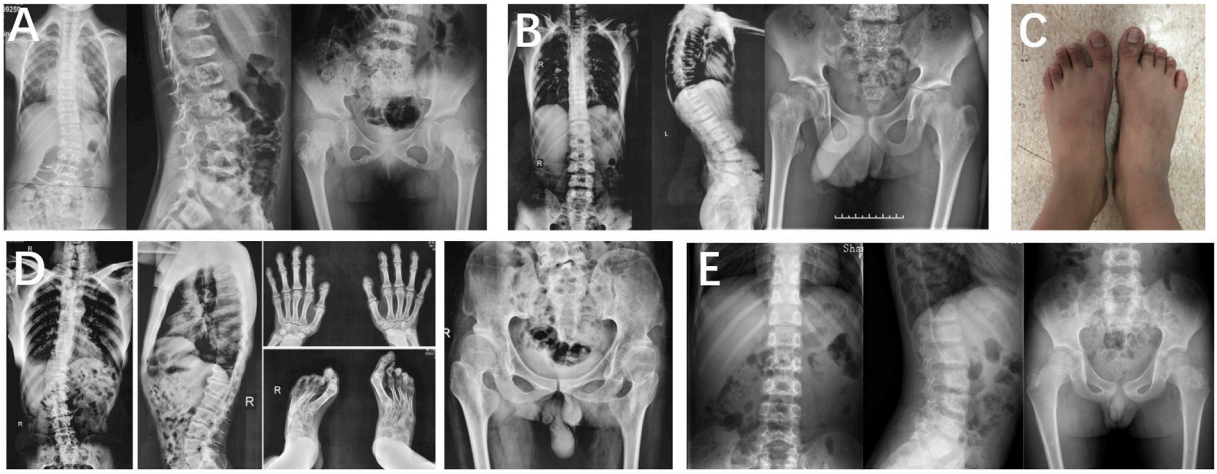

FIGURE 3
Photographs and radiographs of families 1 and 2 with TRPV4-related skeletal dysplasia. **(A)** Radiographs of the spine and pelvis of proband 1 (II-1) in family 1. Mild scoliosis, ovoid vertebral bodies, and rough edges of the vertebral bodies were significant in the spine. Disorganization of metaphysis was in the pelvis. **(B,C)** Radiographs of the spine and pelvis **(B)**, and photographs of feet **(C)** of proband 2 (III-1) in family 2. **(B)** Rough edges of the vertebral bodies and lumbar lordosis were visible in the spine. Disorganization of the metaphysis and shortening of the femoral neck were in the pelvis. **(C)** Fourth metatarsal dysplasia was in the left foot. **(D)** Radiographs of hands, spine, pelvis, and feet of proband 2's father (II-1). Mild contracture of the distal joints was shown in the hands. Scoliosis and depression of the anterior edge of vertebral bodies were displayed in the spine. Flattening of the acetabular roof, shortening of the femoral neck, and stenosis of joint spaces were in the pelvis. Hallux valgus deformity was seen in feet. **(E)** Radiographs of the spine and pelvis of proband 2's brother (III-2). Irregular shape of the vertebral bodies in the spine. Radiographs of the pelvis were normal.

Kniest dysplasia (OMIM# 156550)

In family 4, the 29-year-old male proband 4 (II-1) was 146 cm (−4.4 SDS) tall. He was born with enlarged knee joints, and thereafter, bilateral interphalangeal, elbow, knee, and ankle joints were enlarged gradually. At the age of 5, knee joint pain began and gradually aggravated, resulting in difficulty in walking. Proband 4 had poor visual acuity (retinal detachment in the

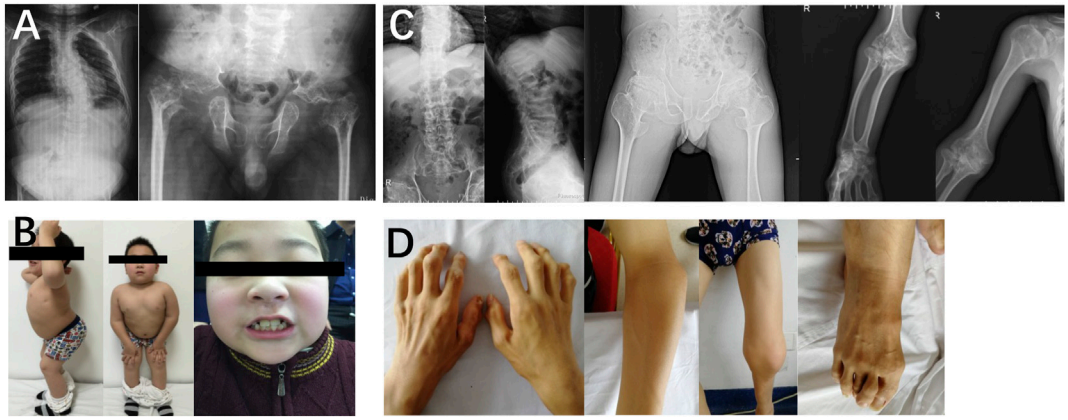

FIGURE 4
Photographs and radiographs of the families 3 and 4 with COL2A1-related skeletal dysplasia. **(A,B)** Radiographs of the spine and pelvis **(A)** and photographs of overall body and face **(B)** of proband 3 (II-1) in family 3. **(A)** Scoliosis and platyspondyly were shown in the spine. Flattening and irregularity of the acetabular roof, femoral head necrosis, and disappearance of the femoral neck were visible in the pelvis. **(B)** Barrel chested and limited hip movement were performed in the overall body. No eruption of bilateral incisors was displayed in the face. **(C,D)** Radiographs of the spine, pelvis, and upper limb **(C)** and photographs of hands, elbows, knees, and feet **(D)** of proband 4 (II-1) in family 4. **(C)** Severe multiple compressions of the vertebral bodies was revealed in the spine. Flattening of the acetabulum, shortening of the femoral neck, enlargement of the trochanter and femoral head, and narrow joint space of bilateral hips were shown in the pelvis. Widened epiphysis and metaphysis and joint cavity stenosis were visible in the elbows. **(D)** Bilateral elbow, knee, ankle, multiple metacarpophalangeal and interphalangeal joints were enlarged.

left eye at the age of 24, cataract in the right eye at the age of 25, and both underwent surgery) and normal hearing. X-rays displayed severe multiple compressions of the vertebral bodies, flattening of the acetabulum, shortening of the femoral neck, narrow joint space of bilateral hips, and enlargement of the trochanter and femoral head (Figure 4).

Progressive pseudorheumatoid dysplasia (OMIM# 208230)

In family 5, the female proband 5 (II-1) was 15 years old, with a height of 154.9 cm (−0.8 SDS). Intermittent large joint pain occurred at the age of 10, and no obvious abnormality was found in physical examinations. At the age of 13, the extension of both elbows was limited, and the elbow, knee, ankle, metacarpophalangeal, and interphalangeal joints gradually enlarged. Physical examinations showed that extension of multiple joints was limited, and no extraosseous manifestations were found. Symptoms aggravated with age. X-rays revealed mild platyspondyly, expansion of the epiphysis, and joint cavity stenosis. The pelvis was normal (Figure 5).

Shwachman–Bodian–Diamond syndrome (OMIM# 260400)

In family 6, the male proband 6 (II-1) was 12 years old and had a height of 116 cm (−4.8 SDS). He was born prematurely, and growth retardation occurred at birth. He developed knee pain at the age of 8, which was aggravated after exercise. Physical examinations revealed mild intellectual disability, tooth dysplasia, and normal gait. X-rays demonstrated irregular shape of the vertebral bodies and epiphysis, expansion of metaphysis, and disorganization of metaphysis (Figure 5).

Aggrecan-related spondyloepiphyseal dysplasia (OMIM# 608361)

In family 7, the 48-year-old male proband 7 (II-2) had a height of 148 cm (−4.0SDS) and an arm span of 135 cm, with a positive family history. Brachydactyly, clubfoot, and growth retardation were found at birth. When learning to walk at the age of 1, he had mild knee valgus and a swinging gait. Pain in the spine, hip, and knee joints appeared at the age of 16, and symptoms worsened after 20 years. Physical examinations revealed stubby fingers and toes, mild knee valgus, and limited hip mobility. X-rays displayed mild flattening and irregular shape of the vertebral bodies, 4–5 lumbar spondylolisthesis, flattening of the acetabulum, hip subluxation, femoral head necrosis, shortening of the femoral neck, osteoarthritis, widened epiphysis, and joint cavity stenosis (Figure 6). Both his mother (I-2, 73 years old, 150 cm, −2.0 SDS) and daughter (III-1, 22 years old, 148 cm, −2.3 SDS) had similar symptoms: short stature with short limbs. Her daughter's X-ray reports showed similar findings, but her pelvis was normal.

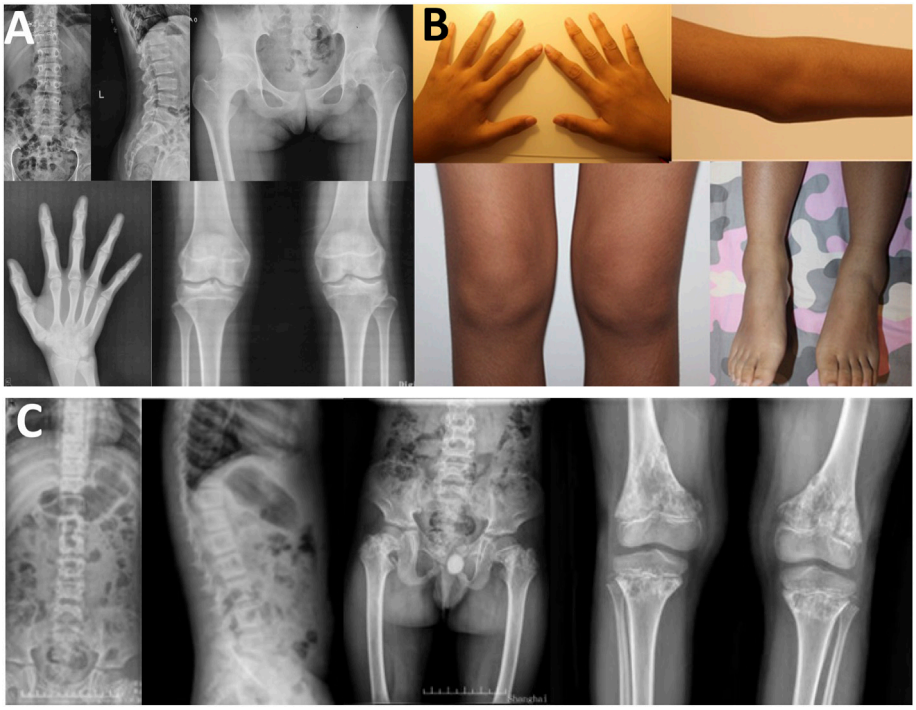

FIGURE 5
Photographs and radiographs of the families 5 and 6. **(A,B)** Radiographs of the spine, pelvis, hands, knees **(A)** and photographs **(B)** of proband 5 (II-1) in family 5. **(A)** Mild platyspondyly was revealed in the spine. The pelvis was normal. Expansion of metaphysis and stenosis of joint spaces were visible in hands. Widened epiphysis and joint cavity stenosis were displayed in the knees. **(B)** Bilateral elbow, knee, ankle, and multiple metacarpophalangeal and interphalangeal joints were enlarged. **(C)** Radiographs of the spine, pelvis, and knees of proband (II-1) in family 6. Irregular shape of the vertebral bodies was significant in the spine. Flattening of the acetabular roof, shortening of the femoral neck, mildly compressed femoral head, and thickening of metaphyseal texture were displayed in the pelvis. Widened epiphysis and metaphysis, irregular shape of the epiphysis, and disorganization of the metaphysis were obvious in the knees.

Genetic analysis

We have identified *TRPV4*, *COL2A1*, *CCN6*, *SBDS*, and *ACAN* gene mutations in 8 p.R232C (c.694C> T) were detected in two probands and three family members. In family 3, a heterozygous deletion mutation in *COL2A1*, p.G1089del (c.3266_3268del), was detected in proband 3. In family 4, a heterozygous splicing mutation in *COL2A1*, c.654+1G > C, was detected in proband 4. In family 5, two missense mutations in *CCN6*, p.C132W (c.396 T>G) and p.C241R (c.721 T>C), were detected in proband 5. Furthermore, proband 5's mother (c.721 T>C) and father (c.396 T>G) carried a mutation, respectively. In family 6, a homozygous splicing mutation in SBDS, c.258+2 T>C, was detected in proband 6. Also, we found a heterozygous splicing mutation (c.258+2 T>C) in proband 6's mother. In family 7, a heterozygous missense mutation in *ACAN*, p.T503K (c.1508C> A), was detected in proband 7 and two affected family members. A total of seven variants were found, and the pathogenicity prediction and classification are shown in Table 2. Combined with literature studies, two variants (c.654 + 1G > C and p.T503K) were novel, and five variants (p.R232C, p.G1089del, p.C132W, p.C241R, and c.258+2 T>C) were reported previously.

Discussion

This study focused on exploring phenotype and genotype in seven families with SEMD caused by *TRPV4*, *SBDS*, *COL2A1*, *CCN6*, and *ACAN* gene mutations, including two *TRPV4*-related skeletal dysplasia, one spondyloepiphyseal dysplasia, one Kniest dysplasia, one progressive pseudorheumatoid dysplasia, one Shwachman–Bodian–Diamond syndrome, and one aggrecan-related SED. The main clinical feature was short stature, and four probands had severe short stature (<-3 SDS). In addition, four probands had extraosseous manifestations. We have reported seven different mutation sites, including two novel sites and five reported sites. These findings expanded the phenotypic and genetic spectrum of SEMD in the Chinese population.

TRPV4 gene encodes a nonselective calcium-permeable ion channel, widely distributed in bone, nerve, lung, heart, and other

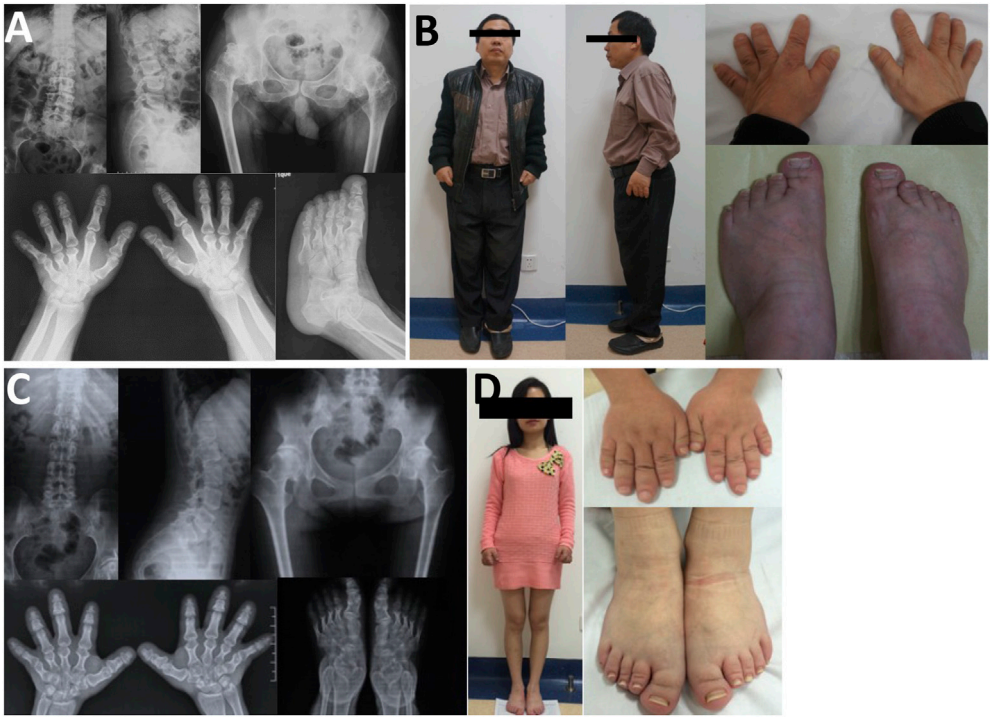

FIGURE 6
Photographs and radiographs of the family 7. **(A,B)** Radiographs of the spine, pelvis, hands, and feet **(A)** and photographs **(B)** of proband 7 (II-2) in family 7. **(A)** Mild flattening and irregular shape of the vertebral bodies and 4–5 lumbar spondylolisthesis were shown in the spine. Flattening of the acetabulum, hip subluxation, femoral head necrosis, and shortening of the femoral neck were revealed in the pelvis. Widened epiphysis and joint cavity stenosis were displayed in the hands and feet. **(B)** Short stature with short limb was visible in the full body. Thick and short fingers and toes were shown in hands and feet. **(C,D)** Radiographs of the spine, pelvis, hands, and feet **(C)** and photographs **(D)** of patient (III-1) in family 7. **(C)** Mild flattening and irregular shape of the vertebral bodies were displayed in the spine. The pelvis was normal. Widened epiphysis and joint cavity stenosis were displayed in the hands and feet. **(D)** Thick and short fingers and toes were shown in hands and feet.

tissues (Everaerts et al., 2010). So far, more than 70 variants in the *TRPV4* gene had been reported to be related to autosomal-dominant skeletal dysplasia and motor and sensory neuropathies, such as Charcot-Marie-Tooth type 2C (CMT2C, OMIM#606482), scapuloperoneal spinal muscular atrophy (SPSMA, OMIM# 181405), spondylometaphyseal dysplasia-Kozlowski type (SMDK, OMIM#184252), and spondylo-epi-metaphyseal dysplasia Maroteaux pseudo-Morquio type 2 (SEDM-PM2, OMIM# 184095). The R232C variant had been reported repeatedly. Two studies reported that patients with R232C had a CMT2C-SPSMA overlap syndrome (Klein et al., 2011; Koutsis et al., 2015). They all had vocal cord paralysis, which was not found in this study. The probands in families 1 and 2 with R232C manifested slight short stature and scoliosis. Moreover, X-rays showed dysplasia of the vertebral bodies. No evidence of distal purely motor neuropathy was found in two probands, but these symptoms progressed very slowly. Therefore, we should follow up closely. Although only a small number of patients have been identified, they had comorbidity of neuromuscular and skeletal dysplasia (Cho et al., 2012; Faye et al., 2019). Interestingly, the clinical manifestations of family members who found the same variants showed intrafamily and interfamily variabilities. We detected that proband 1′s father harbored the R232C variant unexpectedly. He does not seem to be affected. Proband 2′s father and brother harbored the same variant. The phenotype of his father was the most serious, while his brother had no obvious abnormality, and only a mild irregularity in the shape of the vertebral bodies was found on the X-ray. These performances reinforced the notion that clinical features are heterogeneous in *TRPV4*-related neuropathies and skeletal dysplasia (Echaniz-Laguna et al., 2014). Meanwhile, the R232C variant exhibited reduced penetrance, which is the same as other reports (Chen et al., 2010; Koutsis et al., 2015). The R236C and R315W variants had also been reported to have reduced penetrance (Auer-Grumbach et al., 2010; Jędrzejowska et al., 2019). However, this phenomenon has not been reported in families with *TRPV4*-associated skeletal dysplasia (Nishimura et al., 2012).

The *COL2A1* gene encodes the alpha-1 chain of type II procollagen, which is the main component of the nucleus pulposus of intervertebral discs, the vitreous humor of the eyes, and hyaline cartilage extracellular matrix (Li et al.,

TABLE 2 Description of the variants and predictions for pathogenicity.

Patient	Gene	RefSeq number	Mutation	Zygote	Segregation	Mutation Taster	Polyphen2	SIFT	CADD Phred	Evidence of classification	Classification	Reported
P1	*TRPV4*	NM_021625	c.694C>T and p.R232C	Heterozygous	Paternal	Disease causing	Probably damaging	Deleterious	31	PS1, PS3, PS4, PM2, PP2, and PP3	P	Yes
P2	*TRPV4*	NM_021625	c.694C>T and p.R232C	Heterozygous	Paternal	Disease causing	Probably damaging	Deleterious	31	PS1, PS3, PS4, PM2, PP2, and PP4	P	Yes
P3	*COL2A1*	NM_001844	c.3266_3268del and p.G1089del	Heterozygous	De novo	—	—	—	—	PS1, PM2, PM4, and PM6	P	Yes
P4	*COL2A1*	NM_001844	c.654+1G > C	Heterozygous	De novo	—	—	—	—	PVS1 and PM2	P	—
P5	*CCN6*	NM_198239	c.396 T>G and p.C132W	Compound heterozygous	Paternal and maternal	Disease causing	Probably damaging	Deleterious	24/28.4	PS1, PM2, PM3, PP4, and PP2; PS1, PS4, PM2, PM3, PP2, and PP4	P/P	Yes
			c.721 T>C and p.C241R		Paternal and maternal	Disease causing	Probably damaging	Deleterious				
P6	*SBDS*	NM_016038	c.258+2 T>C	Homozygous	Maternal and de novo	-	-	-	25.6	PVS1, PS1, PP1, and PP4	P	Yes
P7	*ACAN*	NM_001135	c.1508C>A and p.T503K	Heterozygous	Maternal	Disease causing	Probably damaging	Deleterious	24.5	PM2, PP1, PP3, PP2, and PP4	LP	-

P, pathogenic; LP, likely pathogenic.

10.3389/fgene.2022.960504

1995). The phenotypic spectrum of *COL2A1*-related diseases is very broad and includes mainly spondyloepiphyseal dysplasia congenita (SEDC, OMIM#183900), Kniest dysplasia, spondyloperipheral dysplasia (SPPD, OMIM#271700), osteoarthritis with mild chondrodysplasia (OSCDP, OMIM# 604864), and spondyloepiphyseal dysplasia-Strudwick type (SED-ST, OMIM#184250). It encompasses a diverse group of clinical phenotypes characterized by short stature and ocular manifestations, whereas later it is manifested as isolated arthritis. SEDC is characterized by a short trunk, flattened vertebral bodies, and abnormal epiphyses. In our study, proband 3 had a short trunk (U/P = 0.91), severe hip joint mobility limitation, and femoral head necrosis. He had a deletion of glycine in Gly-X-Y repeats (p.Gly1089del), which led to severe impairment of protein assembly and stability (Barat-Houari et al., 2016b). Patients with C-propeptide glycine substitutions have been reported to be shorter than those with N-propeptide substitutions (Terhal et al., 2012). Our center has reported that glycine to serine substitution caused milder phenotypes than glycine to nonserine substitutions (Xu et al., 2020). In Kniest dysplasia, the classical phenotypes are short-trunk dwarfism due to severely affected skeletal growth, scoliosis, platyspondyly, and joint enlargement, while extraskeletal features mainly include myopia, prominent eyes, conductive hearing loss, and mid-face hypoplasia (Barat-Houari et al., 2016a). Proband 4 with Kniest dysplasia had severe short stature (−4.4 SDS, U/L = 0.92), severe skeletal deformity, retinal detachment and cataract, and normal face and hearing. It is worth mentioning that proband 4 was misdiagnosed as PPD before, but he was detected with a *COL2A1* mutation. This reminds us that we should pay attention to the differential diagnosis of PPD and *COL2A1*-related SEDC. The onset age of SEDC is usually at birth, while PPD mostly occurs at the age of 3–8 years (Garcia Segarra et al., 2012). At least 33 mutations were reported to cause Kniest dysplasia, and we reported a novel splice-site mutation (c.654 + 1G > C) which led to exon skipping.

Progressive pseudorheumatoid dysplasia (PPD) is a rare autosomal recessive disease caused by the functional loss or abnormality of cellular communication network factor 6 (*CCN6*). The clinical features are progressive joint stiffness and enlargement without inflammation (Dalal et al., 2012). Patients with PPD are usually normal at birth, with an onset ranging from 1 to 16 years of age. (Delague et al., 2005; Dalal et al., 2012). In our study, proband 5 developed symptoms at an average age of 10 years and were misdiagnosed as rheumatoid arthritis, but there was no inflammation. PPD initially presented with swelling and stiffness of the interphalangeal joint, gradually involving all large joints. According to literature statistics, the height of adults is usually less than the 3rd percentile (Garcia Segarra et al., 2012). In the early stages of the disease, the stature and proportion of patients may still be normal. Although patients had enlarged joints and limited mobility, X-rays showed no evidence of osteoarthritis. As cartilage destruction increases, secondary osteoarthritis may develop in adulthood. In our study, we found two reportedly missense mutations (C132W and C241R). The C241R variant has been reported many times in Chinese families and seems to be a hot site in Chinese (Ye et al., 2012; Yu et al., 2015; Hu et al., 2017). One research has reported that most PPD patients carry nonsense mutations in both *WISP3* alleles. They observed that the phenotype of patients homozygous for a missense mutation was not milder than patients with one or both alleles carrying a nonsense mutation (Garcia Segarra et al., 2012).

Shwachman–Bodian–Diamond syndrome (SBDS, OMIM#260400) is an autosomal recessive disease characterized by hematologic abnormalities, exocrine pancreatic dysfunction, immune deficiency, and skeletal abnormalities (Ginzberg et al., 1999). More than 90% of SBDS were caused by *SBDS* gene mutations (Boocock et al., 2003), and the most common variants were c.184A > T and c.258 + 2 T > C (Kuijpers et al., 2005; Nelson and Myers, 2018). The diagnosis of SBDS relied on evidence of exocrine pancreatic dysfunction, hematologic abnormalities, and recurrent infections (Huang and Shimamura, 2011; Nelson and Myers, 2018). However, some patients did not have this classic combination of manifestations (Myers et al., 2014). One study evaluated 102 genetically diagnosed patients with SBDS and found 40% had hematologic complications (Donadieu et al., 2012). According to research in China, the onset age of hemocytopenia ranges from 0 to 12 years old (An et al., 2020). In our study, proband 6 had normal hematological function. Therefore, it is necessary to conduct long-term follow-up on the hematologic complications of proband 6. Skeletal dysplasia is also a common manifestation, Mäkitie reported that the skeletal abnormalities in patients with SBDS varied not only with age but also with individuals (Mäkitie et al., 2004). Proband 6 had obvious skeletal manifestations, severe short stature (< −3.0 SDS), and epiphyseal and metaphyseal dysplasia. One study found that patients with SBDS ranged widely in their neurocognitive impairment compared with controls (Kerr et al., 2010) and had been shown to be related to structural brain alterations (Toiviainen-Salo et al., 2008). It shows that the phenotypic spectrum of SBDS is wider than previously thought. One study summarized the literature for large SBDS cohorts and found that no obvious genotype–phenotype correlation was observed (Mäkitie et al., 2004; Donadieu et al., 2012; Myers et al., 2020).

The cartilage aggrecan proteoglycan is encoded by the *ACAN* gene, the main structural component of the cartilage growth plate, which is essential for skeletal growth and articular cartilage function (Roughley and Mort, 2014). The mutations in the *ACAN* gene can be classified into four categories: spondyloepiphyseal dysplasia, Kimberley type (SEDK, OMIM#608361); spondylo-epi-metaphyseal dysplasia, aggrecan type (SEMD, OMIM#612813); osteochondritis dissecans (OCD, OMIM#165800); and short stature and

advanced bone age. Previously, *ACAN* mutations had been reported as a cause of short stature with a frequency of 1.4–37.5% in the short stature population (Hauer et al., 2017; Stavber et al., 2020). In 2021, Li reported a large cohort of Chinese short-stature children caused by *ACAN* mutations (Lin et al., 2021). Patients with SEDK mostly have brachydactyly, platyspondyly, irregular femoral epiphyses, and precocious arthropathy, similar to the patients in this study. However, other features such as facial dysmorphisms and discopathy were not found. In contrast to previous data, brachydactyly was observed in all probands (Sentchordi-Montané et al., 2018). Nevertheless, there are few reports of SEDK caused by *ACAN* mutations (Gleghorn et al., 2005; Sentchordi-Montané et al., 2018). The new variant we reported expanded the clinical phenotype and genotype of this disease. At present, many clinical trials have proved that combined treatment with growth hormone (GH) or gonadotropin-releasing hormone (GnRH) is used to improve the final height of patients (Lin et al., 2021; Wei et al., 2021). Gkourogianni reported that the average height of patients treated with GH was lower than normal at 2.5 SD, while that of untreated patients was lower than 3 SD (Gkourogianni et al., 2017). The efficacy of GH and GnRH analogs in the treatment of patients with *ACAN* mutations needs more studies to be proved.

This study had some limitations. First, we were unable to perform electromyogram (EMG) testing in patients from family 1 and family 2 because the patients refused. We failed to determine whether the patients had manifestations of distal purely motor neuropathy. Second, as this was a single-center study, the number of probands with SEMD was small. Therefore, we did not have sufficient evidence to elucidate the phenotype–genotype relationship in SEMD. In the future, we hope to accumulate more patient data to illustrate the correlation between the two.

In the present study, we summarized seven families with SEMD caused by *TRPV4, COL2A1, CCN6, SBDS*, and *ACAN* gene mutations. Our results further demonstrated that phenotypic and genotypic spectra of SEMD are very wide. We should pay attention to the complications of SEMD and reduce or prevent their effects. Genetic testing is important for diagnosis, genetic counseling, and prenatal diagnosis. The new findings reported herein would contribute to the investigation of the phenotype–genotype relations among patients with SEMD.

Data availability statement

The datasets for this article are not publicly available due to concerns regarding participant/patient anonymity. Requests to access the datasets should be directed to the corresponding author.

Ethics statement

The studies involving human participants were reviewed and approved by the Ethics Committee of Shanghai Jiao Tong University Affiliated Sixth People's Hospital. Written informed consent to participate in this study was provided by the participants' legal guardian/next of kin. Written informed consent was obtained from the individual(s) and minor(s)' legal guardian/next of kin for the publication of any potentially identifiable images or data included in this article.

Author contributions

Conceptualization: ZZ and SL; data curation: SL, JZ, and LL; formal analysis: ZZ and SL; funding acquisition: ZZ, SL, HY, and CW; methodology: ZZ; project administration: ZZ and SL; resources: HZ and HY; supervision: ZZ, SL, and CW; writing—original draft: SL; writing—review and editing: ZZ and SL.

Funding

The study was supported by the National Key Research and Development Program of China (2018YFA0800801), the National Natural Science Foundation of China (NSFC) (81974123 and 81900807), and the Clinical Science and Technology Innovation Project of Shanghai Shenkang Hospital Development Center (SHDC12018120).

Acknowledgments

We are grateful to Genesky Biotechnologies Inc., (Shanghai) for its technical support and to the patients and their families for their participation in this study.

Conflict of interest

The authors declare that the research was conducted in the absence of any commercial or financial relationships that could be construed as a potential conflict of interest.

Publisher's note

References

Alanay, Y., and Lachman, R. S. (2011). A review of the principles of radiological assessment of skeletal dysplasias. *Jcrpe* 3 (4), 163–178. doi:10.4274/jcrpe.463

An, W. B., Liu, C., Wan, Y., Chang, L. X., Chen, X. Y., and Zhu, X. F. (2020). Clinical features and gene mutations of children with Shwachman-Diamond syndrome and malignant myeloid transformation. *Zhongguo Dang Dai Er Ke Za Zhi* 22 (5), 460–465. doi:10.7499/j.issn.1008-8830.2001133

Auer-Grumbach, M., Olschewski, A., Papić, L., Kremer, H., McEntagart, M. E., Uhrig, S., et al. (2010). Alterations in the ankyrin domain of TRPV4 cause congenital distal SMA, scapuloperoneal SMA and HMSN2C. *Nat. Genet.* 42 (2), 160–164. doi:10.1038/ng.508

Barat-Houari, M., Dumont, B., Fabre, A., Them, F. T., Alembik, Y., Alessandri, J. L., et al. (2016a). The expanding spectrum of COL2A1 gene variants IN 136 patients with a skeletal dysplasia phenotype. *Eur. J. Hum. Genet.* 24 (7), 992–1000. doi:10.1038/ejhg.2015.250

Barat-Houari, M., Sarrabay, G., Gatinois, V., Fabre, A., Dumont, B., Genevieve, D., et al. (2016b). Mutation update forCOL2A1Gene variants associated with type II collagenopathies. *Hum. Mutat.* 37 (1), 7–15. doi:10.1002/humu.22915

Boocock, G. R., Morrison, J. A., Popovic, M., Richards, N., Ellis, L., Durie, P. R., et al. (2003). Mutations in SBDS are associated with Shwachman-Diamond syndrome. *Nat. Genet.* 33 (1), 97–101. doi:10.1038/ng1062

Briggs, M. D., Hoffman, S. M., King, L. M., Olsen, A. S., Mohrenweiser, H., Leroy, J. G., et al. (1995). Pseudoachondroplasia and multiple epiphyseal dysplasia due to mutations in the cartilage oligomeric matrix protein gene. *Nat. Genet.* 10 (3), 330–336. doi:10.1038/ng0795-330

Chen, D. H., Sul, Y., Weiss, M., Hillel, A., Lipe, H., Wolff, J., et al. (2010). CMT2C with vocal cord paresis associated with short stature and mutations in the TRPV4 gene. *Neurology* 75 (22), 1968–1975. doi:10.1212/WNL.0b013e3181ffe4bb

Cho, T. J., Matsumoto, K., Fano, V., Dai, J., Kim, O. H., Chae, J. H., et al. (2012). TRPV4-pathy manifesting both skeletal dysplasia and peripheral neuropathy: A report of three patients. *Am. J. Med. Genet.* 158a (4), 795–802. doi:10.1002/ajmg.a.35268

Cormier-Daire, V. (2008). Spondylo-epi-metaphyseal dysplasia. *Best Pract. Res. Clin. Rheumatology* 22 (1), 33–44. doi:10.1016/j.berh.2007.12.009

Dalal, A., Bhavani G, G. S., Togarrati, P. P., Bierhals, T., Nandineni, M. R., Danda, S., et al. (2012). Analysis of theWISP3gene in Indian families with progressive pseudorheumatoid dysplasia. *Am. J. Med. Genet.* 158a (11), 2820–2828. doi:10.1002/ajmg.a.35620

Delague, V., Chouery, E., Corbani, S., Ghanem, I., Aamar, S., Fischer, J., et al. (2005). Molecular study ofWISP3 in nine families originating from the Middle-East and presenting with progressive pseudorheumatoid dysplasia: Identification of two novel mutations, and description of a founder effect. *Am. J. Med. Genet.* 138a (2), 118–126. doi:10.1002/ajmg.a.30906

Donadieu, J., Fenneteau, O., Beaupain, B., Beaufils, S., Bellanger, F., Mahlaoui, N., et al. (2012). Classification of and risk factors for hematologic complications in a French national cohort of 102 patients with Shwachman-Diamond syndrome. *Haematologica* 97 (9), 1312–1319. doi:10.3324/haematol.2011.057489

Echaniz-Laguna, A., Dubourg, O., Carlier, P., Carlier, R. Y., Sabouraud, P., Pereon, Y., et al. (2014). Phenotypic spectrum and incidence of TRPV4 mutations in patients with inherited axonal neuropathy. *Neurology* 82 (21), 1919–1926. doi:10.1212/wnl.0000000000000450

Everaerts, W., Nilius, B., and Owsianik, G. (2010). The vanilloid transient receptor potential channel TRPV4: From structure to disease. *Prog. Biophysics Mol. Biol.* 103 (1), 2–17. doi:10.1016/j.pbiomolbio.2009.10.002

Faye, E., Modaff, P., Pauli, R., and Legare, J. (2019). Combined phenotypes of spondylometaphyseal dysplasia-kozlowski type and charcot-marie-tooth disease type 2C secondary to a TRPV4 pathogenic variant. *Mol. Syndromol.* 10 (3), 154–160. doi:10.1159/000495778

Garcia Segarra, N., Mittaz, L., Campos-Xavier, A. B., Bartels, C. F., Tuysuz, B., Alanay, Y., et al. (2012). The diagnostic challenge of progressive pseudorheumatoid dysplasia (PPRD): A review of clinical features, radiographic features, and WISP3 mutations in 63 affected individuals. *Am. J. Med. Genet.* 160c (3), 217–229. doi:10.1002/ajmg.c.31333

Ginzberg, H., Shin, J., Ellis, L., Morrison, J., Ip, W., Dror, Y., et al. (1999). Shwachman syndrome: Phenotypic manifestations of sibling sets and isolated cases in a large patient cohort are similar. *J. Pediatr.* 135 (1), 81–88. doi:10.1016/s0022-3476(99)70332-x

Gkourogianni, A., Andrew, M., Tyzinski, L., Crocker, M., Douglas, J., Dunbar, N., et al. (2017). Clinical characterization of patients with autosomal dominant short stature due to aggrecan mutations. *J. Clin. Endocrinol. Metab.* 102 (2), 460–469. doi:10.1210/jc.2016-3313

Gleghorn, L., Ramesar, R., Beighton, P., and Wallis, G. (2005). A mutation in the variable repeat region of the aggrecan gene (AGC1) causes a form of spondyloepiphyseal dysplasia associated with severe, premature osteoarthritis. *Am. J. Hum. Genet.* 77 (3), 484–490. doi:10.1086/444401

Hauer, N. N., Sticht, H., Boppudi, S., Büttner, C., Kraus, C., Trautmann, U., et al. (2017). Genetic screening confirms heterozygous mutations in ACAN as a major cause of idiopathic short stature. *Sci. Rep.* 7 (1), 12225. doi:10.1038/s41598-017-12465-6

Hu, Q., Liu, J., Wang, Y., Wang, J., Shi, H., Sun, Y., et al. (2017). Delayed-onset of progressive pseudorheumatoid dysplasia in a Chinese adult with a novel compound WISP3 mutation: A case report. *BMC Med. Genet.* 18 (1), 149. doi:10.1186/s12881-017-0507-3

Huang, J. N., and Shimamura, A. (2011). Clinical spectrum and molecular pathophysiology of Shwachman-Diamond syndrome. *Curr. Opin. Hematol.* 18 (1), 30–35. doi:10.1097/MOH.0b013e32834114a5

Jędrzejowska, M., Dębek, E., Kowalczyk, B., Halat, P., Kostera-Pruszczyk, A., Ciara, E., et al. (2019). The remarkable phenotypic variability of the p.Arg269HiS variant in the TRPV4 gene. *Muscle Nerve* 59 (1), 129–133. doi:10.1002/mus.26346

Kerr, E. N., Ellis, L., Dupuis, A., Rommens, J. M., and Durie, P. R. (2010). The behavioral phenotype of school-age children with shwachman diamond syndrome indicates neurocognitive dysfunction with loss of Shwachman-Bodian-Diamond syndrome gene function. *J. Pediatr.* 156 (3), 433–438. doi:10.1016/j.jpeds.2009.09.026

Klein, C. J., Shi, Y., Fecto, F., Donaghy, M., Nicholson, G., McEntagart, M. E., et al. (2011). TRPV4 mutations and cytotoxic hypercalcemia in axonal Charcot-Marie-Tooth neuropathies. *Neurology* 76 (10), 887–894. doi:10.1212/WNL.0b013e31820f2de3

Koutsis, G., Lynch, D., Manone, A., Karadima, G., Reilly, M. M., Houlden, H., et al. (2015). Charcot-Marie-Tooth disease type 2C and scapuloperoneal muscular atrophy overlap syndrome in a patient with the R232C TRPV4 mutation. *J. Neurol.* 262 (8), 1972–1975. doi:10.1007/s00415-015-7800-x

Kuijpers, T. W., Alders, M., Tool, A. T., Mellink, C., Roos, D., and Hennekam, R. C. (2005). Hematologic abnormalities in shwachman diamond syndrome: Lack of genotype-phenotype relationship. *Blood* 106 (1), 356–361. doi:10.1182/blood-2004-11-4371

Landrum, M. J., Lee, J. M., Benson, M., Brown, G. R., Chao, C., Chitipiralla, S., et al. (2018). ClinVar: Improving access to variant interpretations and supporting evidence. *Nucleic Acids Res.* 46 (D1), D1062–d1067. doi:10.1093/nar/gkx1153

Li, H. (2009). Growth standardized values and curves based on weight, length/height and head circumference for Chinese children under 7 years of age. *Zhonghua Er Ke Za Zhi* 47 (3), 173–178.

Li, S. W., Prockop, D. J., Helminen, H., Fässler, R., Lapveteläinen, T., Kiraly, K., et al. (1995). Transgenic mice with targeted inactivation of the Col2 alpha 1 gene for collagen II develop a skeleton with membranous and periosteal bone but no endochondral bone. *Genes Dev.* 9 (22), 2821–2830. doi:10.1101/gad.9.22.2821

Liang, H., Hou, Y., Pang, Q., Jiang, Y., Wang, O., Li, M., et al. (2021). Clinical, biochemical, radiological, genetic and therapeutic analysis of patients with COMP gene variants. *Calcif. Tissue Int.* 110, 313–323. doi:10.1007/s00223-021-00920-6

Lin, L., Li, M., Luo, J., Li, P., Zhou, S., Yang, Y., et al. (2021). A high proportion of novel ACAN mutations and their prevalence in a large cohort of Chinese short stature children. *J. Clin. Endocrinol. Metab.* 106 (7), e2711–e2719. doi:10.1210/clinem/dgab088

Lv, S., Zhao, J., Xi, L., Lin, X., Wang, C., Yue, H., et al. (2021). Genetics evaluation of targeted exome sequencing in 223 Chinese probands with genetic skeletal dysplasias. *Front. Cell Dev. Biol.* 9, 715042. doi:10.3389/fcell.2021.715042

Madhuri, V., Santhanam, M., Rajagopal, K., Sugumar, L. K., and Balaji, V. (2016). WISP3 mutational analysis in Indian patients diagnosed with progressive pseudorheumatoid dysplasia and report of a novel mutation at p.Y198*. *Bone & Jt. Res.* 5 (7), 301–306. doi:10.1302/2046-3758.57.2000520

Mäkitie, O., Ellis, L., Durie, P. R., Morrison, J. A., Sochett, E. B., Rommens, J. M., et al. (2004). Skeletal phenotype in patients with Shwachman-Diamond syndrome and mutations in SBDS. *Clin. Genet.* 65 (2), 101–112. doi:10.1111/j.0009-9163.2004.00198.x

Miyoshi, K., Nakamura, K., Haga, N., and Mikami, Y. (2004). Surgical treatment for atlantoaxial subluxation with myelopathy in spondyloepiphyseal dysplasia congenita. *Spine* 29 (21), E488–E491. doi:10.1097/01.brs.0000143621.37688.f3

Mortier, G. R., Cohn, D. H., Cormier-Daire, V., Hall, C., Krakow, D., Mundlos, S., et al. (2019). Nosology and classification of genetic skeletal disorders: 2019 revision. *Am. J. Med. Genet.* 179 (12), 2393–2419. doi:10.1002/ajmg.a.61366

Myers, K. C., Bolyard, A. A., Otto, B., Wong, T. E., Jones, A. T., Harris, R. E., et al. (2014). Variable clinical presentation of shwachman-diamond syndrome: Update from the north American shwachman-diamond syndrome registry. *J. Pediatr.* 164 (4), 866–870. doi:10.1016/j.jpeds.2013.11.039

Myers, K. C., Furutani, E., Weller, E., Siegele, B., Galvin, A., Arsenault, V., et al. (2020). Clinical features and outcomes of patients with shwachman-diamond syndrome and myelodysplastic syndrome or acute myeloid leukaemia: A multicentre, retrospective, cohort study. *Lancet Haematol.* 7 (3), e238–e246. doi:10.1016/s2352-3026(19)30206-6

Nelson, A. S., and Myers, K. C. (2018). Diagnosis, treatment, and molecular pathology of shwachman-diamond syndrome. *Hematology/Oncology Clin. N. Am.* 32 (4), 687–700. doi:10.1016/j.hoc.2018.04.006

Nishimura, G., Lausch, E., Savarirayan, R., Shiba, M., Spranger, J., Zabel, B., et al. (2012). TRPV4-associated skeletal dysplasias. *Am. J. Med. Genet.* 160c (3), 190–204. doi:10.1002/ajmg.c.31335

Richards, S., Aziz, N., Bale, S., Bick, D., Das, S., Gastier-Foster, J., et al. (2015). Standards and guidelines for the interpretation of sequence variants: A joint consensus recommendation of the American College of medical genetics and genomics and the association for molecular pathology. *Genet. Med.* 17 (5), 405–424. doi:10.1038/gim.2015.30

Roughley, P. J., and Mort, J. S. (2014). The role of aggrecan in normal and osteoarthritic cartilage. *J. Exp. Ortop.* 1 (1), 8. doi:10.1186/s40634-014-0008-7

Sentchordi-Montané, L., Aza-Carmona, M., Benito-Sanz, S., Barreda- Bonis, A. C., Sánchez-Garre, C., Prieto-Matos, P., et al. (2018). Heterozygous aggrecan variants are associated with short stature and brachydactyly: Description of 16 probands and a review of the literature. *Clin. Endocrinol.* 88 (6), 820–829. doi:10.1111/cen.13581

Spranger, J. (1989). Radiologic nosology of bone dysplasias. *Am. J. Med. Genet.* 34 (1), 96–104. doi:10.1002/ajmg.1320340117

Stavber, L., Hovnik, T., Kotnik, P., Lovrečić, L., Kovač, J., Tesovnik, T., et al. (2020). High frequency of pathogenic ACAN variants including an intragenic deletion in selected individuals with short stature. *Eur. J. Endocrinol.* 182 (3), 243–253. doi:10.1530/eje-19-0771

Stenson, P. D., Mort, M., Ball, E. V., Chapman, M., Evans, K., Azevedo, L., et al. (2020). The human gene mutation database (HGMD): Optimizing its use in a clinical diagnostic or research setting. *Hum. Genet.* 139 (10), 1197–1207. doi:10.1007/s00439-020-02199-3

Terhal, P. A., van Dommelen, P., Le Merrer, M., Zankl, A., Simon, M. E., Smithson, S. F., et al. (2012). Mutation-based growth charts for SEDC and other COL2A1 related dysplasias. *Am. J. Med. Genet.* 160c (3), 205–216. doi:10.1002/ajmg.c.31332

Toiviainen-Salo, S., Mäkitie, O., Mannerkoski, M., Hämäläinen, J., Valanne, L., and Autti, T. (2008). Shwachman-Diamond syndrome is associated with structural brain alterations on MRI. *Am. J. Med. Genet.* 146a (12), 1558–1564. doi:10.1002/ajmg.a.32354

Wei, M., Ying, Y., Li, Z., Weng, Y., and Luo, X. (2021). Identification of novel ACAN mutations in two Chinese families and genotype-phenotype correlation in patients with 74 pathogenic ACAN variations. *Mol. Genet. Genomic Med.* 9 (11), e1823. doi:10.1002/mgg3.1823

Xu, Y., Li, L., Wang, C., Yue, H., Zhang, H., Gu, J., et al. (2020). Clinical and molecular characterization and discovery of novel genetic mutations of Chinese patients with col2a1-related dysplasia. *Int. J. Biol. Sci.* 16 (5), 859–868. doi:10.7150/ijbs.38811

Ye, J., Zhang, H. W., Qiu, W. J., Han, L. S., Zhang, Y. F., Gong, Z. W., et al. (2012). Patients with progressive pseudorheumatoid dysplasia: From clinical diagnosis to molecular studies. *Mol. Med. Rep.* 5 (1), 190–195. doi:10.3892/mmr.2011.619

Yu, Y., Hu, M., Xing, X., Li, F., Song, Y., Luo, Y., et al. (2015). Identification of a mutation in the WISP3 gene in three unrelated families with progressive pseudorheumatoid dysplasia. *Mol. Med. Rep.* 12 (1), 419–425. doi:10.3892/mmr.2015.3430

frontiers | Frontiers in Pediatrics

TYPE Case Report
PUBLISHED 18 November 2022
DOI 10.3389/fped.2022.975947

OPEN ACCESS

EDITED BY
Pelin Ozlem Simsek-Kiper,
Hacettepe University, Turkey

REVIEWED BY
Yen-Shan Chen,
Indiana University, Purdue University Indianapolis, United States
Santasree Banerjee,
Beijing Genomics Institute (BGI), China
Asmat Ullah,
University of Copenhagen, Denmark

*CORRESPONDENCE
Vanessa Romero
vromero@usfq.edu.ec

SPECIALTY SECTION
This article was submitted to Genetics of Common and Rare Diseases, a section of the journal Frontiers in Pediatrics

RECEIVED 22 June 2022
ACCEPTED 21 October 2022
PUBLISHED 18 November 2022

CITATION
Calvache CA, Vásquez EC, Romero VI, Hosomichi K and Pozo JC (2022) Novel SRY-box transcription factor 9 variant in campomelic dysplasia and the location of missense and nonsense variants along the protein domains: A case report.
Front. Pediatr. 10:975947.
doi: 10.3389/fped.2022.975947

Novel SRY-box transcription factor 9 variant in campomelic dysplasia and the location of missense and nonsense variants along the protein domains: A case report

Carlos A. Calvache[1], Estefanía C. Vásquez[1], Vanessa I. Romero[1]*, Kazuyoshi Hosomichi[2] and Juan C. Pozo[3]

[1]School of Medicine, Universidad San Francisco de Quito, Quito, Ecuador, [2]Department of Bioinformatics and Genomics, Kanazawa University, Kanazawa, Japan, [3]School of Medicine, Universidad de Cuenca, Cuenca, Ecuador

Background: Campomelic dysplasia (CD) is a rare disorder that involves the skeletal and genital systems. This condition has been associated with a diverse set of mutations in the SRY-box transcription factor 9 (*SOX9*) gene.
Case presentation: We herein report a case involving a 4-year-old female patient with CD, female sex reversal, type 1 Arnold–Chiari malformation, and bilateral conductive hearing loss and investigate the causal mutation. Whole-exome sequencing analysis detected a novel Trp115X* variant in the *SOX9* gene. We performed a literature review of the reported cases and demonstrated that the missense variants were located only in the self-dimerization domain (DIM) and high-mobility group box domains. We also reported that variants in the DIM domain do not cause sex reversal and identified that the amino acid sequences that were mutated in the patients with campomelic dysplasia are evolutionarily conserved among primates.
Conclusions: We suggest that missense variants cannot be located in the K2, PQA, and PQS given that these domains function critically for transcriptional activation or repression of target genes and evolve under purifying selection.

KEYWORDS

campomelic dysplasia, high-mobility group box (HMG), self-dimerization domain (DIM), SOX9 gene, Ecuador

Background

Campomelic dysplasia (CD) belongs to the group of almost lethal prenatal skeletal dysplasia, causing abnormalities during bone and sexual development and heart, respiratory, and neurological malformations (1). Mutations in the SRY-box transcription factor 9 (*SOX9*) gene have been associated with CD. We herein report a novel nonsense variant in a child with CD, sex reversal, and Arnold–Chiari malformation type I and discovered that missense variants were located in the self-dimerization domain (DIM) and high-mobility group box (HMG) domains. Further,

we found that no sex reversal when variants were located in the DIM domain, and that the missense variants were limited to humans.

CD is an autosomal dominant skeletal dysplasia that is primarily and clinically characterized by micrognathia, cleft palate, small chest, shortened long-type bones, scapular hypoplasia, clubfoot, and complete sex reversal or ambiguous genitalia. In fact, around one-third of affected men show complete sexual feminization or a degree of ambiguous genitalia. This condition is usually fatal in the perinatal period and has been associated with high postnatal mortality rates due to respiratory failure (2), with mortality rates reaching 77% in the first month and 90% by the second year (3). The main clinical differential diagnosis includes osteogenesis imperfecta, kyphomelic syndrome, thanatophoric dysplasia, mesomelic dysplasia, and Cummings syndrome (3).

SOX gene is the only causal gene for CD. The protein produced by this gene is a transcription factor involved in chondrogenesis that promotes cartilage-specific extracellular matrix components, regulates other SOX family genes, and plays a key role in the development of the endochondral skeleton and male sexual differentiation (4). *SOX9* domains include an HMG domain, a DIM domain, and three transactivation domains (TAD), namely K2, PQA, and PQS. The HMG box creates a twisted L-shaped structure that binds to the minor groove of the DNA. DIM has a dimerization function and directly influences the transactivation activity. The DIM and TAD domains function in the transcriptional regulation of pathways involving *SOX9*. TADs control the transcriptional machinery by mediating protein–protein interactions. K2 and PQS are critical for the appropriate transcriptional activation or repression of target genes. PQA, which is exclusive to mammals, enhances PQS transactivation activity, is unable to activate transcription alone, and is associated with the SRY sex-determining mechanism (5). Most pathological variants are *de novo*; however, there are a few parental germline mosaic cases (2).

This report described a case involving a female patient with skeletal dysplasia in whom whole-exome sequencing (WES) in trio analysis detected a novel nonsense variant, reviewed published cases, determined the locations of the reported variants along the gene domains, and compared the variants with other primates.

Case presentation

Our case involves a 4-year-old patient assigned as female at birth who visited the genetic outpatient clinic for ambiguous genitalia and skeletal dysplasia. She was born *via* cesarean delivery from non-consanguineous parents and had a cleft palate, which was corrected at 4 months. The girl had a moderate developmental delay characterized by being able to stand at 1 year of age and walk at 3 years of age after constant physiotherapy. Physical examination of the head revealed trigonocephaly, a protruding frontal region, almond-shaped eyes with antimongoloid deviation, a flat nasal bridge, a long philtrum, retromicrognathia, and a short neck. Radiography of the head revealed a vertebral fusion between C5 and C6 (**Figure 1**). We observed limb malformations, including prominent hips, shortening of the right lower limb, valgus knees, and rhizomelic arms (**Table 1**). Radiography of the limbs revealed femur bowing, an underdeveloped acetabulum, and a femoral head. At birth, the physicians described the appearance of external female genitalia. Abdominal ultrasonography revealed ovaries, a small uterus, and shortened vagina. Hormone analysis showed increased testosterone, luteinizing hormone, and follicle-stimulating

FIGURE 1
Radiography and computed tomography of the legs, hip, and spine showing femoral, tibial, and fibular bowing, hip rotation, and an abnormal spine curvature.

TABLE 1 Clinical features of the nonsense and missense variants in reported cases.

Nonsense variants	E28X	59X (C155bp)	59X (C155bp)	W86X	261-262insG	W115X	Q117X	Y319X	Q375X	Q391X	R394X	E400X	Q412X	Ser438X	Y440X	Y440X	Y440X	Q458X
General Features																		
'Intellectual disability						X	X									X		
Short stature			X			X					X		X					X
Facial Features																		
Flat face			X		X				X			X	X	X		X	X	X
Macrocephaly		X										X				X		
Depressed nasal bridge		X	X		X	X								X	X	X	X	
Hypertelorism														X				
Low-set ears				X	X				X									
Long philtrum			X															
Cleft palate	X				X				X			X				X	X	
Micrognathia		X	X			X		X				X		X	X	X	X	
Retrognathia	X													X	X	X		
Bone malformation																		
Spinal dysraphism									X	X							X	X
Hypoplastic scapula	X	X	X	X				X	X			X			X			
Bell Shaped Thorax															X		X	
Bowing of the bones	X	X	X	X	X	X	X	X	X	X	X	X		X	X	X	X	
Dislocation of radial head/hip		X												X				
Hypoplastic patellae																		
Respiratory																		
Tracheobronchomalacia														X			X	
Hypoplastic Lungs																		
Respiratory Distress		X		X	X				X			X		X	X			
Neurological																		
Abnormal Brain Convolutions			X															
Hypoplastic of Corpus Collosum						X												
Ventriculomegaly						X												

(*continued*)

10.3389/fped.2022.975947

TABLE 1 Continued

Nonsense variants	E28X	59X (C155bp)	59X (C155bp)	W86X	261-262insG	W115X	Q117X	Y319X	Q375X	Q391X	R394X	E400X	Q412X	Ser438X	Y440X	Y440X	Y440X	Q458X
Absence of the Olfactory Bulbs																	X	
Cardiovascular																		
Abnormalities																		
Renal																		
Hydronephrosis					X												X	X
Other Renal Abnormalities					X				X									X
Status																		
Abortion	14 weeks							21 weeks		20 weeks	14 weeks		14 weeks					27 weeks
Death		Day 1		Day 12					Week 7			Week 10			Month 3			
Last reported age			18 years		39 weeks gestation	4 years	12 years							Newborn		11 years	4 years	
Reproductive system																		
Sex Reversal						X	X		X						X			
External genitalia	Male	Female	Female	Female	Male	Female	Male	Female	Female	Unknown	Female	Male	Unknown	Male	Female	Female	Male	Female
karyotype	XY	XX	XX	XX	ND	XY	XX	XX	XY	ND	XX	XY	ND	XY	XY	XX	XY	XX
Others																		
Hearing Impairment			X			X	X								X	X		
Protein domain	DIM	DIM	DIM	DIM	DIM	HMG	HMG		PQA				PQS	PQS	PQS	PQS	PQS	PQS

	Missense variants																		
	H65Y	A76E	Q79P	V80G	P108L	F112S	M113V	119 (C358bp)	A119V	W143R	R152P	F154L	A158T	A158V	H165Q	H169Q	H169P	P170L	P170L	P170R
General Features																				
Intellectual disability	X			X					X									X	X	
Short stature									X					X				X	X	
Facial Features																				
Flat face					X		X	X	X				X				X		X	X
Macrocephaly	X									X			X	X				X		

(*continued*)

10.3389/fped.2022.975947

TABLE 1 Continued

Nonsense variants	E28X		59X (C155bp)	59X (C155bp)	W86X	261-262insG	W115X	Q117X	Y319X	Q375X	Q391X	R394X	E400X	Q412X	Ser438X	Y440X	Y440X	Y440X	Q458X
Depressed nasal bridge	X										X		X			X	X		
Hypertelorism	X		X								X		X				X		
Low-set ears	X		X		X				X		X		X	X			X	X	X
Long philtrum													X						
Cleft palate	X	X	X	X	X		X	X				X		X	X			X	X
Micrognathia	X		X	X			X	X			X		X	X	X				X
Retrognathia							X									X	X		X
Bone malformations																			
Spinal dysraphism							X			X									
Hypoplastic scapula	X	X			X	X	X	X	X				X	X					X
Bell Shaped Thorax				X			X							X					
Bowing of the bones	X		X	X	X	X		X		X	X	X	X		X	X	X	X	X
Dislocation of radial head/hip	X			X			X							X					
Hypoplastic patellae	X																		
Respiratory																			
Tracheobronchomalacia	X		X	X	X		X		X										
Hypoplastic Lungs														X					
Respiratory Distress	X					X							X				X		
Neurological			X																
Abnormal Brain Convolutions																			
Hypoplastic of Corpus Collosum			X																
Ventriculomegaly																			
Absence of the Olfactory Bulbs																			
Cardiovascular																			
Cardiovascular Abnormalities			X	X														X	
Renal																			

(*continued*)

10.3389/fped.2022.975947

TABLE 1 Continued

Nonsense variants	E28X		59X (C155bp)	59X (C155bp)	W86X	261-262insG	W115X	Q117X	Y319X	Q375X	Q391X	R394X	E400X	Q412X	Ser438X	Y440X	Y440X	Y440X	Q458X
Hydronephrosis																			
Other Renal Abnormalities							X												
Status																			
Abortion or death							Week 21									Week 20			
Death				Month 6					Month 5	Day 2	Day 1								Month 1
Last reported age	11 years	6 years	1.5 years	2 years 2 months	Newborn	Newborn		Newborn				19 years	Newborn	Newborn	10 years		21 years	15 years	
Reproductive system																			
Sex Reversal				X					X			X							
External genitalia	Male	Male	Male	Female	Female	Male	Female	ND	Male	Female	Female	Female	Female	Female	Male	Male	Male	Female	Female	Male
Karyotype	XY	XY	XY	XX	XY	XY	XX	ND	XY	XY	XX	XX	XY	XX	XY	XY	XY	XX	XX	XY
Others																			
Hearing Impairment			X	X													X	X	
Protein domain	DIM	DIM	DIM	DIM	HMG	HMG	HMG	HMG	HMG	HMG	HMG	HMG	HMG	HMG	HMG	HMG	HMG	HMG	HMG	HMG

ND, not described; Blank, not reported on the paper.

10.3389/fped.2022.975947

hormone levels. A peripheral blood karyotype reported a 46XY with a positive SRY gene. Brain magnetic resonance imaging showed Arnold–Chiari malformation type 1 (**Supplementary Figure S1**). Moreover, she had moderate conductive bilateral hearing loss, which was corrected with hearing aids (**Supplementary Figure S2**). Written informed consent was obtained from the parents to perform WES given that this analysis is not covered by the public health system.

We used a capture of target regions using probes, followed by next-generation sequencing with Illumina technology. The total number of reads was 41,660,733, whereas that of the mapped reads was 41,603,016 (99.86%). We aligned the raw data using the Burrows–Wheeler Aligner software, sorted and merged the data using the Picard tools software, and identified the nucleotide variants (SNV) and insertions or deletions (indel) using GATK. The GRCh37 version of the human genome was taken as reference.

After performing WES on the mother, father, and patient, we identified 1,582 variants causing non-synonymous, stop-gain, and frameshift changes; selected those with minor allele frequency (<0.01) in various databases; filtered variants unique to the daughter and absent in the parents; and detected one nonsense heterozygote variant in the *SOX9* gene of the patient. We sequenced only the *SOX9* gene and confirmed the variant. The pathogenic variant was caused by a guanine to adenine change at the 344 bp (c.G344A), resulting in a tryptophan to a premature stop codon change at position 115 (p.Trp115*) of the HMG domain. The frequency of this variant was 0 in the Genome Aggregation Database and Exome Aggregation Consortium databases and was not reported in the Ensembl genome and ClinVar databases. The parents did not have the nonsense variant and were homozygous for the reference allele (G). To the best of our knowledge, no genes have been previously associated with Arnold–Chiari malformation type I.

We subsequently performed a literature review on CD and found 115 reported cases. Thereafter, we filtered the cases with nonsense and missense variants and excluded translocations and papers that did not include the description of the mutation. The results after correlating the variant location with the domains along the gene are shown in **Figure 2** and **Supplementary Table S1**. The final number of research articles included 18 nonsense and 20 missense cases. Although variants p.Asn147Thr, p.Arg121*, and p.Glu134* were mentioned in review articles, no clinical description was provided.

Our literature review (**Supplementary Table S1**) revealed that missense variants were located at the beginning of *SOX9*, with 4 located in the DIM and 12 in the HMG domains. There was no missense variant in the K2, PQA, and PQS domains. There were no reported cases of sex reversal with mutations in the DIM domain, but three cases with mutations in the HMG domains exhibited sex reversal. The reported missense cases shared facial features and bone malformations. Three of these patients had cardiovascular malformations. Premature death did not occur in patients with DIM mutations, unlike those with HMG mutations who died during the first months of life. The oldest reported individual was a 21-year-old woman.

Nonsense variants were located along the whole *SOX9* gene, with three in the DIM, four in the HMG, one in the PQA, and four in the PQS domain. The mutation in our patient was localized in the HMG domain. Four mutations (Tyr319*, Gln391*, Arg394*, and Glu400*) did not occur on a

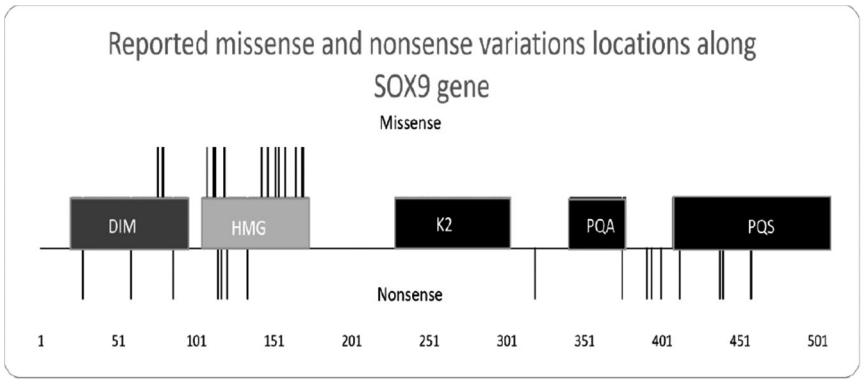

Missense	Domain	Nonsense	Domain
p.His65Tyr	DIM	p.Glu28X	DIM
p.Ala76Glu	DIM	p. 59X	DIM
p.Gln79Pro	DIM	p.Trp86X	DIM
p.Val80Gly	DIM	p.Trp115X	HMG
p.Pro108Leu	HMG	p.Gln117X	HMG
p.Phe112Ser	HMG	p.Arg121X	HMG
p.Met113Val	HMG	p.Glu134X	HMG
p.Ala119Val	HMG	p.Tyr319X	
p.Trp143Arg	HMG	p.Gln375X	PQA
p.Asn147Thr	HMG	p.Gln391X	
p.Arg152Pro	HMG	p. Arg394X	
p.Phe154Leu	HMG	p.Glu400X	
p.Ala158Thr	HMG	p.Gln412X	PQS
p.His165Gln	HMG	p.Ser438X	PQS
p.His169Pro	HMG	p.Tyr440X	PQS
p.Pro170Arg	HMG	p.Gln458X	PQS

FIGURE 2
Graphic description of the *SOX* gene variant. We identified 115 cases of campomelic dysplasia, determined the amino acid variant (right side), and constructed a visual representation of the variant along *SOX9* (left side). Missense variants are the lines over the image, whereas nonsense variants are the lines below the image. Missense variants are limited from amino acids 76 to 170. Ala = alanine, arg = arginine, asn = asparagine, asp = aspartic acid, asx = asparagine or aspartic acid, cys = cysteine, glu = glutamic acid, gln = glutamine, glx = glutamine or glutamic acid, gly = glycine, his = histidine, ile = isoleucine, leu = leucine, lys = lysine, met = methionine, phe = phenylalanine, pro = proline, ser = serine, thr = threonine, trp = tryptophan, tyr = tyrosine, val = valine. The *SOX9* domains include a high-mobility group box (HMG) (gray box), self-dimerization domain (DIM) (dark gray box), and three transactivation domains (TAD), namely K2, PQA, and PQS. Black box includes the reported case.

functional domain and could alter the protein structure. There was no nonsense variant in the K2 domain. The reported nonsense cases shared facial features and bone malformations. Our patient, along with two others, had neurological malformations. Most patients died during gestation or the postnatal period or were aborted by the mothers. The oldest reported individual was an 18-year-old woman. There were no reported cases of sex reversal with mutations in the DIM, whereas two cases with mutations in the HMG, one with mutations in the PQA, and one with mutations in the PQS domains exhibited sex reversal. From the information provided in the reported cases, respiratory and cardiovascular malformations were more common in missense than in nonsense variants.

We considered that the variant causing CD develops only in humans given that *SOX9* alters essential functions during development. There were no reported cases of primates with phenotypes such as CD. We compared and aligned a normal human sequence and all missense variants with *SOX9* from chimpanzees (*Pan troglodytes* NC_036896.1), orangutans (*Pongo abelii* NC_036920.1), gorillas (*Gorilla* NC_044619.1), rhesus monkeys (*Macaca mulatta* NC_041770.1), and house mice (*Mus musculus* NC_000083.7). The protein alignment confirmed that the *SOX* gene was highly preserved between species (similarity between 96.45% and 100%, as described in **Supplementary Figure S3**) and that no other species had the missense or nonsense variants (**Supplementary Figures S4A,B**) (6, 7).

Discussion and conclusion

CD results from missense, nonsense, frameshift, or splice site loss-of-function mutations in one of the three *SOX9* exons (2). *SOX9* is a transcription factor during chondrogenesis that promotes cartilage-specific extracellular matrix components and regulates other SOX family members. We performed WES in trio analysis, which revealed a Trp115* novel variant, conducted a literature review of the reported cases, located the variants along *SOX9* domains, and compared the variants with other primates to determine the conservation (**Supplementary Table S2**).

Our patient presented with skeletal dysplasia, characteristic facial features, and sex reversal. Compared to other cases, she did not exhibit cardiovascular and respiratory abnormalities, which are the main causes of premature death (8). However, she is the first reported case of CD and Arnold–Chiari malformation type 1. The oldest reported nonsense survivor was still alive at 18 years of age (3). Although the reason for the patient's survival was not described in the publication, we believe that it may be attributed to the lack of respiratory and cardiovascular defects, such as tracheobronchomalacia and laryngomalacia (3).

Missense variants are located at the DIM and HMG domains, which are the most conserved between species. The reported missense variant was not located in the K2, PQA, and PQS, which are domains that evolve under purifying selection and sweep away deleterious mutations. The missense and nonsense variants were not between the 66–75 residues of the DIM that interacts with the promoter activation of *Amh*, which is a sex-determining gene that requires only a *SOX9* monomer for its activation. Cases with DIM mutations showed no sex reversal. The HMG box is highly conserved with a significant constraint due to its binding pattern, and mutations reduce the DNA binding affinity (9). Mutations in the DIM domain decrease the dimerization and cease or reduce the transactivation activity for chondrogenic and sex-determining genes without altering other domain functions. We suggest that the lack of missense variants in the K2, PQA, and PQS domains was associated with the critical function during transcriptional activation or repression of target genes or that a single missense variant in the K2, PQA, and PQS domains could be responsible for the CD phenotype when the DIM or HMG domains are intact (5). Moreover, the K2 and PQS domains have evolved under purifying selection and have a relaxed selective pressure (primarily K2), reflecting a higher fixation of mutations (5).

Previous studies have reported that nonsense mutations in the DIM and HMG (64 to 181 aa) present a classical type of CD with a reduced amount of *SOX9*. Cases with DIM mutations showed no sex reversal. Nonsense variants between the K2 and PQA (228 to 401 aa) have more truncated proteins, which escape the nonsense-mediated decay and have a dominant-negative effect. In contrast, the variant along the PQS (402–509 aa) produces a truncated protein but leaves a longer fraction of the TA domain, resulting in a lower transactivation effect and allowing patients to survive for several years (2). Meyer in 1997 reported 12 cases of CD and concluded no phenotype/genotype correlation, although 3 out of the 12 patients were not found to have variants in *SOX9* and gene sequencing was not available. However, not all *SOX9* domains had been identified in 1997, and Meyer suggested the need for a larger sample and research on the residual transactivation activity of a mutant *SOX9* protein. Gene sequencing can be beneficial for detecting point mutations that cause CD. Our study is the first to review the literature that analyzes all reported cases, associates these cases with the functional domains, and agrees with Meyer regarding the phenotype variability and residual activity of mutant *SOX9* (10).

One limitation of the current study was our use of information provided by the articles and not that obtained from the concerned patients. Furthermore, we did not conduct protein quantification in our patient considering that the pathology could have resulted from either a null protein or dominant-negative protein.

SOX9, which binds to response elements of target genes as a homodimer or monomer to activate or repress the transcriptional machinery, has been associated with CD—a rare disorder that involves the skeletal and genital systems. Our study described the first case of CD with Arnold–Chiari type malformation 1 (Trp115*) and found that the reported missense variants were located between amino acids 76–170 in the DIM and HMG domains, Further, we discovered that variants in the DIM domain had no sex reversal and that the mutated amino acid sequences in the human patients with CD were evolutionarily conserved among primates.

Data availability statement

The datasets for this article are not publicly available due to concerns regarding participant/patient anonymity. Requests to access the datasets should be directed to the corresponding author.

Ethics statement

Written informed consent for publication of identifying images or other personal or clinical details was obtained from the parents of the patient. The studies involving human participants were reviewed and approved by the Universidad San Francisco de Quito Ethics Committee. Written informed consent to participate in this study was provided by the participants' legal guardian/next of kin.

Author contributions

CC: performed the literature review, analyzed the WES results, and drafted the manuscript. EV: performed the literature review, analyzed the WES results, and drafted the manuscript. VR: contacted the patient, provided genetic counseling, performed the literature review, analyzed the WES results, and drafted the manuscript. KH: performed the WES analysis. JP: contacted the patient and provided genetic counseling. All authors contributed to the article and approved the submitted version.

Acknowledgments

We would like to thank all individuals who prompted us to conduct this review. We are grateful to our families who have consistently provided us with the necessary support to reach our goals. Finally, we cannot fail to thank the university and the teachers who provided us with the necessary information and equipment to complete this review. The publication of this article was funded by the Academic Articles Publication Fund of Universidad San Francisco de Quito USFQ.

Conflict of interest

The authors declare that the research was conducted in the absence of any commercial or financial relationships that could be construed as a potential conflict of interest.

Publisher's note

Supplementary material

The Supplementary Material for this article can be found online at: https://www.frontiersin.org/articles/10.3389/fped.2022.975947/full#supplementary-material.

References

1. Kumar M, Thakur S, Haldar A, Anand R. Approach to the diagnosis of skeletal dysplasias: experience at a center with limited resources. *J Clin Ultrasound*. (2016) 44(9):529–39. doi: 10.1002/jcu.22371. Available at: https://pubmed.ncbi.nlm.nih.gov/27218215/

2. Csukasi F, Duran I, Zhang W, Martin JH, Barad M, Bamshad M, et al. Dominant-negative SOX9 mutations in campomelic dysplasia. *Hum Mutat*. (2019) 40(12):2344–52. doi: 10.1002/humu.23888. Available at: https://pubmed.ncbi.nlm.nih.gov/31389106/

3. Jain V, Sen B. Campomelic dysplasia. *J Pediatr Orthop B*. (2014) 23(5):485–8. doi: 10.1097/BPB.0000000000000058. Available at: https://pubmed.ncbi.nlm.nih.gov/24800790/

4. Lefebvre V, Dvir-Ginzberg M. SOX9 And the many facets of its regulation in the chondrocyte lineage. *Connect Tissue Res*. (2017) 58(1):2–14. doi: 10.1080/03008207.2016.1183667. Available at: https://www.tandfonline.com/doi/abs/10.1080/03008207.2016.1183667

5. Geraldo MT, Valente GT, Nakajima RT, Martins C. Dimerization and transactivation domains as candidates for functional modulation and diversity of Sox9. *PLos One*. (2016) 11(5):e0156199. doi: 10.1371/journal.pone.0156199. Available at: https://journals.plos.org/plosone/article?id=10.1371/journal.pone.0156199

6. Sievers F, Wilm A, Dineen D, Gibson TJ, Karplus K, Li W, et al. Fast, scalable generation of high-quality protein multiple sequence alignments using clustal

omega. *Mol Syst Biol*. (2011) 7. doi: 10.1038/msb.2011.75. Available at: https://pubmed.ncbi.nlm.nih.gov/21988835/:539

7. Saitou N, Nei M. The neighbor-joining method: a new method for reconstructing phylogenetic trees. *Mol Biol Evol*. (1987) 4(4):406–25. doi: 10.1093/oxfordjournals.molbev.a040454

8. Mortier GR, Cohn DH, Cormier-Daire V, Hall C, Krakow D, Mundlos S, et al. Nosology and classification of genetic skeletal disorders: 2019 revision. *Am J Med Genet A*. (2019) 179(12):2393–419. doi: 10.1002/ajmg.a.61366. Available at: https://pubmed.ncbi.nlm.nih.gov/31633310/

9. Jo A, Denduluri S, Zhang B, Wang Z, Yin L, Yan Z, et al. The versatile functions of Sox9 in development, stem cells, and human diseases. *Genes Dis*. (2014) 1(2):149–61. doi: 10.1016/j.gendis.2014.09.004

10. Meyer J, Südbeck P, Held M, Wagner T, Schmitz ML, Bricarelli FD, et al. Mutational analysis of the SOX9 gene in campomelic dysplasia and autosomal sex reversal: lack of genotype/phenotype correlations. *Hum Mol Genet*. (1997) 6(1):91–8. doi: 10.1093/hmg/6.1.91. Available at: https://academic.oup.com/hmg/article/6/1/91/2357160

frontiers | Frontiers in Genetics

TYPE Mini Review
PUBLISHED 25 November 2022
DOI 10.3389/fgene.2022.996364

OPEN ACCESS

EDITED BY
Yi Zhang,
Xiangya Hospital, Central South University, China

REVIEWED BY
Lianlei Wang,
Peking Union Medical College Hospital (CAMS), China
Yunjia Wang,
Xiangya Hospital, Central South University, China

*CORRESPONDENCE
Muhammad Umair,
khugoo4u@yahoo.com,
umairmu@ngha.med.sa

SPECIALTY SECTION
This article was submitted to Genetics of Common and Rare Diseases, a section of the journal Frontiers in Genetics

RECEIVED 17 July 2022
ACCEPTED 31 October 2022
PUBLISHED 25 November 2022

CITATION
Umair M, Younus M, Shafiq S, Nayab A and Alfadhel M (2022), Clinical genetics of spondylocostal dysostosis: A mini review.
Front. Genet. 13:996364.
doi: 10.3389/fgene.2022.996364

Clinical genetics of spondylocostal dysostosis: A mini review

Muhammad Umair[1]*, Muhammad Younus[2], Sarfraz Shafiq[3], Anam Nayab[4] and Majid Alfadhel[1,5]

[1]Medical Genomics Research Department, Ministry of National Guard Health Affairs (MNGH), King Abdullah International Medical Research Center (KAIMRC), King Saud Bin Abdulaziz University for Health Sciences, Riyadh, Saudi Arabia, [2]State Key Laboratory of Membrane Biology and Beijing Key Laboratory of Cardiometabolic Molecular Medicine, Institute of Molecular Medicine, College of Future Technology and Peking-Tsinghua Center for Life Sciences and PKU-IDG/McGovern Institute for Brain Research, Peking University, Beijing, China, [3]Department of Anatomy and Cell Biology, University of Western Ontario, London, ON, Canada, [4]Department of Biotechnology, Fatima Jinnah Women University, Rawalpindi, Pakistan, [5]Genetics and Precision Medicine Department, King Abdullah Specialized Children Hospital (KASCH), King Abdulaziz Medical City, Ministry of National Guard Health Affairs (MNG-HA), Riyadh, Saudi Arabia

Spondylocostal dysostosis is a genetic defect associated with severe rib and vertebrae malformations. In recent years, extensive clinical and molecular diagnosis advancements enabled us to identify disease-causing variants in different genes for such severe conditions. The identification of novel candidate genes enabled us to understand the developmental biology and molecular and cellular mechanisms involved in the etiology of these rare diseases. Here, we discuss the clinical and molecular targets associated with spondylocostal dysostosis, including clinical evaluation, genes, and pathways involved. This review might help us understand the basics of such a severe disorder, which might help in proper clinical characterization and help in future therapeutic strategies.

KEYWORDS

Spondylocostal dysostosis, SCDO, Genetic skeletal disorders, SCDO1-7, Notch-signaling pathway

1 Introduction

The spondylocostal dysostosis (SCDO), a subclass of a Jarcho–Levin syndrome, represents a rare heritable group of genetic disorders. SCDO is characterized by congenital defective vertebral segmentation and rib deformation due to imperfect alignments, fusion, or reduction in numbers. The patient often presents with a short trunk and scoliosis (Solomon et al., 1978; Mortier et al., 1996; Gucev et al., 2010). SCDO can be characterized as familial or sporadic because of its autosomal recessive and dominant inheritance pattern (Turnpenny et al., 1993). SCDO is generally inherited as an autosomal recessive trait due to mutations of the genes that are involved in the Notch-signaling pathway such as Delta-like canonical Notch ligand 3 (*DLL3*) (Bulman et al., 2000), mesoderm posterior protein 2 (*MESP2*) (Whittock et al., 2004a; Whittock et al., 2004b), *LFNG* (Sparrow et al., 2006), and *HES7* genes (Sparrow et al., 2008). Patients with familial SCDO clinically present with the most common symptoms such as anal and urogenital anomalies, congenital heart disease, limb abnormalities, plagiocephaly-torticollis

TABLE 1 Spondylocostal dysostosis-associated genes, associated clinical representation, and function in the Notch-signaling pathway.

S.No	Gene	Disease	Clinical features observed	Function	Reference
1	*DLL3* (OMIM 602768)	Spondylocostal dysostosis 1 (OMIM 277300)	Dwarfism, respiratory infection, short trunk, rib anomalies, and vertebral fusion	Encodes Delta proteins which functions as Notch ligands and inhibits signaling	Kusumi et al. (2004)
2	*MESP2* (OMIM 605195)	Spondylocostal dysostosis 2 (OMIM 608681)	Disproportionate short stature, fusion of ribs at costovertebral junction, angular vertebrae, vertebral clefts, and sickle-shaped vertebrae	Encodes proteins, basically transcription factors that belong to the bHLH family. It plays an important role in the somite formation *via* interactions with Notch-signaling pathways	Whittock et al. (2004b)
3	*LFNG* (OMIM 602576)	Spondylocostal dysostosis 3 (OMIM 609813)	Short stature, fused ribs, multiple vertebral anomalies, kyphosis, and scoliosis	Encodes a glycosyltransferase, that is, involved in Notch1 receptor signaling *via* post-translational modification of Notch receptors	Sparrow et al. (2006)
4	*HES7* (OMIM 608059)	Spondylocostal dysostosis 4 (OMIM 613686)	Short stature, dextrocardia, cardiovascular anomalies, restrictive ventilatory defect, ribs anomalies, and fusion	Encodes a transcriptional repressor protein which helps in accurate modeling of axial skeleton. It belongs to the hairy and enhancer of split family of bHLH transcription factors. This gene is regulated by Notch signaling	Sparrow et al. (2008)
5	*TBX6* (OMIM 602427)	Spondylocostal dysostosis 5	Disproportionate short stature, fusion of ribs, ribs anomalies, extra or missing ribs, scoliosis, and butterfly vertebrae	Encodes a T-box transcription factor which helps in activating the *MESP2* and *DLL1* gene expression that are key to the regulation of developmental processes It belongs to a conserved gene family that has a common T-box and a DNA-binding domain	Wu et al. (2015)
6	*RIPPLY2* (OMIM 609891)	Spondylocostal dysostosis 6 (OMIM 616566)	Spinal canal stenosis, absence of posterior elements of upper cervical vertebrae, hemi-vertebrae in cervical and thoracic spine, cervical kyphosis, thoracic scoliosis, and spinal cord compression	It encodes a nuclear protein essential for the vertebrate somitogenesis. It acts as a transcriptional repressor protein by interacting with the transcriptional repressor Groucho and a carboxy-terminal RIPPLY homology domain *via* a tetrapeptide WRPW motif. Mutant mice models displays defective somitogenesis	McInerney-Leo et al. (2015)
7	*DLL1* (OMIM 606582)	Spondylocostal dysostosis 7	Kyphosis, scoliosis, delayed development, cortical dysplasia, mall cerebellum, and autistic features	Encodes *DLL1* which is a human homolog of the Notch Delta ligand and has an important role in mediating cell fate decisions during hematopoiesis. Its related pathways involve signaling by Notch1 and Notch2 activation and transmission of signal to the nucleus	Barhoumi et al. (2019)

deformity sequence, diaphragmatic hernia, and neuronal tube defects (in males) (Cetinkaya et al., 2008), while patients with sporadic SCDO present with a wide variety of symptoms such as asymmetrical thoracic region and scoliosis (Mortier et al., 1996). Numerous sporadic SCDO cases have been reported with VATER, VACTERL, and MURCS associations along with DiGeorge, Alagille, and Robinow syndromes. Associations with an intellectual disability and other abnormal neurological syndromes are unusual (Turnpenny et al., 2009; Turnpenny et al., 2017).

In the present review, we have classified spondylocostal dysostosis based on gene identification and associated clinical phenotypes. A total of 185 and 284 entries were obtained using the mesh "spondylocostal dysostosis" in the OMIM and PubMed (NCBI). They include both syndromic and non-syndromic spondylocostal dysostosis. Autosomal recessive spondylocostal dysostoses have been classified into seven types and are presented in Table 1, which might be helpful for researchers and clinicians to have a quick overview of the disorder, help in molecular diagnosis, and further management plans.

1.1 Clinical description

Patients with SCDO have short trunks relative to their height, a short neck, and often present with thoracic insufficiency and mild to severe non-progressive scoliosis. Neonates often clinically present with mild to moderate respiratory insufficiency due to a smaller thorax. Neonatal lung growth may improve by the age of 2 years, which supports their normal growth and development. Such patients can survive but are at a higher risk of life-threatening complications such as pulmonary hypertension. Male patients with SCDO may be at a higher risk of inguinal hernia (Turnpenny et al., 2017).

1.2 Classification

SCDO is classified into seven types based on pathogenic mutations in different genes (Table 1). Autosomal recessive SCDO is isolated in nature, and is confined to the vertebrae

TABLE 2 Mutations reported to date in genes associated with spondylocostal dysostosis (HGMD® Professional 2022.2).

Number of mutation	Gene name	cDNA	Protein	Phenotype	Types of mutation
1	*DLL3*	c.150C>A	p.C50*	Spondylocostal dysostosis	Nonsense
2	*DLL3*	c.621C>A	p.C207*	Spondylocostal dysostosis	Nonsense
3	*DLL3*	c.674G>A	p.S225N	Congenital scoliosis	Missense
4	*DLL3*	c.712C>T	p.R238*	Spondylocostal dysostosis	Nonsense
5	*DLL3*	c.805G>A	p.G269R	Vertebral malformation	Missense
6	*DLL3*	c.810C>A	p.C270*	Spondylocostal dysostosis	Nonsense
7	*DLL3*	c.926G>A	p.C309Y	Spondylocostal dysostosis	Missense
8	*DLL3*	c.1086C>A	p.C362*	Spondylocostal dysostosis	Nonsense
9	*DLL3*	c.1138C>T	p.R380C	Spondylocostal dysostosis	Missense
10	*DLL3*	c.1154G>A	p.G385D	Spondylocostal dysostosis	Missense
11	*DLL3*	c.1164C>A	p.C388*	Spondylocostal dysostosis	Nonsense
12	*DLL3*	c.1511G>A	p.G504D	Spondylocostal dysostosis	Missense
13	*DLL3*	c.329delT	p.(Val110Glyfs*22)	Spondylocostal dysostosis	Small deletion
14	*DLL3*	c.395delG	p.(Gly132Glufs*109)	Spondylocostal dysostosis	Small deletion
15	*DLL3*	c.602delG	p.(Gly201Valfs*40)	Spondylocostal dysostosis	Small deletion
16	*DLL3*	c.618delC	p.(Cys207Alafs*34)	Spondylocostal dysostosis	Small deletion
17	*DLL3*	c.868_870+8del11	p.?	Spondylocostal dysostosis	Small deletion
18	*DLL3*	c.945_946delAT	p.(Ala317Argfs*17)	Spondylocostal dysostosis	Small deletion
19	*DLL3*	c.948_949delTG	p.(Ala317Argfs*17)	Spondylocostal dysostosis	Small deletion
20	*DLL3*	c.1365_1381del17	p.(Cys455Trpfs*5)	Spondylocostal dysostosis	Small deletion
21	*DLL3*	c.1418delC	p.(Ala473Glufs*75)	Spondylocostal dysostosis	Small deletion
22	*DLL3*	c.1440delG	p.(Pro481Argfs*67)	Spondylocostal dysostosis	Small deletion
23	*DLL3*	c.599_603dupGCGGT	p.(Pro202Alafs*41)	Spondylocostal dysostosis	Small insertion
24	*DLL3*	c.602_614dup13	p.(Pro206Serfs*14)	Spondylocostal dysostosis	Small insertion
25	*DLL3*	c.1183_1184insCGCTGC	p.(Cys395delinsSerLeuArg)	Spondylocostal dysostosis	Small insertion
26	*DLL3*	c.1238_1255dup18	p.(His413_Ala418dup)	Spondylocostal dysostosis	Small insertion
27	*DLL3*	c.1291_1307dup17	p.(Pro437Thrfs*117)	Spondylocostal dysostosis	Small insertion
28	*DLL3*	c.661C>T	p.R221*	Hemi-vertebrae and rib fusion	Nonsense
1	*MESP2*	c.307G>T	p.E103*	Spondylocostal dysostosis	Nonsense
2	*MESP2*	c.367G>T	p.E123*	Spondylocostal dysostosis	Nonsense
3	*MESP2*	c.373C>G	p.L125V	Spondylocostal dysostosis	Missense
4	*MESP2*	c.688C>T	p.Q230*	Spondylocostal dysostosis	Nonsense
5	*MESP2*	c.737G>A	p.W246*	Spondylocostal dysostosis	Nonsense
6	*MESP2*	c.1166A>G	p.E389G	Spondylocostal dysostosis	Missense
7	*MESP2*	c.599delA	p.(Gln200Argfs*281)	Spondylocostal dysostosis	Small deletion
8	*MESP2*	c.180_193dup14	p.(Glu65Alafs*60)	Spondylocostal dysostosis	Small insertion
9	*MESP2*	c.500_503dupACCG	p.(Gly169Profs*199)	Spondylocostal dysostosis	Small insertion
1	*LFNG*	c.446C>T	p.T149I	Spondylocostal dysostosis	Missense
2	*LFNG*	c.564C>A	p.F188L	Spondylocostal dysostosis	Missense
3	*LFNG*	c.583T>C	p.W195R	Spondylocostal dysostosis	Missense
4	*LFNG*	c.601G>A	p.D201N	Spondylocostal dysostosis	Missense
5	*LFNG*	c.761C>T	p.T254M	Spondylocostal dysostosis	Missense
6	*LFNG*	c.842C>A	p.T281K	Spondylocostal dysostosis	Missense
7	*LFNG*	c.139_142delGGCC	p.(Gly47Profs*97)	Autism spectrum disorder	Small deletion
8	*LFNG*	c.372delG	p.(Lys124Asnfs*21)	Spondylocostal dysostosis	Small deletion
9	*LFNG*	c.44dupG	p.(Ala16Argfs*135)	Spondylocostal dysostosis	Small insertions
1	*HES7*	c.73C>T	p.R25W	Spondylocostal dysostosis	Missense

(Continued on following page)

TABLE 2 (*Continued*) Mutations reported to date in genes associated with spondylocostal dysostosis (HGMD® Professional 2022.2).

Number of mutation	Gene name	cDNA	Protein	Phenotype	Types of mutation
2	*HES7*	c.86A>G	p.N29S	Spondylocostal dysostosis	Missense
3	*HES7*	c.172A>G	p.I58V	Spondylocostal dysostosis	Missense
4	*HES7*	c.556G>T	p.D186Y	Spondylocostal dysostosis	Missense
5	*HES7*	c.385_394dup10	p.(Arg132Glnfs*42)	Spondylocostal dysostosis	Small insertion
1	*TBX6*	c.422T>C	p.L141P	Spondylocostal dysostosis	Missense
2	*TBX6*	c.449G>A	p. p.R150H	Spondylocostal dysostosis	Missense
3	*TBX6*	c.661C>A	p.H221N	Spondylocostal dysostosis	Missense
4	*TBX6*	c.699G>C	p.W233C	Spondylocostal dysostosis	Missense
5	*TBX6*	c.1148C>A	p.S383*	Spondylocostal dysostosis	Nonsense
6	*TBX6*	c.994delG	p.(Glu332Lysfs*166)	Spondylocostal dysostosis	Small deletion
1	*RIPPLY2*	c.238A>T	p.R80*	Vertebral segmentation defects	Nonsense
2	*RIPPLY2*	c.240–4T>G		Vertebral segmentation defects	Splice site
1	*DLL1*	c.1534G>A	p.G512R	Vertebral malformation	Missense

and ribs. However, additional syndromic types have been reported in some of the subtypes.

1.3 Spondylocostal dysostosis type 1 (SCDO1; *DLL3*)

SCDO1 is caused by pathogenic biallelic mutations in the Delta-like canonical Notch ligand 3 (*DLL3*) gene (MIM 602768) located on chromosome 19q13.2 with autosomal recessive mode of inheritance. The clinical features, reported in the affected individuals having *DLL3* mutations, are the irregularity of the vertebral column on spinal radiographs in early childhood and the prenatal stage. "Pebble beach sign" of each vertebral body in the fetus is a characteristic feature, which is observed having an ovoid or round shape with smooth boundaries (Turnpenny et al., 2003). As a result, the fetus develops the pebble beach appearance of the vertebrae and gives rise to multiple irregularities to the vertebral column. In such a situation, an MRI is more feasible to view the irregularities as compared to X-rays.

The *DLL3* gene (NM_016941.4) consists of eight exons encoding a 618-amino acid (NP_058637.1) long protein. The long encoded *DLL3* protein is composed of different domains such as a Delta–Serrate-Lag2 region (DSL), six epidermal growth factor-like domains (EGF), and a transmembrane (TM) domain. *DLL3* has been shown to be involved in the somite boundary formation and cell-signaling mechanism as it has shown a spatially restricted expression pattern when studied in different animal models (Dunwoodie et al., 2002; Kusumi et al., 2004; Dunwoodie S. L., 2009). To date, only 31 disease-causing mutations have been reported in the *DLL3* (HGMD, 2021). Out of these, 28 homozygous mutations have been identified in the *DLL3* gene associated with SCDO1. These mutations included seven nonsense mutations, six missense mutations, ten small deletions, and five small insertions (Table 2).

1.4 Spondylocostal dysostosis type 2 (SCDO2; *MESP2*)

SCDO2 is reported to be inherited as an autosomal recessive disorder, and is caused due to the mutation in the *MESP2* gene which is located on chromosome 15q26.1. The mutation in mesoderm posterior basic helix–loop–helix transcription factor 2 (*MESP2*) (MIM 605195) may be a homozygous or a compound heterozygous mutation. SCDO2 reported cases that exhibit clinical features such as truncal shortening, short necks, and spondylocostal dysostosis. As compared to SCDO1 (*DLL3*), the affected individuals have relatively mildly affected lumbar vertebrae as compared to the thoracic region (Whittock et al., 2004b).

In an Arab-Lebanese family, reported by Whittock et al. (2004a), two affected individuals exhibited spondylocostal dysostosis features, such as short necks and truncal shortening without any other abnormalities. In the same family, a biallelic 4-bp duplication (c.500_503dup) has been identified in the *MESP2* (NM_001039958.2, NP_001035047.1) gene as the main cause of the disease. It has been found that the mutation occurs in a sequence following the basic helix–loop–helix (bHLH) domain which leads to a frameshift, hence resulting in premature truncation (Whittock et al., 2004b).

MESP2 (MIM 605195; NM_001039958.2) consists of two exons (1614 bp) and encodes a protein comprising 397 amino acids (NP_001035047.1). The full-length *MESP2* protein consists of an N-terminal domain succeeded by a basic helix–loop–helix

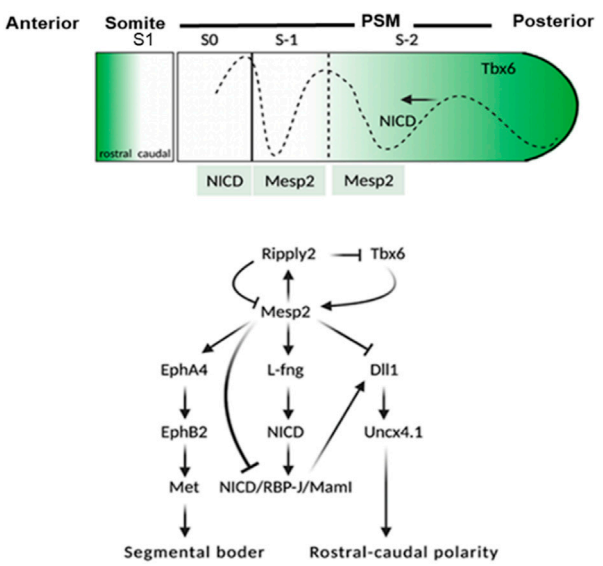

FIGURE 1
Schematic representation of events involved in the activation of *MESP2*. *TBX6* along with Notch1 signaling leads to the expression of *MESP2* in the anterior presomitic mesoderm (NICD dotted line). The dotted line toward the anterior along with the black arrow shows the Notch1 signal wavers in the presomitic mesoderm. As *MESP2* protein is formed within S1, NICD is suppressed indirectly *via* activation of *LFNG*, and directly *via* inhibition of *DLL1*. The expression of *MESP2* protein inhibits the expression of *DLL1* and *Uncx4.1* caudal genes; however, it induces the expression of rostral genes EphA4, EphB2, and followed by mesenchymal-to-epithelial transition (MET) within somites leading to segmentation of the rostral-caudal polarity within the somites is generated *via* a *RIPPLY2–MESP2* negative feedback loop. S1 = formed somite; S0 = somite under formation; S1 and S2 = somite primordia.

(bHLH) domain, a GQ (glycine and glutamine repeats)-rich region, and finally, a C-terminal domain. *MESP2* belongs to a family of transcriptional regulatory proteins that have a core helix–loop–helix (bHLH) domain, and plays a key role in rostro-caudal polarization and somite formation (Figure 1) (Mitsuru Morimoto et al., 2005) (Morimoto et al., 2007). To date, only nine mutations have been reported in the *MESP2* gene and only nine have been associated with SCDO2, which include four nonsense mutations, two missense mutations, one small deletion, and two small insertions (Table 2).

MESP2 is integral to somite boundary formation, and is important for the development of anterior somatic compartment *via* suppression of Notch signaling (Figure 1). *MESP2* expression was analyzed by Cornier et al. (2008) and Saga et al. (1997) in mouse models. They argued that *MESP2* expressed as stripe in the presomitic mesoderm which is indicative of the future somite. It is these stripes that form a support for the vertebral development in the spine of adult mice. *MESP2* expression is localized in the anterior somatic compartment. *MESP2* gene knockout mice show severe vertebral segmentation defects along with proximal rib fusion which is parallel to that observed in STD patients.

1.5 Spondylocostal dysostosis type 3 (SCDO3; *LFNG*)

SCDO3 is clinically characterized by having long slender fingers, camptodactyly, and congenital vertebral anomalies. Radiological scans have revealed multiple vertebral ossification centers in the thoracic region of the vertebral column (Sparrow et al., 2006). SCDO3-carrying individuals exhibit more severe spine shortening as compared to SCDO1 and SCDO2 individuals, although ribs deformities have been reported to be similar to SCDO1 and SCDO2 cases. In 2006, Sparrow *et al* reported a biallelic missense mutation (c.564C>A; p.F188L) in the Leng O-fucosylpeptide 3-beta-N-acetylglucosaminyltransferase (*LFNG*) gene located on chromosome 7p22.3 as a candidate gene in a Lebanese proband. Recently, a proband from a Japanese family has been reported having features of severe multiple vertebral deformities starting from the cervical to sacral spine. Novel compound heterozygous variants [c.372delG (p.K124Nfs*) and c.601G>A (p.D201N)] in the *LFNG* gene have been identified which further validates the role of this gene in causing spondylocostal dysostosis type 3 in humans (Otomo et al., 2019).

LFNG (NM_001040167.2) is composed of a total of eight exons (2377bp) located on chromosome 7p22.3, encoding a 379-aa long protein (NP_001035257.1) To date, fourteen mutations have been reported in the *LFNG* gene responsible for causing SCDO3 phenotypes (HGMD; 2018). To date, only 14 mutations have been reported in the *LFNG* gene and only nine have been associated with SCDO3, including two small deletions, one small insertion, and six missense variants (Table 2). The other phenotypes reported include autism spectrum disorder (ASD), scoliosis, Asperger's syndrome, and tetralogy of Fallot.

Apart from vertebral defects, the proband reported by Sparrow et al. (2006) had camptodactyly of the left index finger. The authors suggested that these features might not be due to the *LFNG* mutation, since according to one study, lack of *LFNG* expression in mouse models did not show limb defects (Zhang et al., 2002). It has been shown that the *LFNG* expression is restricted to the hemangioblasts (precursors of blood vessels) in a developing vertebrate limb. However, the expression of *LFNG* in the human embryo is still elusive, and human limb development might be different from that in the mouse (Sparrow et al., 2006).

1.6 Spondylocostal dysostosis type 4 (SCDO4; *HES7*)

SCDO4 is a severe autosomal recessive disorder triggered by the *HES7* gene mutation located on chromosome 17p13.1. A

proband in a Caucasian Mediterranean origin consanguineous family had features such as lumbosacral myelomeningocele; hydrocephalus; myelomeningocele; bell-shaped, shortened thorax; stenotic anus; and talipes. The radiological examination of the proband also revealed the shortening of the spine and contiguous and multiple vertebral defects. The parents were normal, second cousins, having two healthy kids (Sparrow et al., 2008). Molecular analysis of the proband led to the identification of a homozygous missense mutation (c.73C>T; p. Arg25Trp) in the *HES7* gene.

Later, two affected cases from a non-consanguineous Italian family were reported to have spondylocostal dysostosis. The affected individuals showed multiple anomalies, multiple rib fusions with 11 pairs of bilateral ribs, short trunk, and short stature. MRI results revealed multiple segmentation anomalies in the cervical region of the spine (Sparrow et al., 2010). In 2013, a large consanguineous Arab family was reported to have seven SCDO4 cases. The affected individuals were reported to have consistent features of SCDO4. Three of the affected individuals were presented with dextrocardia along with situs inversus. Two of the affected individuals also exhibited secondary features such as neural tube defects (spina bifida occulta, thoracic myelomeningocele, and Chiari II) (Sparrow et al., 2013).

The *HES7* gene (MIM608059; NM_001165967.2) covers 1674 bp of the genomic region, has four exons, and encodes *HES7* protein. An *HES7* protein is a transcription factor that belongs to the hairy and enhancer of split family of bHLH transcription factors (NP_001159439.1). To date, only seven disease-causing homozygous mutations have been identified in the *HES7* gene (HGMD, 2022). Only five mutations including four missense mutations and one small insertion have been associated with SCDO4 (Table 2).

Gene expression analysis of various transcription factors in an embryonic mouse brain have suggested the low level expression of *HES7* in the mid-brain and thalamus and thus, is limited to PSM (Gray et al., 2004). The expression of other members of the *HES* family (*HES*1, 3, 5, and 6) in the embryonic mouse brain has also been reported (Gray et al., 2004). Furthermore, severe neural tube defects and premature neurogenesis have been reported for *HES1*-null mutants (Ishibashi et al., 1995). Severe somite segmentation defects have been reported in homozygous *HES7*-null mouse embryos; laterality defects, however, have not been described (Bessho et al., 2001).

1.7 Spondylocostal dysostosis type 5 (SCDO5; *TBX6*)

SCDO5 was reported for the first time by Gucev et al. (2010) in a Macedonian descendant family segregating autosomal dominant spondylocostal dysostosis. The affected individuals had several phenotypes, such as disproportionate short trunks, short necks, mild scoliosis with hemi-vertebrae, and vertebral blocks. These affected individuals did not reveal any other abnormalities, dysmorphic features, or neurodevelopment issues. Gucev et al. (2010) identified a pathogenic heterozygous variant in the *TBX6* gene. In total, twenty-three individuals from the Chinese Han population with congenital scoliosis-related compound heterozygous mutations in the *TBX6* gene were identified. The affected individuals revealed hemi-vertebrae and other shared rib abnormalities (Wu et al., 2015). More recently (Lefebvre et al., 2017), identified homozygous disease-causing mutations in the *TBX6* gene justified the recessive inheritance of SCDO5. The affected individuals presented features such as disproportionate short stature, short necks, rib abnormalities, missing ribs, scoliosis, syringomyelia, and butterfly vertebrae.

The *TBX6* gene is located on chromosome 16p11.2 (NM_004608.3, NP_004599.2), and is composed of nine exons encoding a 463-amino acid protein, *TBX6*. *TBX6* belongs to a family that is phylogenetically conserved and shares a common DNA-binding domain, the T-box. The T-box genes encode transcription factors that play an important role in the regulation of developmental processes. The knockout studies in mice have suggested the role of this gene in the specification of paraxial mesoderm structures (Zhao et al., 2018). To date, only 66 disease-causing homozygous mutations have been identified in the *HES7* gene (HGMD, 2022). Only six mutations in the *TBX6* gene have been associated with SCDO5, including four missense mutations, one nonsense mutation, and one small deletion (Table 2). Other phenotypes associated with *TBX6* pathogenesis include scoliosis, Müllerian aplasia, Mayer–Rokitansky–Küster–Hauser syndrome, congenital anomalies of the kidney, tetralogy of Fallot, and autism.

The *TBX6*-null/mh mice exhibited vertebral malformations, similar to those in humans; the lower part of the spine is affected by the vertebral malformations (Liu et al., 2019).

1.8 Spondylocostal dysostosis type 6 (SCDO6; *RIPPLY2*)

SCDO6, an autosomal recessive disorder, is caused by homozygous variants in the *RIPPLY2* gene (NM_001009994.2), which is located on chromosome 6q14.2. SCDO6 exhibits severe phenotypes such as spinal canal stenosis, the descent of an occipital bone, absence of posterior elements of upper cervical vertebrae, hemi-vertebrae, butterfly vertebrae, cervical kyphosis, and thoracic scoliosis (Menger et al., 2021). McInerney-Leo et al. (2015) reported two affected individuals born to non-consanguineous parents having phenotypes such as affected posterior C1–C4 elements, butterfly vertebrae of T2–T7, cervical kyphosis, spinal canal stenosis, mild thoracic scoliosis, and hemi-vertebrae.

The *RIPPLY*2 gene consists of four exons (664 bp) that encode a 128-aa long nuclear protein, *RIPPLY2* (*RIPPLY* transcriptional repressor 2 protein), that belongs to a novel family of proteins required for vertebrate somitogenesis. The members of this family of proteins are characterized by having a tetrapeptide WRPW motif at N-terminal and a *RIPPLY* homology domain at C-terminal (composed of a Bowline-DSCR-Ledgerline conserved region) The *RIPPLY* family of proteins has been reported to be the transcriptional repressors as they negatively regulate the T-box proteins, including *TBX6*, coded by SCDO gene 10 (Kawamura et al., 2008). The transcriptional repression occurs by the interaction of *RIPPLY* proteins with the DNA-binding domain of T-box proteins, *via* their *RIPPLY* homology domain, and with the transcriptional co-repressor Groucho/TLE proteins *via* their WRPW motif (Kawamura et al., 2005). To date, only three disease-causing mutations have been identified in the *RIPPLY*2 gene, including one nonsense, one splice site mutation, and one small deletion (Table 2; HGMD, 2022).

Studies involving mice, which are kept homozygous null for *RIPPLY2*, have been reported to have severe vertebral and ribs malformations. Such mice also displayed defects in axial skeleton segmentations due to defective somitogenesis and finally, died in their prenatal stage. The vertebral defects that have been observed in *RIPPLY2*-null mice had a metameric pattern of vertebral bodies, intervertebral discs, and severely disrupted neural arches (Chan et al., 2007). Such conditions are similar to those of the mice, which are homozygous null for the autosomal recessive SCDO genes *DLL3*, *MESP2*, *LFNG*, and *HES7* (Sparrow et al., 2011).

1.9 Spondylocostal dysostosis type 7 (SCDO7; *DLL1*)

SCDO type 7 is a recently identified type of spondylocostal dysostosis inherited in an autosomal recessive manner. Barhoumi et al. (2019) reported two affected individuals (boys) showing features such as scoliosis, fused thoracic spines (T4–T5, T6–T8, and T11–T12), and multiple spine deformities. The whole-exome sequence analysis of these patients revealed a homozygous missense mutation (c.1534G>A; p. Gly512Arg) in exon 9 of the *DLL1* gene. In addition, 14 patients from unrelated families had neurodevelopmental disorders along with other brain abnormalities. The sequence analysis of these patients revealed the heterozygous mutations in the *DLL1* gene (Fischer-Zirnsak et al., 2019). All these reported patients had kyphosis/scoliosis, hyperextensible joints, hypotonia, and ataxia, as common features.

DLL1, located on chromosome 6q27, comprise a total of 11 exons (3174 bp) encoding a 723-amino acid long protein (NM_005618.4, NP_005609.3, 11). *DLL1* encodes for the protein Delta-like canonical Notch ligand 1 (*DLL1*). *DLL1* belongs to the Delta/Serrate/Jagged Family and is a human homolog of the *Drosophila* Delta ligand. It is important for hematopoiesis as it plays an important role in mediating cell fate decisions *via* cell-to-cell communication (Barhoumi et al., 2019). To date, 38 disease-causing mutations have been identified in the *DLL1* gene associated with different disorders such as neurodevelopmental disorder, autism, hearing loss, congenital heart disease, and cleft lip/or palate. However, only one mutation has been associated in *DLLI* causing vertebral malformations (SCDO7) (Barhoumi et al., 2019).

DLL1 is composed of three domains, mainly intracellular, transmembrane, and an extracellular domain [containing eight epidermal growth factor-like (EGF-like) domains]. The mutation is mainly located in the eight EGF-like domains at a conserved nucleotide region. The mutation resulted in a change of amino acid at 512 position (from glycine to arginine), consequently affecting its binding properties with the target proteins.

Knockout mutations of *DLL1* in the mouse model generated a phenotype that differed significantly from the wild-type mouse in reference to the body size. The KO mouse had a small size and suffered from osteosclerosis because of the loss of function of osteoblasts and osteoclasts. According to the histopathological study, the affected mice had a reduced bone formation rate, decreased osteoblast surface area, and a compromised metabolic bone turnover (Muguruma et al., 2017).

1.10 Molecular genetics of SCDO and involvement of the Notch-signaling pathway

In humans, vertebrae are formed during embryogenesis from somites which are the embryonic segments produced from the presomitic mesoderm (PSM) in approx. 4–5 h. These somites are produced in a rhythmic sequence following an anterior to posterior direction. This periodic series of somite formation involves a molecular segmentation clock which basically operates through a Notch-signaling pathway (Wahi et al., 2016). Most of the genes belonging to the Notch-signaling pathway are involved in the somitogenesis and the molecular oscillation generated by them is synchronized with coupling genes of Wnt and FGF pathways in the PSM. These pathways are vital for normal vertebral development and somitogenesis as the coupled oscillations of the signaling genes under these signaling pathways govern the accurate segmentation in the process of somite formation. The mutations in these genes such as *LFNG*, *DLL3*, and *MESP2* have been shown to be associated with the abnormal molecular oscillations leading to the development of congenital vertebral malformations, that is, recessive spondylocostal dysostosis (SCDO) (Dequéant et al., 2006; Goldbeter and Pourquié, 2008).

The Notch-signaling pathway was identified for the first time in *Drosophila*. It is highly conserved through evolution from invertebrates to vertebrates (Bray, 2006). The Notch-signaling pathway is a very diverse and important pathway, which is known to interact with several other pathways such as hedgehog

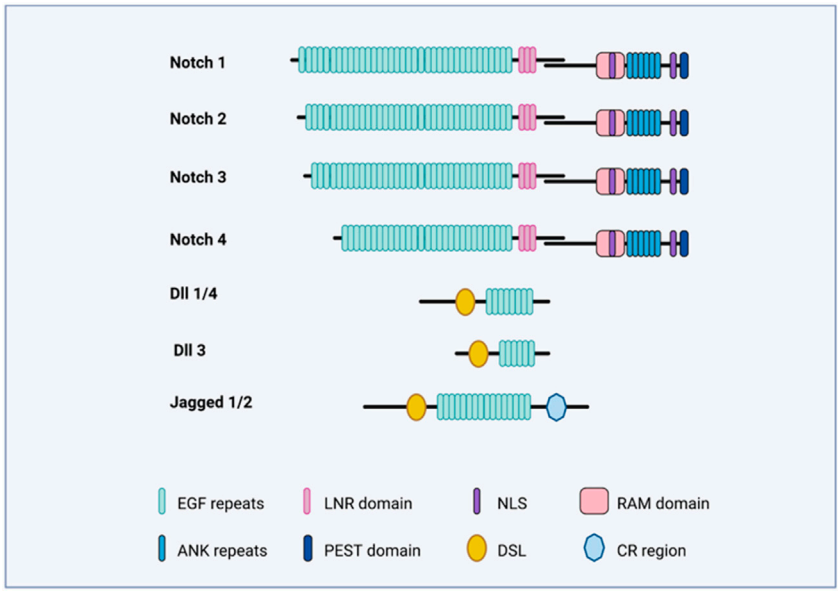

FIGURE 2
Notch-signaling illustration. The figure illustrates the domains of Notch receptors (Notch 1–4) and Notch ligands (*DLL1*,*3*,*4*; Jag1 and Jag2).

(Hh), fibroblast growth factor (FGF), Janus kinase/signal transducers, transcription activation (Jak/STAT), transforming growth factor-β (TGF-β), receptor tyrosine kinase (RTK), hypoxia pathways, and Wnt pathways (Gustafsson et al., 2005; Hurlbut et al., 2007). These signaling pathways have been extensively studied, and the future research might unravel the complex interactions and pathophysiology involved.

Notch receptors bind the Delta/Serrate/Lag2 ligands, also known as DSL ligands. In mammals, the DSL ligands are subdivided into five types, which are grouped into two classes, that is, the Delta-like (homology with *Drosophila* Delta), which includes the *DLL1*, *DLL3*, and *DLL4*, as well as Serrate-like and the Serrate, which included *Jagged1* and *Jagged2* (Figure 2). Both the Delta-like and Serrate-like ligands have an extracellular domain having a signal peptide, an amino-terminal domain, a DSL domain, and several EGF-like repeats (Nye and Kopan, 1995).

In mammals, Notch receptors (Notch1–4) have four types (Figure 2), and it is structurally divided into an extracellular and intracellular domain. The extracellular domain (ECD) has EGF-like 29–36 repeats and three Lin-12/Notch (LIN) repeats. The EGF-like repeats binds the ligand, while the LIN repeats prevent ligand-independent signaling. The intracellular domain (ICD) contains the RBPj-associated molecule (RAM) domain, and a six-ankyrin (ANK) repeats domain. Both of these are protein-interacting domains. Apart from these, the intracellular domain also contains a transactivation domain (TAD), a PEST sequence, and nuclear localization signals (NLSs).

The Notch-signaling pathway is very simple, as the intracellular domain (ICD) of the Notch receptor lacks the second messengers and is thus directly involved in the target gene transcription (Figure 3). However, Notch-signaling modifiers have been involved in the complex signaling specificity (Bray, 2006). Once synthesized as a single polypeptide, Notch protein travels through the Golgi apparatus where it may be further modified (Panin et al., 1997) and is cleaved by a furin-like convertase *via* S1 cleavage in the trans-Golgi network convertase (Logeat et al., 1998). The associated specific epidermal growth factor (EGF)-like repeats are modified in the endoplasmic reticulum (ER) by O-fucosylation *via* O-fucosyltransferase 1 (Pofut1).

The C-terminal transmembrane, N-terminal extracellular truncation (ECN), and intracellular domain (TMIC) of the Notch receptor fragments form a heterodimer that proceeds toward the cell surface (Rand et al., 2000; Sanchez-Irizarry et al., 2004). Once it has reached the cell surface, it is cleaved by disintegrin (S2 cleavage) and proteases (metalloprotease domain, ADAM10 and ADAM17) due to the interaction of the ECN with the respective ligand (in the trans), resulting in the separation of Notch heterodimer separation through transendocytosis of the ECN into the signal-sending cell (Pan and Rubin, 1997; Brou et al., 2000; Hartmann et al., 2002). The Notch-signaling pathway in Figure 3 summarizes the function and involvement of each gene.

1.11 Diagnosis and genetic counseling

SCDO is mostly diagnosed by the radiological features in association with NGS (WES/WGS). The identification of the

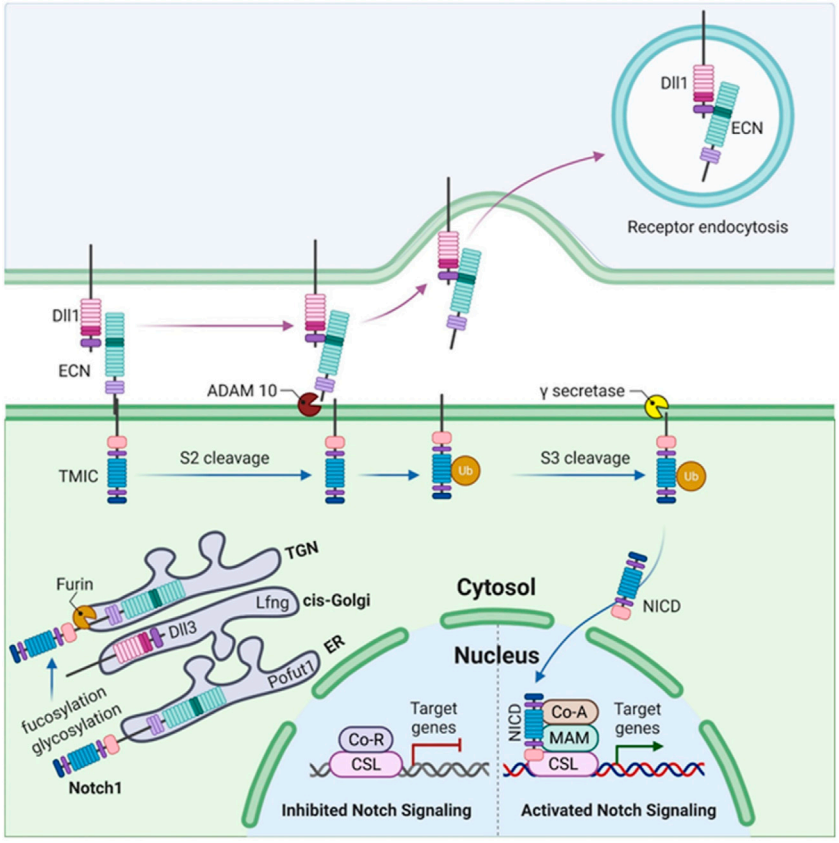

FIGURE 3
Somitogenesis in mammals illustrating Notch1 signaling. The figure illustrates the synthesis of Notch1 as a single polypeptide. O-fucosylation of specific EGF-like repeats occurs in the endoplasmic reticulum (ER) by O-fucosyltransferase 1 (Pofut1), followed by the elongation of these O-fucosylated EGF-like repeats (upon addition of GlcNAc by lunatic fringe, Lfng) as the Notch1 polypeptide passes through the cis-Golgi. S1 cleavage occurs in the trans-Golgi network (TGN) by a furin-like convertase. The Notch1 heterodimer (composed of an N-terminal extracellular truncation, ECN, and a C-terminal transmembrane and intracellular domain, TMIC) moves toward the cell surface where it binds *DLL1 via* ECN in trans. This binding leads to the activation of S2 cleavage by the disintegrin and metallopeptidase domain (ADAM) proteases, ADAM10 or ADAM17. This liberates the Notch1 ECN which then undergoes ubiquitylation (Ub) and is endocytosed. S3 cleavage of Notch1 ECN occurs in the transmembrane domain *via* γ-secretase which releases the Notch1 intracellular domain (NICD). NICD binds CSL which is a DNA-binding protein. Upon binding to CSL, co-repressor (CoR) proteins and histone deacetylases (HDACs) are released while the binding of coactivators (CoAs) occurs simultaneously which results in the activation of Notch signaling, leading to the transcription of target genes such as *MESP2*, *LFNG*, and *HES7*.

culprit gene defines the type of SCDO. It is characterized into different subtypes as a result of homozygous mutations in several genes causing autosomal recessive SCDO, such as *DLL3*, *DLL1*, *LFNG*, *RIPPLY2*, *MESP2*, *HES7*, and *TBX6*. Once the mutation in the specific gene is identified, genetic counseling and family carrier testing can be performed. Carrier testing will help to reduce the occurrence of diseases in coming generations (Umair et al., 2017).

2 Discussion

Genetic deformities of the skeletal system are characterized by malformation, inconsistent growth, and distortion of individual bones or groups of bones, which can cause syndromic and non-syndromic forms (Umair et al., 2019). Genetic skeletal deformities can occur due to disruption in the intricate processes of skeletal development, growth, and homeostasis. The inheritance pattern of genetic skeletal deformities can be either autosomal (dominant or recessive) or X-linked (dominant or recessive) (Umair et al., 2018b; Umair and Hayat, 2020; Ahmad et al., 2022). Similarly, spondylocostal dysostosis is a severe form of skeletal deformity that leads to severe ribs and vertebrae malformations. With the advent of NGS technology, molecular diagnosis of rare skeletal deformities such as spondylocostal dysostosis is now cost effective and quick (Umair et al., 2018a). Screening the associated seven genes in patients suffering from disorders such as spondylocostal dysostosis will enable the researchers and clinicians to treat

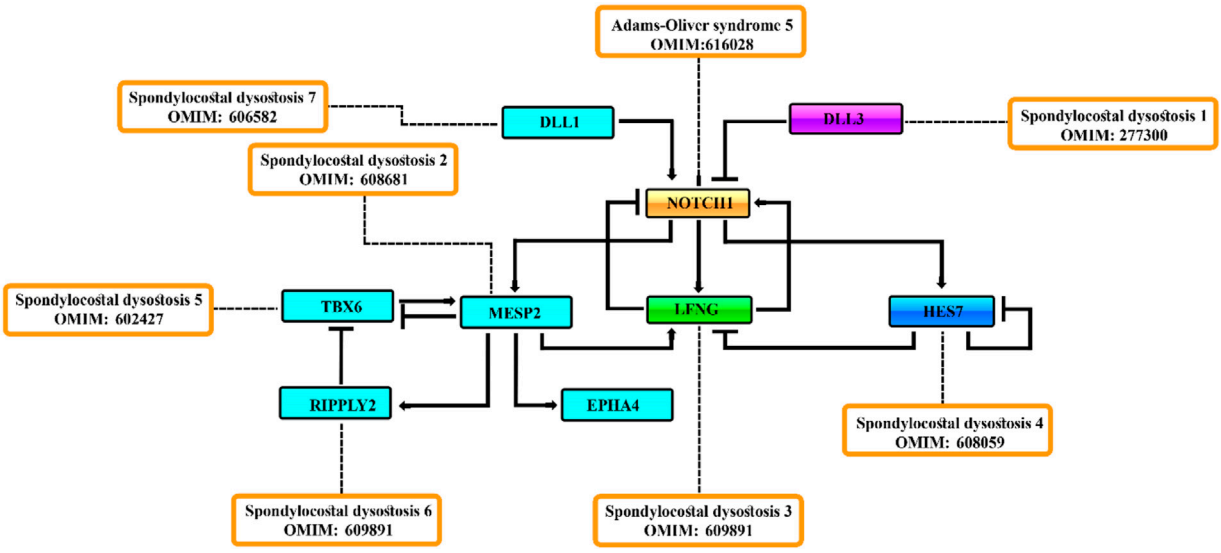

FIGURE 4
Negative feedback [act as repressors] loop consisting of the *MESP2*, *LFNG*, *HES7*, and *DLL3* genes regulate the Notch-signaling activity during somitogenesis.

the patient at an early stage. In addition, techniques such as Noninvasive prenatal testing (NIPT), Pre-implantation genetic testing for aneuploidy (PGT-A) and Pre-implantation genetic testing for monogenic disorders (PGT-M) have been employed to reduce the occurrence of severe genetic disorders (Alyafee et al., 2021a; Alyafee et al., 2021b; Alyafee et al., 2022). Therapeutic interventions are only possible if we know the exact molecular origin of a disease that might help the researchers to identify the exact biomarkers. In such a scenario, knowledge about the molecular etiology and pathophysiology of such a rare genetic disease is a must to implement and draw future therapeutic interventions.

The Notch-signaling pathway plays a major role in numerous cell developmental processes, the major one being the skeletal system development and bone homeostasis. The Notch-signaling system utilizes Notch receptors as a key component in the regulation of cell differentiation and function. The four Notch receptors carry out cell-specific functions in the skeletal system and any mutations in them cause alterations in the Notch signaling. Several skeletal malignancies and development of various congenital bone disorders have been reported to be associated with the variations in the Notch-signaling pathway (Canalis, 2018).

The Notch-signaling pathway is an absolute requirement for normal somitogenesis in vertebrates which has been confirmed by mouse models and cell culture studies. The somite boundary formation and its patterning largely depend on the Notch1 activity. The Notch pathway genes are largely involved in the rostral-caudal patterning, synchronized oscillations in the segmentation clock in PSM, and the segmental border formation. Disease causing genetic mutations encoding the protein involved in these essential processes has been reported to be the source of severe vertebral deformities in humans Notch pathway components (Dunwoodie SL., 2009).

Investigation of the genetic causes of abnormal vertebral segmentation (AVS), using mouse models, has reported certain genes that are important for normal vertebral development as they are the activators of Notch, FGF, and Wnt signaling pathways. These signaling pathways are pivotal for normal somite production and bones development in vertebrates. Mutations in these genes, that is, *DLL3*, *MESP2*, *LFNG*, and *HES7*, cause congenital AVS disorder, SCDO. *DLL3* and *DLL1* are worth mentioning as these genes serve as the DSL ligands of Notch and are likely to inhibit the pathway by acting as an inhibitor of signaling (Dunwoodie S. L., 2009).

Disease-causing variants in Notch-signaling pathway members cause different types of developmental disorders that affect different parts of the body, including the skeleton, heart, liver, kidneys, eye, face, and vasculature. Notch-associated disorders include different types of severe disorders such as Alagille syndrome caused by mutations in both ligand JAG1 and receptor Notch2 and autosomal recessive spondylocostal dysostosis, caused by mutations in ligand *DLL3*, and many other members of the Notch-signaling pathway (Penton et al., 2012). Similarly, the other genes associated with recessive spondylocostal dysostosis (*MESP2*, *LFNG*, and *HES7*) have been associated with regulating

Notch-signaling activity during somitogenesis (Penton et al., 2012).

It has been observed that *DLL3* interacts with full-length Notch1 in the late endocytic compartment and that high levels of *DLL3* expression are correlated with low levels of Notch1, suggesting that *DLL3* targets Notch1 for lysosomal degradation (Chapman et al., 2010). The *LFNG* is an N-acetylglucosaminyltransferase that adds N-acetylglucosamine to fucose residues on Notch receptors and acts to suppress Notch signaling during somitogenesis in mice (Sparrow et al., 2006). *HES7* acts to downregulate *LFNG* expression. *LFNG*, *DLL3*, and *MESP2* mutant embryos display a broadening of Notch-signaling activity during somitogenesis, detected by antibodies to NICD (Chapman et al., 2010; Feller et al., 2008) (Figures 3, 4). *DLL3* is predicted to participate in lysosomal degradation of Notch1, *MESP2* destabilizes MAML, and *LFNG* down-regulates Notch signaling immediately posterior to the forming somite (Chapman et al., 2010; Sasaki et al., 2011) (Figures 2, 4). Not surprisingly, ubiquitous activation of Notch in the presomitic mesoderm results in abnormal somite formation (Feller et al., 2008).

3 Conclusion

In conclusion, proper somite formation is dependent on the Notch-signaling pathway which regulates the skeletal homeostasis. SCDO is an abnormal congenital disorder of vertebral and rib deformation which occurs due to the mutations of the genetic components of the Notch-signaling pathway. SCDO is diagnosed based on characteristic symptoms, family history, an extensive clinical evaluation (radiographs of the spine), and molecular diagnosis (WGS/WES). No specific treatment is available; however, surgery can be performed to repair an inguinal hernia and scoliosis, and antibiotics can be suggested for recurrent respiratory infections. As a rare genetic disorder, the exact incidence or prevalence of SCDO is unknown, and a proper genetic and molecular analysis is required to identify the culprit gene, which might help in proper diagnosis and timely treatments.

Author contributions

MU: idea and wrote the first draft; MY, SS, and AN: edited and approved the final draft. MA: edited the final version.

Funding

This study was funded by King Abdullah International Medical Research Center (KAIMRC) (RC19/352/R).

Conflict of interest

The authors declare that the research was conducted in the absence of any commercial or financial relationships that could be construed as a potential conflict of interest.

Publisher's note

References

Alyafee, Y., Alam, Q., Altuwaijri, A., Umair, M., Haddad, S., Alharbi, M., et al. (2021a). Next-generation sequencing-based pre-implantation genetic testing for aneuploidy (PGT-A): First report from Saudi arabia. *Genes (Basel)* 12 (4), 461. doi:10.3390/genes12040461

Alyafee, Y., Al Tuwaijri, A., Alam, Q., Umair, M., Haddad, S., Alharbi, M., et al. (2021b). Next generation sequencing based non-invasive prenatal testing (nipt): First report from Saudi Arabia. *Front. Genet.* 12, 630787. doi:10.3389/fgene.2021.630787

Alyafee, Y., Al Tuwaijri, A., Umair, M., Alharbi, M., Haddad, S., Ballow, M., et al. (2022). Non-invasive prenatal testing for autosomal recessive disorders: A new promising approach. *Front. Genet*. doi:10.3389/fgene.2022.1047474

Ahmad, Z., Liaqat, R., Palander, O., Bilal, M., Zeb, S., Ahmad, F., et al. (2022). Genetic overview of postaxial polydactyly (PAP): Updated classification. *Clin. Genet*. doi:10.1111/cge.14224

Barhoumi, T., Nashabat, M., Alghanem, B., Alhallaj, A., Boudjelal, M., Umair, M., et al. (2019). Delta like-1 gene mutation: A novel cause of congenital vertebral malformation. *Front. Genet.* 510, 534. doi:10.3389/fgene.2019.00534

Bessho, Y., Sakata, R., Komatsu, S., Shiota, K., Yamada, S., and Kageyama, R. (2001). Dynamic expression and essential functions of Hes7 in somite segmentation. *Genes Dev.* 15, 2642–2647. doi:10.1101/gad.930601

Bray, S. J. (2006). Notch signalling: A simple pathway becomes complex. *Nat. Rev. Mol. Cell Biol.* 7, 678–689. doi:10.1038/nrm2009

Brou, C., Logeat, F., Gupta, N., Bessia, C., LeBail, O., Doedens, J. R., et al. (2000). A novel proteolytic cleavage involved in notch signaling: The role of the disintegrin-metalloprotease TACE. *Mol. Cell* 5, 207–216. doi:10.1016/s1097-2765(00)80417-7

Bulman, M. P., Kusumi, K., Frayling, T. M., McKeown, C., Garrett, C., Lander, E. S., et al. (2000). Mutations in the human delta homologue, *DLL3*, cause axial skeletal defects in spondylocostal dysostosis. *Nat. Genet.* 24, 438–441. doi:10.1038/74307

Canalis, E. (2018). Notch in skeletal physiology and disease. *Osteoporos. Int.* 29 (12), 2611–2621. doi:10.1007/s00198-018-4694-3

Cetinkaya, M., Ozkan, H., Köksal, N., Yazici, Z., and Yalçinkaya, U. (2008). Spondylocostal dysostosis associated with diaphragmatic hernia and neural tube defects. *Clin. Dysmorphol.* 17, 151–154. doi:10.1097/MCD.0b013e3282f2699c

Chan, T., Kondow, A., Hosoya, A., Hitachi, K., Yukita, A., Okabayashi, K., et al. (2007). Ripply2 is essential for precise somite formation during mouse early development. *FEBS Lett.* 581, 2691–2696. doi:10.1016/j.febslet.2007.05.017

Chapman, G., Sparrow, D. B., Kremmer, E., and Dunwoodie, S. L. (2010). Notch inhibition by the ligand DELTA-LIKE 3 defines the mechanism of abnormal vertebral segmentation in spondylocostal dysostosis. *Hum. Mol. Genet.* 20 (5), 905–916. doi:10.1093/hmg/ddq529

Cornier, A. S., Staehling-Hampton, K., Delventhal, K. M., Saga, Y., Caubet, J. F., Sasaki, N., et al. (2008). Mutations in the MESP2 gene cause spondylothoracic dysostosis/Jarcho-Levin syndrome. *Am. J. Hum. Genet.* 82, 1334–1341. doi:10.1016/j.ajhg.2008.04.014

Dequéant, M. L., Glynn, E., Gaudenz, K., Wahl, M., Chen, J., Mushegian, A., et al. (2006). A complex oscillating network of signaling genes underlies the mouse segmentation clock. *Science* 314, 1595–1598. doi:10.1126/science.1133141

Dunwoodie, S. L. (2009b). Mutation of the fucose-specific beta1, 3 N-acetylglucosaminyltransferase LFNG results in abnormal formation of the spine. *Biochim. Biophys. Acta* 1792 (2), 100–111. doi:10.1016/j.bbadis.2008.11.003

Dunwoodie, S. L., Clements, M., Sparrow, D. B., Sa, X., Conlon, R. A., and Beddington, R. S. (2002). Axial skeletal defects caused by mutation in the spondylocostal dysplasia/pudgy gene *DLL3* are associated with disruption of the segmentation clock within the presomitic mesoderm. *Development* 129, 1795–1806. doi:10.1242/dev.129.7.1795

Dunwoodie, S. L. (2009a). The role of Notch in patterning the human vertebral column. *Curr. Opin. Genet. Dev.* 19 (4), 329–337. doi:10.1016/j.gde.2009.06.005

Feller, J., Schneider, A., Schuster-Gossler, K., and Gossler, A. (2008). Noncyclic Notch activity in the presomitic mesoderm demonstrates uncoupling of somite compartmentalization and boundary formation. *Genes Dev.* 22 (16), 2166–2171. doi:10.1101/gad.480408

Fischer-Zirnsak, B., Segebrecht, L., Schubach, M., Charles, P., Alderman, E., Brown, K., et al. (2019). Haploinsufficiency of the notch ligand DLL1 causes variable neurodevelopmental disorders. *Am. J. Hum. Genet.* 105 (3), 631–639. doi:10.1016/j.ajhg.2019.07.002

Goldbeter, A., and Pourquié, O. (2008). Modeling the segmentation clock as a network of coupled oscillations in the Notch, Wnt and FGF signaling pathways. *J. Theor. Biol.* 252, 574–585. doi:10.1016/j.jtbi.2008.01.006

Gray, P. A., Fu, H., Luo, P., Zhao, Q., Yu, J., Ferrari, A., et al. (2004). Mouse brain organization revealed through direct genome-scale TF expression analysis. *Science* 306, 2255–2257. doi:10.1126/science.1104935

Gucev, Z. S., Tasic, V., Pop-Jordanova, N., Sparrow, D. B., Dunwoodie, S. L., Ellard, S., et al. (2010). Autosomal dominant spondylocostal dysostosis in three generations of a Macedonian family: Negative mutation analysis of *DLL3*, MESP2, HES7, and LFNG. *Am. J. Med. Genet. A* 152a, 1378–1382. doi:10.1002/ajmg.a.33471

Gustafsson, M. V., Zheng, X., Pereira, T., Gradin, K., Jin, S., Lundkvist, J., et al. (2005). Hypoxia requires notch signaling to maintain the undifferentiated cell state. *Dev. Cell* 9, 617–628. doi:10.1016/j.devcel.2005.09.010

Hartmann, D., de Strooper, B., Serneels, L., Craessaerts, K., Herreman, A., Annaert, W., et al. (2002). The disintegrin/metalloprotease ADAM 10 is essential for Notch signalling but not for alpha-secretase activity in fibroblasts. *Hum. Mol. Genet.* 11, 2615–2624. doi:10.1093/hmg/11.21.2615

Hurlbut, G. D., Kankel, M. W., Lake, R. J., and Artavanis-Tsakonas, S. (2007). Crossing paths with Notch in the hyper-network. *Curr. Opin. Cell Biol.* 19, 166–175. doi:10.1016/j.ceb.2007.02.012

Ishibashi, M., Ang, S. L., Shiota, K., Nakanishi, S., Kageyama, R., and Guillemot, F. (1995). Targeted disruption of mammalian hairy and Enhancer of split homolog-1 (HES-1) leads to up-regulation of neural helix-loop-helix factors, premature neurogenesis, and severe neural tube defects. *Genes Dev.* 9, 3136–3148. doi:10.1101/gad.9.24.3136

Kawamura, A., Koshida, S., Hijikata, H., Ohbayashi, A., Kondoh, H., and Takada, S. (2005). Groucho-associated transcriptional repressor ripply1 is required for proper transition from the presomitic mesoderm to somites. *Dev. Cell* 9, 735–744. doi:10.1016/j.devcel.2005.09.021

Kawamura, A., Koshida, S., and Takada, S. (2008). Activator-to-repressor conversion of T-box transcription factors by the Ripply family of Groucho/TLE-associated mediators. *Mol. Cell. Biol.* 28, 3236–3244. doi:10.1128/MCB.01754-07

Kusumi, K., Mimoto, M. S., Covello, K. L., Beddington, R. S., Krumlauf, R., and Dunwoodie, S. L. (2004). *DLL3* pudgy mutation differentially disrupts dynamic expression of somite genes. *Genesis* 39, 115–121. doi:10.1002/gene.20034

Lefebvre, M., Duffourd, Y., Jouan, T., Poe, C., Jean-Marçais, N., Verloes, A., et al. (2017). Autosomal recessive variations of *TBX6*, from congenital scoliosis to spondylocostal dysostosis. *Clin. Genet.* 91, 908–912. doi:10.1111/cge.12918

Liu, J., Wu, N., Yang, N., Takeda, K., Chen, W., Li, W., et al. (2019). *TBX6*-associated congenital scoliosis (TACS) as a clinically distinguishable subtype of congenital scoliosis: Further evidence supporting the compound inheritance and *TBX6* gene dosage model. *Genet. Med.* 21, 1548–1558. doi:10.1038/s41436-018-0377-x

Logeat, F., Bessia, C., Brou, C., LeBail, O., Jarriault, S., Seidah, N. G., et al. (1998). The Notch1 receptor is cleaved constitutively by a furin-like convertase. *Proc. Natl. Acad. Sci. U. S. A.* 95, 8108–8112. doi:10.1073/pnas.95.14.8108

McInerney-Leo, A. M., Harris, J. E., Leo, P. J., Marshall, M. S., Gardiner, B., Kinning, E., et al. (2015). Whole exome sequencing is an efficient, sensitive and specific method for determining the genetic cause of short-rib thoracic dystrophies. *Clin. Genet.* 88, 550–557. doi:10.1111/cge.12550

Mitsuru Morimoto, M., Takahashi, Y., Endo, M., and Saga, Y. (2005). The Mesp2 transcription factor establishes segmental borders by suppressing Notch activity. *Nature* 19435 (7040), 354–359. doi:10.1038/nature03591

Morimoto, M., Sasaki, N., Oginuma, M., Kiso, M., Igarashi, K., Aizaki, K., et al. (2007). The negative regulation of Mesp2 by mouse Ripply2 is required to establish the rostro-caudal patterning within a somite. *Development* 134 (8), 1561–1569. doi:10.1242/dev.000836

Mortier, G. R., Lachman, R. S., Bocian, M., and Rimoin, D. L. (1996). Multiple vertebral segmentation defects: Analysis of 26 new patients and review of the literature. *Am. J. Med. Genet.* 61, 310–319. doi:10.1002/(SICI)1096-8628(19960202)61:4<310::AID-AJMG3>3.0.CO;2-Y

Muguruma, Y., Hozumi, K., Warita, H., Yahata, T., Uno, T., Ito, M., et al. (2017). Maintenance of bone homeostasis by *DLL1* -mediated notch signaling. *J. Cell. Physiol.* 232, 2569–2580. doi:10.1002/jcp.25647

Nye, J. S., and Kopan, R. (1995). Developmental signaling. Vertebrate ligands for Notch. *Curr. Biol.* 5, 966–969. doi:10.1016/s0960-9822(95)00189-8

Otomo, N., Mizumoto, S., Lu, H. F., Takeda, K., Campos-Xavier, B., Mittaz-Crettol, L., et al. (2019). Identification of novel LFNG mutations in spondylocostal dysostosis. *J. Hum. Genet.* 64, 261–264. doi:10.1038/s10038-018-0548-2

Pan, D., and Rubin, G. M. (1997). Kuzbanian controls proteolytic processing of Notch and mediates lateral inhibition during Drosophila and vertebrate neurogenesis. *Cell* 90, 271–280. doi:10.1016/s0092-8674(00)80335-9

Panin, V. M., Papayannopoulos, V., Wilson, R., and Irvine, K. D. (1997). Fringe modulates Notch-ligand interactions. *Nature* 387, 908–912. doi:10.1038/43191

Penton, A. L., Leonard, L. D., and Spinner, N. B. (2012). Notch signaling in human development and disease. *Semin. Cell Dev. Biol.* 23 (4), 450–457. doi:10.1016/j.semcdb.2012.01.010

Rand, M. D., Grimm, L. M., Artavanis-Tsakonas, S., Patriub, V., Blacklow, S. C., Sklar, J., et al. (2000). Calcium depletion dissociates and activates heterodimeric notch receptors. *Mol. Cell. Biol.* 20, 1825–1835. doi:10.1128/mcb.20.5.1825-1835.2000

Saga, Y., Hata, N., Koseki, H., and Taketo, M. M. (1997). Mesp2: A novel mouse gene expressed in the presegmented mesoderm and essential for segmentation initiation. *Genes Dev.* 11, 1827–1839. doi:10.1101/gad.11.14.1827

Sanchez-Irizarry, C., Carpenter, A. C., Weng, A. P., Pear, W. S., Aster, J. C., and Blacklow, S. C. (2004). Notch subunit heterodimerization and prevention of ligand-independent proteolytic activation depend, respectively, on a novel domain and the LNR repeats. *Mol. Cell. Biol.* 24, 9265–9273. doi:10.1128/MCB.24.21.9265-9273.2004

Sasaki, N., Kiso, M., Kitagawa, M., and Saga, Y. (2011). The repression of Notch signaling occurs via the destabilization of mastermind-like 1 by Mesp2 and is essential for somitogenesis. *Development* 138 (1), 55–64. [PubMed] [Google Scholar]. doi:10.1242/dev.055533

Solomon, L., Jimenez, R. B., and Reiner, L. (1978). Spondylothoracic dysostosis: Report of two cases and review of the literature. *Arch. Pathol. Lab. Med.* 102, 201–205.

Sparrow, D. B., Chapman, G., and Dunwoodie, S. L. (2011). The mouse notches up another success: Understanding the causes of human vertebral malformation. *Mamm. Genome* 22, 362–376. doi:10.1007/s00335-011-9335-5

Sparrow, D. B., Chapman, G., Wouters, M. A., Whittock, N. V., Ellard, S., Fatkin, D., et al. (2006). Mutation of the LUNATIC FRINGE gene in humans causes spondylocostal dysostosis with a severe vertebral phenotype. *Am. J. Hum. Genet.* 78, 28–37. doi:10.1086/498879

Sparrow, D. B., Faqeih, E. A., Sallout, B., Alswaid, A., Ababneh, F., Al-Sayed, M., et al. (2013). Mutation of HES7 in a large extended family with spondylocostal dysostosis and dextrocardia with situs inversus. *Am. J. Med. Genet. A* 161a, 2244–2249. doi:10.1002/ajmg.a.36073

Sparrow, D. B., Guillén-Navarro, E., Fatkin, D., and Dunwoodie, S. L. (2008). Mutation of Hairy-and-Enhancer-of-Split-7 in humans causes spondylocostal dysostosis. *Hum. Mol. Genet.* 17, 3761–3766. doi:10.1093/hmg/ddn272

Sparrow, D. B., Sillence, D., Wouters, M. A., Turnpenny, P. D., and Dunwoodie, S. L. (2010). Two novel missense mutations in HAIRY-AND-ENHANCER-OF-SPLIT-7 in a family with spondylocostal dysostosis. *Eur. J. Hum. Genet.* 18, 674–679. doi:10.1038/ejhg.2009.241

Turnpenny, P. D., Sloman, M., and Dunwoodie, S.; ICVS (international consortium for vertebral anomalies and scoliosis) (2009). "Spondylocostal dysostosis, autosomal recessive," in *GeneReviews® [internet]*. M. P. Adam, H. H. Ardinger, R. A. Pagon, et al. (Seattle (WA): University of Washington, Seattle). [Updated 2017 Dec 21]Available from: https://www.ncbi.nlm.nih.gov/books/NBK8828/.

Turnpenny, P. D., Sloman, M., and Dunwoodie, S.; ICVS (International Consortium for Vertebral Anomalies and Scoliosis) (1993). "Spondylocostal dysostosis, autosomal recessive," in *GeneReviews(®)*. Editors M. P. Adam, H. H. Ardinger, R. A. Pagon, S. E. Wallace, L. J. H. Bean, G. Mirzaa, et al. (Seattle (WA): University of Washington, Seattle Copyright © 1993-2021University of Washington, Seattle. GeneReviews is a registered trademark of the University of Washington, Seattle. All rights reserved.).

Turnpenny, P. D., Whittock, N., Duncan, J., Dunwoodie, S., Kusumi, K., and Ellard, S. (2003). Novel mutations in *DLL3*, a somitogenesis gene encoding a ligand for the Notch signalling pathway, cause a consistent pattern of abnormal vertebral segmentation in spondylocostal dysostosis. *J. Med. Genet.* 40, 333–339. doi:10.1136/jmg.40.5.333

Umair, M., Ahamd, F., Bilal, M., Asiri, A., Younus, M., and Khan, A. (2019). A comprehensive review of genetic skeletal disorders reported from Pakistan: A brief commentary. *Meta Gene* 20, 100559. doi:10.1016/j.mgene.2019.100559

Umair, M., Ahmad, F., and Ullah, A. (2018a). Whole exome sequencing as a diagnostic tool for genetic disorders in Pakistan. *PJMR* 57 (2), 90–91.

Umair, M., Ahmad, F., Bilal, M., and Arshad, M. (2018b). Frontonasal dysplasia: A review. *J. Biochem. Clin. Gene.* 1 (2), 1–14.

Umair, M., and Hayat, A. (2020). Nonsyndromic split-hand/foot malformation: Recent classification. *Mol. Syndromol.* 10 (5), 243–254. doi:10.1159/000502784

Umair, M., Rafique, A., Ullah, A., Ahmad, F., Ali, R. H., Nasir, A., et al. (2017). Novel homozygous sequence variants in the GDF5 gene underlie acromesomelic dysplasia type-grebe in consanguineous families. *Congenit. Anom.* 57 (2), 45–51. doi:10.1111/cga.12187

Wahi, K., Bochter, M. S., and Cole, S. E. (2016). The many roles of Notch signaling during vertebrate somitogenesis. *Semin. Cell Dev. Biol.* 49, 68–75. doi:10.1016/j.semcdb.2014.11.010

Whittock, N. V., Ellard, S., Duncan, J., de Die-Smulders, C. E., Vles, J. S., and Turnpenny, P. D. (2004a). Pseudodominant inheritance of spondylocostal dysostosis type 1 caused by two familial delta-like 3 mutations. *Clin. Genet.* 66, 67–72. doi:10.1111/j.0009-9163.2004.00272.x

Whittock, N. V., Sparrow, D. B., Wouters, M. A., Sillence, D., Ellard, S., Dunwoodie, S. L., et al. (2004b). Mutated MESP2 causes spondylocostal dysostosis in humans. *Am. J. Hum. Genet.* 74, 1249–1254. doi:10.1086/421053

Wu, N., Ming, X., Xiao, J., Wu, Z., Chen, X., Shinawi, M., et al. (2015). *TBX6* null variants and a common hypomorphic allele in congenital scoliosis. *N. Engl. J. Med.* 372, 341–350. doi:10.1056/NEJMoa1406829

Zhang, N., Norton, C. R., and Gridley, T. (2002). Segmentation defects of Notch pathway mutants and absence of a synergistic phenotype in lunatic fringe/radical fringe double mutant mice. *Genesis* 33, 21–28. doi:10.1002/gene.10081

Zhao, W., Oginuma, M., Ajima, R., Kiso, M., Okubo, A., and Saga, Y. (2018). Ripply2 recruits proteasome complex for Tbx6 degradation to define segment border during murine somitogenesis. *Elife* 15, 7e33068. doi:10.7554/eLife.33068

Frontiers in Genetics

Highlights genetic and genomic inquiry relating to all domains of life

The most cited genetics and heredity journal, which advances our understanding of genes from humans to plants and other model organisms. It highlights developments in the function and variability of the genome, and the use of genomic tools.

Discover the latest Research Topics

See more →

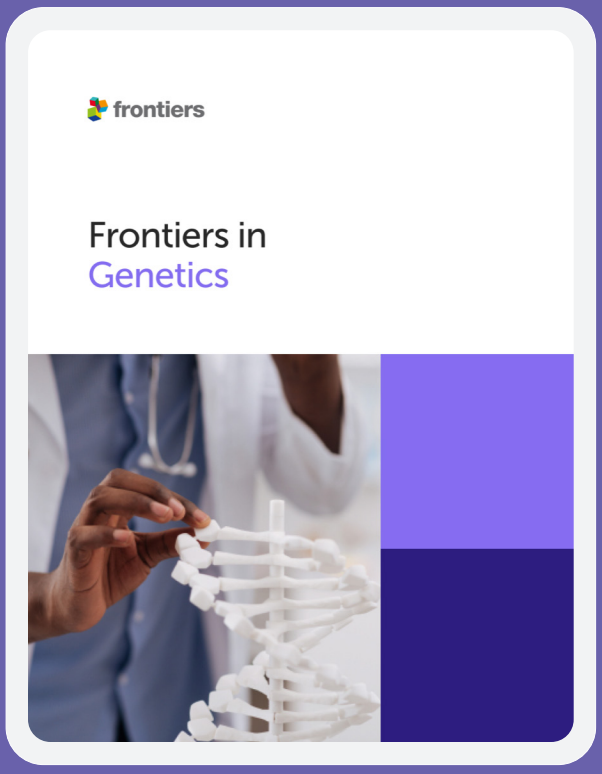

Frontiers

Avenue du Tribunal-Fédéral 34
1005 Lausanne, Switzerland
frontiersin.org

Contact us

+41 (0)21 510 17 00
frontiersin.org/about/contact